Journal of Applied Mechanics

(*Contributions of the ASME Applied Mechanics Division*)

SEPTEMBER, 1949

VOL. 16, NO. 3

Transactions of The American Society of Mechanical Engineers

Journal of Applied Mechanics

Papers Contributed to the Transactions by the ASME Applied Mechanics Division

Published Quarterly by

The American Society of Mechanical Engineers

Publication Office, 20th and Northampton Streets, Easton, Pa.
Editorial Department at the Headquarters of the Society, 29 West Thirty-Ninth Street, New York 18, N. Y.

Published quarterly by The American Society of Mechanical Engineers. Publication office at 20th and Northampton Streets, Easton, Pa. The editorial department is located at the headquarters of the Society, 29 West Thirty-Ninth Street, New York 18, N. Y. Cable address, "Dynamic," New York. Price $1.35 a copy, $5.00 a year; to members $2.50 a year. Changes of address must be received at Society headquarters three weeks before they are to be effective on the mailing list. Please send old as well as new address. . . . By-Law: The Society shall not be responsible for statements or opinions advanced in papers or . . . printed in its publications (B13, Par. 4). . . . Entered as second-class matter March 14, 1933, at the Post Office at Easton, Pa., under the act of August 24, 1912 . . . .

Primary Creep in the Design of Internal-Pressure Vessels

By L. F. COFFIN, JR.,[1] P. R. SHEPLER,[2] AND G. S. CHERNIAK[3]

The paper evaluates the stresses and the permanent strains at a particular time, resulting from loading a thick-walled cylinder under constant internal pressure and elevated temperature when account is taken of the primary creep characteristics of a given material. The results are compared with permanent strains obtained by considering secondary creep as the general basis for pressure-vessel design. For a thick-walled cylinder of wall ratio of R_1/R_0 = 2 and of 12 per cent chromium steel, operating under 12,000 psi at 850 F, the permanent strain at the end of 25 hr by the primary-creep analysis was found to be equal to the strain at the end of 2000 hr, considering only secondary creep. The methods formulated are shown to be suitable for design of pressure vessels intended for short life.

Nomenclature

The following nomenclature is used in the paper:

α = thermal coefficient of expansion, in./in./deg F
Δ = increment
ξ_1, ξ_2, ξ_3 = principal strains, Cartesian co-ordinates, in./in.
$\dot{\xi}_1, \dot{\xi}_2, \dot{\xi}_3$ = principal strain rates, in./in./sec
ξ_r, ξ_t, ξ_z = principal strains, cylindrical co-ordinates, in./in.
$\dot{\xi}_r, \dot{\xi}_t, \dot{\xi}_z$ = principal strain rates, in./in./sec
ξ^* = effective strain, in./in.
$\dot{\xi}^*$ = effective strain rate, in./in./sec
ϵ_p = plastic component of strain, in./in.
$\theta, \theta_0, \theta_1$ = temperature, deg F, subscript refers to position
ν = Poisson's ratio
$\sigma_1, \sigma_2, \sigma_3$ = principal stresses, Cartesian co-ordinates, psi
$\sigma_r, \sigma_t, \sigma_z$ = principal stresses, cylindrical co-ordinates, psi
σ^* = effective stress, psi
$\omega_1 = 1 + D$
$\omega_2 = \nu + D/2$
$A, b, B, c, C^*_1, C_1, C_2, k, m, n', N_1, N_2$ = const
D = variable coefficient relating stresses and strains with plastic flow
E = modulus of elasticity, psi
p_0 = bore pressure, psi
r = radius, in.
R_0, R_1 = bore or outside radius, in.
t = time, hr

[1] Consultant to Lessells and Associates, Boston, Mass., and Assistant Professor of Mechanical Engineering, Massachusetts Institute of Technology, Cambridge, Mass. Mem. ASME.
[2] Consulting Engineer, Lessells and Associates.
[3] Chief Engineer, Lessells and Associates. Jun. ASME.

Contributed by the Applied Mechanics Division and presented at the Petroleum-Mechanical Engineering Conference, Amarillo, Texas, October 3–6, 1948, of THE AMERICAN SOCIETY OF MECHANICAL ENGINEERS.

Discussion of this paper should be addressed to the Secretary, ASME, 29 West 39th Street, New York, N. Y., and will be accepted until October 10, 1949, for publication at a later date. Discussion received after the closing date will be returned.

NOTE: Statements and opinions advanced in papers are to be understood as individual expressions of their authors and not those of the Society. Paper No. 48—PET-18.

Introduction

In the design of thick-walled pressure vessels, Fig. 1, for elevated temperatures in the power, oil, and chemical fields, numerous situations may arise where factors other than strength considerations impose limitations on useful life. Among such factors may be included surface corrosion, intergranular corrosion, grain growth, life of fittings, contamination, etc. Under the condition of short service life imposed by the foregoing factors, a rational design procedure for internal-pressure vessels should be such as to set the stresses at a level where permissible creep is attained at this service life. By such a procedure higher pressures and temperatures may be reached, which would greatly facilitate chemical reaction or power-plant efficiency.

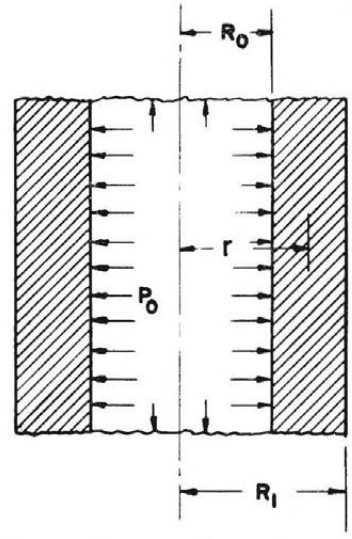

FIG. 1 THICK-WALLED CYLINDER UNDER INTERNAL PRESSURE OF 12,000 PSI AND CONSTANT θ = 850 F

To date the commonly accepted basis for design of pressure vessels at elevated temperatures has been by the use of tensile secondary-creep data applied to combined steady stress such as the methods used by Bailey (1),[4] by Marin (2), and by Soderberg (3). In short life, secondary-creep conditions are rarely attained and primary creep must be the basis for any analysis. Soderberg (4) pointed out in 1936, that there has been a general tendency to ignore the initial period of varying creep rate and to treat the problem as one of constant rate; it is evident that this procedure is unsuitable for cases where stresses are influenced by the plastic deformations themselves. Such is nearly always the case in practical problems.

The present paper attempts to show how the tensile primary-creep characteristics may be utilized in the design of thick-walled pressure vessels. In other words, it attempts to trace the stress-deformation history of the tube from the time when the pressure is applied initially until its life expectancy, or to the time when steady-state conditions corresponding to secondary creep are reached.

[4] Numbers in parentheses refer to the Bibliography at the end of the paper.

In this paper, for the sake of simplicity, analysis has been made for the case of a thick-walled cylinder under constant temperature throughout the wall. Any temperature could have been used for which there were sufficient data in good form. It appeared that the McVetty data for 12 per cent Cr steel at 850 F, as presented by Soderberg (4) fitted this condition rather well. This is shown in Fig. 2. As will be noted in the following section, inclusion of heat flow does not complicate the problem unduly. In such a case of course, tensile creep data at various stress levels and at various temperature levels would be necessary for the material in question. The same type of analysis as presented herein may at some future date be extended to the problem of cyclic loading of pressure vessels.

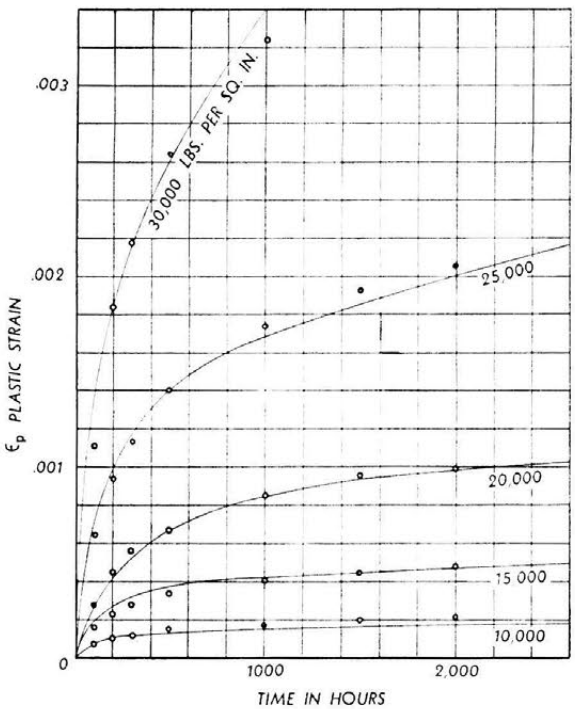

FIG. 2 CREEP CURVES FOR 12 PER CENT CR STEEL AT 850 F

The analysis as presented with but slight modification may be applied to other systems of combined stresses in cylindrical problems such as rotating disks, turbine rotors, etc.

By use of the maximum shear theory of plastic flow and by a unique trial-and-error procedure, stresses and strains have been found that are compatible with a stress versus strain curve occurring at any instant of time. The method requires the conversion of conventional tensile creep data to curves of stress versus strain with time constant. Experimental work is necessary to verify the validity of using these converted curves for a mechanism of varying stresses at a point in the material. The trial-and-error system may be too lengthy to allow solution of the great number of cases of thick-walled cylinders under internal pressure which need attention, and to that end, a computer to handle this procedure automatically is suggested.

BASIC THEORY AND FORM OF CALCULATION

Transient State. In the long thick-walled cylinder subjected to a constant internal pressure and heat flow with temperature equilibrium, the transient state is defined as that portion of the deformation history of the tube when the stresses throughout the cylinder vary with time. It may be considered to start when the pressure is first applied, at which point the stress distribution in the tube is entirely elastic in nature, and is completed when the complex creep-relaxation process in the tube has adjusted itself to the point where the entire stress distribution is constant with respect to time. The transient state is a result of primary creep of the metal. This state is examined first.

At all instants of time during the life of the tube, certain basic relationships must be fulfilled throughout the tube. These include the condition of radial equilibrium of stresses

$$r\frac{d\sigma_r}{dr} = \sigma_t - \sigma_r \quad \ldots\ldots [1]$$

and the condition of compatibility of the strains, which can be expressed in the form

$$r\frac{d\xi_t}{dr} = \xi_r - \xi_t \quad \ldots\ldots [2]$$

The creep process is thought of as a plastic phenomenon to which the basic laws of plastic flow of a homogeneous ductile metal apply, namely, the constancy of volume of plastic strains, and the geometric similarity of Mohr's three principal strain circles to Mohr's three principal stress circles. These laws are quite well known (5), and have been extended to the creep problem by Soderberg (4). A generalized stress-strain relationship (6), can be formulated applying these laws, together with the well-known Hooke's law for elastic behavior; thus

$$\left.\begin{aligned} E\xi_r &= \omega_1\sigma_r - \omega_2(\sigma_t + \sigma_z) \\ E\xi_t &= \omega_1\sigma_t - \omega_2(\sigma_z + \sigma_r) \\ E\xi_z &= \omega_1\sigma_z - \omega_2(\sigma_r + \sigma_t) \end{aligned}\right\} \quad \ldots\ldots [3]$$

where

$$\left.\begin{aligned} \omega_1 &= 1 + D \\ \omega_2 &= \nu + \frac{D}{2} \end{aligned}\right\} \quad \ldots\ldots [4]$$

It will be seen that Equations [3] satisfy the plastic-flow law of constancy of volume, since the volume change per unit volume is

$$(\xi_r + \xi_t + \xi_z) = \frac{1 - 2\nu}{E}(\sigma_r + \sigma_t + \sigma_z)$$

where the term in the right-hand side represents only an elastic bulk-modulus effect. Also, from Equation [3] the second plastic law is fulfilled since

$$\frac{\xi_r - \xi_t}{\sigma_r - \sigma_t} = \frac{\xi_t - \xi_z}{\sigma_t - \sigma_z} = \frac{\xi_z - \xi_r}{\sigma_z - \sigma_r}$$

When a temperature gradient exists in the tube, Equations [3] become

$$\left.\begin{aligned} E\xi_r &= \omega_1\sigma_r - \omega_2(\sigma_t + \sigma_z) + \alpha\theta \\ E\xi_t &= \omega_1\sigma_t - \omega_2(\sigma_z + \sigma_r) + \alpha\theta \\ E\xi_z &= \omega_1\sigma_z - \omega_2(\sigma_r + \sigma_t) + \alpha\theta \end{aligned}\right\} \quad \ldots\ldots [3a]$$

Further conditions to be applied to the tube under load must be the constancy of axial strain for all radii or

$$\xi_z = k \quad \ldots\ldots [5]$$

and the end load condition, namely

$$2\pi\int_{R_0}^{R_1}\sigma_z r dr = \pi R_0^2 p_0 \quad \ldots\ldots [6]$$

The final condition needed for the evaluation of the transient-creep problem is the formulation of a unique relationship between stress, strain, temperature, and time for the material, regardless

of the stress condition. Obviously, this is no simple matter and involves the introduction of certain assumptions regarding the mechanism of creep. Considering for the moment the plastic behavior of homogeneous ductile metals under combined stress and small time intervals, it has been found possible to establish a relationship of stress and strain, namely

$$\sigma^* = f(\xi^*) \quad [7]$$

regardless of the stress ratio imposed on the material. Equation [7] usually is valid for strains less than 10 per cent. The widely accepted distortion energy theory for plastic flow can be applied to Equation [7] where

$$\sigma^* = \frac{1}{\sqrt{2}} \sqrt{(\sigma_r - \sigma_t)^2 + (\sigma_t - \sigma_z)^2 + (\sigma_z - \sigma_r)^2} \quad [8]$$

and

$$\xi^* = \frac{\sqrt{2}}{3} \sqrt{(\xi_r - \xi_t)^2 + (\xi_t - \xi_z)^2 + (\xi_z - \xi_r)^2} \quad [9]$$

However, because of the formidable analytical difficulties introduced by the complexity of Equations [8] and [9] for the present analysis the maximum shear theory will be adopted where

$$\sigma^* = \sigma_t - \sigma_r \quad [10]$$

$$\xi^* = \xi_t - \xi_r \quad [11]$$

Aside from simplicity in form, it will be shown that for the thick-walled cylinder the maximum shearing stress is always the difference between the tangential and radial stresses, the axial stress always being intermediate. This makes for simplicity of analysis. Other experimenters (7, 8) have found no basic violation to the uniqueness of maximum shearing stress - shearing strain relationship within the range of variables of their tests.

A further assumption is now made that in creep tests, time, temperature, and strain may be treated as independent variables so that one may write

$$\sigma^* = f(\xi^*, t, \theta) \quad [12]$$

This implies that for a particular temperature, tests such as, for example, standard tensile creep tests, as in Fig. 3, may be converted to curves of stress versus strain with time as a parameter as in Fig. 4. Temperature gradients in a thick-walled cylinder may then be taken into account by determining a family of curves similar to Fig. 4 for each temperature level. This procedure has been applied to various constant total strain relaxation data found in the literature using the given creep data converted to the total strain (elastic plus plastic), such as Fig. 3, and determining the stress and time for a particular constant total strain. Agreement with observed relaxation tests in the various cases has been very good.

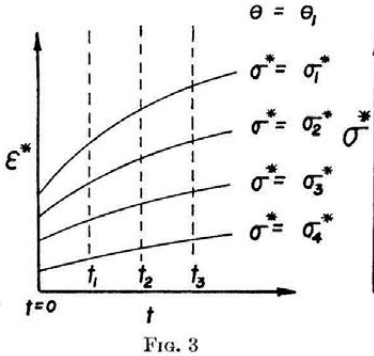

FIG. 3

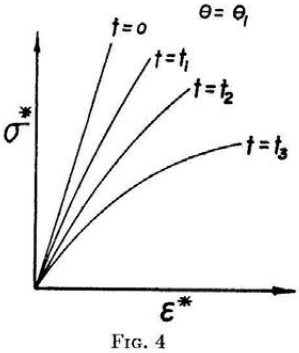

FIG. 4

With this assumption, the formulation of Equation [12], using tension-creep data, the analysis of transient creep with no heat flow (constant temperature) in thick-walled cylinders can be carried out at a particular time as though one is dealing with a static problem with the material following the arbitrary stress-strain curves such as in Fig. 5. If there is a temperature variation throughout the tube (assumed to be steady with time), then a family of curves with temperature as parameter can be used as in Fig. 6.

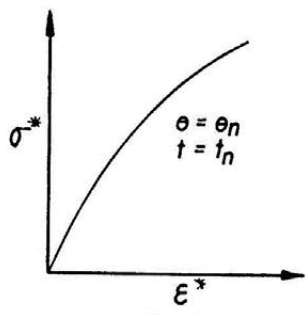

FIG. 5

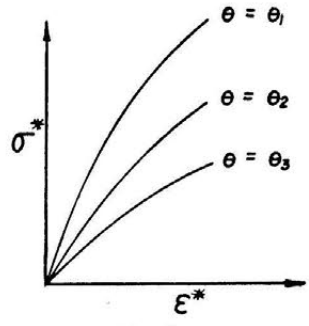

FIG. 6

Analysis can now be undertaken using the basic relationships given by Equations [1], [2], [3], or [3a], [5], [6], [10], [11], and Fig. 5 or Fig. 6, depending upon whether there is heat flow in the tube or not. First consideration is given to the determination of Fig. 5 or Fig. 6, from tension-creep data.

Assuming the tension-creep test to be performed in the z-direction, from these tests experimental curves exist of the form

$$\sigma_z = f(\xi_z) \quad [13]$$

for a particular time and temperature. For this test $\sigma_r = \sigma_t = 0$. Hence Equation [3]

$$\begin{aligned} E\xi_r &= -\omega_2\sigma_z \\ E\xi_t &= -\omega_2\sigma_z \\ E\xi_z &= \omega_1\sigma_z = (1 + D)\sigma_z \end{aligned}$$

Hence

$$D = \frac{E\xi_z}{\sigma_z} - 1$$

Then $\xi^* = \xi_z - \xi_t$ for a tension test. Thus

$$\xi^* = \xi_z + \omega_2 \frac{\sigma_z}{E} = \xi_z + \left(\nu + \frac{D}{2}\right)\frac{\sigma_z}{E}$$

or

$$\xi^* = \frac{3}{2}\xi_z - \left(\frac{1}{2} - \nu\right)\frac{\sigma_z}{E} \quad [14]$$

and

$$\sigma^* = \sigma_Z - \sigma_t = \sigma_Z \quad [15]$$

Equations [14] and [15] then determine the effective stress and strain values from tensile stress and strain values on the basis of the maximum shear theory.

For radial heat flow in thick cylinders, the temperature as a function of radius is given by

$$\theta = \theta_0 + \frac{\theta_1 - \theta_0}{\ln \frac{R_1}{R_0}} \ln \frac{r}{R_0} \quad [16]$$

Since the form of calculation to be presented is a numerical one, values of temperature at five equally spaced radial points, including the bore and outside surface, are found from which curves of the type of Fig. 6 are constructed. Assuming a wall ratio of $R_1/R_0 = 2$ for the purpose of discussion, each of the five curves Fig. 6, would then apply at the particular ratio $r/R_0 =$ 1, 1.25, 1.50, 1.75, and 2.

A distribution of the quantity $E\xi^*$ versus r/R_0 is now assumed throughout the tube. If there is no basis for the assumed distribution, a constant value of $E\xi^*$ may be selected. Using Fig. 6, σ^* is then determined for each r/R_0. Applying Equation [1]

$$r\frac{d\sigma_r}{dr} = \sigma_t - \sigma_r = \sigma^*$$

or in better form

$$\frac{d\sigma_r}{d\left(\frac{r}{R_0}\right)} = \frac{\sigma^*}{\left(\frac{r}{R_0}\right)} \quad \ldots\ldots\ldots\ldots\ldots\ldots [17]$$

Since the right-hand side of Equation [17] is known, numerical integration using Lagrangian integration coefficients (9, 10) gives the quantity $\Delta\,\sigma_r$ for each $\Delta(r/R_0)$. Since $\sigma_r = -p_0$ for internal pressure when $r/R_0 = 1$, the values of σ_r at $r/R_0 = 2$ can be found. This value should be equal to zero, but may not, in which case the quantity $\sigma^*/(r/R_0)$ is corrected by the σ_r at $r/R_0 = 2$, and a new integration performed giving $\sigma_r = 0$ at $r/R_0 = 2$. From the values of σ_r and $\sigma^*/(r/R_0)$ after adjustment, σ^* and σ_t can be found as well as the corresponding values of $E\xi^*$ from Fig. 6.

The next step in the calculation is to obtain the quantities ω_1, ω_2, and D. From Equation [3a]

$$E(\xi_t - \xi_r) = (\omega_1 + \omega_2)(\sigma_t - \sigma_r)$$

or substituting Equations [4], [10], and [11]

$$E\xi^* = \left(1 + \nu + \frac{3}{2}D\right)\sigma^*$$

Hence

$$D = \frac{2}{3}\frac{E\xi^*}{\sigma^*} - \frac{2}{3}(1 + \nu) \quad \ldots\ldots\ldots\ldots [18]$$

for each value of r/R_0, and ω_1 and ω_2 are found from Equation [4].

Now applying condition Equation [5], the constancy of axial strain, together with the last equation in Equations [3a]

$$\sigma_z = \frac{Ek}{\omega_1} + \frac{\omega_2}{\omega_1}(\sigma_t + \sigma_r) - \frac{\alpha\theta}{\omega_1} \quad \ldots\ldots\ldots\ldots [19]$$

The stress σ_z can be solved for if k were known. This can be found by trial and error using Equation [6]. Generally, three trials for Ek (with $Ek = 0$ for one) give the correct value of Ek, and the distribution of σ_z versus r/R_0. In the integration involved in Equation [6], Lagrangian integration coefficients again are used.

Knowing for the assumed and corrected distribution of $E\xi^*$, the quantities σ_t, σ_r, σ_z and k, $E\xi_t$ is found from the second of Equation [3a]. The compatibility Equation [2] has yet to be used, and this equation is a check and a means of improving the solution. Writing Equation [2] in the form

$$\frac{dE\xi_t}{d\left(\frac{r}{R_0}\right)} = -\frac{E\xi^*}{\left(\frac{r}{R_0}\right)} \quad \ldots\ldots\ldots\ldots [20]$$

numerical integration is performed giving the increments $\Delta E\xi$ for each increment of $\Delta(r/R_0)$, the right-hand side of Equation [20] having been computed from the assumed and corrected $E\xi^*$. If the correct value of $E\xi^*$ had been used at the beginning of the calculation, then the increments $\Delta E\xi_t$ found from Equation [20] should equal the increments of $E\xi_t$ from Equations [3a]. This will probably not be the case in the first trial, and a new trial is undertaken to improve the solution.

Rapid convergence of the solution is possible by selecting a new distribution of the quantity $E\xi^*$ in the following way: The strain ξ_z will be found to be small in comparison with ξ_t and ξ_r, and if the elastic strain components of the total strains are also small then

$$\xi_r + \xi_t + \xi_z \approx 0$$

or

$$\xi_t \approx -\xi_r$$

Hence

$$\xi^* = \xi_t - \xi_r \approx +2\xi_t$$

and thus

$$\Delta E\xi^* \approx +2\Delta E\xi_t \quad \ldots\ldots\ldots\ldots [21]$$

The error in the first trial is measured by the difference in increments of $E\xi_t$ found from Equations [3a], and that of [20]. By Equation [21], doubling this difference gives the error in each increment of $E\xi^*$. Hence the increments of $E\xi^*$ found from the first trial can be corrected by twice the error in $\Delta E\xi_t$. A new distribution of $E\xi^*$ for the second trial is then found keeping the same $E\xi^*$ at $r/R_0 = 1.5$ as before and determining the remaining values of $E\xi^*$ by the corrected increments of $E\xi^*$.

The second trial is carried out in an identical fashion and the errors in the increments of $E\xi_t$ observed. A third trial is then performed if necessary. Convergence by this method is more rapid for those curves having higher degrees of plastic flow or creep than for those with low creep.

Thus for the particular time parameter in Fig. 6, the complete stress-strain distribution in the tube is found. A new time parameter is then selected leading to new curves for Fig. 6, and the analysis repeated. Enough time parameters are selected to give a clear picture of the stresses and strains throughout the tube as a function of time from the case when $t = 0$ (the elastic solution) to where t approaches steady-state conditions when the stresses are constant with time.

A particular problem is treated in this paper where there is no heat flow in the tube, in which case Equations [3] and Fig. 5 are used in the analysis rather than Equations [3a] and Fig. 6. A wall ratio of 2 is selected, together with a bore pressure of 12,000 psi, using a 12 per cent Cr steel at 850 F. The creep data for these curves have been taken from reference (4), and are replotted as Figs. 7, 8, and 9. A sample calculation sheet, Table 1, has been included to show the form of calculation which the foregoing analysis assumes. Table 5 shows the data for Fig. 9.

Steady State. After a certain time the creep-relaxation process of strain in the thick-walled cylinder under constant internal pressure reaches a steady state, defined by the condition that the stresses remain constant with time. This state is associated with secondary creep. The analysis just given and assumptions can be extended readily to this case, leading to expressions for stresses and strain rates which appear in closed form. The problem is first considered from a general point of view and is then applied to the thick-walled cylinder.

If one is dealing with a homogeneous ductile metal, subjected to plastic flow or creep to such an extent that the elastic com-

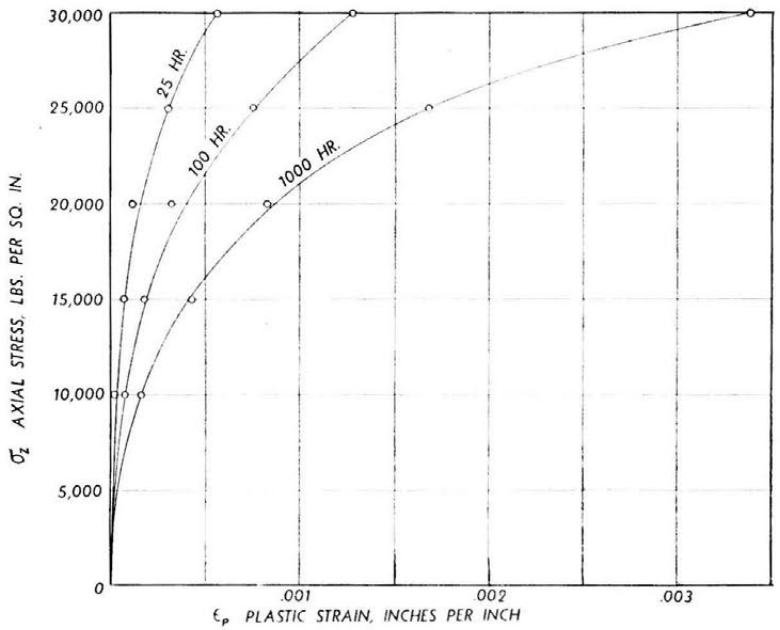

FIG. 7 AXIAL STRESS VERSUS PLASTIC STRAIN

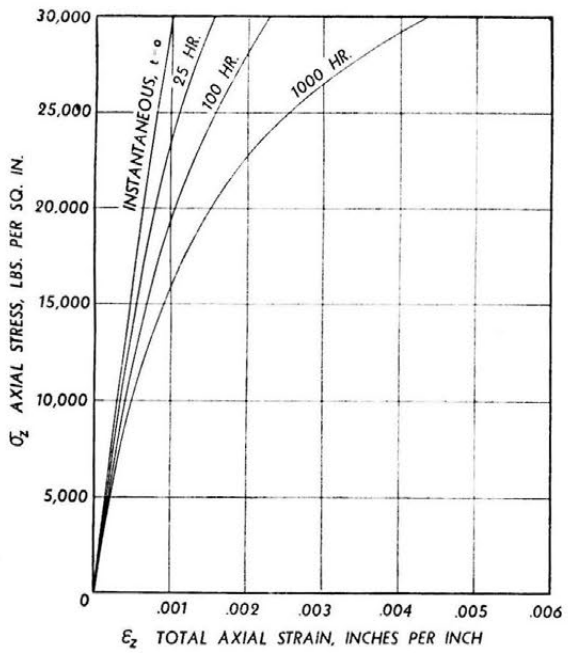

FIG. 8 AXIAL STRESS VERSUS TOTAL AXIAL STRAIN FOR 12 PER CENT CR STEEL AT 850 F

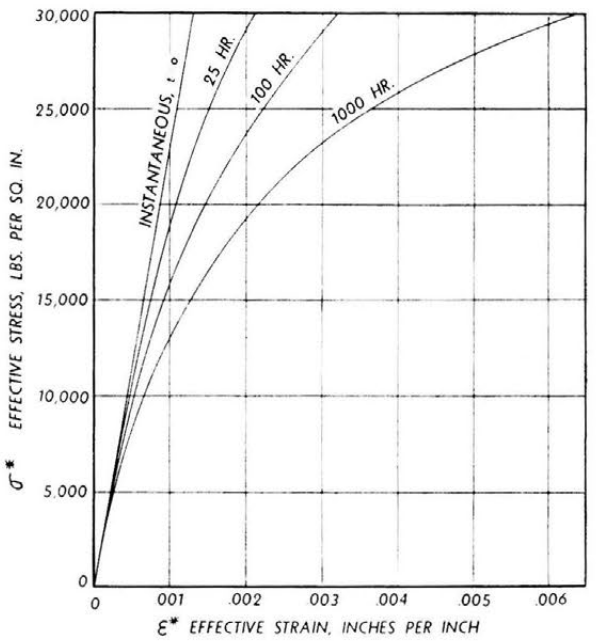

FIG. 9 EFFECTIVE STRESS VERSUS EFFECTIVE STRAIN FOR 12 PER CENT CR STEEL AT 850 F

ponent of the strains may be neglected, a state of combined stress of constant value exists such that

$$\sigma_1 > \sigma_2 > \sigma_3$$

then on the basis of the maximum shear theory

$$\sigma^* = \sigma_1 - \sigma_3 \quad \ldots\ldots [10]$$

$$\xi^* = \xi_1 - \xi_3 \quad \ldots\ldots [11]$$

and

$$\dot{\xi}^* = \dot{\xi}_1 - \dot{\xi}_3 \quad \ldots\ldots [22]$$

It is then assumed that a steady-state creep law can be formulated (1), namely

$$\dot{\xi}^* = Ae^{b\theta}(\sigma^*)^n \quad \ldots\ldots [23]$$

Applying equations of the form of Equations [3a], when the elastic strains are small and differentiating with time

$$\left.\begin{aligned} \dot{\xi}_1 &= \frac{dD}{dt}\left[\sigma_1 - \frac{1}{2}(\sigma_2 + \sigma_3)\right] \\ \dot{\xi}_2 &= \frac{dD}{dt}\left[\sigma_2 - \frac{1}{2}(\sigma_3 + \sigma_1)\right] \\ \dot{\xi}_3 &= \frac{dD}{dt}\left[\sigma_3 - \frac{1}{2}(\sigma_1 + \sigma_2)\right] \end{aligned}\right\} \quad \ldots\ldots [24]$$

Noting that

$$\dot{\xi}_1 - \dot{\xi}_3 = \dot{\xi}^*$$

TABLE 1 SAMPLE CALCULATION SHEET STRESS-STRAIN SOLUTION OF THICK-WALLED CYLINDER BY PRIMARY CREEP

TRIAL H-25	MAT'L: 12% CR STEEL			t = 25 HR.		θ = 850°F		P_0 = 12,000 p.s.i.	E = 30×10⁶	$\frac{R}{R_0}$ = 2.0	SOURCE OF DATA RP-58-15		
r/R_0	$-E\varepsilon^*$ from G-25	$E\varepsilon_t$ from G-25	a $\Delta E\varepsilon_t$ from G-25	$-\frac{E\varepsilon^*}{r/R_0}$ from G-25	b $\int(\leftarrow)$ from G-25	b − a from G-25	Corr. next trial 2× Σ diff.	New $-E\varepsilon^*$	ε^*	σ^*	$\frac{\sigma^*}{r/R_0}$	Corr. $\sigma^*/r/R_0$	Corr. σ^*	Corr. ε^*
1.0	-55,350	28,129		-55,350			+274	-55,076	.001836	27,750	27,750	27,768	27,768	.001838
1.25	-33,720	18,203	-9,926	-26,976	-9,785	+143 Same	-12	-33,732	.001124	20,340	16,272	16290	20,362	.001126
1.50	-22,920	13,134	-5,069	-15,280	-5,075	-6 Sign	0	-22,920	.000764	15,150	10,100	10,118	15,177	.000766
1.75	-16,650	10,144	-2,990	-9,514	-3,039	-49 Change	+98	-16,552	.000552	11,520	6,583	6601	11,552	.000553
2.0	-12,630	8,175	-1,669	-6,315	-1,911	+58 Sign	-18	-12,648	.000442	9,020	4,510	4,528	9,056	.000424

$-E\varepsilon_z$		σ_r	σ_t			D	ω_1	ω_2		σ_{z_0}		σ_z		
$-E\varepsilon^*$	$\Delta\sigma_r\left(\frac{\sigma^*}{r/R_0}\right)$	σ_r	$\sigma^*+\sigma_r$	$\sigma_r+\sigma_t$	$\frac{2}{3}\left(\frac{E\varepsilon^*}{\sigma^*}\right)$	$\frac{2}{3}\frac{E\varepsilon^*}{\sigma^*}-\frac{2.6}{3}$	D+1	$\frac{D}{2}+U$	$\frac{\omega_2}{\omega_1}$	$\frac{\omega_2}{\omega_1}(\sigma_r+\sigma_t)$	$\frac{ER}{\omega_1}=\frac{1616}{\omega_1}$	$\sigma_{z_0}+\frac{1616}{\omega_1}$	$\sigma_z\left(\frac{r}{R_0}\right)$	$\sigma_r+\sigma_z$
-55,140		-12,000	+15,768	3,768	1.3238	.4572	1.4571	.5285	.3627	1,367	1,109	2,476	2,476	-9,524
-33,780	5,360	-6,640	13,722	7,082	1.1060	.2393	1.2393	.4196	.3386	2,398	1,304	3,702	4,627	-2,938
-22,980	3,224	-3,416	11,761	8,345	1.0094	.1427	1.1427	.3714	.3250	2,712	1,414	4,126	6,189	+710
-16,590	2,053	-1,363	10,189	8,826	9574	.0907	1.0907	.3454	.3167	2,795	1,482	4,277	7,485	+2,914
-12,720	1,364	0	9,056	9,056	.9364	.0697	1.0697	.3394	.3131	2,835	1,511	4,346	8,692	+4,346

3,16 numerical integrating constants

$-\omega_2(\sigma_r+\sigma_t)$	$\omega_1\sigma_t$	$E\varepsilon_t$ $\omega_1\sigma_t-\omega_2(\sigma_r+\sigma_t)$	a $\Delta E\varepsilon_t$	$-\frac{E\varepsilon^*}{r/R_0}$	b $\int(\leftarrow)$	b − a difference	Corr. for next trial 2× Σ diff.	New $E\varepsilon^*$			a	b	c	d
+5033	22,976	28,009		-55,140			-50	-55,190			.34861	-.02639	+.01528	-.02639
+1,234	17,006	18,240	-9,769	-27,024	-9,770	-1 Same	-48	-33,828			.89722	+.48056	-.10278	+.14722
+264	13,459	13,175	-5,065	-15,320	-5,089	-24 Sign	0	-22,980		× 1/4	-.36667	+.63333	+.63333	-.36667
-1,006	11,113	10,107	-3,068	-9,480	-3,039	+29 Change	-58	-16,648			+.14722	-.10278	+.48056	+.89722
-1,455	9,687	8,232	-1,875	-6,360	-1,907	-32 Sign	+6	-12,714			-.02639	+.01528	-.02639	+.34861

TABLE 2 COMPARISON OF PRINCIPAL CREEP RATES OF VARIOUS THEORIES WITH COMBINED STRESS-CREEP EXPERIMENTS

A. TESTS OF TAPSELL AND JOHNSON ENGINEERING VOL. 150, 1940
.17% CARBON STEEL AT 850°F, CREEP RATES AT 150 HOURS

			EXPERIMENTAL			BAILEY THEORY			SODERBERG & MARIN'S THEORY			MAXIMUM SHEAR THEORY		
			IN./IN./HR. × 10⁻⁶											
σ_1 (P.S.I.)	σ_2 (P.S.I.)	σ_3	$\dot{\varepsilon}_1$	$\dot{\varepsilon}_2$	$\dot{\varepsilon}_3$	$\dot{\varepsilon}_1$	$\dot{\varepsilon}_2$	$\dot{\varepsilon}_3$	$\dot{\varepsilon}_1$	$\dot{\varepsilon}_2$	$\dot{\varepsilon}_3$	$\dot{\varepsilon}_1$	$\dot{\varepsilon}_2$	$\dot{\varepsilon}_3$
14,660	-660	0	0.89	-0.80	-0.19	0.95	-0.49	-0.46	0.96	-0.50	-0.46	1.00	-0.53	-0.47
12,360	-350	0	0.72	-0.57	-0.15	0.68	-0.35	-0.33	0.68	-0.36	-0.32	0.67	-0.35	-0.32
12,080	-2,080	0	1.04	0.37	-1.41	0.76	-0.45	-0.31	0.77	-0.48	-0.29	0.80	-0.49	-0.31
14,980	-2,580	0	1.76	-0.24	-1.52	1.22	-0.73	-0.49	1.17	-0.72	-0.45	1.28	-0.79	-0.49
9,720	-3,720	0	0.75	-0.21	-0.54	0.59	-0.42	-0.17	0.60	-0.44	-0.16	0.66	-0.49	-0.17
8,100	-3,100	0	0.47	0.15	-0.62	0.39	-0.28	-0.11	0.40	-0.30	-0.10	0.44	-0.33	-0.11
7,630	-4,470	0	0.52	-0.30	-0.22	0.42	-0.35	-0.07	0.43	-0.36	-0.07	0.49	-0.41	-0.08
10,240	-6,240	0	1.09	-1.13	0.04	0.84	-0.70	-0.14	0.86	-0.73	-0.13	0.97	-0.83	-0.14
5,900	-5,900	0	0.34	-0.34	0	0.36	-0.36	0	0.37	-0.37	0	0.43	-0.43	0
7,720	-7,720	0	0.68	-0.58	0	0.66	-0.66	0	0.68	-0.68	0	0.78	-0.78	0

B. TESTS OF NORTON-ASME TRANS. 63, 1941
CARBON-MOLYBDENUM STEEL AT 900° AND 1050° F

TEMERATURE OF TEST				EXPERIMENTAL	SODERBERG & MARIN'S THEORY	MAXIMUM SHEAR THEORY	DURATION OF TEST HOURS
				IN./IN./HR. × 10⁻⁶			
	σ_1 (P.S.I.)	σ_2 (P.S.I.)	σ_3 (P.S.I.)	$\dot{\varepsilon}_1$	$\dot{\varepsilon}_1$	$\dot{\varepsilon}_1$	
900°	23,000	11,500	0	0.15	0.104	0.140	1,400
1050°	9,200	4,600	0	0.87	0.740	1.14	2,600

one obtains from Equations [24]

$$\dot{\xi}^* = \frac{3}{2}\frac{dD}{dt}(\sigma_1 - \sigma_3) = \frac{3}{2}\frac{dD}{dt}\sigma^*$$

then from Equation [23]

$$\frac{dD}{dt} = \frac{2}{3}Ae^{b\theta}(\sigma^*)^{n-1}$$

and Equations [24] become

$$\left.\begin{aligned}\dot{\xi}_1 &= \frac{2}{3}Ae^{b\theta}(\sigma_1 - \sigma_3)^{n-1}\left[\sigma_1 - \frac{1}{2}(\sigma_2 + \sigma_3)\right]\\ \dot{\xi}_2 &= \frac{2}{3}Ae^{b\theta}(\sigma_1 - \sigma_3)^{n-1}\left[\sigma_2 - \frac{1}{2}(\sigma_3 + \sigma_1)\right]\\ \dot{\xi}_3 &= \frac{2}{3}Ae^{b\theta}(\sigma_1 - \sigma_3)^{n-1}\left[\sigma_3 - \frac{1}{2}(\sigma_1 + \sigma_2)\right]\end{aligned}\right\} \quad [25]$$

The correlation with the tensile-creep data is made by assuming the tensile-creep results to be of the form

$$\dot{\xi}_1 = Be^{b\theta}\sigma_1^n \quad [26]$$

For simple tension $\sigma_1 = \sigma^*$ and the first of Equations [25] gives

$$\dot{\xi}_1 = \frac{2}{3}Ae^{b\theta}\sigma_1^n$$

Hence from Equation [26] $B = 2/3\,A$ and Equations [25] become

$$\left.\begin{aligned}\dot{\xi}_1 &= Be^{b\theta}(\sigma_1 - \sigma_3)^{n-1}\left[\sigma_1 - \frac{1}{2}(\sigma_2 + \sigma_3)\right]\\ \dot{\xi}_2 &= Be^{b\theta}(\sigma_1 - \sigma_3)^{n-1}\left[\sigma_2 - \frac{1}{2}(\sigma_3 + \sigma_1)\right]\\ \dot{\xi}_3 &= Be^{b\theta}(\sigma_1 - \sigma_3)^{n-1}\left[\sigma_3 - \frac{1}{2}(\sigma_1 + \sigma_2)\right]\end{aligned}\right\} \quad [27]$$

Equations [27] may then be considered as the generalized creep laws for constant combined stresses based upon the maximum shear theory for yielding. Their validity when applied to practical engineering problems can be shown only through actual experimental results in combined stress creep tests. Table 2 has been prepared to show the creep rates predicted by these laws, as compared with those proposed by Bailey (1), Soderberg (3), and Marin (2), for some of the rather scanty published experimental work on this subject. Agreement in most cases is quite favorable. For purposes of comparison, the Bailey creep laws are

$$\left.\begin{aligned}\dot{\xi}_1 &= \frac{Be^{b\theta}}{2^m}[(\sigma_1-\sigma_2)^2 + (\sigma_2-\sigma_3)^2 + (\sigma_3-\sigma_1)^2]^m\\ &\quad [(\sigma_1-\sigma_2)^{n-2m} - (\sigma_3-\sigma_1)^{n-2m}]\\ \dot{\xi}_2 &= \frac{Be^{b\theta}}{2^m}[(\sigma_1-\sigma_2)^2 + (\sigma_2-\sigma_3)^2 + (\sigma_3-\sigma_1)^2]^m\\ &\quad [(\sigma_2-\sigma_3)^{n-2m} - (\sigma_1-\sigma_2)^{n-2m}]\\ \dot{\xi}_3 &= \frac{Be^{b\theta}}{2^m}[(\sigma_1-\sigma_2)^2 + (\sigma_2-\sigma_3)^2 + (\sigma_3-\sigma_1)^2]^m\\ &\quad [(\sigma_3-\sigma_1)^{n-2m} - (\sigma_2-\sigma_3)^{n-2m}]\end{aligned}\right\} \quad [28]$$

and the Soderberg-Marin creep laws based on distortion energy theory are

$$\left.\begin{aligned}\dot{\xi}_1 &= \frac{Be^{b\theta}}{2^{\frac{n-1}{2}}}[(\sigma_1-\sigma_2)^2 + (\sigma_2-\sigma_3)^2 + (\sigma_3-\sigma_1)^2]^{\frac{n-1}{2}}\left[\sigma_1 - \frac{1}{2}(\sigma_2+\sigma_3)\right]\\ \dot{\xi}_2 &= \frac{Be^{b\theta}}{2^{\frac{n-1}{2}}}[(\sigma_1-\sigma_2)^2 + (\sigma_2-\sigma_3)^2 + (\sigma_3-\sigma_1)^2]^{\frac{n-1}{2}}\left[\sigma_2 - \frac{1}{2}(\sigma_3+\sigma_1)\right]\\ \dot{\xi}_3 &= \frac{Be^{b\theta}}{2^{\frac{n-1}{2}}}[(\sigma_1-\sigma_2)^2 + (\sigma_2-\sigma_3)^2 + (\sigma_3-\sigma_1)^2]^{\frac{n-1}{2}}\left[\sigma_3 - \frac{1}{2}(\sigma_1+\sigma_2)\right]\end{aligned}\right\} \quad [29]$$

Using the time derivatives of Equations [8] and [9], Equations [29] can be reduced to

$$\left.\begin{aligned}\dot{\xi}_1 &= \frac{\partial\sigma^*}{\partial\sigma_1}\dot{\xi}^*\\ \dot{\xi}_2 &= \frac{\partial\sigma^*}{\partial\sigma_2}\dot{\xi}^*\\ \dot{\xi}_3 &= \frac{\partial\sigma^*}{\partial\sigma_3}\dot{\xi}^*\end{aligned}\right\} \quad [29a]$$

Comparing Equations [27] and [29], the ratio of predicted creep rates is

$$\frac{\dot{\xi}_{\text{max shear}}}{\dot{\xi}_{\text{D.E.T.}}} = \left(\frac{\sigma^*_{\text{max shear}}}{\sigma^*_{\text{D.E.T.}}}\right)^{n-1} \quad [30]$$

The steady-state stresses and strain rates may now be found using the maximum shear creep laws, Equation [27], when transformed to cylindrical co-ordinates, namely

$$\left.\begin{aligned}\dot{\xi}_r &= Be^{b\theta}(\sigma_t - \sigma_r)^{n-1}\left[\sigma_r - \frac{1}{2}(\sigma_t + \sigma_z)\right]\\ \dot{\xi}_t &= Be^{b\theta}(\sigma_t - \sigma_r)^{n-1}\left[\sigma_t - \frac{1}{2}(\sigma_z + \sigma_r)\right]\\ \dot{\xi}_z &= Be^{b\theta}(\sigma_t - \sigma_r)^{n-1}\left[\sigma_z - \frac{1}{2}(\sigma_r + \sigma_t)\right]\end{aligned}\right\} \quad [27a]$$

The assumption is now made that $\dot{\xi}_z = 0$. Adding the three strain rates of Equations [27a]

$$\dot{\xi}_r + \dot{\xi}_t + \dot{\xi}_z = 0 \quad [31]$$

Hence

$$\dot{\xi}_r = -\dot{\xi}_t$$

Now differentiating Equation [2] with respect to time

$$r\frac{d\dot{\xi}_t}{dr} = \dot{\xi}_r - \dot{\xi}_t = -2\dot{\xi}_t$$

Hence

$$\dot{\xi}_t = \frac{c}{r^2} = -\dot{\xi}_r \quad [32]$$

where c is an arbitrary constant. Now setting the last of Equations [27a] to zero

$$\sigma_z = \frac{\sigma_r + \sigma_t}{2} \quad [33]$$

Thus from Equations [27a]

$$\dot{\xi}_t = \frac{3}{4} B e^{b\theta} (\sigma_t - \sigma_r)^n \quad [34]$$

or, using Equation [32]

$$\sigma_t - \sigma_r = \left(\frac{4}{3}\frac{c}{B}\right)^{\frac{1}{n}} \left(\frac{1}{r^2 e^{b\theta}}\right)^{\frac{1}{n}}$$

From the condition of radial equilibrium, Equation [1], and rearranging

$$d\sigma_r = C_1 r^{-\frac{2+n}{n}} e^{-\frac{b\theta}{n}} dr$$

where

$$C_1 = \left(\frac{4}{3}\frac{c}{B}\right)^{\frac{1}{n}}$$

or

$$\sigma_r = C_1 \int r^{-\frac{2+n}{n}} e^{-\frac{b\theta}{n}} dr + C_2 \quad [35]$$

where C_2 is a constant of integration. For simplicity Equation [16] is expressed as

$$\theta = N_1 + N_2 \log_e \frac{r}{R_0}$$

Hence

$$e^{-\frac{b\theta}{n}} = e^{-\frac{bN_1}{n}} \left(\frac{r}{R_0}\right)^{-\frac{bN_2}{n}} \quad [36]$$

Substituting Equation [36] into [35], and integrating, one obtains

$$\sigma_r = -C_1^* \frac{n' r^{-\frac{2}{n'}}}{2} + C_2 \quad [37]$$

where C_1^* is a new constant and

$$n' = \frac{n}{1 + \frac{bN_2}{2}} \quad [38]$$

The constants of Equation [37] are found from the boundary conditions, namely, $\sigma_r = -p_0$ at $r = R_0$, $\sigma_r = 0$ at $r = R_1$, then Equation [37] becomes, upon solving for the boundary conditions

$$\sigma_r = -p_0 \frac{\left(\frac{R_1}{r}\right)^{\frac{2}{n'}} - 1}{\left(\frac{R_1}{R_0}\right)^{\frac{2}{n'}} - 1} \quad [39]$$

from Equation [1]

$$\sigma_t = p_0 \frac{\frac{2 - n'}{n'}\left(\frac{R_1}{r}\right)^{\frac{2}{n'}} + 1}{\left(\frac{R_1}{R_0}\right)^{\frac{2}{n'}} - 1} \quad [40]$$

and from Equation [33]

$$\sigma_z = p_0 \frac{\frac{1 - n'}{n'}\left(\frac{R_1}{r}\right)^{\frac{2}{n'}} + 1}{\left(\frac{R_1}{R_0}\right)^{\frac{2}{n'}} - 1} \quad [41]$$

These equations are identical to those evaluated by Bailey (1). The creep rate $\dot{\xi}_t$ is found from Equation [34], giving with the aid of Equations [39] and [40]

$$\dot{\xi}_t = \frac{3}{4} B e^{b\theta} \left(\frac{2}{n'}\right)^n \left(\frac{R_1}{r}\right)^{\frac{2n}{n'}} \left[\frac{p_0}{\left(\frac{R_1}{R_0}\right)^{\frac{2}{n'}} - 1}\right]^n \quad [42]$$

and

$$\dot{\xi}_r = -\dot{\xi}_t$$

$$\dot{\xi}_z = 0$$

The tangential creep rate predicted by Soderberg, Equations [29], is

$$\dot{\xi}_t = \left(\frac{3}{4}\right)^{\frac{n+1}{2}} B e^{b\theta} \left(\frac{2}{n'}\right)^n \left(\frac{R_1}{r}\right)^{\frac{2n}{n'}} \left[\frac{p_0}{\left(\frac{R_1}{R_0}\right)^{\frac{2}{n'}} - 1}\right]^n \quad [43]$$

Comparing Equations [42] and [43]

$$\frac{\dot{\xi}_t \text{ Eq. [43]}}{\dot{\xi}_t \text{ Eq. [42]}} = \left(\frac{3}{4}\right)^{\frac{n-1}{2}} \quad [44]$$

Results

The resulting stresses based upon elastic conditions and primary creep are shown in Fig. 10 for $t = 0$, 25 hr, 100 hr, 1000 hr, and for steady state. Table 6 indicates elastic data for the curves. Here total stresses are plotted against radial position for 12 per cent chromium steel at constant temperature of 850 F, in a thick-walled cylinder of $R_1/R_0 = 2$, under an internal pressure of 12,000 psi. It can be seen from this figure that stress distributions gradually change from those of pure elasticity, $t = 0$, to those of increasing plasticity, $t = 25$ hr, 100, and then 1000 hr. Finally, the purely plastic case of the steady-state or secondary-creep condition is attained. According to the σ_t curves, it appears that the steady state for the specific conditions of this problem would fall beyond 10,000 hr, probably in the neighborhood of 100,000 hr.

In Fig. 11 is shown the resulting total strain versus radial position, based on the primary-creep condition. Tangential strains are numerically approximately equal to radial strains. The axial strain is of very small magnitude and practically invarient with time. As regards the tangential and radial strain, there is approximately the same increase for the time interval $t =$ 0 to 25 hr as for the time interval $t = 25$ hr to 100 hr. The increase in strains from 100 hr to 1000 hr is roughly double that for $t = 25$ to 100 hr. Tangential strains for a particular time are usually about 4 times as great at the bore as on the outside. This indicates strains to be approximately inversely proportional to r^2. Table 3 shows the data from which Figs. 10 and 11 were plotted.

Fig. 12 indicates the residual stress versus radial position resulting from instantaneous elastic unloading. This would be

TABLE 3 SUMMARY OF STRESSES AND STRAINS FOR THICK-WALLED CYLINDER
(R_1/R_0 = 2.0) at 850 F and 12,000 Psi

	$\frac{r}{R_o}$	σ_r	σ_t	σ_z	σ^*	E_{ε^*}	ε^*	ε_r	ε_t	ε_z
Elastic	1.0	-12,000	20,000	4,000	32,000	41,600	.001387	-.000640	.000747	.000053
	1.25	-6,240	14,240	4,000	20,480	26,620	.000887	-.000390	.000497	.000053
	1.50	-3,110	11,110	4,000	14,220	18,490	.000616	-.000255	.000361	.000053
	1.75	-1,220	9,220	4,000	10,440	13,590	.000452	-.000173	.000280	.000053
	2.0	0	8,000	4,000	8,000	10,400	.000347	-.000120	.000227	.000053
25 HR.	1.0	-12,000	15,770	2,480	27,770	55,140	.001838	-.000904	.000934	.000054
	1.25	-6,640	13,720	3,700	20,360	33,780	.001126	-.000518	.000608	.000054
	1.50	-3,420	11,740	4,120	15,160	22,950	.000765	-.000326	.000438	.000054
	1.75	-1,370	10,200	4,280	11,570	16,620	.000554	-.000217	.000337	.000054
	2.0	0	8,030	4,340	8,030	12,660	.000422	-.000149	.000273	.000054
100 HR.	1.0	-12,000	14,080	1,660	26,080	72,240	.002408	-.001206	.001202	.000055
	1.25	-6,870	13,110	3,370	19,980	44,250	.001475	-.000701	.000774	.000055
	1.50	-3,640	11,980	4,160	15,610	29,850	.000995	-.000442	.000553	.000055
	1.75	-1,480	10,870	4,520	12,360	21,420	.000714	-.000292	.000422	.000055
	2.0	0	10,020	4,720	10,020	16,260	.000541	-.000201	.000341	.000055
1000 HR.	1.0	-12,000	12,460	770	24,460	102,570	.003419	-.001729	.001690	.000055
	1.25	-7,070	12,610	3,020	19,680	63,120	.002104	-.001023	.001081	.000055
	1.50	-3,730	12,190	4,220	15,920	42,500	.001417	-.000651	.000765	.000055
	1.75	-1,600	11,490	4,760	13,090	30,540	.001018	-.000438	.000579	.000055
	2.0	0	10,900	6,110	10,900	22,980	.000766	-.000304	.000462	.000055
							$\dot{\varepsilon}^*$	$\dot{\varepsilon}_r$	$\dot{\varepsilon}_t$	$\dot{\varepsilon}_z$
Steady State Sec. creep $n = 3.885$ $B = 2.089 \cdot 10^{-16}$	1.0	-12,000	8,580	-1,710	20,580		.000120	-.000090	+.000090	0
	1.25	-7,660	10,680	+1,510	18,340		.000078	-.000058	+.000058	0
	1.50	-4,460	12,240	+3,890	16,700		.000054	-.000041	+.000041	0
	1.75	-1,990	13,440	+5,730	15,430		.000040	-.000029	+.000029	0
	2.0	0	14,400	+7,200	14,400		.000030	-.000022	+.000022	0

TABLE 4 RESIDUAL STRESSES AND PERMANENT PLASTIC STRAIN FOR ELASTIC UNLOADING

	$\frac{r}{R}$	σ_r''	σ_t''	σ_z''	$\sigma^{*\prime\prime}$	$\varepsilon^{*\prime\prime}$	ε_r''	ε_t''	ε_z''
ELASTIC	1.0	0	0	0	0	0	0	0	0
	1.25	0	0	0	0	0	0	0	0
	1.50	0	0	0	0	0	0	0	0
	1.75	0	0	0	0	0	0	0	0
	2.0	0	0	0	0	0	0	0	0
25 HR.	1.0	0	-4,230	-1,520	-4,230	+.000451	-.000264	.000187	.000001
	1.25	-400	- 520	- 300	-120	+.000238	-.000128	.000111	.000001
	1.50	-310	+630	+120	+940	+.000149	-.000071	.000077	.000001
	1.75	-150	+980	+280	+1,130	+.000102	-.000044	.000057	.000001
	2.0	0	+1030	+340	+1,030	.000075	-.000029	.000046	.000001
100 HR.	1.0	0	-5,920	-2,340	-5,920	.001021	-.000566	.000455	.000002
	1.25	-630	-1,130	-630	-500	.000588	-.000311	.000277	.000002
	1.50	-530	+870	+160	+1,390	.000379	-.000187	.000192	.000002
	1.75	-260	+1,650	+520	+1,920	.000262	-.000119	.000142	.000002
	2.0	0	+2,020	+720	+2,020	.000194	-.000081	.000114	.000002
1000 HR.	1.0	0	-7,540	-3,230	-7,540	.002032	-.001089	.000943	.000002
	1.25	-830	-1,630	-870	-800	.001217	-.000633	.000584	.000002
	1.50	-620	+1,080	+220	+1,700	.000801	-.000396	.000404	.000002
	1.75	-380	+2,270	+760	+2,650	.000566	-.000266	.000299	.000002
	2.0	0	+2,900	+1,110	+2,900	.000419	-.000184	.000235	.000002
ESTIMATED 10,000 HR.	1.0							+.002000	
	1.25							+.001240	
	1.50							+.000856	
	1.75							+.000635	
	2.0							+.000499	
						$\dot{\varepsilon}^*$	$\dot{\varepsilon}_r$	$\dot{\varepsilon}_t$	$\dot{\varepsilon}_z$
STEADY STATE SEC. CREEP n = 3.885	1.0	0	-11,420	-5,710	-11,420	.000120	-.000090	+.000090	0
	1.25	-1420	-3,560	-2,490	-2,140	.000078	-.000058	+.000058	0
	1.50	-1350	+1,130	-110	+2,480	.000054	-.000041	+.000041	0
	1.75	-770	+4,220	+1,730	+4,990	.000040	-.000029	+.000029	0
	2.0	0	+6,400	+3,200	+6,400	.000030	-.000022	+.000022	0

the case if the unloading could be sufficiently fast to insure that it would be elastic in nature. Such is equivalent to subtracting in Fig. 10 the $t = 0$ curve from the stress curves at the times indicated. Although the residual axial stresses have been calculated as shown in Table 4, these were not included in the figure to avoid confusion. Roughly, they are about one half of the residual tangential stresses. It can be seen from Fig. 12 that for the

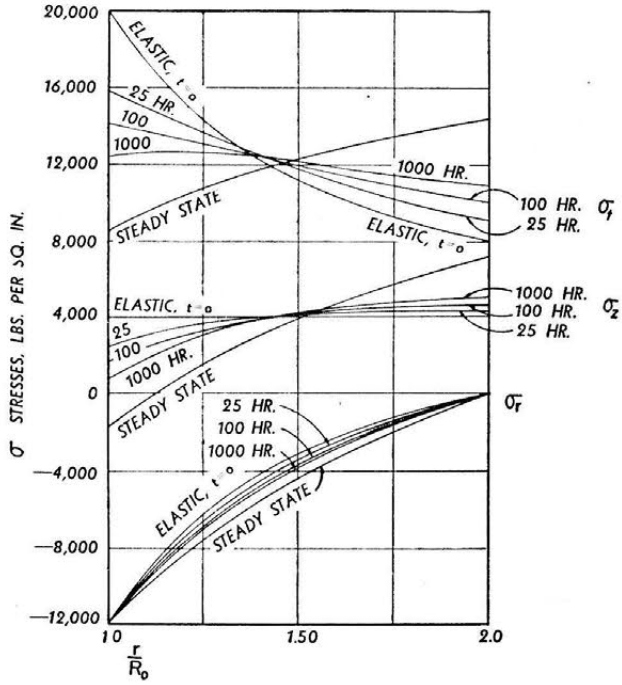

FIG. 10 TOTAL STRESSES VERSUS RADIAL POSITION IN A THICK-WALLED CYLINDER ($R_1/R_0 = 2.0$) OF 12 PER CENT CR STEEL AFTER BEING HELD AT 850 F AND 12,000 PSI FOR TIMES SHOWN

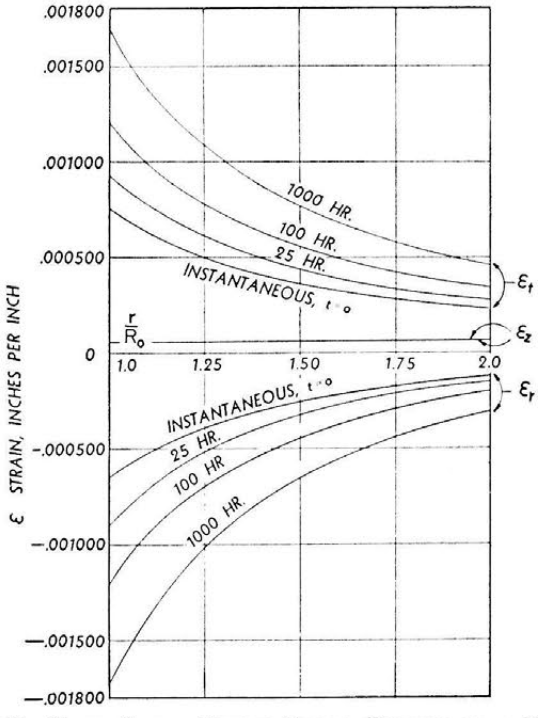

FIG. 11 TOTAL STRAIN VERSUS RADIAL POSITION IN A THICK-WALLED CYLINDER ($R_1/R_0 = 2.0$) OF 12 PER CENT CR STEEL AFTER BEING HELD AT 850 F AND 12,000 PSI FOR TIMES SHOWN

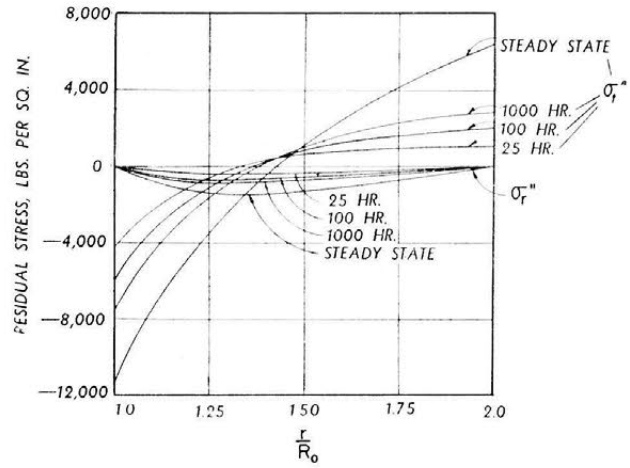

FIG. 12 RESIDUAL STRESSES VERSUS RADIAL POSITION UPON INSTANTANEOUS ELASTIC UNLOADING FROM 850 F AND p_0 = 12,000 PSI IN A THICK-WALLED CYLINDER ($R_1/R_0 = 2.0$) OF 12 PER CENT CR STEEL

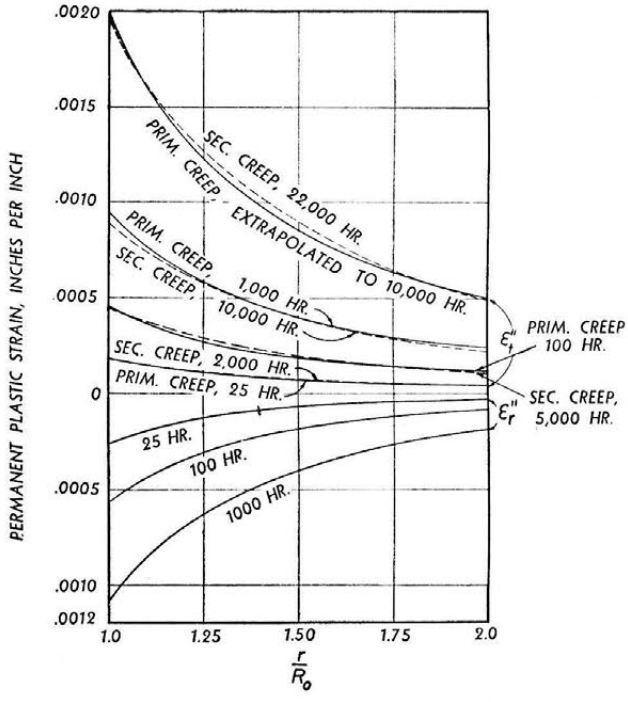

FIG. 13 PERMANENT PLASTIC STRAIN VERSUS RADIAL POSITION UPON INSTANTANEOUS ELASTIC UNLOADING FROM 850 F AND p_0 = 12,000 PSI IN A THICK-WALLED CYLINDER ($R_1/R_0 = 2.0$) OF 12 PER CENT CR STEEL

case where the load has been left on for a long period of time, instantaneous unloading would cause high compressive stresses at the bore and high tensile stresses at the outside. If the load were to be reapplied at a very fast rate, it would be expected that the stresses would not be far from the particular curve in Fig. 10 from which the cylinder was unloaded.

Fig. 13 shows that during the primary-creep stage, much greater strains occur throughout the vessel than would be indicated by considerations of secondary creep alone. The solid curves in this figure are based on primary-creep analysis and show the permanent strains in both tangential and radial directions occurring after 25 hr, 100 hr, and 1000 hr at 850 F, and 12,000 psi. By the use of Fig. 14 the permanent strain in the tangential direction for primary creep has been extrapolated to

	σ^*	0	25 HR.	100 HR.	1000 HR.	
	0	0	0	0	0	
	1,000	.000043	.000043	.000044	.000046	
	2,000	.000087	.000088	.000090	.000096	
	3,000	.000130	.000133	.000137	.000150	
	4,000	.000173	.000179	.000186	.000208	
	5,000	.000217	.000226	.000238	.000271	
	6,000	.000260	.000273	.000292	.000340	
	7,000	.000303	.000321	.000349	.000414	
	8,000	.000347	.000371	.000409	.000495	
	9,000	.000390	.000421	.000472	.000582	
	10,000	.000433	.000472	.000539	.000676	
	11,000	.000477	.000524	.000610	.000778	
	12,000	.000520	.000578	.000685	.000889	
	13,000	.000563	.000635	.000764	.001009	
	14,000	.000607	.000694	.000848	.001138	
	15,000	.000650	.000755	.000937	.001277	
	16,000	.000693	.000818	.001032	.001428	
	17,000	.000737	.000884	.001133	.001593	
	18,000	.000780	.000952	.001240	.001771	
	19,000	.000823	.001024	.001355	.001965	
	20,000	.000867	.001099	.001478	.002175	
	21,000	.000910	.001177	.001608	.002404	
	22,000	.000953	.001259	.001745	.002657	
	23,000	.000997	.001346	.001891	.002941	
	24,000	.001040	.001438	.002048	.003262	
	25,000	.001083	.001535	.002215	.003626	
	26,000	.001127	.001638	.002394	.004041	
	27,000	.001170	.001749	.002584	.004515	
	28,000	.001213	.001866	.002785	.005055	
	29,000	.001257	.001991	.002997	.005670	
	30,000	.001300	.002125	.003222	.006368	
	σ^*	ε^*	ε^*	ε^*	ε^*	

TABLE 5 (*left*) TENSION-CREEP DATA IN TERMS OF EFFECTIVE STRESS AND EFFECTIVE STRAIN FOR 12 PER CENT CR STEEL AT 850 F

$$\sigma_r' = -\frac{\left(\frac{R_i}{r}\right)^2 - 1}{\left(\frac{R_i}{R_o}\right)^2 - 1} P_o \qquad \sigma_t' = \frac{\left(\frac{R_i}{r}\right)^2 + 1}{\left(\frac{R_i}{R_o}\right)^2 - 1} P_o$$

$\frac{r}{R_o}$	$\frac{R_i}{r}$	$\left(\frac{R_i}{r}\right)^2$	$\left(\frac{R_i}{r}\right)^2 - 1$	$\frac{-\left(\frac{R_i}{r}\right)^2 - 1}{3}$	$\left(\frac{R_i}{r}\right)^2 + 1$	$\frac{\left(\frac{R_i}{r}\right)^2 + 1}{3}$	σ_r'	σ_t'
1.0	2.0	4.0	3.0	-1.0	5.0	.166667	-12,000	20,000
1.1	1.81818	3.30578	2.30578	-.7686	4.30578	1.43526	-9,220	17,220
1.2	1.66667	2.77777	1.77777	-.5926	3.77777	1.2592	-7,110	15,110
1.25	1.60	2.56	1.56	-.52	3.56		-6,240	14,240
1.3	1.53846	2.36686	1.36686	-.4556	3.36686	1.12229	-5,470	13,470
1.4	1.42857	2.04081	1.04081	-.3469	3.04081	1.01360	-4,160	12,160
1.5	1.33333	1.77777	.77777	-.259259	2.77777	.92592	-3,111	11,111
1.6	1.25	1.5625	.5625	-.1875	2.5625	.85417	-2,250	10,250
1.7	1.17647	1.38408	.38408	-.1280	2.38408	.79469	-1,540	9,540
1.75	1.142857	1.306122	.306122	-.102041	2.306122		-1220.1	9,224
1.8	1.11111	1.23456	.23456	-.0782	2.23456	.74485	-940	8,940
1.9	1.05263	1.10803	.10803	-.0360	2.10803	.70267	-430	8430
2.0	1.0	1.0	0	0	2.0	.66667	0	8000

TABLE 6 (*left*) ELASTIC STRESS IN THICK-WALLED TUBE FOR p_0 = 12,000 PSI

ELASTIC STRAINS

$E\varepsilon_r = \sigma_r - \nu(\sigma_t + \sigma_z)$ $E\varepsilon_t = \sigma_t - \nu(\sigma_r + \sigma_z)$ $E\varepsilon_z = \sigma_z - \nu(\sigma_r + \sigma_t)$

r/R_o	σ_r	σ_t	σ_z	$\sigma_r + \sigma_t$	$\sigma_r + \sigma_z$	$\sigma_t + \sigma_z$	$.3(\sigma_r + \sigma_t)$	$-.3(\sigma_r + \sigma_z)$	$-.3(\sigma_t + \sigma_z)$
1.0	-12,000	20,000	4,000	8,000	-8,000	24,000	-2,400	+2,400	-7,200
1.25	-6,240	14,240	4,000	8,000	-2240	18,240	-2,400	+670	-5,470
1.5	-3,110	11,110	4,000	8,000	+890	15,110	-2,400	-270	-4,530
1.75	-1,220	9,220	4,000	8,000	+2,780	13,220	-2,400	-830	-3,970
2.0	0	8,000	4,000	8,000	+4,000	12,000	-2,400	-1,200	-3,600

		$E\varepsilon_r$		$E\varepsilon_t$		$E\varepsilon_z$		
	$\frac{r}{R_o}$	$\sigma_r - .3(\sigma_t + \sigma_z)$	ε_r	$\sigma_t - .3(\sigma_r + \sigma_z)$	ε_t	$\sigma_z - .3(\sigma_r + \sigma_t)$	ε_z	
	1.0	-19,200	.000640	22,400	.000747	1,600	.000053	
	1.25	-11,710	-.000390	14,910	.000497	1,600	.000053	
	1.5	-7640	-.000255	10,840	.000361	1,600	.000053	
	1.75	-5,190	-.000173	8,390	.000280	1,600	.000053	
	2.0	-3,600	-.000120	6,800	.000227	1,600	.000053	

TABLE 7 STEADY STATE BY MAXIMUM SHEAR THEORY FOR THICK-WALLED TUBE
$n = 3.995$ $B = 2.098 \times 10^{-19}$ Per Cent/1000 Hr $p = 12{,}000$ Psi

$$\sigma_r = -\frac{\left(\frac{R_1}{r}\right)^{\frac{2}{n}} - 1}{\left(\frac{R_1}{R_0}\right)^{\frac{2}{n}} - 1} \cdot P_0 \qquad \sigma_t = \frac{\frac{2-n}{n}\left(\frac{R_1}{r}\right)^{\frac{2}{n}} + 1}{\left(\frac{R_1}{R_0}\right)^{\frac{2}{n}} - 1} \cdot P_0$$

STRESSES

					σ_r			σ_t	σ_z
$\frac{r}{R_0}$	$\frac{R_1}{r}$	$\log\left(\frac{R_1}{r}\right)^{.5148}$	$\left(\frac{R_1}{r}\right)^{.5148}$	$\left(\frac{R_1}{r}\right)^{.5148}-1$	$-27972(\ )$	$.4851\left(\frac{R_1}{r}\right)^{.5148}$	$-.4851\left(\frac{R_1}{r}\right)^{.5148}+1$	$27972(\ )$	$\frac{\sigma_r+\sigma_t}{2}$
1.0	2.0	.15497	1.429	.429	-12,000	.6932	.3068	8,582	-1,709
1.25	1.6	.10508	1.274	.274	-7,664	.8180	.3820	10,685	+1,510
1.50	1.3333	.06431	1.1595	.1595	-4,462	.5625	.4375	12,238	+3888
1.75	1.1429	02986	1.071	.071	-1,986	.5195	.4805	13,441	+5,728
2.0	1.0	0	1.0	0	0	.4851	.5149	14,403	+7,202

STRAIN RATE

$\dot{\epsilon}_t = -\dot{\epsilon}_r = .00225\left(\frac{R_1}{r}\right)^2$ %/1000 HOURS

				$\dot{\epsilon}_t$	$\dot{\epsilon}_t$			
	$\frac{r}{R_0}$	$\frac{R_1}{r}$	$\left(\frac{R_1}{r}\right)^2$	$.00225\left(\frac{R_1}{r}\right)^2$ in/in/1000 hrs				
	1.0	2.00	4.0000	.009	.000090			
	1.25	1.60	2.5600	.00576	.000058			
	1.50	1.3333	1.7777	.00410	.000041			
	1.75	1.1429	1.3061	.00294	.000029			
	2.0	1.0	1.0000	.00225	.000022			

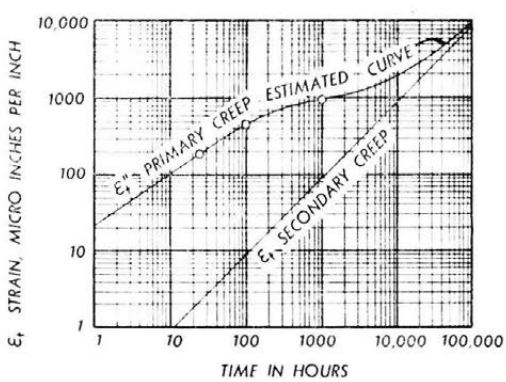

FIG. 14 EXTRAPOLATION CURVE FOR DETERMINING BORE TANGENTIAL STRAIN TO 10,000 HR IN A THICK-WALLED CYLINDER (R_1/R_0 = 2.0) OF 12 PER CENT CR STEEL AT 850 F AND 12,000 PSI

10,000 hr. The dashed curves are those calculated by the steady-state analysis and are plotted for the tangential direction only (see Table 7 for data from which the dashed curves were calculated). Radial strains by such analysis are numerically equal to and opposite in sign to the tangential strains, but are not shown in the figure. It is apparent from tangential strain that primary creep at 25 hr gives about the same permanent strain that secondary creep produces at 2000 hr. Similarly, primary creep at 100 hr is approximately equal to secondary creep at 5000 hr; primary creep at 1000 hr to secondary creep at 10,000 hr and primary creep at 10,000 hr to secondary creep at 22,000 hr. It thus becomes apparent that secondary-creep analysis is at considerable variance with primary-creep considerations in the early stages, i.e., up to 1000 hr. As we approach 10,000 to 100,000 hr duration, the strains occurring in these two creep stages approach the same order of magnitude.

For a case where the maximum permanent strain at any part of the vessel is to be limited to 1 per cent as might occur in turbine parts, Fig. 13 would indicate a life of about 1000 hr by primary creep and 10,000 hr by secondary creep.

In cases where the over-all life of a vessel is expected to be small, it appears that primary-creep considerations are essential. For those cases where long life in the neighborhood of 5 to 10 years is expected, secondary creep would appear quite adequate.

Conclusions

1 In the design of pressure vessels for short life, consideration of elastic conditions and primary creep is essential.

2 In the design of pressure vessels for long life, secondary-creep analysis is sufficient.

3 For the particular problem conditions of a thick-walled cylinder of 12 per cent chromium steel, of wall ratio $R_1/R_0 = 2$, at 850 F and 12,000 psi, primary creep should govern up to 10,000 hr.

Recommended Experimental Program

Because of the complexity of the creep-relaxation process in the transient case where primary creep is involved, this problem should be investigated experimentally and the results compared with the conclusions of this paper. Once experimentally verified, short-cut design procedures may be developed, or a machine computer constructed for handling the great number of cases of pressures, temperatures, wall ratios, and materials which are of practical importance.

A further research that requires more attention is the checking of the various secondary-creep-strength theories in applying

tensile-creep data to the biaxial condition. Under the maximum shear theory used in this paper, the tangential-strain rate for the problem developed is under steady-state conditions 0.000090 in./in./1000 hr at the bore. Bailey's (1) creep equation, based on distortion energy, indicates this strain rate to be 0.000057 in./in./1000 hr., Soderberg's (4) and Marin's (2) analyses, the latter of which is a modification of Bailey's, show a strain rate of 0.000059 in./in./1000 hr. It would be well to know how closely experiments fit the maximum shear analysis and what errors are involved in its adoption.

As mentioned in the "Introduction," experimental work is necessary to verify the validity of converting available tensile creep-time data to stress versus strain at each instant of time and applying this to a varying stress condition. If a specimen, as shown in Fig. 15, were to be placed under a constant load and temperature, diameter measurements for each instant of time could be taken at the gaging lines. Then if a second specimen were to be subjected to one load for a time and then a second load for a time, history effects could be studied at numerous stress levels. The same history effects could also be studied on standard tensile-creep specimens; this would require more specimens but would be much more accurate because of longer gage length.

Acknowledgments

The authors wish to express their appreciation to Mr. William Raisch and the members of the Petroleum Division Executive Committee for their encouragement and co-operation in providing valuable background on the industry's practices.

BIBLIOGRAPHY

1 "The Utilization of Creep Test Data in Engineering Design," by R. W. Bailey, *The Institution of Mechanical Engineers*, vol. 131, November, 1935, pp. 131–349.

2 "Mechanical Properties of Materials and Design," by Joseph Marin, McGraw-Hill Book Company, Inc., New York, N. Y., chapt. 7 on Combined Creep Stresses, 1942.

3 Discussion by C. R. Soderberg of "Design Aspects of Creep," by R. W. Bailey, JOURNAL OF APPLIED MECHANICS, Trans. ASME, vol. 58, 1936, p. A-150.

4 "The Interpretation of Creep Tests for Machine Design," by C. R. Soderberg, Trans. ASME, vol. 58, 1936, p. 733.

5 "Plasticity," by A. Nadai, McGraw-Hill Book Company, Inc., New York, N. Y., chapt. 14, 1931.

6 "Partially Plastic Thick-Walled Tubes," by C. W. MacGregor, L. F. Coffin, Jr., and J. C. Fisher, *Journal of The Franklin Institute*, vol. 245, February, 1948, pp. 135–158.

7 "Yielding and Fracture of Medium Carbon Steel Under Combined Stress," by E. A. Davis, JOURNAL OF APPLIED MECHANICS, Trans. ASME, vol. 67, 1945, p. A-13.

8 "Combined Stress Tests on 24S-T Aluminum Alloy Tubes," by W. R. Osgood, JOURNAL OF APPLIED MECHANICS, Trans. ASME, vol. 69, 1947, p. A-147.

9 "An Application of Polynominal Approximation to the Solution of Integral Equations Arising in Physical Problem," by J. D. Crout, *Journal of Mathematics and Physics*, vol. 19, January, 1940, pp. 34–92.

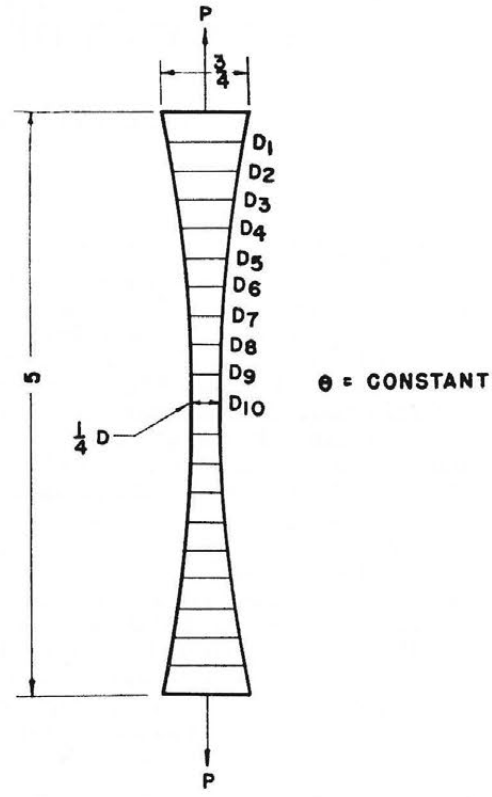

FIG. 15 PROPOSED TAPERED CREEP SPECIMEN FOR OBTAINING TENSILE CREEP DATA AT SEVERAL STRESSES SIMULTANEOUSLY

10 Work Progress Administration of the Federal Works Agency, "Tables of Lagrangian Interpolation Coefficients," prepared by the Mathematical Tables Project of WPA, Columbia University Press, New York, N. Y., 1944.

11 "Thick-Walled Tubes and Cylinders Under High Pressure and Temperature," by R. W. Bailey, *Engineering*, vol. 130, June 13, 1930, p. 772; June 20, 1930, p. 785, and June 27, 1930, p. 818.

12 "Approximate Solutions for Symmetrically Loaded Thick-Walled Cylinders," by C. W. MacGregor and L. F. Coffin, Jr., JOURNAL OF APPLIED MECHANICS, Trans. ASME, vol. 69, 1947, p. A-301.

13 "The Stress Analysis and Design of Radially Expanded Guns," by C. W. MacGregor, L. F. Coffin, Jr., J. C. Fisher, L. F. Lawrie, and M. E. Graham, Project G, Report No. 2, Contract NOrd 9107—Task F, Nov. 22, 1946

14 "Heat Transmission," by W. H. McAdams, McGraw-Hill Book Company, Inc., New York, N. Y., second edition, 1942.

15 "Progress Report on Tubular Creep Test," by F. H. Norton, Trans. ASME, vol. 63, 1941, pp. 735–736.

16 "Creep Under Combined Tension and Torsion—Part I—Behavior of 17% C Steel at 455° C," by H. J. Tapsell and A. E. Johnson, *Engineering*, vol. 150, 1940, p. 24.

Analysis of a Single Stiffener on an Infinite Sheet

By S. U. BENSCOTER,[1] PASADENA, CALIF.

The use of stiffened-sheet construction in aircraft design has brought about the study of many problems in mechanics in which concentrated loads are introduced into stiffeners and transferred to the sheet. In the present paper a basic problem of this type is considered. A single stiffener of finite length is assumed to be attached to a sheet of infinite extent. A concentrated force is applied to the stiffener at each end. Any given problem may be divided into symmetrical and antisymmetrical parts. The physical condition that governs the problem is that the axial strain in the stiffener must be equal to the normal strain in the sheet at all points along the stiffener. In order to formulate the solution, it is necessary to employ an influence function for the strain in the sheet. This function is known from the classical theory of elasticity. The solution is found to be governed by an integral equation which has the same form as the equation which governs spanwise air-load distribution on an airplane wing. Hence a number of mathematical methods are known for solving the equation. A numerical example is presented.

Nomenclature

The following nomenclature is used in the paper:

A = area of stiffener
a = half-length of stiffener
E = Young's modulus
E_1 = Young's modulus for stiffener
E_2 = Young's modulus for sheet
f = force reduction in stiffener
$\bar{f}$ = dimensionless force reduction in stiffener
K = influence function
P = external concentrated force
p = axial force in stiffener
$\bar{p}$ = dimensionless axial force in stiffener
q = shear flow
r = radial co-ordinate
t = thickness of sheet
x = horizontal rectangular co-ordinate
y = vertical rectangular co-ordinate
ϵ = axial strain in stiffener
ϵ_x = horizontal normal strain in sheet
μ = Poisson's ratio
σ_x = horizontal normal stress in sheet
σ_y = vertical normal stress in sheet
θ = angle variable
ξ = horizontal rectangular co-ordinate
η = physical parameter

Introduction

The use of semimonocoque, or stiffened-sheet construction in airplane design has given rise to a class of problems in mechanics in which concentrated loads are introduced into the stiffeners in various ways. The stress-analysis problem consists of determining the variation of axial forces in the stringers, and the stress distribution in the sheet. In the present paper a solution will be given for a fundamental problem in this class of problems. It is assumed that a single stiffener of finite length is attached to a sheet of infinite extent. The stiffener is acted upon by a concentrated force at each end of the stiffener. It is found that the variation of axial force along the stringer is governed by an integral equation which is of the same form as Prandtl's lifting-line equation for spanwise air-load distribution on an airplane wing. The problem of a semi-infinite sheet with a single stiffener has been previously investigated by E. Reissner,[2] who noted the mathematical similarity between this type of stress problem and the aerodynamic-lift problem.

Influence Function

In order to determine the stress variation in a stringer attached to an infinite sheet, it is necessary to have available an influence function for the normal strain in the sheet at one point on the x-axis due to a concentrated force acting horizontally at another point on the x-axis. Such a function may be obtained from the classical solution of two-dimensional stresses in an infinite plate of unit thickness due to a concentrated force at the origin. For the case of a concentrated force P, acting horizontally at the origin on a plate of unit thickness, as shown in Fig. 1(a), the normal stress formulas are due to Timoshenko.[3]

$$\sigma_x = -\frac{P}{2\pi}\frac{x}{r^2}\left[\frac{\mu+3}{2} - (\mu+1)\frac{y^2}{r^2}\right] \quad [1]$$

$$\sigma_y = -\frac{P}{2\pi}\frac{x}{r^2}\left[\frac{\mu-1}{2} + (\mu+1)\frac{y^2}{r^2}\right] \quad [2]$$

From Hooke's law the strain in the direction of the x-axis at an arbitrary point in the sheet is given by

$$\epsilon_x = \frac{1}{E}(\sigma_x - \mu\sigma_y) \quad [3]$$

Substituting Equations [1] and [2] gives

$$\epsilon_x(x, y) = -\frac{P}{2\pi E}\frac{x}{r^2}\left[\frac{(3-\mu)(1+\mu)}{2} - (1+\mu)^2\frac{y^2}{r^2}\right] \quad [4]$$

The value of ϵ_x on the x-axis is given by

---

[1] Aeronautical Research Scientist, National Advisory Committee for Aeronautics, Langley Field, Va.; on leave as graduate student at the California Institute of Technology.

Presented at the National Meeting of the Applied Mechanics Division, Ann Arbor, Mich., June 13–15, 1949, of The American Society of Mechanical Engineers.

Discussion of this paper should be addressed to the Secretary, ASME, 29 West 39th Street, New York, N. Y., and will be accepted until October 10, 1949, for publication at a later date. Discussion received after the closing date will be returned.

Note: Statements and opinions advanced in papers are to be understood as individual expressions of their authors and not those of the Society. Paper No. 49—APM-13.

[2] "Note on the Problem of the Distribution of Stress in a Thin Stiffened Elastic Sheet," by E. Reissner, Proceedings of the National Academy of Sciences, vol. 26, 1940, pp. 300–305.

[3] "Theory of Elasticity," by S. Timoshenko, McGraw-Hill Book Company, Inc., New York, N. Y., 1934, p. 111.

$$\epsilon_x(x, 0) = -\frac{P(3 - \mu)(1 + \mu)}{4\pi Ex} \quad [5]$$

Referring to Fig. 1(*b*), the influence function that is needed expresses the strain at station x on the x-axis due to a unit force at

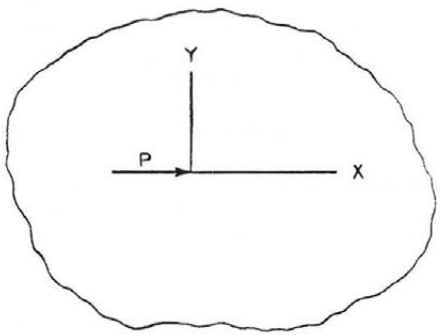

(a) Central Force

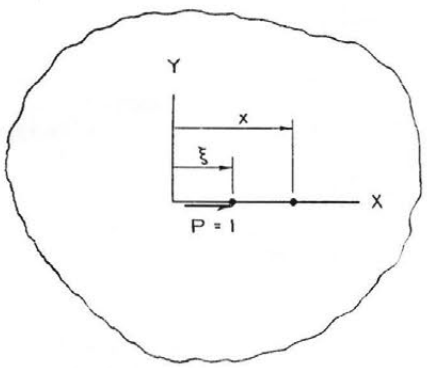

(b) Eccentric Force

FIG. 1 CONCENTRATED FORCE ACTING ON AN INFINITE PLATE

station ξ. The factor x in Equation [5] must be replaced by $(x - \xi)$. For a unit force acting on a sheet of thickness t, the factor P must be replaced by $1/t$. The influence function becomes

$$K(x, \xi) = -\frac{(3 - \mu)(1 + \mu)}{4\pi Et(x - \xi)} \quad [6]$$

INTEGRAL EQUATION

The physical condition which governs the solution is that the normal strain ϵ_x, in the sheet at points along the x-axis from $-a$ to $+a$ must be the same as the normal strain in the stiffener. In order to allow for the use of different materials in the stiffener and the sheet, the value of Young's modulus for the stiffener will be indicated by E_1 and for the sheet by E_2.

If a tensile force P is applied at either end of the stiffener, the axial force p at any point along the stringer will vary as indicated in Fig. 2. The strain ϵ in the stringer may be expressed in terms of the stress σ or the axial force p

$$\epsilon = \frac{\sigma}{E_1} = \frac{p}{AE_1} \quad [7]$$

The area A of the stringer may be variable along its length.

The sheet may be considered to be acted upon by a variable shear flow q, as shown in Fig. 3. The strain ϵ_x in the sheet on the x-axis must be computed by using the influence function given by Equation [6] and integrating over the length of the applied load

$$\epsilon_x = \int_{-a}^{+a} (\xi)K(x, \xi)d\xi \quad [8]$$

The shear flow acting on the sheet and the axial force in the stringer are related by the equation of equilibrium of a differential length of the stiffener

$$q(\xi) = \frac{dp}{d\xi} \quad [9]$$

Equation [8] becomes

$$\epsilon_x = \int_{-a}^{+a} \frac{dp}{d\xi} K(x, \xi)d\xi \quad [10]$$

The strain as given by Equation [7] may be equated to the strain as given by Equation [10]

$$\frac{p}{AE_1} = \int_{-a}^{+a} \frac{dp}{d\xi} K(x, \xi)d\xi \quad [11]$$

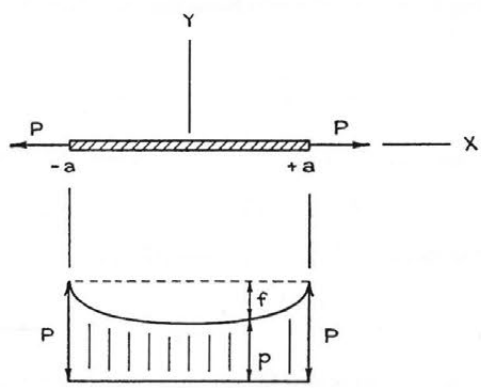

FIG. 2 VARIATION OF AXIAL FORCE IN STRINGER WITH SYMMETRICAL LOADING

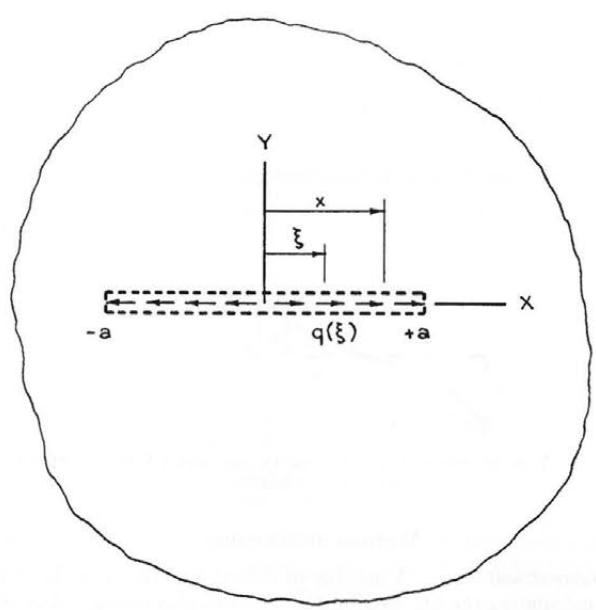

FIG. 3 SHEAR FLOW ACTING ON PLATE

The influence function from Equation (6) may be substituted to obtain

$$\frac{p}{AE_1} = -\frac{(3-\mu)(1+\mu)}{4\pi E_2 t}\int_{-a}^{+a}\left(\frac{1}{x-\xi}\right)\frac{dp}{d\xi}\,d\xi \quad [12]$$

This equation may be written in the following form

$$\eta p + \frac{a}{4\pi}\int_{-a}^{+a}\frac{dp}{x-\xi} = 0 \quad [13]$$

where

$$\eta = \frac{E_2 ta}{E_1 A(3-\mu)(1+\mu)} \quad [14]$$

Equation [13] must be solved to obtain the variation of the axial force. Referring to Fig. 2, it is convenient to represent the reduction of force at any point by a symbol f which satisfies the following relations

$$p = P - f \quad [15]$$

$$\frac{dp}{d\xi} = -\frac{df}{d\xi} \quad [16]$$

Substituting these formulas into Equation [13] gives the following equation

$$\eta f + \frac{a}{4\pi}\int_{-a}^{+a}\frac{df}{x-\xi} = \eta P \quad [17]$$

It is convenient to introduce dimensionless forces defined by

$$f = P\bar{f},\quad p = P\bar{p} = P(1-\bar{f}) \quad [18]$$

Substituting this formula into Equation [17] gives

$$\eta\bar{f} + \frac{a}{4\pi}\int_{-a}^{+a}\frac{d\bar{f}}{x-\xi} = \eta \quad [19]$$

This integral equation is seen to bear an accurate correspondence to Prandtl's lifting-line equation for spanwise air-load distribution on airplane wings. The force reduction f corresponds to the wing circulation.

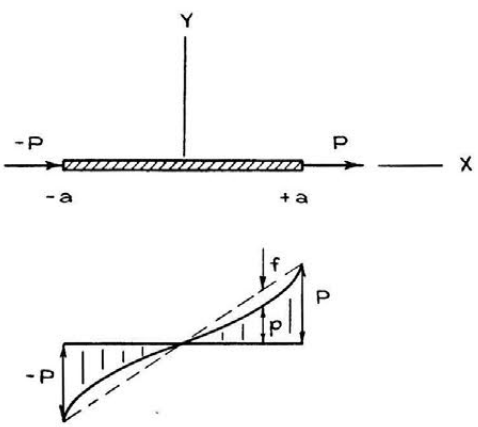

FIG. 4 VARIATION OF AXIAL FORCE IN STRINGER WITH ANTISYMMETRICAL LOADING

METHOD OF SOLUTION

Symmetrical Case. A number of different methods are known for calculating the lift distribution on an airplane wing. Any of these methods may be used in the present problem. A convenient method due to H. Multhopp[4] will be used in the present paper. The integral equation which governs the unknown function is replaced by a system of linear algebraic equations which govern a finite set of ordinates to the unknown function.

Since the axial-force distribution is symmetrical about the origin, it is only necessary to calculate ordinates at points on the semispan extending from $x = 0$ to $x = a$. The points at which the ordinates are determined are not equally spaced but are defined by introducing a new variable θ by the following relation

$$x = a\cos\theta \quad [20]$$

The angle variable θ ranges from zero to $\pi/2$ and this interval is divided into equal parts. If four ordinates, f_1 to f_4, are to be computed, the corresponding values of x and θ are as follows

$$\left.\begin{array}{ll}\theta_1 = 22.5^\circ & x_1 = 0.9239\\ \theta_2 = 45^\circ & x_2 = 0.7071\\ \theta_3 = 67.5^\circ & x_3 = 0.3827\\ \theta_4 = 90^\circ & x_4 = 0\end{array}\right\} \quad [21]$$

The equations governing the force reduction values may be written in the following matrix form

$$\begin{bmatrix}(2.6131+\eta_1) & -0.9571 & 0 & -0.0732\\ -0.5179 & (1.4141+\eta_2) & -0.5972 & 0\\ 0 & -0.4571 & (1.0824+\eta_3) & -0.4268\\ -0.0560 & 0 & -0.7886 & (1+\eta_4)\end{bmatrix}\begin{bmatrix}\bar{f}_1\\ \bar{f}_2\\ \bar{f}_3\\ \bar{f}_4\end{bmatrix} = \begin{bmatrix}\eta_1\\ \eta_2\\ \eta_3\\ \eta_4\end{bmatrix} \quad [22]$$

The corresponding equations for wing airload distribution have been developed by simple methods by the author.[5] The values of η for the particular case to be solved may be substituted into the equations and a solution immediately obtained. For the common case of a prismatic stiffener η is a constant.

It is of some interest to note that if the variation of stiffener area is chosen to give a constant value of stress at all points in the stiffener, the force reduction will be of elliptical distribution. This corresponds to the elliptical distribution of lift on a wing having minimum induced drag.

Antisymmetrical Case. Referring to Fig. 4, the stiffener is considered to be acted upon by a tensile force P at $x = a$ and a compressive force $-P$ at $x = -a$. The resultant force acting on the stiffener is $2P$. This force must be transmitted into the sheet and carried to infinity where the reaction occurs. If the shear flow q between the stiffener and the sheet is uniformly distributed, the variation of axial force in the stiffener is linear as indicated by the dotted line in Fig. 4. The force-reduction quantity f, in this case, may be defined as the difference between a linear distribution and the true distribution.

The axial force and its derivative are related to the force-reduction quantity by the following equations

$$p = \frac{Px}{a} - f \quad [23]$$

[4] "Die Berechnung der Auftriebsverteilung von Tragflügeln," by H. Multhopp, *Luftfahrtforschung*, vol. 15, April, 1938, pp. 153–169 (translated by British Ministry of Aircraft Production, Translation no. 2392.)

[5] "Matrix Development of Multhopp's Equations for Spanwise Air-Load Distribution," by S. U. Benscoter, *Journal of the Aeronautical Sciences*, vol. 15, February, 1948, pp. 113–120.

$$\frac{dp}{d\xi} = \frac{P}{a} - \frac{df}{d\xi} \quad \ldots\ldots\ldots\ldots\ldots\ldots [24]$$

Equation [13] takes the following form

$$\frac{\eta P x}{a} - \eta f + \frac{P}{4\pi}\int_{-a}^{+a}\frac{d\xi}{x-\xi} - \frac{a}{4\pi}\int_{-a}^{+a}\frac{df}{x-\xi} = 0 \quad \ldots [25]$$

The first integral in this equation may be evaluated without difficulty. The principal value must be determined and is given by the formula

$$\int_{-a}^{+a}\frac{d\xi}{x-\xi} = -\ln\left(\frac{a-x}{a+x}\right) \quad \ldots\ldots\ldots [26]$$

Substituting Equation [26] into Equation [25] gives

$$\eta f + \frac{a}{4\pi}\int_{-a}^{+a}\frac{df}{x-\xi} = \frac{\eta P x}{a} - \frac{P}{4\pi}\ln\left(\frac{a-x}{a+x}\right) \quad \ldots [27]$$

Introducing the dimensionless function, as defined by Equation [18], gives

$$\eta \bar{f} + \frac{a}{4\pi}\int_{-a}^{+a}\frac{d\bar{f}}{x-\xi} = \frac{\eta x}{a} - \frac{1}{4\pi}\ln\left(\frac{a-x}{a+x}\right) \quad \ldots [28]$$

It is convenient to introduce a symbol k to represent the quantity on the right-hand side of Equation [28].

$$k(x) = \frac{x}{a}\eta(x) - \frac{1}{4\pi}\ln\left(\frac{a-x}{a+x}\right) \quad \ldots\ldots\ldots [29]$$

This quantity may be expressed in terms of the variable θ by substituting Equation [20]

$$k(\theta) = \eta(\theta)\cos\theta - \frac{1}{4\pi}\ln\left(\frac{1-\cos\theta}{1+\cos\theta}\right) \quad \ldots\ldots [30]$$

The system of linear algebraic equations, which replace Equation [28], take the following form

$$\begin{bmatrix} (2.6131+\eta_1) & -0.9239 & 0 \\ -0.5 & (1.4141+\eta_2) & -0.5 \\ 0 & -0.3827 & (1.0824+\eta_3) \end{bmatrix}\begin{bmatrix}\bar{f}_1\\ \bar{f}_2\\ \bar{f}_3\end{bmatrix} = \begin{bmatrix}k_1\\ k_2\\ k_3\end{bmatrix} [31]$$

Numerical Example

In order to illustrate the application of the theory, a numerical solution has been made for a sheet and a prismatic stringer having the following dimensions and properties

$$\frac{E_2}{E_1} = 1 \qquad t = 0.1 \text{ in.}$$
$$\mu = 0.3 \qquad a = 10 \text{ in.}$$
$$A = 1 \text{ sq in.}$$

The parameter η is computed to have the following value

$$\eta = \frac{1}{(3-\mu)(1+\mu)} = 0.2849 \quad \ldots\ldots\ldots [32]$$

The symmetrical case will be considered first. The given value of η may be substituted into Equation [22] to obtain the following

$$\begin{bmatrix} 2.8980 & -0.9571 & 0 & -0.0732 \\ -0.5179 & 1.6990 & -0.5972 & 0 \\ 0 & -0.4571 & 1.3673 & -0.4268 \\ -0.0560 & 0 & -0.7886 & 1.2849 \end{bmatrix}\begin{bmatrix}\bar{f}_1\\ \bar{f}_2\\ \bar{f}_3\\ \bar{f}_4\end{bmatrix} = \begin{bmatrix}0.2849\\ 0.2849\\ 0.2849\\ 0.2849\end{bmatrix} [33]$$

This equation may be solved to obtain values of $\bar{f}$. Subtraction of these values from unity gives the values of $\bar{p}$ The following values are obtained

$$\bar{f}_1 = 0.2543 \qquad \bar{p}_1 = 0.7457$$
$$\bar{f}_2 = 0.4299 \qquad \bar{p}_2 = 0.5701$$
$$\bar{f}_3 = 0.5254 \qquad \bar{p}_3 = 0.4746$$
$$\bar{f}_4 = 0.5553 \qquad \bar{p}_4 = 0.4447$$

This symmetrical solution is illustrated in Fig. 5(*a*) where the dimensionless axial force is plotted for the semispan.

The antisymmetrical case may now be considered. The constant terms may be determined from Equation [30] and substituted into Equation [31] to obtain

$$\begin{bmatrix} 2.8980 & -0.9239 & 0 \\ -0.5 & 1.6990 & -0.5 \\ 0 & -0.3827 & 1.3673 \end{bmatrix}\begin{bmatrix}\bar{f}_1\\ \bar{f}_2\\ \bar{f}_3\end{bmatrix} = \begin{bmatrix}0.5202\\ 0.3417\\ 0.1732\end{bmatrix} [34]$$

This equation may be solved for the values of $\bar{f}$. From Equation [23] it is seen that the dimensionless axial force may be computed from the formula

$$\bar{p} = \cos\theta - \bar{f} \quad \ldots\ldots\ldots\ldots\ldots [35]$$

The values of $\bar{f}$ and $\bar{p}$ are found to be as follows

$$\bar{f}_1 = 0.2922 \qquad \bar{p}_1 = 0.6317$$
$$\bar{f}_2 = 0.3535 \qquad \bar{p}_2 = 0.3536$$
$$\bar{f}_3 = 0.2256 \qquad \bar{p}_3 = 0.1571$$

The antisymmetrical solution is illustrated graphically in Fig 5(*b*).

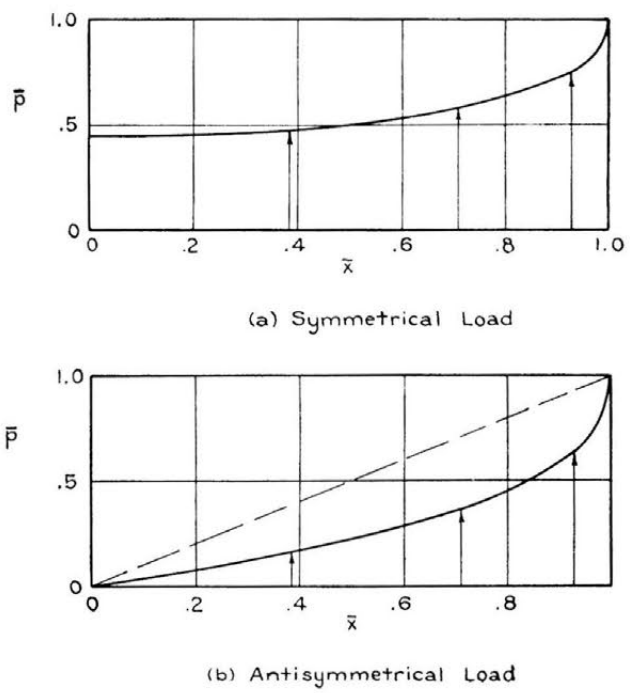

Fig. 5 Variation of Dimensionless Force in Stringer From Numerical Example

Conclusions

The axial-force distribution in a stringer of finite length attached to an infinite sheet may be computed by numerical methods. An influence function is employed which is obtained from the classical theory of elasticity. The distribution is found to be governed by an integral equation which has the same form as

the equation governing spanwise air-load distribution on an airplane wing. The integral equation may be replaced by a system of linear algebraic equations by any of the methods that are known to be applicable to the spanwise air-load problem.

Acknowledgment

The author is indebted to Miss L. B. Evans, mathematician, NACA, for having performed the calculations required for the preparation of the paper.

Application of Electric-Analog Computers to Heat-Transfer and Fluid-Flow Problems

By G. D. McCANN,[1] JR., AND C. H. WILTS,[2] PASADENA, CALIF.

There are two general classes of mathematical problems encountered in science and engineering for which high-speed mechanical computation is required. One of these embraces those problems of such complexity that it is impractical to obtain even a few solutions by conventional analysis. In the other class are problems which may be of only moderate complexity, but in which it is necessary to obtain a large number of solutions before the results become of practical value. It is the intent of this paper to discuss some of the applications that have been made of the California Institute of Technology "electric-analog computer" to heat-transfer and fluid-flow problems of both of the classes mentioned.

Introduction

ONE important attribute of the electric-analog computer described in this paper is that once the electric circuits which specify the mathematical form of the problem have been set up, it is a simple matter to obtain quickly successive solutions. A wide range of parameters can be scanned rapidly, delineating regions of interest. This not only saves time when a large number of solutions are desired as for the more general types of studies, but also saves a great deal of time in preliminary analysis and planning of calculations. This method also greatly facilitates an understanding of the physics of the problem through the analogy concept.

Unlike the large-scale digital computers being developed, the field of application of an analog computer is limited by the number of each component element it contains. It will be attempted therefore to indicate here ranges of applications and techniques for extending those ranges.

Description of Computer

In June, 1947, although then only partially completed, the Institute's computer[3,4,5] was placed in active service. Since then it has been in full-time use for the solution of commercial engineering problems and Institute research. Now that it is almost completed, it has been possible to apply it to certain of the partial differential equations of heat transfer and fluid flow and to evaluate partially its applicability to these general fields.

The computer was designed to handle linear ordinary algebraic and differential equations of high order of complexity, ordinary nonlinear equations of moderate complexity, and a limited group of partial differential equations. A special effort was made so to design all elements of the computer that additions can readily be made if sufficiently important problems arise which require greater facilities.

The computer is best described by referring to Fig. 1 and Table 1, which show its general layout and list the component parts. Briefly, its design is based around 110 separate sets of precision inductors, resistors, and capacitors, and 25 special transformers. These are used to set up circuits for solving ordinary or partial differential equations. There are, at present, 20 separate forcing functions for introducing (as known voltages, currents, or charges) the known functions of the independent variable. These may be steady-state variable-frequency sinusoidal functions, square-wave transient functions, or perfectly arbitrary functions of time. As listed in Table 1, amplifiers are used for negative impedance terms or unilateral terms such as the unsymmetrical terms of a matrix. For simulating the nonlinear terms of an equation, multipliers are provided for multiplying any two variables, and nonlinear functions elements are provided for forming arbitrary functions of any dependent variables. The dependent variables which constitute the desired solutions are simulated as circuit voltages, currents, or charges. For transient solutions, they are recorded or viewed on cathode-ray oscilloscopes while for steady-state or algebraic solutions they are measured with dynamometer-type meters.

Important elements of the computer are the synchronous switches used to switch in the forcing functions, remove energy from the circuits to restore them to their proper initial condition, and to accomplish other sudden changes in circuit conditions. These switches are required only for transient solutions which may be obtained in either of two ways. One of these is to apply the transient only once and record it photographically or on some other memory device such as magnetic tape. The other method is to apply the transient cyclically (usually 10 times per sec) so that the solution appears as a steady image on a cathode-ray oscilloscope for viewing and recording. Other important features are the plugboard arrangement and metering circuits which enable rapid and accurate hook-up of the desired circuits, and rapid metering of all solutions.

The methods of formulating analogies and converting results to numerical values[3,4,5] cannot be treated in a perfectly general way in this paper. However, detailed discussions of some analogies are given in connection with individual examples.

Problems Described by Ordinary Differential Equations

The application of electric-analog techniques to ordinary linear equations has been apparent for many years. The extension (in the case of the Cal Tech computer) to ordinary nonlinear equations has been discussed in detail.[4] Except for the example

---

[1] Professor of Electrical Engineering, California Institute of Technology. Mem. ASME.

[2] Assistant Professor of Applied Mechanics, California Institute of Technology.

[3] "A New Device for the Solution of Transient Vibration Problems by the Method of Electrical Analogy," by H. E. Criner, G. D. McCann, and P. E. Warren, JOURNAL OF APPLIED MECHANICS, Trans. ASME vol. 67, 1945, p. A-135.

[4] "The Mechanical Transients Analyzer," by G. D. McCann, Proceedings of the National Electronics Conference, vol. 2, 1946, p. 372.

[5] "A Large Scale General Purpose Electric Analog Computer," by E. L. Harder and G. D. McCann, AIEE Technical Paper 48-112, 1948.

Contributed by the Applied Mechanics Division of THE AMERICAN SOCIETY OF MECHANICAL ENGINEERS and presented at the first Heat Transfer and Fluid Mechanics Institute, Los Angeles, Calif., June 21–23, 1948.

Discussion of this paper should be addressed to the Secretary, ASME, 29 West 39th Street, New York, N. Y., and will be accepted until October 10, 1949, for publication at a later date. Discussion received after the closing date will be returned.

NOTE: Statements and opinions advanced in papers are to be understood as individual expressions of their authors and not those of the Society. Paper No. 48—HFT-1.

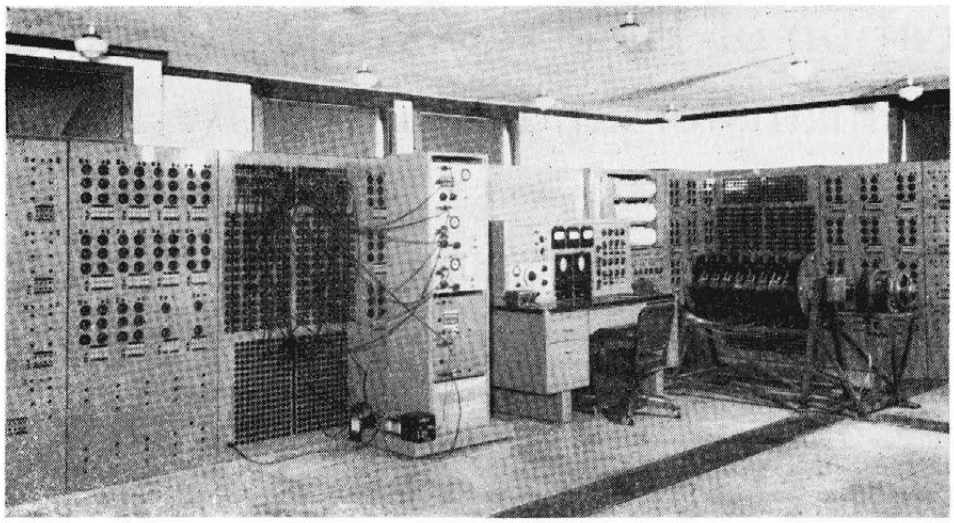

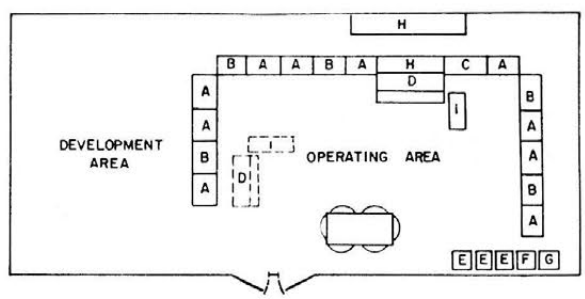

[(*Above*) General view of computer (*Right*) Block diagram of computer.]

FIG. 1 CALIFORNIA INSTITUTE OF TECHNOLOGY ELECTRIC-ANALOG COMPUTER

TABLE 1 BASIC ELEMENTS OF CALIFORNIA INSTITUTE OF TECHNOLOGY ELECTRIC-ANALOG COMPUTER

(See schematic diagram, Fig. 1)

(*A*)	*Ten Passive Circuit Elements Cabinets*		
	1	100 high "Q" inductors	0 to 1.0 henrys in 0.001-henry steps
	2	20 high "Q" inductors	0 to 1.50 henrys in 0.01-henry steps
	3	100 resistors	0 to 7000 ohms in 2-ohm steps
	4	20 resistors	0 to 500,000 ohms in 200-ohm steps
	5	60 capacitors	0 to 1.0 mfd in 0.01-mfd steps
	6	40 capacitors	0 to 4.0 mfd in 0.01-mfd steps
	7	10 capacitors	0 to 80 mfd in 10-mfd steps
	8	25 special transformers[a]	
(*B*)	*Five Plugboards*		
	1	Plugboards for all elements of two-circuit elements cabinets	
	2	Receptable patch board for 500 element connections and 25 main buses	
(*C*)	*One Forcing Functions Cabinet*[a]		
	1	6 sinusoidal variable-frequency and phase-position voltage sources (0 to 50 volts, 1 ampere, 1 ohm)	
	2	6 separate square-wave voltage sources (0 to 12 volts, or one 72 volt source in 2-volt steps)	
	3	6 arbitrary voltage sources (maximum 50 volts, 1 ohm)	
	4	3 arbitrary current sources (controllable from any voltage source)	
(*D*)	*One Metering Desk*[a]		
	1	3 dynamometer-type meters for metering sinusoidal current, voltage, power, etc.	
	2	2 cathode-ray oscillographs for transient solution (current, voltage, or charge)	
	3	1 three-wire metering circuit (and selector system) for metering all passive circuit elements and source forcing functions	
	4	1 manual metering selector circuit for 16 of 25 main buses	
	5	Circuits for connecting 8 synchronous switches to any of 16 main buses	
(*E*)	*Amplifier Cabinets (portable)*		
	1	5 negative gain (0 to 50) d-c amplifiers (15 ohm impedance), each having an RC time-delay circuit for servo problems	
	2	5 positive gain (0 to 100) d-c amplifiers with isolated input and 1 ohm output impedance[a]	
(*F*)	*Multiplier Cabinets (portable)*		
	1	1 multiplier with isolated input and 1 ohm output impedance[a] (five more to be constructed)	
(*G*)	*Arbitrary Functions of Dependent Variable (portable)*		
	1	2 voltage limiters	
	2	2 current limiters	
	3	2 perfectly arbitrary function devices[a]	

[a] Additional elements are contemplated. Table lists only elements of computer in its present operating form.

given below, no thermal or fluid-flow problem specified by ordinary equations has been solved as yet with the Cal Tech computer. However, there are many important problems of this sort which can be treated readily.

Temperature Rise in Rotating Electric Machines During Variable-Load Cycles. Many calculations of the temperature rise of machinery involve the solution of ordinary linear equations since each thermal medium can be considered to have equal temperature throughout. An example of the application of an electric-analog computer to such a "lumped constant" thermal system is in the calculation of temperature variations in an electric motor during a complex variable-load cycle. This is typical of numerous problems encountered in the proper application of electrical and mechanical equipment. In this problem it is assumed that the motor is composed of two materials with high thermal capacity, the magnetic iron and the copper conductors. Generated in each are energy losses. In the iron these are eddy-current and hysteresis losses which are a function of the applied voltage. In the copper are I^2R losses which are a function of the motor load. Heat can be transmitted from each into the ambient air and can also be exchanged between each through the winding insulation.

The following differential equations then apply

$$W_c = c_c G_c \frac{dT_c}{dt} + \alpha_c S_c T_c + \alpha_{ci} S_{ci} (T_c - T_i) \quad [1]$$

$$W_i = c_i G_i \frac{dT_i}{dt} + \alpha_i S_i T_i + \alpha_{ci} S_{ci} (T_i - T_c) \quad [2]$$

where

W_c and W_i are copper and iron losses
T_c and T_i are temperature rises above ambient air
c_c and c_i are specific heats of both metals
G_c and G_i are weights of each metal

S_c and S_i are surface areas of each metal in contact for direct transmission of heat to air

α_c and α_i are heat-transmission coefficients from metal to air

α_{ci} is heat-transmission coefficient through insulation between copper and iron

Electric Analog. Several electric analogies can be used for Equations [1] and [2]. That of Fig. 2 is used as an illustration: It satisfies the voltage equations

$$E_c = L_c \frac{di_c}{dt} + R_c i_c + R_{ci}\,(i_c - i_i) \quad [3]$$

$$E_i = L_i \frac{di_i}{dt} + R_i i_i + R_{ci}\,(i_i - i_c) \quad [4]$$

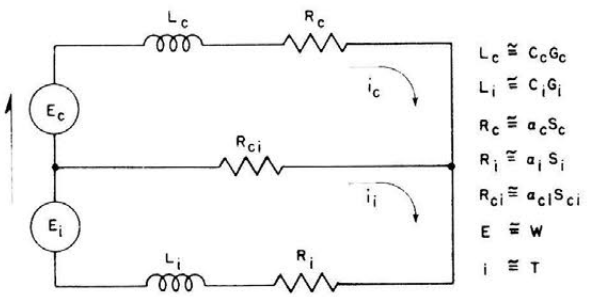

(a) ANALOGY FOR MOTOR RUNNING CONTINUOUSLY

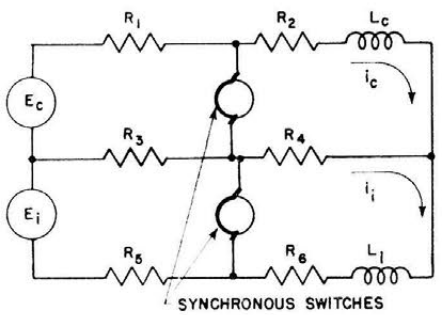

$R_1 + R_2 = R_c$ WHILE MOTOR IS RUNNING

$R_2 = R_c$ WHEN MOTOR IS STOPPED

(b) ANALOGY FOR MOTOR STOPPED PART OF CYCLE

FIG. 2 ELECTRIC ANALOG FOR TEMPERATURE RISE IN ELECTRIC MOTOR DURING VARIABLE-LOAD CYCLE

Such a circuit can be solved rather simply unless the voltages E_c and E_i corresponding to the copper and iron losses are complex functions of time. When set up on the computer, these functions readily can be made to have any arbitrary form. If the motor is running continuously with constant applied voltage, the function ($E_i \cong W_i$) is constant, and only the voltage corresponding to the copper losses ($E_c \cong W_c$) need be varied. This condition is illustrated in Fig. 2(*a*). However, if the motor is shut down for any part of the load cycle, not only must the iron losses be varied, but also all of the heat-transfer coefficients. As shown in Fig. 2(*b*), the proper circuit conditions for representing the period that the motor is shut down are obtained by closing the two switches. The circuit to the right of the switch then represents the thermal system with no thermal energy being generated, and the thermal conductivities reduced because of its lack of air circulation.

In choosing the proper circuit elements for quantitative simulation and to convert from electrical to thermal units, the following relationships are applicable as long as consistent sets of units are used in both the thermal system and the analogous electric system

$$L = \frac{a}{n} cG,\ R = a\alpha S \quad [5]$$

Where a is an arbitrary impedance factor and n determines the time base change made for the computer. Thus $t = nt'$ where t is actual time and t' is time on the computer time base. To obtain actual temperature values one uses the relations

$$T_c = a i_c \frac{W}{E}, \text{ etc.} \quad [6]$$

where $\frac{W}{E}$ is the ratio of thermal energy to analogous computer voltage.

Figs. 3 and 4 present typical analog-computer solutions for the two conditions of motor operation. In these figures the effect of stopping the motor during its no-load period is apparent. The maximum copper and iron temperatures are both greater than when the motor runs continuously. A solution of this type requires only about 15 min of setup time, and a few minutes for each successive set of solutions. From the analogous circuit it is apparent that simple basic tests on actual machines can be made readily to determine the thermal coefficients. Routine computations of this type for complex motor loads would be quite simple, rapid, and economical, and greatly improve such motor applications.

PROBLEMS SPECIFIED BY PARTIAL DIFFERENTIAL EQUATIONS

Most of the heat-transfer and fluid-flow problems so far solved with the analog computer have involved "distributed constants." Several important types of such partial differential equations in the field of fluid and thermal flow are well-suited to such computation methods. These include both linear and nonlinear systems. The general applications of electric circuits to partial equations have been treated by Kron.[6,7] However, many of the techniques discussed by him are not practicable, in general, either because they involve too many circuit elements for any but a special-purpose computer, apply only to limited cases, or require too much setup and computation time. Nevertheless, the range of application of electric-analog methods to partial differential equations is broader than one would at first suppose.

The electric analogies and computing techniques so far found practicable will be presented. Following this are several numerical solutions which illustrate the methods and give information on computation time and expected accuracy. The general methods of determining electric analogies are best described by first considering some of the simpler specific examples. Since computers of the type being considered here consist of "lumped-constant" elements, it is necessary (except in special cases) to resort to the finite-difference method of representing the space variables. For this purpose the region of interest is divided into "cells," and the differential equation is approximated by a difference equation involving the values of the dependent variable at the centers of neighboring cells. The number of cells required to give results to suitable accuracy is surprisingly small. Specific data on this matter are meager, although the numerical examples to be given will give some idea of the requirements in general.

---

[6] "Numerical Solution of Ordinary and Partial Differential Equations by Means of Equivalent Circuits," by G. Kron, *Journal of Applied Physics*, vol. 16, March, 1945, p. 172.

[7] "Equivalent Circuits of Compressible and Incompressible Fluid Flow Fields," by G. Kron, *Journal of Aeronautical Sciences*, vol. 12, 1945, p. 221.

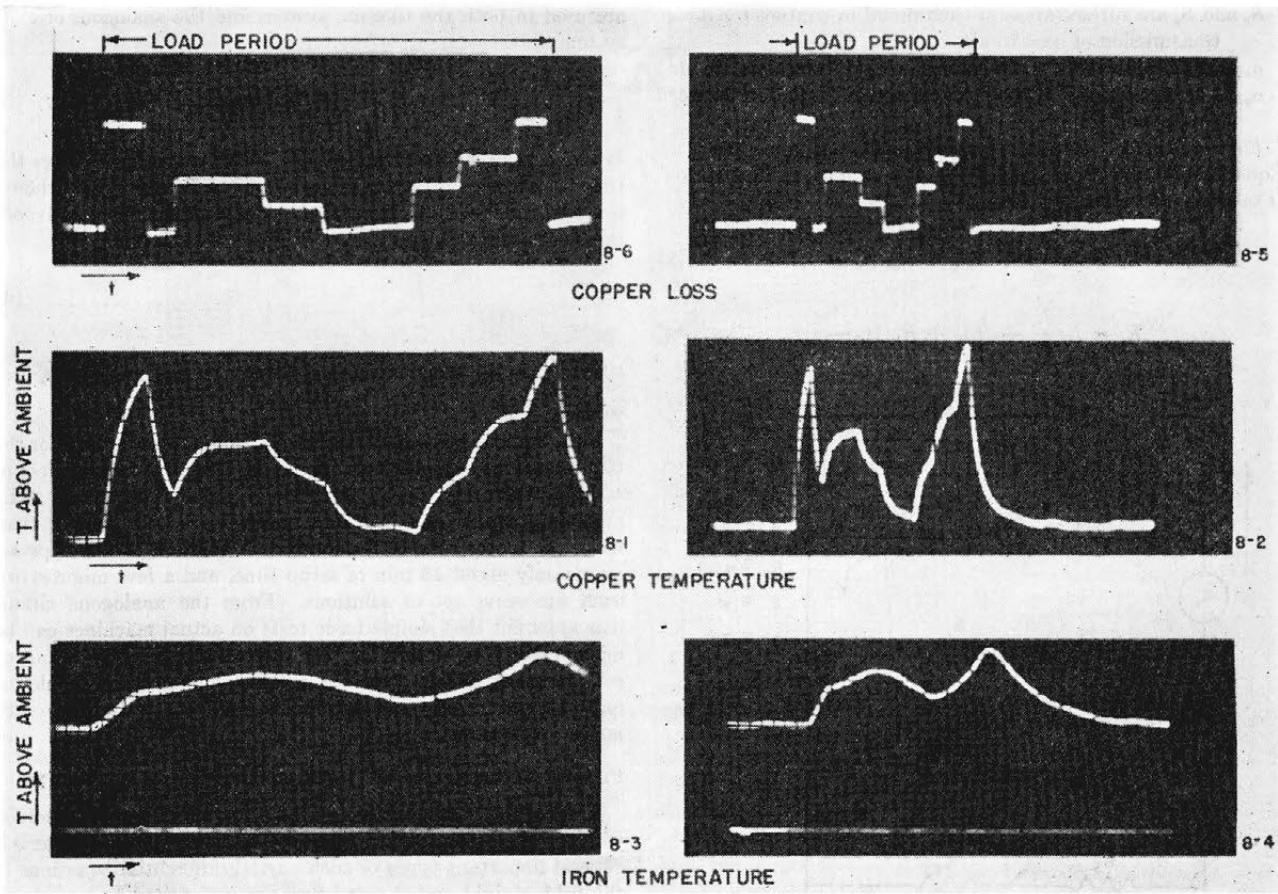

FIG. 3 TEMPERATURE RISE IN ELECTRIC MOTOR DURING VARIABLE-LOAD CYCLE—MOTOR RUNNING CONTINUOUSLY

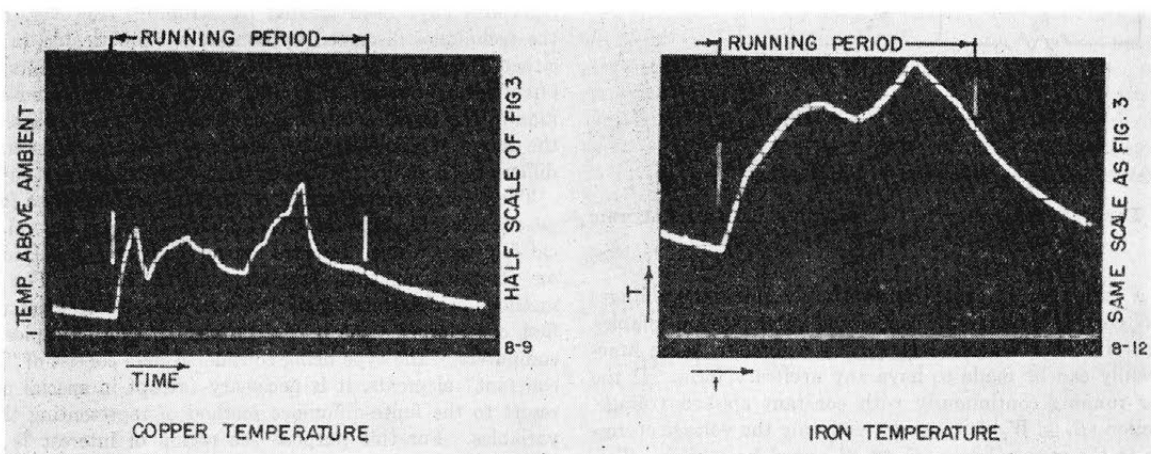

FIG. 4 TEMPERATURE RISE IN ELECTRIC MOTOR DURING VARIABLE-LOAD CYCLE—MOTOR STOPPED FOR HALF OF LOAD CYCLE

In certain cases it is expedient to treat the time variable in the same manner, and use a finite-difference equation in time as well as in space. In the electrical analogy for such a problem, the time co-ordinate is then treated the same as a space co-ordinate, and a static network results. There are also some problems in which a space co-ordinate in the problem of interest becomes a time co-ordinate in the computer solution, although the other space co-ordinates are still treated by finite-difference methods.

Laplace's Equation $\nabla^2 \phi = 0$. In Fig. 5 are shown the more common analogies for Laplace's equation in two dimensions. The analogies are obtained by applying Kirchhoff's law for the summation of currents at a junction point of a mesh. If the resistance grid is used either direct current or steady-state sinusoidal currents and voltages may be applied. If alternating current is used, inductors or capacitors may be used also. It is readily apparent that the method applies to any co-ordinate system and to the three-dimensional case.

Transient Heat-Flow Equation $\nabla^2\phi = k(\partial\phi/\partial t) + f(t)$. The transient heat-flow equation has two additional terms, one representing the effect of heat stored in the conducting medium, and another the

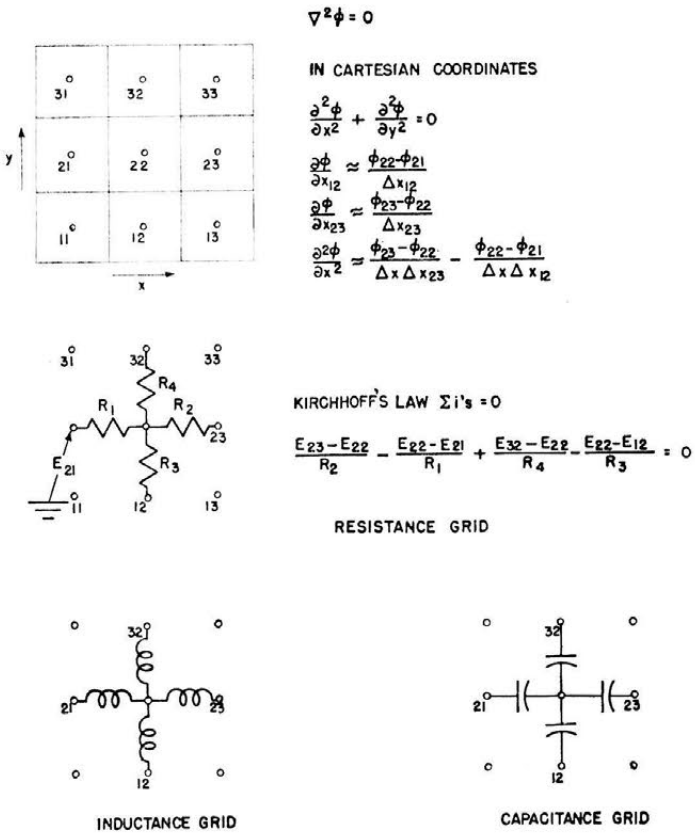

FIG. 5 ANALOGIES FOR LAPLACE'S EQUATIONS

effect of heat generated within the medium. If time is to be represented as such in the analog, it is desirable to employ the resistance grid for the Laplacian. The linear transient heat-flow problem can then be solved using the analogies of Fig. 6. The finite-difference equation approximating the differential equation is still taken as an expression of Kirchhoff's law for the summation of currents at a junction point of a mesh. The current proportional to $\partial\phi/\partial t$ is obtained with a capacitor, Fig. 6*a*, and the current proportional to $f(t)$ is inserted at each point with a current generator, Fig. 6*b*. The transient boundary condition and the arbitrary heat-generation function $f(t)$ can be simulated readily with the electric-analog computer.

Combined Eddy and Thermal Conductivity. In systems involving steady-state flow of fluid, the equation for heat flow can be written in terms of the usual thermal and an eddy conductivity coefficient. When proper symmetry prevails, it is expedient to represent one of the space variables as the time variable on the computer. In particular, if the direction of fluid flow can be taken along one co-ordinate axis, the equations of thermal flow can be expressed by the equation in Fig. 6(*a*) with the co-ordinates perpendicular to the direction of flow represented as a space grid and distance along the flow axis represented by time.

Viscous Damping in Small-Diameter Tubes. The analogies in Fig. 7 represent the damping system employed on a special testing machine for dynamic loading of material. It is an incompressible hydraulic system in which viscous flow is required between two chambers in the system. This is achieved by connecting a large number of very small-diameter tubes in parallel. Application of a pressure differential between the headers gives rise to laminar flow which is a function of radial co-ordinate only and which is described by an equation identical to that of Fig. 6(*b*), but where $f(t)$ is now proportional to the pressure differential. Thus the same analogy can be used, or if it is preferred to insert the functions $f(t)$ as voltages instead of currents, the second analogy in Fig. 7 may be employed.

Nonlinear Thermal System. The nonlinearities arising in thermal equations may be of two types. Variations in the coefficients of heat capacity and conductivity give rise to equations of the form

$$f_1(\phi)\frac{\partial^2\phi}{\partial x^2} + f_2(\phi)\frac{\partial^2\phi}{\partial y^2} = \frac{k\partial\phi}{\partial t} \quad \ldots\ldots\ldots\ldots [7]$$

Unless the system can be represented by a relatively small number of finite-difference equations in space variables, such problems cannot be handled on the Cal Tech computer without representing time as a space variable and employing iteration methods. This process will be discussed later.

The other type of nonlinearity arises from heat sources within the thermal medium which are functions of temperature. This condition is illustrated by the equations in Figs. 8 and 9. When the problem is one-dimensional in space it is sometimes practical to represent the nonlinear functions in a direct time analogy as shown in Fig. 8. There the function $F_1(t)\cdot F_2(x_n)\cdot\phi_n$ must be introduced as a current into each junction point of the space mesh. This is obtained with a multiplier taking the inputs ϕ_n and $F_1(t)\cdot F_2(x_n)$ and producing a current proportional to the product.

In Fig. 9, this same type of equation is simulated with a static alternating-current network. Referring to the equations in Fig. 9 it will be noted that to represent terms of the form $\partial\phi/\partial t$ or $\partial\phi/\partial x$ by finite-difference methods, it

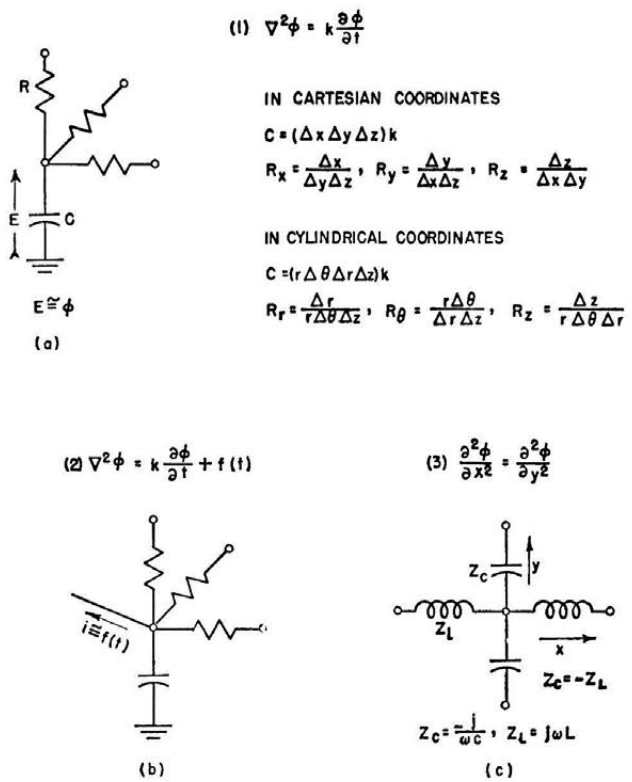

FIG. 6 ANALOGIES FOR OTHER PARTIAL DIFFERENTIAL EQUATIONS OF THERMAL AND FLUID FLOW

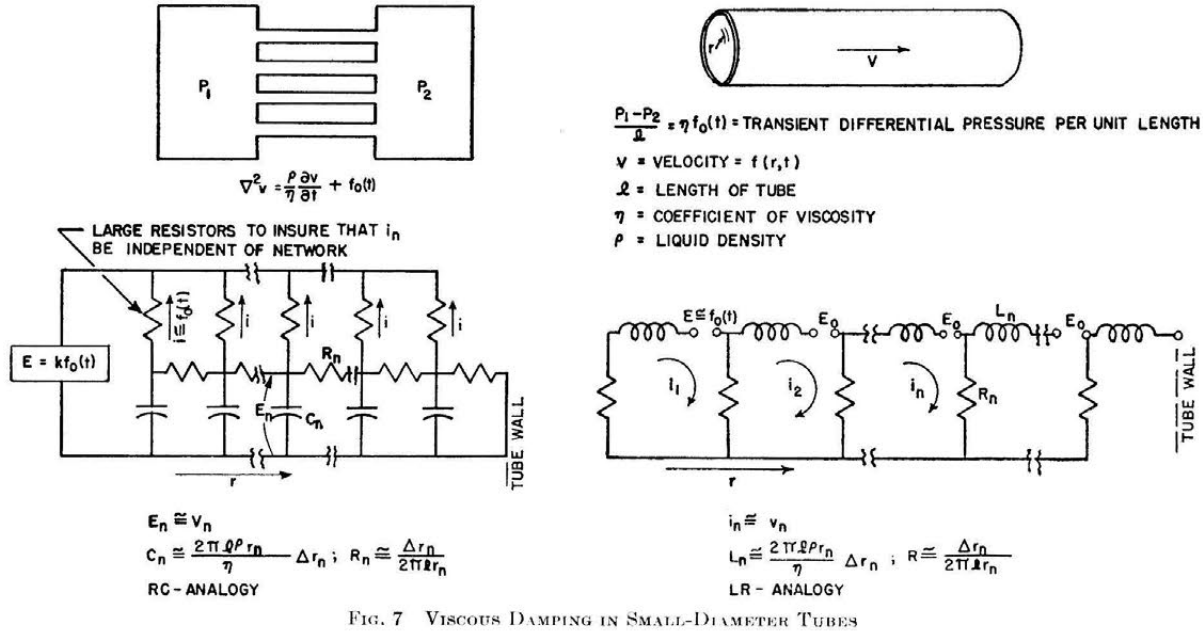

FIG. 7 VISCOUS DAMPING IN SMALL-DIAMETER TUBES

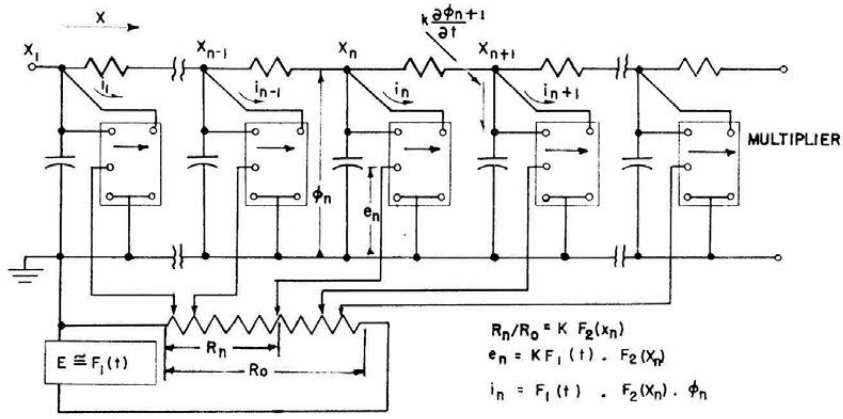

FIG. 8 ANALOG FOR NONLINEAR PARTIAL DIFFERENTIAL EQUATION OF HEAT TRANSFER

is necessary to have negative impedances. With a very extensive resistance grid this would be impractical, but with an alternating-current-static network it is accomplished with capacitive and inductive impedances. However, as will be shown later, such terms can sometimes be represented in the resistance-type grid when combined with higher-order terms which make the combined resistors positive. With circuits of this sort, functions of the dependent variable are handled by iterative methods. In this case the function $F_1(t_m) \cdot F_2(x_n) \cdot \phi_{nm}$ must be inserted as a current at the appropriate junction. To accomplish this, an estimate of ϕ is used, and the correct solution is approached by a series of successive approximations.

Analogy for Compressible Fluid Flow. The equations for laminar nonviscous compressible fluid flow are commonly expressed in the following form[8] for which an electric analogy can be developed

$$\left(1 - \frac{u^2}{a^2}\right)\frac{\partial^2 \phi}{\partial x^2} - \frac{2uv}{a^2}\frac{\partial^2 \phi}{\partial x\, y} + \left(1 - \frac{v^2}{a^2}\right)\frac{\partial^2 \phi}{\partial y^2} = 0 \quad \ldots\ldots [8]$$

where

$$u = \frac{\partial \phi}{\partial x},\ v = \frac{\partial \phi}{\partial y} \text{ and } a^2 = \frac{\gamma - 1}{2}(a_0^2 - u^2 - v^2)$$

This equation can be rewritten as follows

$$A\frac{\partial^2 \phi}{\partial x^2} - 2B\frac{\partial^2 \phi}{\partial x \partial y} + C\frac{\partial^2 \phi}{\partial y^2} = 0 \quad \ldots\ldots\ldots\ldots [9]$$

This equation can also be solved by an analogous circuit and a series of successive approximations. Referring to Fig. 10, its terms in finite-difference form can be written as follows

$$\frac{\partial^2 \phi}{\partial x^2} = \frac{\phi_{23} - \phi_{22}}{\Delta x\, \Delta x_{23}} - \frac{\phi_{22} - \phi_{21}}{\Delta x\, \Delta x_{12}} \quad \ldots\ldots\ldots\ldots [10]$$

[8] "Partial Differential Equations," by Harry Bateman, Dover Publications, New York, N. Y., 1944.

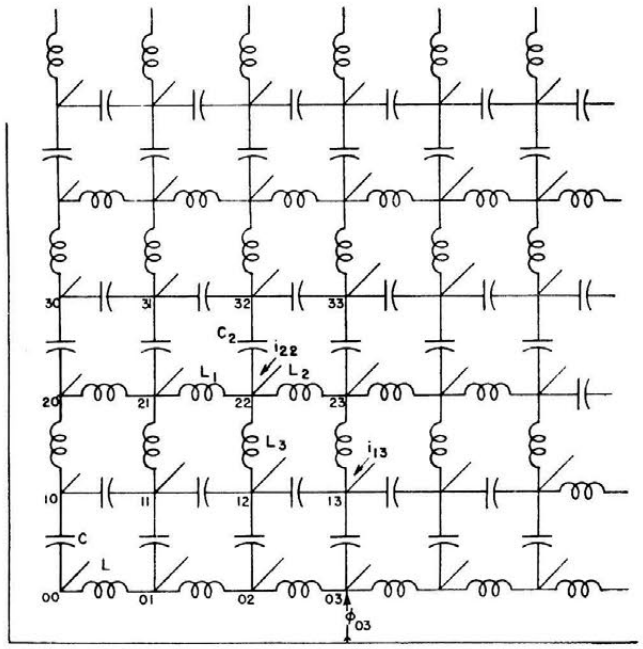

FIG. 9 (*left*) ANALOGOUS CIRCUIT FOR THE NONLINEAR EQUATION $(\partial^2\phi/\partial x^2) = (k\partial\phi/\partial t) + F(x, t, \phi)$

$i_{nm} \cong F(X_n, t_m, \phi_{nm})$ VOLTAGE $\cong \phi$

FINITE DIFFERENCE EQUATION AT JUNCTION 22:

$$\frac{\phi_{23}-\phi_{22}}{\Delta x \Delta x_{23}} - \frac{\phi_{22}-\phi_{21}}{\Delta x \Delta x_{12}} = \frac{k}{2}\left[\frac{\phi_{32}-\phi_{22}}{\Delta t_{23}} + \frac{\phi_{22}-\phi_{12}}{\Delta t_{12}}\right] + F(X_{21}, t_{21}, \phi_{22})$$

BY SUMMATION OF CURRENTS AT JUNCTION 22:

$$\frac{\phi_{23}-\phi_{22}}{j\omega L_2} - \frac{\phi_{22}-\phi_{21}}{j\omega L_1} = \frac{\phi_{32}\ \phi_{22}}{j\left(\frac{1}{\omega C_2}\right)} + \frac{\phi_{22}\ \phi_{12}}{j\omega L_3} + i_{22}$$

$$\frac{\partial^2\phi}{\partial y^2} = \frac{\dfrac{\phi_{32}-\phi_{22}}{\Delta y_{23}} - \dfrac{\phi_{22}-\phi_{12}}{\Delta y_{12}}}{\Delta y} \quad \ldots\ldots\ldots\ldots [11]$$

Where Δx without a subscript is the average value for two intervals; $(\partial^2\phi)/(\partial x \partial y)$ can be defined by four relationships which should be averaged over at least two of them to define the quantity at the same point in space as used for the terms $(\partial^2\phi)/(\partial x^2)$ and $(\partial^2\phi)/(\partial y^2)$. These terms are the following

(*a*) $\dfrac{\dfrac{\phi_{33}-\phi_{32}}{\Delta x_{23}} - \dfrac{\phi_{23}-\phi_{22}}{\Delta x_{23}}}{\Delta y_{23}}$ (*c*) $\dfrac{\dfrac{\phi_{32}-\phi_{21}}{\Delta x_{12}} - \dfrac{\phi_{22}-\phi_{21}}{\Delta x_{12}}}{\Delta y_{23}}$

(*b*) $\dfrac{\dfrac{\phi_{22}-\phi_{21}}{\Delta x_{12}} - \dfrac{\phi_{12}-\phi_{11}}{\Delta x_{12}}}{\Delta y_{12}}$ (*d*) $\dfrac{\dfrac{\phi_{23}-\phi_{22}}{\Delta x_{23}} - \dfrac{\phi_{13}-\phi_{12}}{\Delta x_{23}}}{\Delta y_{12}}$

For instance, choosing (*c*) and (*d*), adding and dividing by 2

$$\frac{\partial^2\phi}{\partial x \partial y} = \frac{1}{2}\left(\frac{\dfrac{\phi_{32}-\phi_{31}}{\Delta x_{12}} - \dfrac{\phi_{22}-\phi_{21}}{\Delta x_{12}}}{\Delta y_{23}} + \frac{\dfrac{\phi_{23}-\phi_{22}}{\Delta x_{23}} - \dfrac{\phi_{13}-\phi_{12}}{\Delta x_{23}}}{\Delta y_{12}}\right) \quad [12]$$

Combining all the terms for Equation [9]

$$(\phi_{23} - \phi_{22})\left[\frac{A}{\Delta x_{23}\Delta x} - \frac{B}{\Delta x_{23}\ \Delta y_{12}}\right]$$

FIG. 10 (*below*) ELECTRICAL ANALOGIES FOR COMPRESSIBLE FLUID EQUATIONS

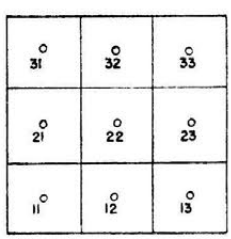

$$\left(1-\frac{u^2}{a^2}\right)\frac{\partial^2\phi}{\partial x^2} - \frac{2uv}{a^2}\frac{\partial^2\phi}{\partial x \partial y} + \left(1-\frac{v^2}{a^2}\right)\frac{\partial^2\phi}{\partial y^2} = 0$$

WHERE $u = \dfrac{\partial\phi}{\partial x}$, $v = \dfrac{\partial\phi}{\partial y}$

$$a^2 = \frac{\gamma-1}{2}\left[a_0^2 - u^2 - v^2\right]$$

ANALOGIES FOR EQUATION $A\dfrac{\partial^2\phi}{\partial x^2} - B\dfrac{\partial^2\phi}{\partial x \partial y} + C\dfrac{\partial^2\phi}{\partial y^2} = 0$

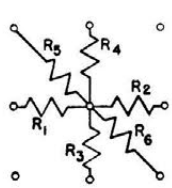

(a) B POSITIVE

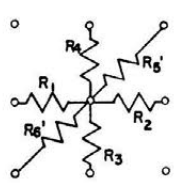

(b) B NEGATIVE

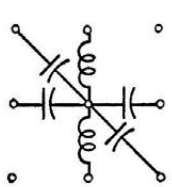

(c)

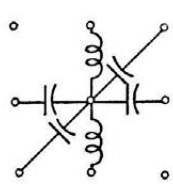

(d)

A OR C NEGATIVE

$$- (\phi_{22} - \phi_{21}) \left[\frac{A}{\Delta x_{12}\ \Delta x} - \frac{B}{\Delta x_{12}\ \Delta y_{23}} \right]$$

$$+ (\phi_{32} - \phi_{22}) \left[\frac{C}{\Delta y_{23}\ \Delta y} - \frac{B}{\Delta x_{12}\ \Delta y_{23}} \right]$$

$$- (\phi_{22} - \phi_{12}) \left[\frac{C}{\Delta y_{12}\ \Delta y} - \frac{B}{\Delta x_{23}\ \Delta y_{12}} \right]$$

$$+ (\phi_{31} - \phi_{22}) \left[\frac{B}{\Delta x_{12}\ \Delta y_{23}} \right] - (\phi_{22} - \phi_{13}) \left[\frac{B}{\Delta x_{23}\ \Delta y_{12}} \right] = 0 \quad [13]$$

This set of difference equations is simulated by the mesh in Fig. 10(a) where the resistors are given by the following equations

$$\left.\begin{aligned} \frac{1}{R_1} &= \left[\frac{A}{\Delta x_{12}\ \Delta x} - \frac{B}{\Delta x_{12}\ \Delta y_{23}} \right] & \frac{1}{R_4} &= \left[\frac{C}{\Delta y_{23}\ \Delta y} - \frac{B}{\Delta x_{12}\ \Delta y_{23}} \right] \\ \frac{1}{R_2} &= \left[\frac{A}{\Delta x_{23}\ \Delta x} - \frac{B}{\Delta x_{23}\ \Delta y_{12}} \right] & \frac{1}{R_5} &= \frac{B}{\Delta x_{12}\ \Delta y_{23}} \\ \frac{1}{R_3} &= \left[\frac{C}{\Delta y_{12}\ \Delta y} - \frac{B}{\Delta x_{23}\ \Delta y_{12}} \right] & \frac{1}{R_6} &= \frac{B}{\Delta x_{23}\ \Delta y_{12}} \end{aligned}\right\} \quad [14]$$

If either u or v is negative so that the term B is negative, then $(\partial^2\phi)/(\partial x \partial y)$ must be formed using terms (a) and (b) instead of (c) and (d). This gives rise to the circuit in Fig. 10(b) where the resistors have the values just given with obvious change of certain subscripts, but the absolute value of B is used.

The values of A, B, and C can be computed from the first derivative of ϕ taken between the appropriate pair of cells. Since the mesh resistors depend upon the potential ϕ, which is unknown, the solution for the incompressible case is used to calculate more nearly correct mesh impedances, and this process is iterated until the desired precision is obtained.

More General Forms of Partial Differential Equations. The foregoing examples have illustrated two basic types of circuits for representing certain thermal and fluid-flow problems. In one of these, time is actually represented as time in the computer. In the other, time is represented by finite-difference terms and a static alternating-current network results. These examples have illustrated the methods of obtaining the analogies for such terms in the finite-difference equations as $(\partial^2\phi)/(\partial x^2)$, $(\partial\phi)/(\partial x)$, and $(\partial^2\phi)/(\partial x \partial y)$.

Thus the methods of formulating analogies for the more general form of equations given in Fig. 11 now become apparent. In cases where finite-difference equations for the space functions lead to a positive resistance grid and the functions (f, F) are not functions of the dependent variable, the analogy of Fig. 11(a) may be employed. Otherwise the static-network method of Fig. 11(b) must be used. In Fig. 11 only two-dimensional grids are illustrated. If sufficient elements were available three- or four-dimensional grids could be formed. It is believed to be generally impracticable to employ the static-network method for any more than a two-dimensional grid. Ordinarily, it would be used for nonlinear problems, and even though time required for changing parameters and recording solutions can be made quite small on a properly planned computer, the intervening numerical computations for each trial calculation might require excessive time. However, for two-dimensional problems, such as illustrated here, computations can be made quite rapidly.

Illustrative Numerical Examples

Temperature Distribution in Gas-Turbine Rotor. As a first example of a numerical solution, consider the system in Fig. 12(a),

$$f_1(x,y)\frac{\partial^2\phi}{\partial x^2} + f_2(x,y)\frac{\partial\phi}{\partial x} + f_3(x,y)\frac{\partial^2\phi}{\partial y^2} + f_4(x,y)\frac{\partial\phi}{\partial y} + f_5(x,y)\frac{\partial^2\phi}{\partial x \partial y} = F(x,y,t) + k_1\frac{\partial\phi}{\partial t} + k_2\phi$$

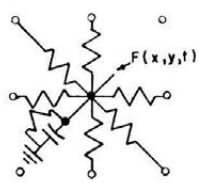

(a) TRANSIENT PROBLEMS WITH ACTUAL TIME REPRESENTED AS TIME IN COMPUTER.

Z may be $R, j\omega L$, or $\frac{-j}{\omega C}$

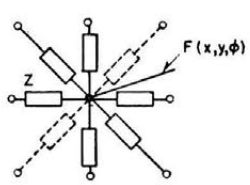

(b) STEADY STATE PROBLEMS, OR TRANSIENT PROBLEMS WITH TIME REPRESENTED AS SPACE VARIABLE. (IF ANY OF FUNCTIONS f ARE DEPENDENT ON ϕ, ITERATIVE METHOD EMPLOYED.)

FIG. 11 ELECTRICAL ANALOGIES FOR MORE GENERAL FORMS OF PARTIAL DIFFERENTIAL EQUATIONS OF HEAT TRANSFER OR FLUID FLOW

in which it is desired to determine the temperature distribution within a gas-turbine rotor being subjected to hot propellant gas at its periphery and cooling gases along one surface. The temperature distribution along its cooling surface is not known. The boundary condition can be specified only in an integral form in terms of the amount of heat being extracted by the cooling gas and the temperature at the location of the propellant gas and at the point of entry of the cooling gas. This type of problem can be solved quite rapidly by trial and error, assuming a temperature gradient, measuring only the heat flow into the gas; readjusting and remeasuring until the desired total heat into the gas is attained. Only one of these calculations is illustrated here.

The analogous circuit used is shown in Fig. 12(*b*). Under steady-state conditions, since the temperature is not varying with time, the heat being stored in each element is constant, and a resistance mesh results. It should be noted that the cells into which the medium has been divided are not of constant size. This will be discussed in more detail later.

The circuit is shown in Fig. 12(*b*), which consists of 116 resistances, representing 58 volume elements and 9 surface heat-transfer coefficients. The time required for calculating these constants was approximately 2 hr. One-half hour was required to set up and check the circuit on the computer. As shown in Fig. 12(*b*), the assumed relative boundary temperatures were obtained as voltages from a bleeder circuit connected to the power supply. Because all points on the rim of the disk were assumed to be at the same temperature, the resistors at the top of Fig. 12(*b*) are shorted out. The resistors near the axis of rotation were omitted because no heat was assumed to flow through them. This condition is of course necessary at the axis itself from the symmetry of the problem.

Tables 2 and 3 list the complete solution to this problem in the form of the temperatures at the centers of each volume element and at the surface from which heat is flowing into the gas. Also given are the rates of heat flow at the boundary surfaces. The flow within the body also could have been measured readily or can be determined from the known resistances and the measured voltage gradients. About 15 min were required for recording the solution. This type of problem can be handled readily by one man. A total of about $2^3/_4$ hr was required for one man to solve this one problem completely. However, it should be emphasized that the greatest amount of time was consumed in determining the analogous circuit and setting it up. The time required for each approximation process was only about 20 min.

Although no tests were made with this specific problem to determine the number of elements required, experience with other problems indicates that the temperature differences obtained should be in error less than 5 or 10 per cent.

Potential Problem; Laplace's Equation. A typical potential problem, Fig. 13, has been chosen to illustrate this application of the computer. Solutions for the problem with different boundary conditions were available, thus offering a convenient way of assessing the accuracy of the solution for varying "coarseness" of the equivalent mesh.

As with all potential problems, this problem can be interpreted in many ways with slight changes in boundary conditions. For example, as one involving the flow of heat from a series of equally spaced cylinders embedded in a conducting medium, flow of heat from a plate with equally spaced semicircular cylindrical bosses, flow of liquid past a series of pipes, etc.

By symmetry considerations, this problem reduces to the one shown in Fig. 14, where in the first problem above, A is a streamline and C is an equipotential, in the second problem A and C constitute an equipotential, and in the third problem A is an equipotential and C is a streamline. Data were taken for the

TABLE 2 (*a*) VOLTAGE DISTRIBUTION IN ELECTRICAL ANALOG OF TURBINE ROTOR—5A-1660, 24 C UNIT. (*b*) TEMPERATURE DISTRIBUTION IN TURBINE ROTOR

Junction no.	Voltage	Temperature, deg F
012	38	944
12	41	986
14	42	1000
16	43.4	1020
18	44.0	1030
20	44.0	1030
022	37	930
22	38	944
24	39	958
26	39.3	962
28	39.7	968
30	39.8	970
032	29	815
32	31	844
34	31.8	855
36	31.8	855
038	18.2	660
38	23.3	734
40	24.5	750
042	16.0	650
42	19.6	680
44	21.0	700
046	14.5	608
46	15.0	614
48	16.2	602
50	18.5	604
52	19.0	672
54	19.7	682
056	14	600
56	15	614
58	16	628
60	18	658
62	18.5	664
64	18.8	670
0114	.2	400
114	7.4	500
66	9.6	537
68	11.4	565
70	13.4	592
72	15.6	625
74	17.7	653
76	18.0	658
78	18.2	660
0116	.2	400
116	7.4	506
80	9.6	537
82	11.5	565
84	13.2	589
86	15.7	624
88	17.2	646
90	17.8	656
92	18.0	558
094	11.8	569
94	13.0	586
96	14.0	600
98	17.7	654
100	17.7	654
102	18.0	658
0104	14.0	600
104	15.5	622
106	17.0	644
108	17.0	644
110	17.2	646
112	17.3	648

NOTE: Temperatures given in the table are temperatures at the labeled junctions, beginning with outside surface next to cooling air.
Conversion between temperature in degrees F and volts is given by $T = 400 + 14.3\ V$.

TABLE 3 HEAT FLOW INTO AND OUT OF 5A-1660 24 C UNIT

(Conversion between heat flow and current is given by 1 milliamp—229 Btu per hr)

	—Heat flow out of surface element—	
Element no.	Milliamperes	Btu per hr
12	12	2750
22	13	2900
32	9	2060
38	13	2900
42	5	1150
46	1	230
56	(*a*)	(*a*)
68	(*a*)	(*a*)
66	(*a*)	(*a*)
	—Heat flow into surface element—	
Element no.	Milliamperes	Btu per hr
2	14	3200
4	12	2750
6	10	2290
8	10	2290
10	8	1830

NOTE: (*a*) Trace of current noted.

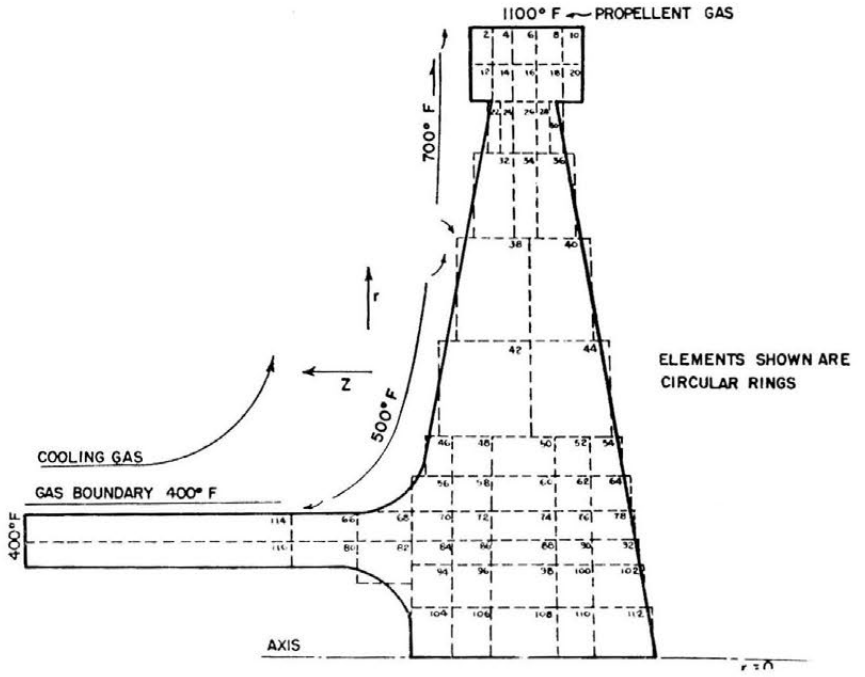

FIG. 12(*a*) TEMPERATURE DISTRIBUTION IN GAS-TURBINE ROTOR; CROSS SECTION OF TURBINE DISK

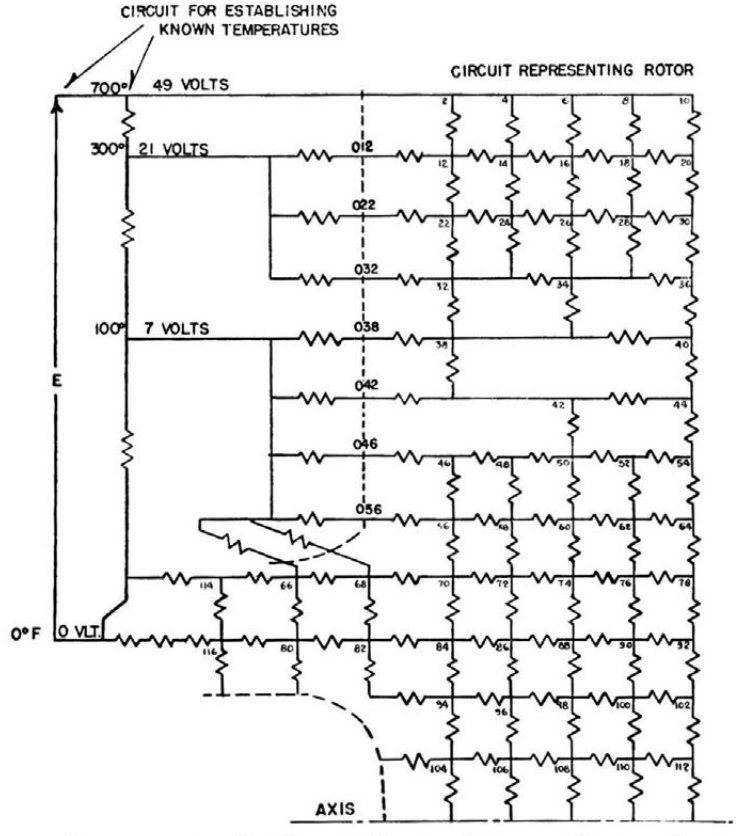

FIG. 12(*b*) TEMPERATURE DISTRIBUTION IN GAS-TURBINE ROTOR; ANALOGOUS ELECTRIC CIRCUIT FOR TURBINE DISK

second and third cases since these were the only ones for which solutions were available.

The two meshes used for this problem are shown in Fig. 14. It should be noted that in rectangular co-ordinates the mesh size need not be constant and must be relatively "fine" only in those regions where the equipotentials have greatest curvature. This usually occurs only near the regions where the boundaries do not coincide with the co-ordinate system chosen.

The correct equipotentials for these problems are shown in Fig. 12. Taking the unit of potential to be the difference between adjacent equipotentials shown, the maximum deviations observed between the analog solution and the known solution are as follows:

	Problem 13(*a*)	Problem 13(*b*)
Fine mesh	0.04 unit	0.07 unit
Coarse mesh	0.08	0.10

Since the potentials were only known to an accuracy of about 0.05 unit, this does not indicate the absolute precision of the fine mesh, but it seems probable that the maximum deviation for the fine mesh is of the order of 0.04 unit. The coarse mesh yields definitely poorer results, but even in this case the results are sufficiently accurate for most engineering applications. It should be remarked that methods are available for improving the accuracy of these solutions, but this was not attempted because of the relatively poor accuracy of the known solutions.

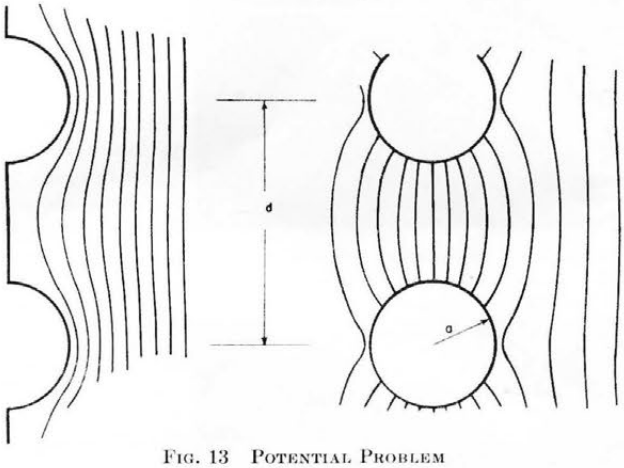

FIG. 13 POTENTIAL PROBLEM

Transient Heat-Flow Problem. The analog circuit can be adapted readily to transient problems as shown in Fig. 6. As an example, the application of a sudden constant temperature rise to the cylindrical surfaces was considered. Solutions for the temperature as a function of time are shown in Fig. 15 for various locations throughout the thermal medium. These points are marked in Fig. 14.

Both problems cited can be set up and solved in a very short time, approximately 3 or 4 hr being required for either of them.

Compressible Fluid Flow. The third interpretation of the foregoing problem is suitable for examining the extension to compressible fluid-flow problems. It was realized that turbulence effects would arise before those of compressibility, thus invalidating this particular solution, but not the process for a practical example. As mentioned before, the solution of the equation of compressible fluid flow must, in general, be achieved by successive approximations, since the mesh impedances are no longer functions only of the cell size, but depend also on the components of velocity at each cell. It appears that three such approximations will give the velocity components for this particular problem with an error less than 5 per cent if the Mach number is not in excess of about 0.75. As the Mach number increases toward unity, more approximations are required. Because of the iterative nature of the solution, such a problem requires 6 to 8 hr for solution.

The solution for this problem, when the maximum velocity (between the tubes) corresponds to a Mach number of 0.73 is shown in Fig. 16. The solution for the incompressible fluid (or low Mach numbers) is also shown for comparison.

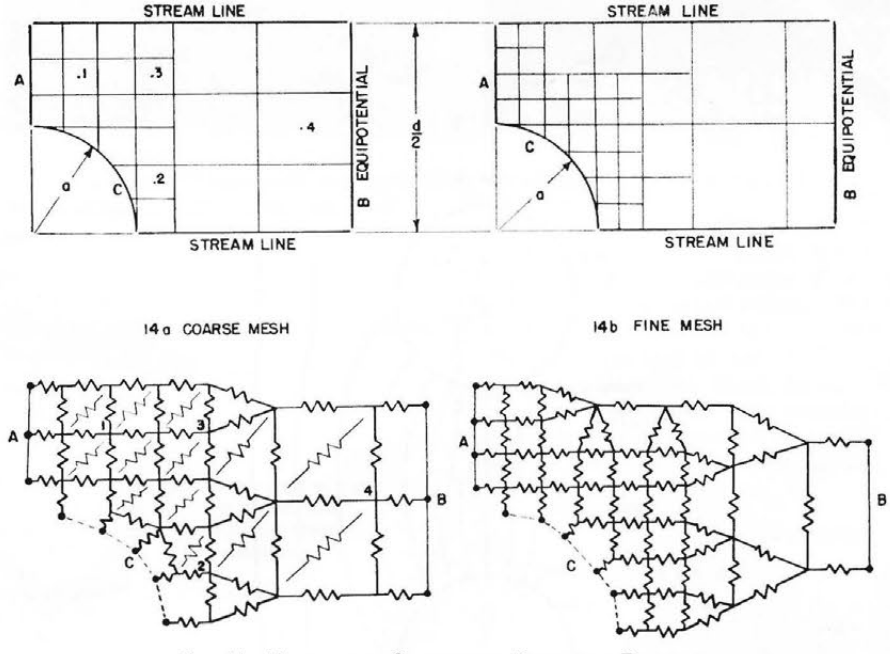

FIG. 14 EQUIVALENT CIRCUIT FOR POTENTIAL PROBLEM

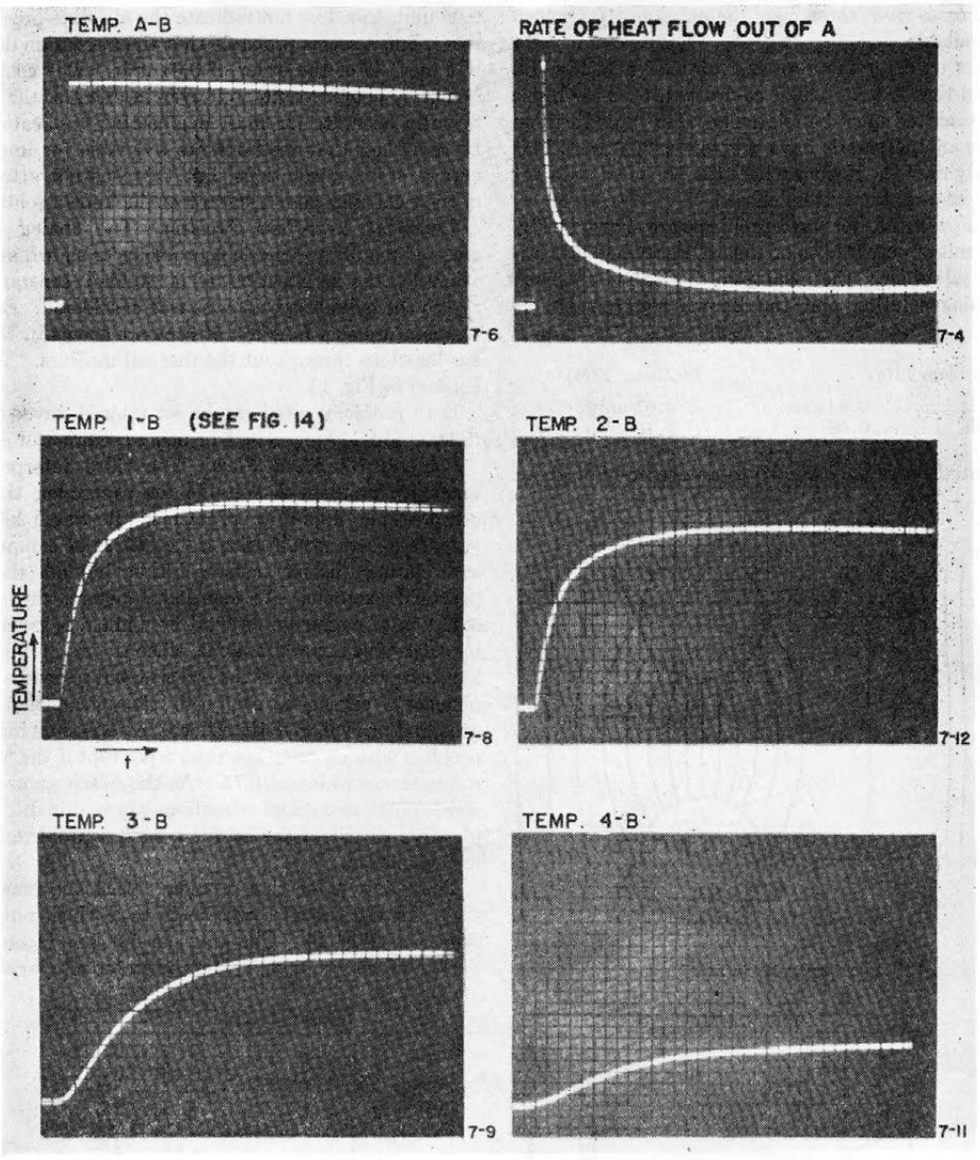

FIG. 15 TRANSIENT HEAT-TRANSFER SOLUTIONS OF POTENTIAL PROBLEM

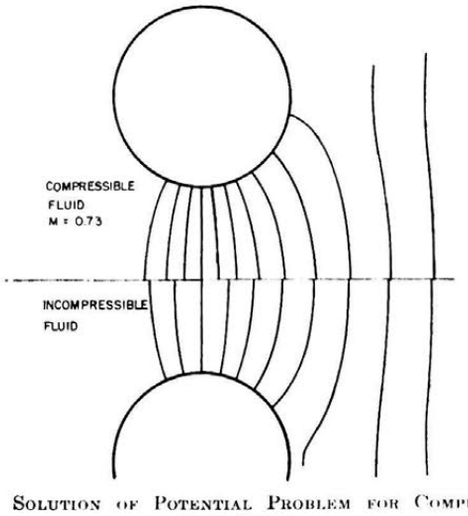

FIG. 16 SOLUTION OF POTENTIAL PROBLEM FOR COMPRESSIBLE FLUID FLOW

Compliance of Elastic Bodies in Contact

By R. D. MINDLIN,[1] NEW YORK, N. Y.

A small tangential force and a small torsional couple are applied across the elliptic contact surface of a pair of elastic bodies which have been pressed together. If there is no slip at the contact surface, considerations of symmetry and continuity lead to the conclusion that there is no change in the normal component of traction across the surface and, aside from warping of the surface, there is no relative displacement of points on the contact surface. The problem is thus reduced to a "problem of the plane" in which the tangential displacements and normal component of traction are given over part of the boundary and the three components of traction are given over the remainder. In the case of the tangential force it is observed that, when Poisson's ratio is zero, the problem is a simple one, in potential theory, which is then generalized by means of a special device. An expression for tangential compliance is found as a linear combination of complete elliptic integrals. In general, the compliance is greater in the direction of the major axis of the elliptic contact surface than in the direction of the minor axis. Both components of tangential compliance increase as Poisson's ratio decreases and become equal when Poisson's ratio is zero. Over the practical range of Poisson's ratio, the tangential compliance is greater than the normal compliance, but never more than twice as great as long as there is no slip. The tangential traction on the contact surface is everywhere parallel to the applied force. Contours of constant traction are ellipses homothetic with the elliptic boundary. The magnitude of the traction rises from one half the average at the center of the contact surface to infinity at the edge. Due to this infinity, there will be slip, the effect of which is studied for the circular contact surface. In the case of the torsional couple, the solution is obtained by generalizing a solution by H. Neuber pertaining to a hyperbolic groove in a twisted shaft. The torsional compliance is expressed in terms of complete elliptic integrals and, for the circular contact area, reduces to that found by E. Reissner and H. F. Sagoci. The resultant traction at a point rises from zero at the center to infinity at the edge of the contact surface, but is constant along and parallel to homothetic ellipses only in the case of the circular contact area.

Notation

Love's notation is used for elastic constants and components of displacement and traction:

μ = modulus of rigidity
σ = Poisson's ratio
$\lambda = 2\mu\sigma/(1 - 2\sigma)$, Lamé's constant
u, v, w = rectangular components of displacement
X_ν, Y_ν, Z_ν = rectangular components of traction at a point on plane surface $z = 0$ of body $z \geqslant 0$.

Additional symbols are defined where they are introduced.

Introduction

Consider two homogeneous, isotropic, elastic bodies in contact at a point, O, in an unstressed state, as shown in Fig. 1(a). The surfaces of the bodies have a common tangent plane and a common normal at O. Let the tangent plane be the plane of x and y, and the normal the z-axis of a rectangular co-ordinate system. If the bodies are pressed together with a force P_z, parallel to Oz, they will come into contact over a small surface in the neighborhood of O, as illustrated in Fig. 1(b). According

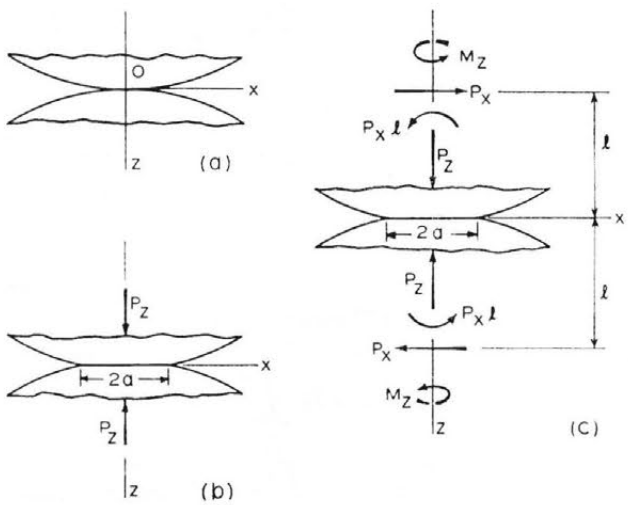

Fig. 1 (a) Bodies in Contact in Unstressed State; (b) Bodies Pressed Together With Hertz Force P_z; (c) Tangential Force P_x and Torsional Couple M_z on Contact Surface of Bodies Pressed Together With Normal Force P_z

to the Hertz theory,[2] the boundary of the contact surface is an ellipse. The theory gives the magnitudes and orientations of the principal axes of the ellipse, the relative approach of the two bodies and the distribution of the normal component of traction across the contact surface. The compliance of the two bodies can be calculated from these results.

Suppose, now, that an additional system of forces is applied to the bodies such that, across the contact surface, one body exerts on the other a small force perpendicular to Oz and a small couple with axis Oz, leaving P_z unchanged, as shown in Fig. 1(c). It is required to find the tangential and torsional compliances of the two bodies.

Hertz Solution

The results of the Hertz solution are[2]

$$p = \frac{3P_z}{2\pi ab}\left(1 - \frac{x^2}{a^2} - \frac{y^2}{b^2}\right)^{1/2} \quad \ldots\ldots\ldots\ldots [1]$$

[1] Professor of Civil Engineering, Columbia University, and Consultant, Bell Telephone Laboratories, Inc. Mem. ASME.

Presented at the National Meeting of the Applied Mechanics Division, Chicago, Ill., June 17–19, 1948, of The American Society of Mechanical Engineers.

Discussion of this paper should be addressed to the Secretary, ASME, 29 West 39th Street, New York, N. Y., and will be accepted until October 10, 1949, for publication at a later date. Discussion received after the closing date will be returned.

Note: Statements and opinions advanced in papers are to be understood as individual expressions of their authors and not those of the Society. Paper No. 48—APM-24.

[2] "Treatise on the Mathematical Theory of Elasticity," by A. E. H. Love, Cambridge University Press, fourth edition, 1927, pp. 193–198.

$$\alpha = \frac{3}{4} P_z(\vartheta_1 + \vartheta_2) \int_0^\infty [(a^2 + \tau)(b^2 + \tau)\tau]^{-1/2} d\tau \ldots [2]$$

$$A = \frac{3}{4} P_z (\vartheta_1 + \vartheta_2) \int_0^\infty (a^2 + \tau)^{-3/2} [(b^2 + \tau)\tau]^{-1/2} d\tau \ldots [3]$$

$$B = \frac{3}{4} P_z (\vartheta_1 + \vartheta_2) \int_0^\infty (b^2 + \tau)^{-3/2} [(a^2 + \tau)\tau]^{-1/2} d\tau \ldots [4]$$

where p is the normal pressure on the contact surface, a and b are the principal semiaxes of the elliptic boundary of the contact surface, α is the relative approach of the two bodies, A and B depend only the shapes and relative orientation of the two bodies in the unstressed state and ϑ_1 and ϑ_2 are elastic constants:

$$\vartheta_1 = \frac{\lambda_1 + 2\mu_1}{4\pi\mu_1(\lambda_1 + \mu_1)} = \frac{1 - \sigma_1}{2\pi\mu_1} \ldots [5]$$

$$\vartheta_2 = \frac{\lambda_2 + 2\mu_2}{4\pi\mu_2(\lambda_2 + \mu_2)} = \frac{1 - \sigma_2}{2\pi\mu_2} \ldots [6]$$

where λ and μ are Lamé's constants and σ is Poisson's ratio, the subscripts referring to the two bodies. Equations [3] and [4] determine a and b, while Equation [2] determines α when a and b are known.

To obtain the normal compliance

$$C_z = \frac{d\alpha}{dP_z} \ldots [7]$$

in a form suitable for quantitative comparison with the tangential compliance, let

$$\tau = a^2 \tan^2 \varphi$$

whereby Equations [2] to [4] are transformed to

$$2b\alpha = 3P_z(\vartheta_1 + \vartheta_2) \int_0^{\frac{\pi}{2}} a^{-1} \Phi^{-1/2} d\varphi \ldots [8]$$

$$2a^2bA = 3P_z(\vartheta_1 + \vartheta_2) \int_0^{\frac{\pi}{2}} a^{-1} \Phi^{-1/2} \cos^2 \varphi \, d\varphi \ldots [9]$$

$$2b^3B = 3P_z(\vartheta_1 + \vartheta_2) \int_0^{\frac{\pi}{2}} a^{-3} \Phi^{-3/2} \cos^2 \varphi \, d\varphi \ldots [10]$$

where

$$\Phi = a^{-2} \cos^2 \varphi + b^{-2} \sin^2 \varphi \ldots [11]$$

The integrals in Equations [8] to [10] are complete elliptic integrals and are functions of a/b only. But a/b is a function of A/B only, as may be seen by dividing Equation [9] by Equation [10]. Since A/B is independent of P_z, each of the integrals is independent of P_z. The calculation of the compliance is now straightforward (remembering that b in Equation [8] is, according to Equation [10], proportional to the cube root of P_z) with the result

$$C_z = (\vartheta_1 + \vartheta_2)\, a^{-1} b^{-1} \int_0^{\frac{\pi}{2}} \Phi^{-1/2} d\varphi \ldots [12]$$

Tangential Force: Boundary Conditions

We shall consider, first, the effect of the tangential force. Taking the axes of x and y to coincide with the principal axes of the elliptic boundary of the contact surface, we resolve the tangential force into components P_x and P_y parallel to x and y, respectively. Without loss of generality, we may consider the effect of P_x alone.

To simplify the establishment of the boundary conditions we impose, temporarily, the following restrictions on the shape, orientation and elastic properties of the unstressed bodies:

1 If R_1, R_1' are, respectively, the maximum and minimum radii of curvature of the unstressed surface, at O, of one body and R_2, R_2' the corresponding radii of the other, then $R_1 = R_2$, $R_1' = R_2'$. (The radii are positive when the centers of curvature are inside the respective bodies.)

2 The normal sections of the two surfaces at O, containing the radii R_1 and R_2, coincide.

3 The two bodies have the same elastic properties.

With these restrictions the contact surface, under the action of P_x alone, is the portion of a plane bounded by an ellipse. We shall designate the contact surface by the symbol S_1 when its elliptic boundary curve is not included and by $\bar{S}_1$, when the boundary curve is included.

The system composed of the two bodies is geometrically and elastically symmetrical with respect to each of the three coordinate planes. To this system is applied the force system P_x, which is symmetrical with respect to the x, z-plane and antisymmetrical with respect to the x, y, and y, z-planes.

If u, v, w are the x, y, z components of displacement due to P_x and if we set (as we may, by Saint Venant's principle)

$$\lim_{x, y, z \to \infty} (u, v, w) = 0 \ldots [13]$$

then, in consequence of the foregoing symmetries, we must have

$$u(x, y, z) = -u(x, y, -z) + \delta_x \ldots [14]$$

$$v(x, y, z) = -v(x, y, -z) \ldots [15]$$

$$w(x, y, z) = w(x, y, -z) \ldots [16]$$

where δ_x is a component of rigid-body displacement, the only one of the six components permissible in view of Equation [13], the x, z-symmetry and the y, z-antisymmetry.

We now assume that there is no slip between the two bodies; i.e., u and v are continuous across $\bar{S}_1$. Setting $z = 0$ in Equations [14] and [15], we find

$$u = \delta_x/2, \; v = 0 \text{ on } \bar{S}_1 \ldots [17]$$

The third boundary condition on $\bar{S}_1$ is found by examining the expression, in terms of displacements, of the normal component of traction, due to P_x, exerted on the plane surface of the body lying in the region $z \geqslant 0$:

$$Z_\nu = -\lambda \left(\frac{\partial u}{\partial x} + \frac{\partial v}{\partial y} \right) - (\lambda + 2\mu) \frac{\partial w}{\partial z} \ldots [18]$$

Using Equation [17], Equation [18] reduces to

$$Z_\nu = -(\lambda + 2\mu) \frac{\partial w}{\partial z} \text{ on } \bar{S}_1 \ldots [19]$$

We now suppose that the two bodies remain in contact and in equilibrium across the contact surface. Then w and Z_ν are continuous across $\bar{S}_1$. The latter requires $\partial w/\partial z$ to be continuous across $\bar{S}_1$, by Equation [19]. Since w and $\partial w/\partial z$ are continuous across $\bar{S}_1$ and, by Equation [16], w is an even function of z, it is necessary that $\partial w/\partial z = 0$ on $\bar{S}_1$. Hence, by Equation [19],

$$Z_\nu = 0 \text{ on } \bar{S}_1 \ldots [20]$$

Considering the body lying in the region $z \geqslant 0$, the part of its boundary outside and in the neighborhood of $\bar{S}_1$ is approximated, as in the Hertz theory, by the plane $z = 0$. This part of the

boundary, designated as S_2, is required to be free of traction. We can now assemble the complete boundary conditions for the body $z \geqslant 0$:

$$u = \delta_x/2, \quad v = Z_\nu = 0 \text{ on } \bar{S}_1 \quad [21]$$

$$X_\nu = Y_\nu = Z_\nu = 0 \text{ on } S_2 \quad [22]$$

$$\lim_{x, y, z \to \infty} (u, v, w) = 0 \quad [23]$$

where

$$X_\nu = -\mu \left(\frac{\partial u}{\partial z} + \frac{\partial w}{\partial x} \right)_{z=0}, \quad Y_\nu = -\mu \left(\frac{\partial v}{\partial z} + \frac{\partial w}{\partial y} \right)_{z=0} \quad [24]$$

It may be seen that the contact surface, as regards displacements in the x, y-plane, shifts uniformly in the x-direction, without change of size or shape. This shift is proportional to P_x since the differential equations of the system are linear. Hence, if there is no slip on the contact surface, the tangential compliance of the two bodies is simply

$$C_x = \delta_x/P_x \quad [25]$$

and the problem of finding it is the problem of finding the value of δ_x corresponding to a given P_x. In the case of slip (see section entitled "Influence of Slip"), the displacement is not simply proportional to P_x because, although the differential equations are linear, the boundary conditions vary with P_x.

We now remove the restrictions imposed on the shapes, relative orientation and elastic properties of the bodies. Elimination of restrictions 1 and 2 introduces a slight warping of the contact surface under P_z alone. Within the limits of the small strain, small rotation theory, this warping may be ignored, as in the Hertz theory. Removal of restriction 3 makes the conditions of continuity of w and vanishing of Z_ν across $\bar{S}_1$ incompatible. In general, to insure continuity of w across the contact surface, there is required a component Z_ν on $\bar{S}_1$. This corresponds to the components X_ν and Y_ν which are ignored in the Hertz theory in the case of bodies of unlike elasticities. We shall adopt the analogous expedient here by retaining the condition $Z_\nu = 0$ on $\bar{S}_1$.

When the elastic properties of the two bodies are different, the relative displacement of S_1 with respect to a distant point in the body $z > 0$ is not the same as the relative displacement with respect to a distant point in the body $z < 0$. Designating the former displacement by $\delta_x'/2$ and the latter by $\delta_x''/2$, the tangential compliances of the two bodies individually are

$$C_x' = \frac{\delta_x'}{2P_x}, \quad C_x'' = \frac{\delta_x''}{2P_x} \quad [26]$$

and the tangential compliance of the two bodies together is

$$C_x = \frac{\delta_x' + \delta_x''}{2P_x} \quad [27]$$

Method of Solution

In the case of the tangential force, we require the solution of the three equations of equilibrium

$$\mu \nabla^2 (u, v, w) + (\lambda + \mu) \left(\frac{\partial}{\partial x}, \frac{\partial}{\partial y}, \frac{\partial}{\partial z} \right) \left(\frac{\partial u}{\partial x} + \frac{\partial v}{\partial y} + \frac{\partial w}{\partial z} \right) = 0 \quad [28]$$

satisfying the boundary conditions given in Equations [21] to [23].

It is convenient to express the components of displacement in terms of the potential functions of Boussinesq and Cerruti in the following two forms:[3]

$$u = \frac{1}{2\pi\mu} \frac{\partial^2 F_1}{\partial z^2} + \frac{\lambda}{4\pi\mu(\lambda + \mu)} \frac{\partial}{\partial x} \left(\frac{\partial F_1}{\partial x} + \frac{\partial G_1}{\partial y} \right) - \frac{1}{4\pi\mu} z \frac{\partial^2}{\partial x \partial z} \left(\frac{\partial F_1}{\partial x} + \frac{\partial G_1}{\partial y} \right) \quad [29]$$

$$v = \frac{1}{2\pi\mu} \frac{\partial^2 G_1}{\partial z^2} + \frac{\lambda}{4\pi\mu(\lambda + \mu)} \frac{\partial}{\partial y} \left(\frac{\partial F_1}{\partial x} + \frac{\partial G_1}{\partial y} \right) - \frac{1}{4\pi\mu} z \frac{\partial^2}{\partial y \partial z} \left(\frac{\partial F_1}{\partial x} + \frac{\partial G_1}{\partial y} \right) \quad [30]$$

$$w = \frac{1}{4\pi(\lambda + \mu)} \frac{\partial}{\partial z} \left(\frac{\partial F_1}{\partial x} + \frac{\partial G_1}{\partial y} \right) - \frac{1}{4\pi\mu} z \frac{\partial^2}{\partial z^2} \left(\frac{\partial F_1}{\partial x} + \frac{\partial G_1}{\partial y} \right) \quad [31]$$

$$F_1 = \int\int X_\nu(\xi, \eta) \Omega d\xi d\eta, \quad G_1 = \int\int Y_\nu(\xi, \eta) \Omega d\xi d\eta \quad [32]$$

$$\Omega = z \log (r + z) - r \quad [33]$$

$$r^2 = (\xi - x)^2 + (\eta - y)^2 + z^2 \quad [34]$$

$$\nabla^2 F_1 = 0, \quad \nabla^2 G_1 = 0 \quad [35]$$

$$u = -\frac{1}{2\pi} \frac{\partial L}{\partial z} + \frac{\lambda + \mu}{2\pi(\lambda + 2\mu)} z \frac{\partial}{\partial x} \left(\frac{\partial L}{\partial x} + \frac{\partial M}{\partial y} \right) \quad [36]$$

$$v = -\frac{1}{2\pi} \frac{\partial M}{\partial z} + \frac{\lambda + \mu}{2\pi(\lambda + 2\mu)} z \frac{\partial}{\partial y} \left(\frac{\partial L}{\partial x} + \frac{\partial M}{\partial y} \right) \quad [37]$$

$$w = -\frac{\mu}{2\pi(\lambda + 2\mu)} \left(\frac{\partial L}{\partial x} + \frac{\partial M}{\partial y} \right) + \frac{\lambda + \mu}{2\pi(\lambda + 2\mu)} z \frac{\partial}{\partial z} \left(\frac{\partial L}{\partial x} + \frac{\partial M}{\partial y} \right) \quad [38]$$

$$L = \int\int \frac{u(\xi, \eta)}{r} d\xi d\eta, \quad M = \int\int \frac{v(\xi, \eta)}{r} d\xi d\eta \quad [39]$$

$$\nabla^2 L = 0, \quad \nabla^2 M = 0 \quad [40]$$

In either form, the equations of equilibrium are satisfied and five of the nine boundary conditions are satisfied, namely, those expressed by Equation [23] and the last of Equations [21] and [22]. If either X_ν, Y_ν or u, v were specified over the whole boundary $z = 0$, the solution of the problem would reduce to the evaluation of the integrals in Equations [32] or [39]. However, in our case, u, v are specified over part of the boundary and X_ν, Y_ν over the remainder.

The four boundary conditions which are yet to be satisfied are expressed in terms of the functions L and M as follows:

$$u = -\frac{1}{2\pi} \frac{\partial L}{\partial z} = \frac{\delta_x'}{2} \text{ on } \bar{S}_1 \quad [41]$$

$$v = -\frac{1}{2\pi} \frac{\partial M}{\partial z} = 0 \text{ on } \bar{S}_1 \quad [42]$$

$$X_\nu = \frac{\mu}{2\pi} \frac{\partial^2 L}{\partial z^2} - \frac{\mu\lambda}{2\pi(\lambda + 2\mu)} \frac{\partial}{\partial x} \left(\frac{\partial L}{\partial x} + \frac{\partial M}{\partial y} \right) = 0 \text{ on } S_2 \quad [43]$$

$$Y_\nu = \frac{\mu}{2\pi} \frac{\partial^2 M}{\partial z^2} - \frac{\mu\lambda}{2\pi(\lambda + 2\mu)} \frac{\partial}{\partial y} \left(\frac{\partial L}{\partial x} + \frac{\partial M}{\partial y} \right) = 0 \text{ on } S_2 \quad [44]$$

We note that, if Poisson's ratio is zero (so that $\lambda = 0$), the boundary conditions reduce to

[3] Reference 2, pp. 242 and 244.

$$\frac{\partial L_0}{\partial z} = -\pi\delta_x', \quad \frac{\partial M_0}{\partial z} = 0 \text{ on } \bar{S}_1 \ldots\ldots\ldots [45]$$

$$\frac{\partial^2 L_0}{\partial z^2} = 0, \quad \frac{\partial^2 M_0}{\partial z^2} = 0 \text{ on } S_2 \ldots\ldots\ldots [46]$$

where L_0 and M_0 are the values of L and M for $\lambda = 0$. Hence, $M_0 = 0$ and the problem of finding $\partial L_0/\partial z$ is the same as that of finding the velocity potential of the irrotational flow of a perfect fluid through a circular or elliptic aperture in an infinite plane; or, it is same as the problem of finding the distribution of electric charge on a circular or elliptic disk whose potential is held constant. The solutions of these problems are known, so that we can find L_0.

To find L and M for an arbitrary value of Poisson's ratio, we assume, tentatively,

$$\frac{\partial L}{\partial x} + \frac{\partial M}{\partial y} = C_1 \frac{\partial L_0}{\partial x} \ldots\ldots\ldots [47]$$

$$\frac{\partial M}{\partial x} - \frac{\partial L}{\partial y} = -C_2 \frac{\partial L_0}{\partial y} \ldots\ldots\ldots [48]$$

where C_1 and C_2 are constants which are equal when λ and M are zero, i.e., the tentative solution reduces to $L = L_0$ when Poisson's ratio is zero.

From Equations [47] and [48] we find, using $\nabla^2 L = 0$,

$$-\frac{\partial^2 L}{\partial z^2} = C_1 \frac{\partial^2 L_0}{\partial x^2} + C_2 \frac{\partial^2 L_0}{\partial y^2} \ldots\ldots\ldots [49]$$

$$-\frac{\partial^2 M}{\partial z^2} = (C_1 - C_2) \frac{\partial^2 L_0}{\partial x \partial y} \ldots\ldots\ldots [50]$$

Substituting Equations [47] and [49] in Equation [43], there results, on $z = 0$,

$$X_\nu = -\frac{C_1\mu(\lambda + \mu)}{\pi(\lambda + 2\mu)} \frac{\partial^2 L_0}{\partial x^2} - \frac{C_2\mu}{2\pi} \frac{\partial^2 L_0}{\partial y^2} \ldots\ldots [51]$$

If we set

$$C_2 = \frac{2(\lambda + \mu)}{(\lambda + 2\mu)} C_1 \ldots\ldots\ldots [52]$$

Equation [51] reduces (using $\nabla^2 L_0 = 0$) to

$$X_\nu = \frac{C_1\mu(\lambda + \mu)}{\pi(\lambda + 2\mu)} \frac{\partial^2 L_0}{\partial z^2} \ldots\ldots\ldots [53]$$

whence, by Equation [46], the boundary condition expressed by Equation [43] is satisfied.

Again, substituting Equations [47] and [50] in Equation [44] and using Equation [52], we find

$$Y_\nu = 0 \ldots\ldots\ldots [54]$$

i.e., Y_ν vanishes over the entire boundary $z = 0$.

To verify the assumed form of solution, it remains to ascertain that the boundary conditions expressed by Equations [41] and [42] are satisfied. These become, using Equations [49], [50], [52], [40], [45],

$$\frac{C_1(3\lambda + 4\mu)}{4\pi(\lambda + 2\mu)} \frac{\partial L_0}{\partial z} + \frac{C_1\lambda}{4\pi(\lambda + 2\mu)} \int \left(\frac{\partial^2 L_0}{\partial x^2} - \frac{\partial^2 L_0}{\partial y^2} \right) dz = -\frac{\delta_x'}{2} \ldots\ldots [55]$$

$$\frac{C_1\lambda}{2\pi(\lambda + 2\mu)} \int \frac{\partial^2 L_0}{\partial x \partial y} dz = 0 \ldots\ldots [56]$$

Since $\partial L_0/\partial z$ is a constant on $\bar{S}_1$, and since the solution must hold for $0 \lessgtr \lambda \lessgtr \infty$, we require

$$\int \left(\frac{\partial^2 L_0}{\partial x^2} - \frac{\partial^2 L_0}{\partial y^2} \right) dz = \text{const on } \bar{S}_1 \ldots\ldots [57]$$

$$\int \frac{\partial^2 L_0}{\partial x \partial y} dz = 0 \text{ on } \bar{S}_1 \ldots\ldots [58]$$

There is an alternative method of testing the displacement boundary conditions. In view of the result $Y_\nu = 0$ over the entire plane $z = 0$, we conclude that, if the assumptions embodied in Equations [47] and [48] are indeed valid, the displacements must be expressible in terms of the function F_1 alone, i.e., we should set $G_1 = 0$ and F_1 proportional to

$$\int\int \frac{\partial^2 L_0}{\partial z^2} \Omega d\xi d\eta \ldots\ldots [59]$$

Then, using Equations [29, 30, 35], the displacement boundary conditions become

$$\frac{3\lambda + 4\mu}{8\pi\mu(\lambda + \mu)} \frac{\partial^2 F_1}{\partial z^2} + \frac{\lambda}{8\pi\mu(\lambda + \mu)} \left(\frac{\partial^2 F_1}{\partial x^2} - \frac{\partial^2 F_1}{\partial y^2} \right) = \frac{\delta_x'}{2} \text{ on } \bar{S}_1 \ldots\ldots [60]$$

$$\frac{\lambda}{4\pi\mu(\lambda + \mu)} \frac{\partial^2 F_1}{\partial x \partial y} = 0 \text{ on } \bar{S}_1 \ldots\ldots [61]$$

Since the boundary conditions must hold for $0 \lessgtr \lambda \lessgtr \infty$, we require

$$\frac{\partial^2 F_1}{\partial x^2} - \frac{\partial^2 F_1}{\partial y^2} = \text{const on } \bar{S}_1 \ldots\ldots [62]$$

$$\frac{\partial^2 F_1}{\partial x \partial y} = 0 \text{ on } \bar{S}_1 \ldots\ldots [63]$$

$$\frac{\partial^2 F_1}{\partial z^2} = \text{const on } \bar{S}_1 \ldots\ldots [64]$$

The method outlined in this section will be applied, first, to the special case of the circular contact area because of its simplicity.

Tangential Force, Circular Contact Area, $\lambda = 0$

Let the boundary of the contact surface be a circle of radius a and let $\rho^2 = x^2 + y^2$. For the case $\lambda = 0$, we must find the harmonic function L_0 satisfying the boundary conditions (see Equations [45, 46])

$$\frac{\partial L_0}{\partial z} = -\pi\delta_x', \ \rho \lessgtr a \ldots\ldots [65]$$

$$\frac{\partial^2 L_0}{\partial z^2} = 0, \ \rho > a \ldots\ldots [66]$$

From the analogous problem in hydrodynamics, we have[4]

$$\frac{\partial L_0}{\partial z} = -2\delta_x' \int_0^\infty e^{-kz} J_0(k\rho) k^{-1} \sin ka \, dk \ldots\ldots [67]$$

where J_0 is the zero order Bessel function of the first kind. Hence

$$L_0 = 2\delta_x' \int_0^\infty e^{-kz} J_0(k\rho) k^{-2} \sin ka \, dk \ldots\ldots [68]$$

Tangential Force, Circular Contact Area, $\lambda \neq 0$

To remove the restriction $\lambda = 0$, we apply the first procedure

[4] "Hydrodynamics," by H. Lamb, sixth edition, Cambridge University Press, 1932, p. 137.

of the section entitled "Method of Solution." We find, from Equation [68],

$$\int\left(\frac{\partial^2 I_0}{\partial x^2}-\frac{\partial^2 I_0}{\partial y^2}\right)dz = -2\delta_x'\cos 2\theta\int_0^\infty e^{-kz}J_2(k\rho)k^{-1}\sin ka\,dk \quad [69]$$

$$\int\frac{\partial^2 I_0}{\partial x\partial y}dz = -\delta_x'\sin 2\theta\int_0^\infty e^{-kz}J_2(k\rho)k^{-1}\sin ka\,dk \quad [70]$$

where $\theta=\tan^{-1}(y/x)$. Now[5]

$$\int_0^\infty J_2(k\rho)k^{-1}\sin ka\,dk = \left\{\begin{array}{l}0,\ \rho\leqslant a,\\ a(\rho^2-a^2)^{1/2}/\rho^2,\ \rho\geqslant a\end{array}\right\} \quad [71]$$

Hence Equations [57] and [58] are satisfied.

To evaluate the constant C_1, we substitute Equations [65, 69, 71] in Equation [55], with the result

$$C_1=\frac{2(\lambda+2\mu)}{(3\lambda+4\mu)} \quad [72]$$

The tangential traction over the contact surface is found by inserting the values of C_1 and I_0 from Equations [72] and [68] into Equation [53]. Noting that

$$\left.\frac{\partial^2 I_0}{\partial z^2}\right]_{z=0}=2\delta_x'\int_0^\infty J_0(k\rho)\sin ka\,dk = \left\{\begin{array}{l}2\delta_x'(a^2-\rho^2)^{-1/2},\ \rho<a\\ \infty,\ \rho=a\\ 0,\ \rho>a\end{array}\right\} \quad [73]$$

we find

$$X_\nu=\frac{4\mu(\lambda+\mu)\delta_x'}{\pi(3\lambda+4\mu)}(a^2-\rho^2)^{-1/2},\ \rho<a \quad [74]$$

The relation between the tangential force and the displacement is found from

$$P_x=\int_0^a\int_0^{2\pi}X_\nu\rho\,d\rho\,d\theta=\frac{8\mu(\lambda+\mu)a\delta_x'}{3\lambda+4\mu} \quad [75]$$

so that

$$X_\nu=\frac{P_x}{2\pi a}(a^2-\rho^2)^{-1/2},\ \rho<a \quad [76]$$

We see that, in the case of a tangential force across a circular contact area, the tangential traction is everywhere parallel to the direction of the applied force. Contours of constant tangential traction are concentric circles. The magnitude of the traction rises from one-half the average at the center to infinity at the edge.

The tangential compliance of one body is

$$C_x'=\frac{\delta_x'}{2P_x}=\frac{3\lambda+4\mu}{16\mu(\lambda+\mu)a}=\frac{2-\sigma}{8\mu a} \quad [77]$$

The tangential compliance of two bodies, with unlike elastic constants, is

$$C_x=\frac{1}{8a}\left(\frac{2-\sigma_1}{\mu_1}+\frac{2-\sigma_2}{\mu_2}\right) \quad [78]$$

It is interesting to notice that all of the results of this section can be extracted from a solution by H. Neuber[6] for the stress concentration at a hyperbolic notch.

Influence of Slip

A practical feature of the foregoing solution which requires additional study is the infinite traction at the edge of the contact surface. Presumably, the tangential component of traction cannot exceed the product of the coefficient of friction f and the normal component of traction p. Thus, for the circular contact area, we should have, from Equation [1],

$$X_\nu=\frac{3fP_z}{2\pi a^2}\left(1-\frac{\rho^2}{a^2}\right)^{1/2},\ a'\leqslant\rho\leqslant a \quad [79]$$

$$X_\nu\leqslant\frac{3fP_z}{2\pi a^2}\left(1-\frac{\rho^2}{a^2}\right)^{1/2},\ \rho\leqslant a' \quad [80]$$

$$Y_\nu=0 \quad [81]$$

where we have assumed that slip has penetrated from the outer radius a to an inner radius a' and that, in the included annulus, the tangential traction remains at its greatest possible value fp.

If slip has just progressed over the entire contact surface, so that Equation [79] holds throughout, we may calculate the corresponding tangential displacements by substituting Equation [79] into Equation [32], and the combination into Equations [29] and [30], with the results

$$8\pi^2\mu a^2 u=3fP_z\int_0^{\omega_0}\int_0^{2\pi}(2-\sigma+\sigma\cos 2\varphi)\Lambda_0\,d\omega\,d\varphi \quad [82]$$

$$8\pi^2\mu a^2 v=3\sigma fP_z\int_0^{\omega_0}\int_0^{2\pi}\Lambda_0\sin 2\varphi\,d\omega\,d\varphi \quad [83]$$

where $\Lambda_0=(-\Phi_0\omega^2-2\Psi_0\omega-\Gamma_0)^{1/2}$ and

$$\omega=[(\xi-x)^2+(\eta-y)^2]^{1/2}=-\Omega_{z=0} \quad [84]$$

$$\varphi=\tan^{-1}\frac{\eta-y}{\xi-x} \quad [85]$$

$$\Phi_0=a^{-2} \quad [86]$$

$$\Psi_0=(x\cos\varphi+y\sin\varphi)a^{-2} \quad [87]$$

$$\Gamma_0=(\rho^2-a^2)a^{-2} \quad [88]$$

and ω_0 is the distance from the point (x, y) to the circle, i.e.,

$$\omega_0=\left(-\Psi_0+\sqrt{\Psi_0^2-\Phi_0\Gamma_0}\right)\Phi_0^{-1} \quad [89]$$

Considering the surface integral in Equation [83], and integrating with respect to ω, we arrive at

$$\int_0^{2\pi}\frac{(\Psi_0^2-\Phi_0\Gamma_0)\pi}{4\Phi_0^{3/2}}\sin 2\varphi\,d\varphi - \int_0^{2\pi}\left[\frac{\Psi_0(-\Gamma_0)^{1/2}}{2\Phi_0}\right]\sin 2\varphi\,d\varphi - \int_0^{2\pi}\left[\frac{\Psi_0^2-\Phi_0\Gamma_0}{2\Phi_0^{3/2}}\sin^{-1}\frac{\Psi_0}{\sqrt{\Psi_0^2-\Phi_0\Gamma_0}}\right]\sin 2\varphi\,d\varphi$$

We note that the algebraic signs of the quantities in brackets change if we substitute $\varphi-\pi$ for φ. Hence, the integrals of the bracketed terms, over the interval 2π, vanish. The same terms occur in Equation [82]. The remaining integrations in Equations [82] and [83] are straightforward, and we find

[5] "Treatise on the Theory of Bessel Functions," by G. N. Watson, Cambridge University Press, 1922, p. 405.

[6] "Kerbspannungslehre," by H. Neuber, Julius Springer, Berlin, Germany, 1937, pp. 85–90.

$$64\ \mu a^3 u = 3fP_z[2(2-\sigma)(2a^2-\rho^2) + \sigma\rho^2\cos 2\theta] \quad [90]$$

$$64\ \mu a^3 v = 3fP_z\,\sigma\rho^2 \sin 2\theta \quad [91]$$

If we now consider a distribution of traction

$$X_\nu = -\frac{3fP_z Q}{2\pi a'^2}\left(1-\frac{\rho^2}{a'^2}\right)^{1/2}, \quad \rho \leqslant a' \quad [92]$$

$$Y_\nu = 0 \quad [93]$$

where Q is a constant, we find corresponding displacements u' and v':

$$64\mu a'^3 u' = -3QfP_z[2(2-\sigma)(2a'^2-\rho^2) + \sigma\rho^2\cos 2\theta] \quad [94]$$

$$64\ \mu a'^3 v' = -3QfP_z\,\sigma\rho^2 \sin 2\theta \quad [95]$$

If, now, we set $Q = a'^3/a^3$ and add the two sets of displacements we have

$$u + u' = \frac{3fP_z(2-\sigma)}{16\ \mu a}\left(1-\frac{a'^2}{a^2}\right), \quad \rho \leqslant a' \quad [96]$$

$$v + v' = 0, \quad \rho \leqslant a' \quad [97]$$

Hence, the system of surface tractions[7]

$$X_\nu = \frac{3fP_z}{2\pi a^2}\left(1-\frac{\rho^2}{a^2}\right)^{1/2}, \quad a' \leqslant \rho \leqslant a \quad [98]$$

$$X_\nu = \frac{3fP_z}{2\pi a^2}\left(1-\frac{\rho^2}{a^2}\right)^{1/2} - \frac{3fP_z a'}{2\pi a^3}\left(1-\frac{\rho^2}{a'^2}\right)^{1/2}, \quad \rho \leqslant a' \quad [99]$$

produces displacements which satisfy the conditions of no slip within the circle of radius a'. To find a' we calculate

$$P_x = \int_0^a \int_0^{2\pi} X_\nu\,\rho\,d\rho\,d\theta$$

$$= fP_z\left(1-\frac{a'^3}{a^3}\right) \quad [100]$$

whence

$$a' = a\left(1-\frac{P_x}{fP_z}\right)^{1/3} \quad [101]$$

The distribution of traction, represented by Equations [98] and [99], is illustrated in Fig. 2 for the case $P_x/fP_z = 0.3$.

To find the compliance, first eliminate a' between Equations [101] and [96] and obtain

$$u + u' = \frac{3fP_z(2-\sigma)}{16\mu a}\left[1-\left(1-\frac{P_x}{fP_z}\right)^{2/3}\right] \quad [102]$$

Then the tangential compliance of one body is

$$C_s' = \frac{d(u+u')}{dP_x} = \frac{2-\sigma}{8\mu a}\left(1-\frac{P_x}{fP_z}\right)^{-1/3} \quad [103]$$

This is to be compared the with compliance without slip given in Equation [77]. The ratio

$$\frac{C_x'}{C_s'} = \left(1-\frac{P_x}{fP_z}\right)^{-1/3} \quad [104]$$

is plotted in Fig. 3, which shows the range over which the compliance calculated on the assumption of no slip is useful. For small ratios of P_x to fP_z the error is small. The remainder of this paper is confined to the case of no slip.

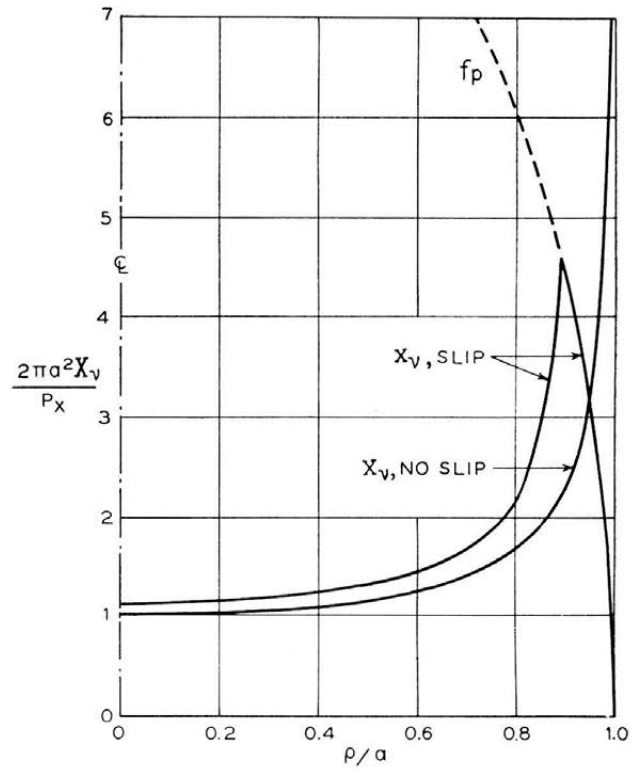

FIG. 2 DISTRIBUTION OF TANGENTIAL TRACTION X_ν DUE TO A TANGENTIAL FORCE P_x ACROSS A CIRCULAR CONTACT AREA (Curve marked "X_ν, SLIP" is for $P_x/fP_z = 0.3$.)

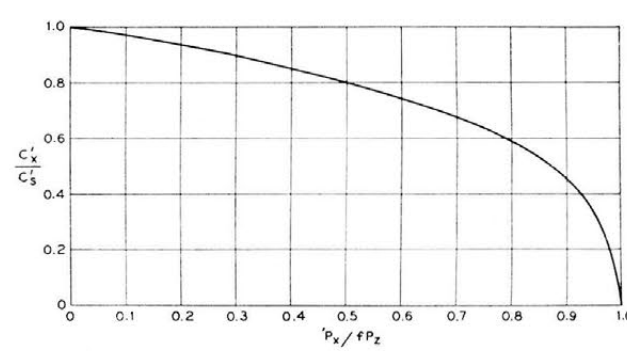

FIG. 3 RATIO OF INITIAL TANGENTIAL COMPLIANCE C_x' TO TANGENTIAL COMPLIANCE WITH SLIP C_s' FOR CIRCULAR CONTACT AREA

TANGENTIAL FORCE, ELLIPTIC CONTACT AREA

As observed in the section entitled "Method of Solution," when $\lambda = 0$ and the contact area is bounded by an ellipse, the problem of finding $\partial L_0/\partial z$ is identical with that of finding the velocity potential of the irrotational flow of a perfect fluid through an elliptic aperture in an infinite plane. From the solution[8] of that problem we need only the result that $\partial^2 L_0/\partial z^2$ is proportional to

$$(1-a^{-2}x^2-b^{-2}y^2)^{-1/2} \quad [105]$$

on $\bar{S}_1$ and vanishes on S_2.

Applying the alternative procedure for $\lambda \neq 0$, described at the

[7] Dr. Stewart Way has called the author's attention to a paper by C. Cattaneo, "Sul contatto di due corpi elastici: distribuzione locale degli sforzi," Accademia dei Lincei, Rendiconti, series 6, vol. XXVII, 1938 pp. 342–348, 434–436, 474–478, in which formulas, corresponding to Equations [98] and [99], are derived for the elliptic contact surface.

[8] Reference 4, p. 151.

end of the section entitled "Method of Solution," we take

$$X_\nu = D(1 - a^{-2}x^2 - b^{-2}y^2)^{-1/2}, \quad Y_\nu = 0, \text{ on } \bar{S}_1 \ldots [106]$$

$$X_\nu = Y_\nu = 0, \text{ on } S_2 \ldots [107]$$

where D is a constant, determined by the condition

$$P_x = \int\int_{S_1} X_\nu \, dx \, dy \ldots [108]$$

To evaluate the integral in Equation [108] let

$$x = \rho \cos\theta, \quad y = \rho \sin\theta \ldots [109]$$

Then

$$P_x = D \int_0^{\rho_1} \int_0^{2\pi} \frac{\rho \, d\rho \, d\theta}{(1 - \Theta \rho^2)^{1/2}} \ldots [110]$$

where

$$\Theta = a^{-2}\cos^2\theta + b^{-2}\sin^2\theta \ldots [111]$$

and ρ_1 is the distance from the origin of x and y to a point on the ellipse, i.e.,

$$\rho_1 = \Theta^{-1/2} \ldots [112]$$

The integration then proceeds without difficulty, with the result

$$P_x = 2\pi abD \ldots [113]$$

Subject to verification of the displacement boundary conditions, we conclude that the tangential traction on the contact surface is everywhere parallel to the applied tangential force. Contours of constant tangential traction are homothetic ellipses, i.e., geometrically similar, and with principal axes parallel to the elliptic boundary. The magnitude of the traction rises from one half the average at the center to infinity at the edge.

It remains to test the displacement boundary conditions, as given in Equations [62] to [64], and to determine δ_x'. To do this we have to find the values of the second derivatives of

$$F_1 = \int\int_{\bar{S}_1} X_\nu(\xi, \eta)\Omega \, d\xi \, d\eta \ldots [114]$$

on $\bar{S}_1$.

As before, let

$$\omega = [(\xi - x)^2 + (\eta - y)^2]^{1/2} = \Omega_{z=0} \ldots [115]$$

$$\xi - x = \omega \cos\varphi \ldots [116]$$

$$\eta - y = \omega \sin\varphi \ldots [117]$$

Then

$$X_\nu = D(-\Phi\omega^2 - 2\Psi\omega - \Gamma)^{-1/2} \ldots [118]$$

where

$$\Phi = a^{-2}\cos^2\varphi + b^{-2}\sin^2\varphi \ldots [119]$$

$$\Psi = a^{-2}x\cos\varphi + b^{-2}y\sin\varphi \ldots [120]$$

$$\Gamma = a^{-2}x^2 + b^{-2}y^2 - 1 \ldots [121]$$

Accordingly, on $\bar{S}_1$,

$$\frac{\partial^2 F_1}{\partial x^2} - \frac{\partial^2 F_1}{\partial y^2} = D \int_0^{\omega_1} \int_0^{2\pi} \frac{\cos 2\varphi \, d\omega d\varphi}{(-\Phi\omega^2 - 2\Psi\omega - \Gamma)^{1/2}} \ldots [122]$$

$$\frac{\partial^2 F_1}{\partial x \partial y} = \frac{D}{2} \int_0^{\omega_1} \int_0^{2\pi} \frac{\sin 2\varphi \, d\omega d\varphi}{(-\Phi\omega^2 - 2\Psi\omega - \Gamma)^{1/2}} \ldots [123]$$

$$\frac{\partial^2 F_1}{\partial z^2} = D \int_0^{\omega_1} \int_0^{2\pi} \frac{d\omega d\varphi}{(-\Phi\omega^2 - 2\Psi\omega - \Gamma)^{1/2}} \ldots [124]$$

where ω_1 is the distance from the point (x, y) to a point on the ellipse. This distance is expressed in terms of φ by noting that, on the ellipse,

$$a^{-2}\xi^2 + b^{-2}\eta^2 - 1 = 0 \ldots [125]$$

or

$$\Phi\omega^2 + 2\Psi\omega + \Gamma = 0 \ldots [126]$$

The significant root of Equation [126] is

$$\omega_1 = (-\Psi + \sqrt{\Psi^2 - \Phi\Gamma})\Phi^{-1} \ldots [127]$$

Returning to Equation [122] and performing the integration with respect to ω, we find

$$\frac{\partial^2 F_1}{\partial x^2} - \frac{\partial^2 F_1}{\partial y^2} = D \int_0^{2\pi} \left[\Phi^{-1/2} \sin^{-1} \frac{\Phi\omega + \Psi}{\sqrt{\Psi^2 - \Phi\Gamma}} \right]_0^{\omega_1} \cos 2\varphi \, d\varphi$$

$$= \frac{\pi D}{2} \int_0^{2\pi} \Phi^{-1/2} \cos 2\varphi \, d\varphi$$

$$- D \int_0^{2\pi} \Phi^{-1/2} \cos 2\varphi \sin^{-1} \frac{\Psi}{\sqrt{\Psi^2 - \Phi\Gamma}} \, d\varphi. \quad [128]$$

In the second integral in Equation [128], we note that

$$\Phi(\varphi) = \Phi(\varphi + \pi)$$

$$\Psi(\varphi) = -\Psi(\varphi + \pi)$$

$$\cos 2\varphi = \cos 2(\varphi + \pi)$$

and Γ is independent of φ. Hence, the integrand reverses sign on substituting $\varphi + \pi$ for φ. Accordingly, the second integral of Equation [128] vanishes and we have

$$\left.\begin{aligned} \frac{\partial^2 F_1}{\partial x^2} - \frac{\partial^2 F_1}{\partial y^2} &= \frac{\pi D}{2} \int_0^{2\pi} \Phi^{-1/2} \cos 2\varphi \, d\varphi \\ &= 2\pi D \int_0^{\frac{\pi}{2}} \Phi^{-1/2} \cos 2\varphi \, d\varphi \\ &= \text{const} \end{aligned}\right\} \ldots [129]$$

so that Equation [62] is satisfied.

Similarly, from Equation [123],

$$\frac{\partial^2 F_1}{\partial x \partial y} = \frac{\pi D}{4} \int_0^{2\pi} \Phi^{-1/2} \sin 2\varphi \, d\varphi$$

$$- \frac{D}{2} \int_0^{2\pi} \Phi^{-1/2} \sin 2\varphi \sin^{-1} \frac{\Psi}{\sqrt{\Psi^2 - \Phi\Gamma}} \, d\varphi \ldots [130]$$

Since $\sin 2\varphi = \sin 2(\varphi + \pi)$ the second integral in Equation [130] may be shown to vanish for the same reason that the second integral in Equation [128] vanished. Regarding the first integral in Equation [130], calling the integrand $g(\varphi)$, we note

$$g(\varphi) = g(\varphi + \pi)$$

and

$$\int_0^{2\pi} g(\varphi) d\varphi = 2 \int_0^{\pi} g(\varphi) \, d\varphi$$

$$= 2 \int_0^{\frac{\pi}{2}} g(\varphi) \, d\varphi + 2 \int_{\frac{\pi}{2}}^{\pi} g(\varphi) \, d\varphi$$

But

$$\sin 2\varphi = -\sin 2(\pi - \varphi)$$

$$\Phi(\varphi) = \Phi(\pi - \varphi)$$

Hence

$$\int_{\frac{\pi}{2}}^{\pi} g(\varphi)d\varphi = -\int_0^{\frac{\pi}{2}} g(\varphi)d\varphi$$

and, therefore,

$$\int_0^{2\pi} g(\varphi)d\varphi = 0$$

Thus

$$\frac{\partial^2 F_1}{\partial x \partial y} = 0$$

on $\bar{S}_1$ and Equation [63] is satisfied.

Finally

$$\left.\begin{aligned}\frac{\partial^2 F_1}{\partial z^2} &= \frac{\pi D}{2}\int_0^{2\pi} \Phi^{-1/2}\,d\varphi \\ &\quad - D\int_0^{2\pi} \Phi^{-1/2}\sin^{-1}\frac{\Psi}{\sqrt{\Psi^2 - \Phi\Gamma}}\,d\varphi \\ &= 2\pi D\int_0^{\frac{\pi}{2}} \Phi^{-1/2}\,d\varphi \\ &= \text{const}\end{aligned}\right\} \quad [131]$$

so that the last displacement boundary condition, given in Equation [64], is satisfied.

To find the displacement δ_x' due to the force P_x we substitute the results expressed by Equations [129] and [131] into Equation [60] and use Equation [113] to obtain

$$2\pi ab\mu_1\delta_x' = P_x(2-\sigma_1)\int_0^{\frac{\pi}{2}} \Phi^{-1/2}\,d\varphi + P_x\sigma_1\int_0^{\frac{\pi}{2}} \Phi^{-1/2}\cos 2\varphi\;d\varphi \quad [132]$$

in which μ has been replaced by μ_1 and λ by $2\mu_1\sigma_1/(1-2\sigma_1)$.

Formulas for Tangential Compliance

To find numerical values of the tangential compliance from Equation [132], it is advisable to transform the integrals in that equation to forms that are tabulated. For the first integral we write

$$\int_0^{\frac{\pi}{2}} \Phi^{-1/2}\,d\varphi = \int_0^{\frac{\pi}{2}} \frac{d\varphi}{\sqrt{a^{-2}\cos^2\varphi + b^{-2}\sin^2\varphi}} = \begin{cases} a\displaystyle\int_0^{\frac{\pi}{2}} \frac{d\varphi}{\sqrt{1-k^2\sin^2\varphi}}, & a < b \\ a\pi/2, & a = b \\ b\displaystyle\int_0^{\frac{\pi}{2}} \frac{d\varphi}{\sqrt{1-k_1^2\sin^2\varphi}}, & a > b \end{cases} \quad [133]$$

where

$$k^2 = 1 - \frac{a^2}{b^2}, \quad k_1^2 = 1 - \frac{b^2}{a^2} \quad [134]$$

Hence

$$\int_0^{\frac{\pi}{2}} \Phi^{-1/2}\,d\varphi = \begin{cases} a\mathbf{K}, & a < b \\ a\pi/2, & a = b \\ b\mathbf{K}_1, & a > b \end{cases} \quad [135]$$

where $\mathbf{K}$ and $\mathbf{K}_1$ are the complete elliptic integrals of the first kind of arguments $(\pi/2, k)$ and $(\pi/2, k_1)$ respectively.

For the second integral, considering first the case $a < b$, we write

$$\int_0^{\frac{\pi}{2}} \Phi^{-1/2}\cos 2\varphi\,d\varphi = a\int_0^{\frac{\pi}{2}} \frac{(1-2\sin^2\varphi)d\varphi}{\sqrt{1-k^2\sin^2\varphi}} = a\mathbf{K} - 2a\int_0^{\frac{\pi}{2}} \frac{\sin^2\varphi d\varphi}{\sqrt{1-k^2\sin^2\varphi}}$$

Now

$$\int_0^{\frac{\pi}{2}} \frac{\sin^2\varphi\,d\varphi}{\sqrt{1-k^2\sin^2\varphi}} = \frac{1}{k^2}\int_0^{\frac{\pi}{2}} \frac{d\varphi}{\sqrt{1-k^2\sin^2\varphi}} - \frac{1}{k^2}\int_0^{\frac{\pi}{2}} \sqrt{1-k^2\sin^2\varphi}\,d\varphi = k^{-2}(\mathbf{K}-\mathbf{E})$$

where $\mathbf{E}$ is the complete elliptic integral of the second kind, of argument $(\pi/2, k)$. Hence

$$\int_0^{\frac{\pi}{2}} \Phi^{-1/2}\cos 2\varphi\,d\varphi = -\frac{a}{k}\left[\left(\frac{2}{k} - k\right)\mathbf{K} - \frac{2}{k}\mathbf{E}\right], a < b \quad [136]$$

The expression in brackets in Equation [136] appears in electromagnetic theory as a quantity proportional to the mutual inductance of a pair of coaxial circular currents. An elaborate tabulation of the quantity

$$\mathbf{N} = 4\pi\left[\left(\frac{2}{k} - k\right)\mathbf{K} - \frac{2}{k}\mathbf{E}\right] \quad [137]$$

has been made by Nagaoka and Sakurai.[9]

For the case $a > b$, we replace φ by $\pi/2 - \varphi$ in the second integral of Equation [132] and find, by a similar procedure

$$\int_0^{\frac{\pi}{2}} \Phi^{-1/2}\cos 2\varphi\,d\varphi = \frac{b}{k_1}\left[\left(\frac{2}{k_1} - k_1\right)\mathbf{K}_1 - \frac{2}{k_1}\mathbf{E}_1\right], a > b \quad [138]$$

where $\mathbf{E}_1$ is the complete elliptic integral of the second kind of argument $(\pi/2, k_1)$.

The difference in algebraic sign between Equation [138] and Equation [136] arises from the fact that

$$\cos 2\varphi = -\cos 2\left(\frac{\pi}{2} - \varphi\right)$$

We find, then,

$$\int_0^{\frac{\pi}{2}} \Phi^{-1/2}\cos 2\varphi\,d\varphi = \begin{cases} -a\mathbf{N}/4\pi k, & a < b \\ 0, & a = b \\ b\,\mathbf{N}_1/4\pi k_1, & a > b \end{cases} \quad [139]$$

[9] "Table No. 2," by H. Nagaoka and S. Sakurai, Scientific Papers of the Institute of Physical and Chemical Research, Tokyo, Sept., 1927. See also Table No. 1, Dec., 1922, for $\mathbf{K}$ and $\mathbf{E}$.

Inserting the expressions given in Equations [136] and [139] into Equation [132], we find for $a < b$:

$$\frac{2\mu_1 b\delta_x'}{P_x} = \frac{2-\sigma_1}{2}\left[\frac{2\mathbf{K}}{\pi} - \frac{\sigma_1}{2\pi^2(2-\sigma_1)}\frac{\mathbf{N}}{k}\right] \quad [140]$$

for $a = b$:

$$\frac{2\mu_1 a\delta_x'}{P_x} = \frac{2-\sigma_1}{2} \quad [141]$$

and for $a > b$:

$$\frac{2\mu_1 a\delta_x'}{P_x} = \frac{2-\sigma_1}{2}\left[\frac{2\mathbf{K}_1}{\pi} + \frac{\sigma_1}{2\pi^2(2-\sigma_1)}\frac{\mathbf{N}_1}{k_1}\right] \quad [142]$$

The last three equations express the ratio of the tangential compliance to the tangential compliance of a body with Poisson's ratio zero and a circular contact area of diameter equal to the maximum diameter of the elliptic contact area. This ratio is plotted as the ordinate in Fig. 4, using Nagaoka and Sakurai's tables.

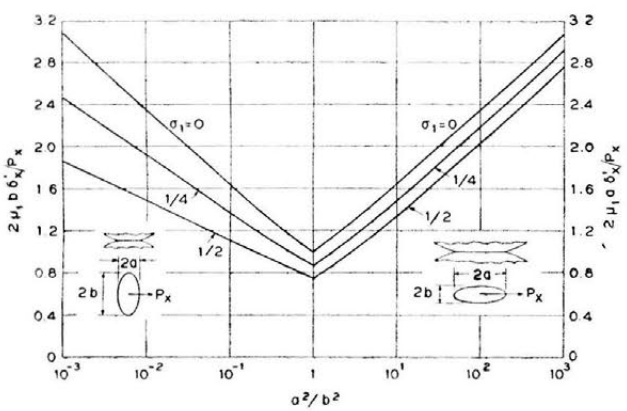

a, b = principal semi-axes of elliptic contact surface
P_x = force in direction of axis a
δ_x' = relative displacement in direction a
μ_1 = modulus of rigidity
σ_1 = Poisson's ratio

FIG. 4 INITIAL TANGENTIAL COMPLIANCE OF ELASTIC BODIES IN CONTACT

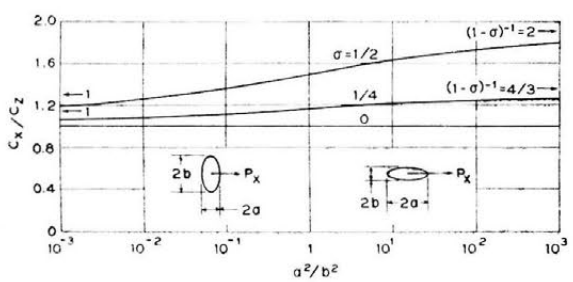

FIG. 5 RATIO OF INITIAL TANGENTIAL COMPLIANCE C_x TO NORMAL COMPLIANCE C_z OF BODIES WITH LIKE ELASTIC CONSTANTS

It may be seen that the tangential compliance decreases as Poisson's ratio increases. When $\sigma = 0$, the tangential compliance is isotropic, but when $0 < \sigma \lessapprox 1/2$ the compliance in the direction of the major axis is greater than the compliance in the direction of the minor axis. Hence, if the tangential force is not parallel to a principal axis of the ellipse, the displacement is parallel to the force only if $\sigma = 0$.

RATIO OF TANGENTIAL TO NORMAL COMPLIANCE

The interesting features of the ratio of the tangential to the normal compliance are illustrated adequately by examining the case in which the two bodies have the same elastic properties. Then, from Equation [12],

$$C_z = \begin{cases} (1-\sigma)\,\mathbf{K}/\pi\mu b, & a < b \\ (1-\sigma)/2\mu a, & a = b \\ (1-\sigma)\,\mathbf{K}_1/\pi\mu a, & a > b \end{cases} \quad [143]$$

Hence, from Equations [143] and [140] to [142],

$$\frac{C_x}{C_z} = \begin{cases} \dfrac{\pi(2-\sigma)}{4(1-\sigma)}\cdot\dfrac{1}{\mathbf{K}}\left[\dfrac{2\mathbf{K}}{\pi} - \dfrac{\sigma}{2\pi^2(2-\sigma)}\dfrac{\mathbf{N}}{k}\right], & a < b \\ \dfrac{2-\sigma}{2(1-\sigma)}, & a = b \\ \dfrac{\pi(2-\sigma)}{4(1-\sigma)}\cdot\dfrac{1}{\mathbf{K}_1}\left[\dfrac{2\mathbf{K}_1}{\pi} + \dfrac{\sigma}{2\pi^2(2-\sigma)}\dfrac{\mathbf{N}_1}{k_1}\right], & a > b \end{cases}$$

To plot this ratio it is only necessary to divide the ordinates in Fig. 4 by $2(1-\sigma)\mathbf{K}/\pi$, for $a < b$ and by $2(1-\sigma)\,\mathbf{K}_1/\pi$ for $a > b$. The results are plotted in Fig. 5. Several limiting cases of interest are as follows:

For $\sigma = 0$, $\dfrac{C_x}{C_z} = 1$

For $\dfrac{a}{b} \to 0$, $\dfrac{C_x}{C_z} = 1$

For $\dfrac{a}{b} \to \infty$, $\dfrac{C_x}{C_z} = \dfrac{1}{1-\sigma}$

For $\dfrac{a}{b} = 1$, $\dfrac{C_x}{C_z} = \dfrac{2-\sigma}{2(1-\sigma)}$

It may be seen that the tangential compliance, over the practical range $0 < \sigma < 1/2$, is always greater than the normal compliance, but never more than twice as great as long as there is no slip.

TWISTING COUPLE: BOUNDARY CONDITIONS

By considerations of symmetry and continuity similar to those in the section entitled "Tangential Force: Boundary Conditions," it may be shown that, in the case of a moment about the z-axis, no normal component of traction is induced on the contact surface and the surface rotates about the z-axis without distortion in the x, y-plane. The boundary conditions for the case of twist are, therefore,

$$u = \beta y/2,\ v = -\beta x/2,\ Z_\nu = 0 \text{ on } \bar{S}_1 \quad [144]$$

$$X_\nu = Y_\nu = Z_\nu = 0 \text{ on } S_2 \quad [145]$$

$$\lim_{x,\,y,\,z\to\infty}(u, v, w) = 0 \quad [146]$$

where $\beta/2$ is the angle of rotation of the contact surface with respect to a distant point in the body $z \gg 0$. For the circular contact area, these boundary conditions are satisfied by a limiting case of a solution by Neuber[10] for the stress concentration at a hyperbolic groove in a twisted shaft. In that solution the traction across the contact surface is found to be

$$X_\nu = \frac{3M_z y}{4\pi a^4}\left(1-\frac{\rho^2}{a^2}\right)^{-1/2},\quad Y_\nu = -\frac{3M_z x}{4\pi a^4}\left(1-\frac{\rho^2}{a^2}\right)^{-1/2} \quad [147]$$

and the compliance of a single body is

[10] See ref. 6, pp. 90–92. See also "Forced Torsional Oscillations of an Elastic Half-Space," by E. Reissner and H. F. Sagoci, *Journal of Applied Physics*, vol. 15, 1944, pp. 652–654.

$$\frac{\beta}{2M_z} = \frac{3}{16\mu a^3} \quad \text{[148]}$$

By analogy with our previous results, we consider the possibility that, in the case of the elliptic contact area, the traction may be

$$\left.\begin{aligned} X_\nu &= T'y(1 - a^{-2}x^2 - b^{-2}y^2)^{-1/2}, \\ Y_\nu &= -T''x(1 - a^{-2}x^2 - b^{-2}y^2)^{-1/2}, \\ Z_\nu &= 0 \end{aligned}\right\} \text{on } S_1 \quad \text{[149]}$$

$$X_\nu = Y_\nu = Z_\nu = 0 \text{ on } S_2 \quad \text{[150]}$$

where T' and T'' are constants. With these surface tractions, all of the boundary conditions, except possibly the first two of Equations [144], are satisfied. If the assumed tractions give the required values of u and v on $\bar{S}_1$, the assumptions expressed in Equations [149] are verified as correct.

Torsional Compliance

To calculate u and v, we substitute Equations [149] and [150] in Equations [29], [30], and [32] and perform the indicated operations. We find, on $\bar{S}_1$,

$$\mu u = y\left[T'a^{-2}\int_0^{\frac{\pi}{2}} \Phi^{-3/2}\cos^2\varphi d\varphi + \sigma(T''b^{-2} - T'a^{-2})\int_0^{\frac{\pi}{2}} \Phi^{-3/2}\sin^2\varphi\cos^2\varphi\, d\varphi\right] \quad \text{[151]}$$

$$\mu v = x\left[-T''b^{-2}\int_0^{\frac{\pi}{2}} \Phi^{-3/2}\sin^2\varphi\, d\varphi + \sigma(T''b^{-2} - T'a^{-2})\int_0^{\frac{\pi}{2}} \Phi^{-3/2}\sin^2\varphi\cos^2\varphi\, d\varphi\right] \quad \text{[152]}$$

These expressions have the correct form.

We note that

$$\int_0^{\frac{\pi}{2}} \Phi^{-3/2}\sin^2\varphi\, d\varphi = a^3[\mathbf{E} - (1-k^2)\mathbf{K}]/[k^2(1-k^2)]$$

$$\int_0^{\frac{\pi}{2}} \Phi^{-3/2}\cos^2\varphi\, d\varphi = a^3[\mathbf{K} - \mathbf{E}]/k^2$$

$$\int_0^{\frac{\pi}{2}} \Phi^{-3/2}\sin^2\varphi\cos^2\varphi\, d\varphi = a^3[(2-k^2)\mathbf{K} - 2\mathbf{E}]/k^4$$

The functions

$$\mathbf{D} = (\mathbf{K} - \mathbf{E})/k^2$$
$$\mathbf{B} = [\mathbf{E} - (1-k^2)\mathbf{K}]/k^2$$
$$\mathbf{C} = [(2-k^2)\mathbf{K} - 2\mathbf{E}]/k^4$$

are tabulated by Jahnke and Emde.[11] Using the values of u and v from Equations [144], we solve Equations [151] and [152] for T' and T'' with the following results:

$$T' = \frac{\mu\beta}{2a}\frac{\mathbf{B} - 2\sigma(1-k^2)\mathbf{C}}{\mathbf{BD} - \sigma\mathbf{CE}} \quad \text{[153]}$$

$$T'' = \frac{\mu\beta}{2a}\frac{\mathbf{D} - 2\sigma\mathbf{C}}{\mathbf{BD} - \sigma\mathbf{CE}} \quad \text{[154]}$$

To find the relation between β and M_z, we calculate

$$M_z = \iint_{S_1}(X_\nu y - Y_\nu x)dx\,dy = \frac{2}{3}\pi ab(T'b^2 + T''a^2) = \frac{1}{3}\pi b^3\mu\beta\frac{\mathbf{E} - 4\sigma(1-k^2)\mathbf{C}}{\mathbf{BD} - \sigma\mathbf{CE}} \quad \text{[155]}$$

Hence, the torsional compliance of one body is

$$\frac{\beta}{2M_z} = \frac{3}{16b^3\mu}\frac{8\{\mathbf{BD} - \sigma\mathbf{CE}\}}{\pi\{\mathbf{E} - 4\sigma(1-k^2)\mathbf{C}\}} \quad \text{[156]}$$

Equation [156] is plotted in Fig. 6.

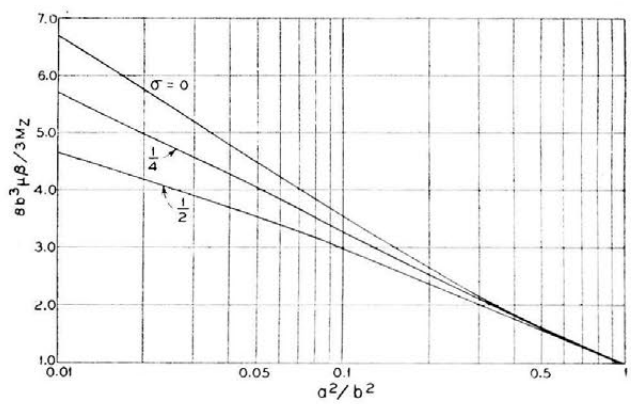

Fig. 6 Initial Torsional Compliance

Noting that

$$\mathbf{B}\left(\frac{\pi}{2}, 0\right) = \mathbf{D}\left(\frac{\pi}{2}, 0\right) = \pi/4, \quad \mathbf{C}\left(\frac{\pi}{2}, 0\right) = \pi/16$$

it may be verified that T', T'' and the compliance reduce to the appropriate values for the limiting case of the circular contact area.

[11] "Tables of Functions," by E. Jahnke and F. Emde, Dover Publications, New York, N. Y., 1943, pp. 82–83.

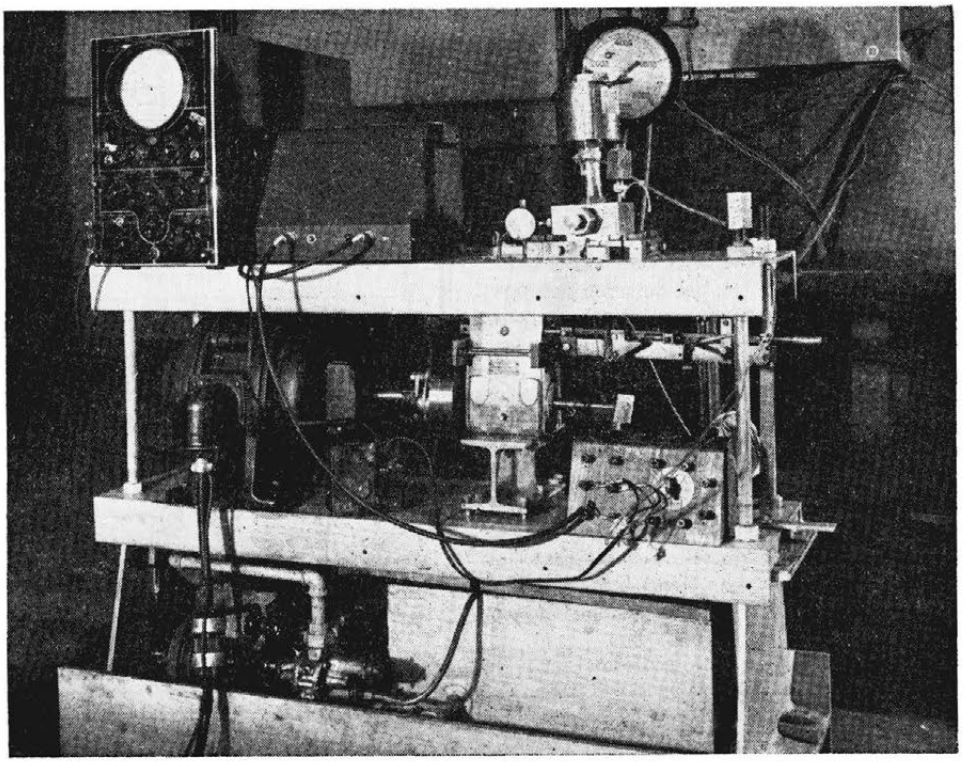

FIG. 1 VIEW OF COMBINED-STRESS PULSATOR

Fatigue Under Combined Pulsating Stresses

BY H. MAJORS, JR.,[1] B. D. MILLS, JR.,[2] AND C. W. MACGREGOR[3]

A special combined stress pulsator is described which was used to subject thin-walled cylindrical tubes to various ratios of combined (in phase) pulsating stresses. The material investigated was annealed SAE-1020 steel. Stress ratios in both the (+, +) and the (+, −) quadrants were applied. In addition, tension tests and uniaxial completely reversed rotating bending fatigue tests were made in the axial and tangential directions to study the anisotropy of the material. The combined stress-fatigue tests agreed best with the distortion-energy theory of strength.

[1] Assistant Professor of Mechanical Engineering, Department of Mechanical Engineering, Massachusetts Institute of Technology, Cambridge, Mass. Mem. ASME.

[2] Professor of Mechanical Engineering, University of Washington, Seattle, Wash. Mem. ASME.

[3] Professor of Applied Mechanics, Department of Mechanical Engineering, Massachusetts Institute of Technology. Mem. ASME.

Contributed by the Applied Mechanics Division and presented at the Annual Meeting, New York, N. Y., November 28–December 3, 1948, of THE AMERICAN SOCIETY OF MECHANICAL ENGINEERS.

Discussion of this paper should be addressed to the Secretary, ASME, 29 West 39th Street, New York, N. Y., and will be accepted until October 10, 1949, to be published at a later date. Discussion received after the closing date will be returned.

NOTE: Statements and opinions advanced in papers are to be understood as individual expressions of their authors and not those of the Society. Paper No. 48—A-7.

INTRODUCTION

WHEN machine parts or structures are subjected to oscillating or fluctuating loads, these generally produce a system of vibratory combined stresses of the biaxial or triaxial types. With few exceptions, however, most of the experiments conducted to investigate the fatigue of metals under fluctuating stresses have been carried out under uniaxial conditions. Thus despite the pragmatic significance of the problem of fatigue under combined stresses, a considerable hiatus now exists in our knowledge of the subject.

Supplemental to the common variables inherent in fatigue under uniaxial stress, namely, surface conditions, range of stress, temperature, frequency, cold work, heat-treatment, and the like, the combined stress-fatigue problem includes such considerations as the influence of the ratio of the stress magnitudes in different directions, the time-phase relationship of these stresses, and so forth.

The alternating torsion test is perhaps the simplest of all the combined stress-fatigue experiments, and it has been widely employed (1–4).[4] The superposition of a static torque upon completely reversed bending stresses has been used by Ono (5), Lea and Budgen (6), and Davies (7). Completely reversed

[4] Numbers in parentheses refer to the Bibliography at the end of the paper.

bending and torsion was studied by Gough and Pollard (8). This yielded test results in the (+, —) quadrant of stress ratios and showed that the distortion-energy theory agreed well with experiments for the mild steel tested. Both cast iron and a $3^1/_2$ per cent nickel-chromium steel did not follow the distortion-energy theory. Maier (9) subjected thin-walled cylindrical tubes of cast iron and mild steel to fluctuating internal pressure with a static axial load. Sufficient data were not presented to permit incontrovertible conclusions to be drawn, but the results indicated that the fatigue limit in the tangential direction was unaffected by the axial force. Further tests have also been conducted by Morikawa and Griffis (10) on thin-walled tubes under pulsating combined stresses for annealed SAE-1020 steel, using a special machine described by Marin (11). This machine subjects a tubular specimen to internal pressure by means of a gear-driven piston and to an axial tensile load by a separate lever system at the rate of 300 cycles per min. Morikawa and Griffis also concluded that the maximum-stress theory agreed with their experiments when modified by the anisotropy of the material.

Two interpretations of the data of combined stress-fatigue tests have been suggested by C. R. Soderberg (12) and J. Marin (13), respectively. The former is based upon the maximum-shear theory and the latter on the distortion-energy theory.

Owing to the paucity of test data on combined stress fatigue, an experimental study of the problem was begun in the Research Laboratories for Mechanics of Materials at the Massachusetts Institute of Technology sometime before the last war. This resulted in the development of a special combined-stress pulsator to subject tubular specimens to various ratios of tangential to axial stresses. The experimental work had to be interrupted for various reasons shortly after the beginning of hostilities, but was resumed during the past year. The present study is restricted to combined pulsating stresses, in phase, applied to thin-walled tubes of SAE-1020 annealed steel. It is the purpose of this paper to describe the special pulsator used, the effect of various ratios of combined pulsating stresses on the fatigue limit, and the interpretation of the results. Fatigue data are included for the first time on the same material in both the (+, +) and (+, —) quadrants of stress ratios.

The Combined-Stress Pulsator

Fig. 1 shows the combined-stress pulsator developed for these experiments. A schematic diagram listing the various component parts is given in Fig. 2.

Filtered machine oil is pumped from a return-flow reservoir to the inlet of a Bosch fuel-injection pump by a small motor-driven gear pump. The injection pump has two high-pressure cylinders which simultaneously deliver high pulsating oil pressure by means of two cam-driven plungers at 880 times per min. A high-pressure oil manifold receives the outlet oil of the Bosch pump for delivery to the lower threaded head into which the tubular test specimens are screwed. When the specimen develops a fatigue crack, a fine spray of oil, penetrating the tube wall through the crack, is caught in a metal box surrounding the specimen. The oil stream flows through tubes to a small cup at the end of a lever shown in Fig. 3. The weight of the escaped oil in the cup lowers the lever which trips a microswitch, shutting off the equipment. The number of pulsations is determined by a revolution counter.

In order to maintain a constant maximum pressure, it has been found necessary to adjust the pressure manually for the first hour of testing, after which the maximum pressure remains essentially constant.

Various ratios of tangential to longitudinal stresses are obtained by attaching suitably designed heads to the upper threaded ends of the tubular test specimens. For example, Fig. 4 shows

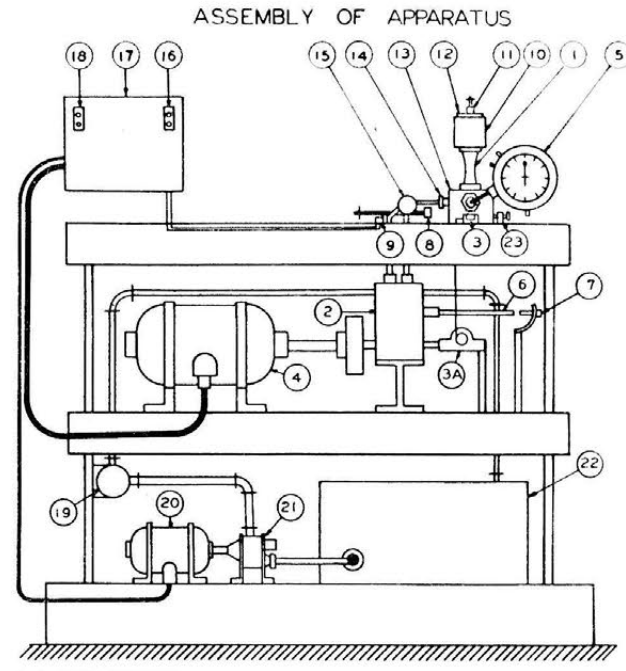

(1) TEST SPECIMEN.
(2) BOSCH HIGH PRESSURE PUMP.
(3) REVOLUTION COUNTER.
(3A) 100 TO 1 SPEED REDUCER.
(4) MOTOR FOR DRIVING BOSCH PUMP (2).
(5) CROSBY PRESSURE GAGE.
(6) BOSCH PUMP CONTROL ROD.
(7) MICROMETER FOR ADJUSTING CONTROL ROD (6).
(8) CUP TO CATCH OVERFLOW OIL FROM (24).
(9) MICRO-SWITCH ACTUATED BY HANDLE OF OVERFLOW CUP (8).
(10) UPPER THREADED HEAD FOR TUBULAR SPECIMEN.
(11) ASSEMBLY OF PISTON AND PLUG (WITHIN SPECIMEN).
(12) OIL LEAKAGE COLLECTOR.
(13) LOWER THREADED HEAD FOR TUBULAR SPECIMEN.
(14) THREADED HIGH-PRESSURE CONNECTION
(15) HIGH PRESSURE MANIFOLD
(16) PUSHBUTTON CONTROL FOR MOTOR (20).
(17) CONTROL PANEL.
(18) PUSH-BUTTON CONTROL FOR MOTOR (4).
(19) OIL FILTER.
(20) D.C. MOTOR FOR DRIVING LOW-PRESSURE GEAR PUMP.
(21) LOW PRESSURE GEAR PUMP.
(22) OIL RESERVOIR.
(23) STEEL BLOCK.
(24) TIN BOX AROUND SPECIMEN TO COLLECT OIL ESCAPING FROM FATIGUE CRACK (NOT SHOWN).

Fig. 2 Schematic Diagram of Combined-Stress Pulsator

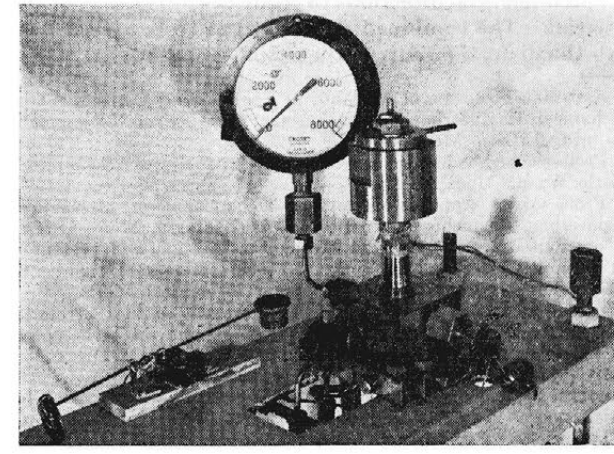

Fig. 3 Close-Up View of Upper and Lower Head Assembly

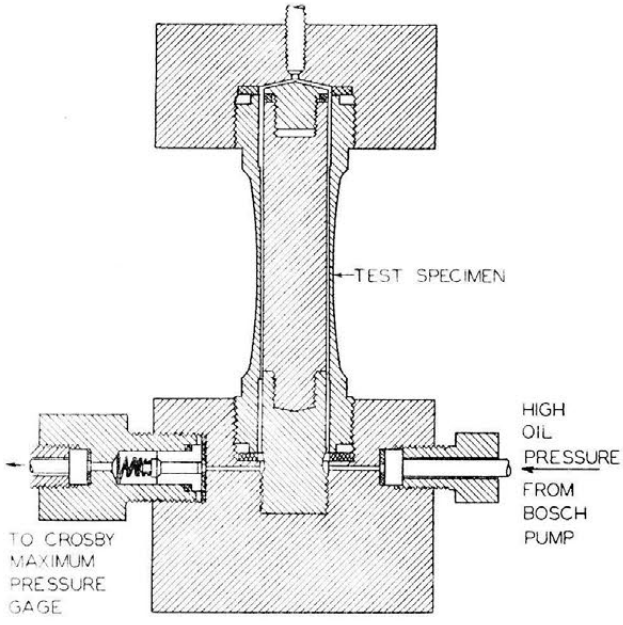

FIG. 4 UPPER AND LOWER HEADS FOR A RATIO OF TANGENTIAL TO LONGITUDINAL STRESS OF ABOUT 2 TO 1

the head used to obtain a ratio of tangential tension to longitudinal tension of about 2 to 1. The central plug inside the test specimen serves to reduce the oil volume in order to allow the Bosch pump to develop the required pressure. From dynamic-stress measurements to be described later on, this solid-type head produces a ratio of tangential tension to longitudinal tension of 1.84 to 1.00 at the outside surface. For other ratios it was necessary to use an oiltight composition cup piston in the upper head. The desired ratios are obtained essentially by selecting the proper areas in the upper head over which the oil pressure acts relative to the cross-sectional bore areas of the tubes and attaching the central axial plug within the tube to carry tension or thrust as the case may be.

For example, the arrangement to produce a ratio of tangential tension to longitudinal tension of approximately 1 to 1 is shown in Fig. 5. In this case the area of the upper head over which the pressure acts is increased over that of Fig. 4 so as to obtain a higher axial stress. The downward thrust of the oil pressure is carried by the central plug unattached to the test specimen. When axial compression is desired, the arrangement is similar to that shown in Fig. 6 where a ratio of tangential tension stress to longitudinal compression stress is approximately 1 to 1. This is accomplished by allowing the central bore plug to carry the axial tensile load due to the oil pressure acting upon the upper area of the plug recess (attached to the plug), while the downward thrust on the same area (but over the head attached to the specimen) is carried by the test specimen.

For a uniaxial tangential stress, the system shown in Fig. 7 is utilized. In this case all axial load due to the internal pressure is carried by the central bore plug. This produces a ratio of tangential tensile stress to longitudinal stress of about 1 to 0. The same general principle can be utilized to give a wide variety of other stress ratios. Dynamic-stress measurements at the outside surface showed the actual stress ratios for the cases shown in Figs. 4, 5, 6, and 7 to be +1.84 to +1.00, +1.04 to +1.00, +1.27 to —1.00, and +1.00 to +0.03, respectively.

DYNAMIC-STRESS STUDIES

Before actual combined stress-fatigue tests were undertaken

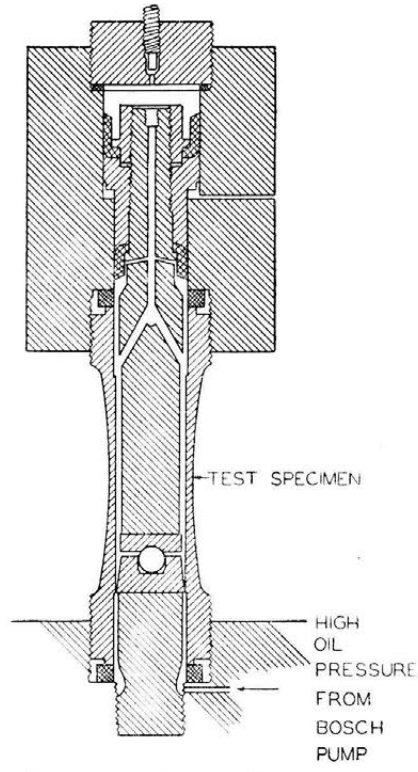

FIG. 5 GRIP SYSTEM FOR A RATIO OF TANGENTIAL TO LONGITUDINAL STRESS OF ABOUT 1 TO 1

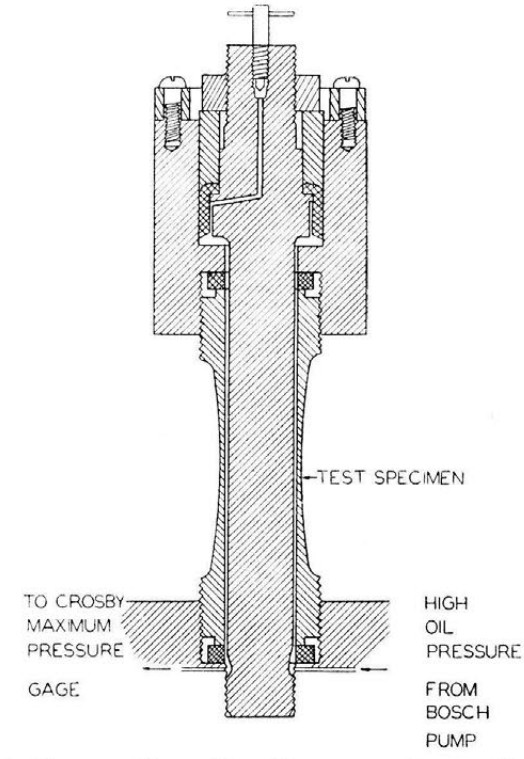

FIG. 6 UPPER AND LOWER HEAD SYSTEM FOR A RATIO OF TANGENTIAL TENSILE STRESS TO LONGITUDINAL COMPRESSIVE STRESS OF ABOUT 1 TO 1

it was necessary to determine: (*a*) if the axial and tangential stresses were in phase; (*b*) the dynamic correction necessary in order to compute the stress magnitudes; and (*c*) the correction necessary for tubes having a curved-tapered wall of the form used in the present study.

Tangential and longitudinal resistance-wire strain gages were attached to the tubes at the position of minimum wall thickness.

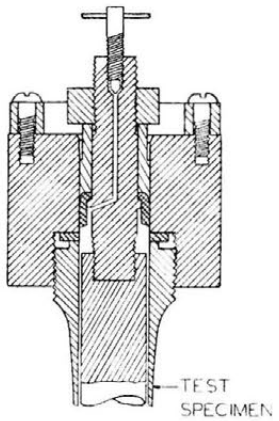

FIG. 7 GRIP SYSTEM FOR A RATIO OF TANGENTIAL STRESS TO LONGITUDINAL STRESS OF ABOUT 1 TO 0

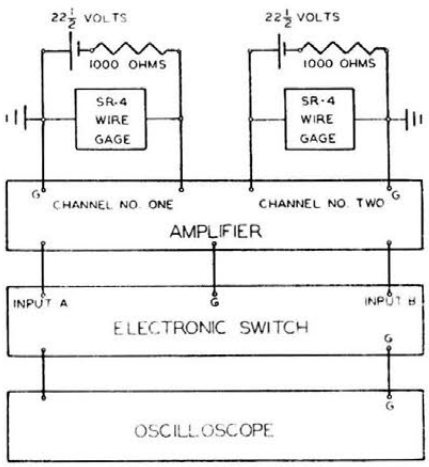

FIG. 8 ELECTRONIC CIRCUIT TO DETERMINE PHASE RELATIONSHIP OF STRESSES

A two-channel amplifier was used to feed the signals from the wire gages to an electronic switch connected to an oscilloscope as shown in Fig. 8. The phase relationships were determined for each of the pressure heads discussed under the previous section both on the previously unstressed tubes and on tubes which had been plastically deformed through cyclic stressing. Fig. 9 shows typical oscilloscopic records of the dynamic strains, tangential and axial, for the stress ratios +1.27 to —1.00, and +1.04 to +1.00. As can be seen, the axial and tangential strains are in phase. Similar results were obtained for the other heads.

In addition, the SR-4 wire strain gages were used to measure dynamic strains on the previously unstressed tubes by the use of the electronic circuit shown in Fig. 10. These strains were converted into dynamic stresses by the usual conversion formulas. The dynamic-strain readings were calibrated by means of three precision resistors each of which was shunted across the gage measuring strain by means of a vibrator switch. The average of three calibrations was used to convert oscilloscopic readings to unit strains. For each pressure head, the Crosby gage pressure was plotted as a function of the peak reading on the oscilloscope scale for each of the four wire gages on the calibrating test specimen. From these data, curves were constructed of Crosby gage pressure versus dynamic longitudinal and tangential stresses. All dynamic stresses were corrected for slightly different ratios of outside to inside radius by using the Lamé solution of stress variation for thick tubes under internal pressure. The ratios of

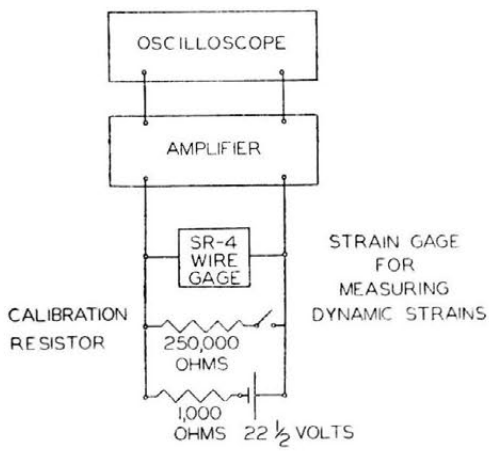

FIG. 10 ELECTRONIC CIRCUIT FOR MEASUREMENT OF DYNAMIC STRAINS

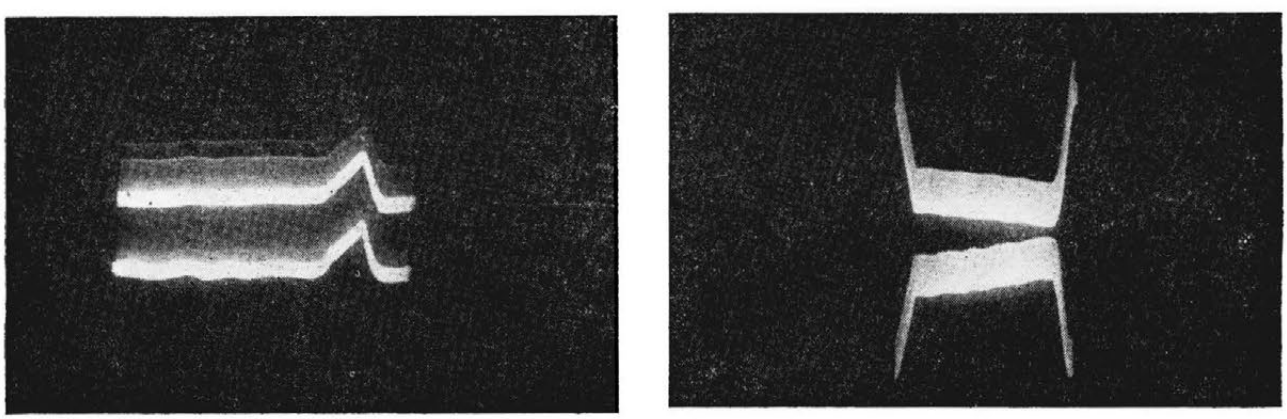

(*a*) (*b*)

FIG. 9 OSCILLOGRAPHIC RECORDS FOR STRESS RATIOS OF TANGENTIAL TO LONGITUDINAL STRESSES (*a*, Ratio of +1.04 to +1.00; and *b*, ratio of +1.27 to —1.00. Both signals in phase.)

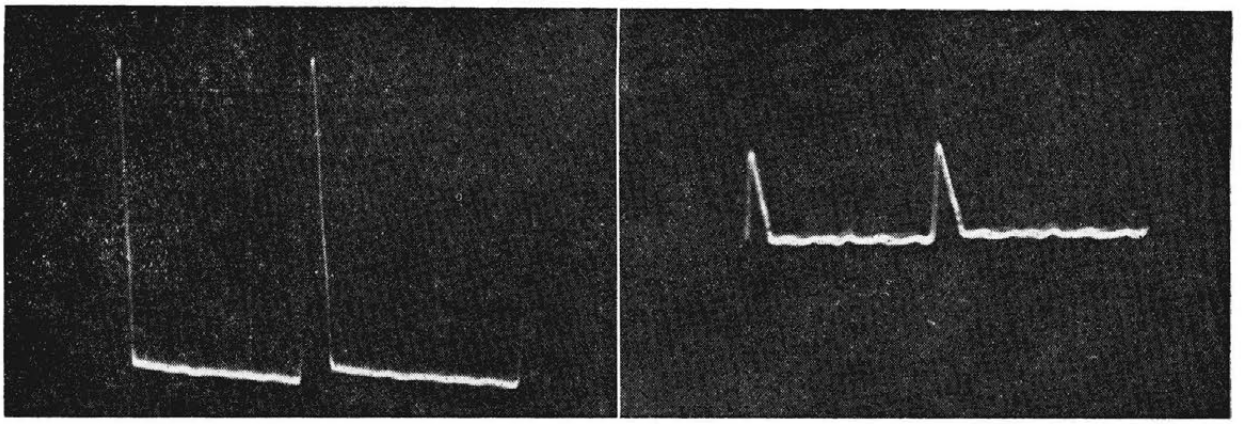

Tangential Strain-Tension Longitudinal Strain-Tension

FIG. 11 OSCILLOGRAPHIC RECORDS OF DYNAMIC STRAINS TO PRODUCE

$$\frac{\sigma_t}{\sigma_z} = \frac{+1.84}{+1.00}$$

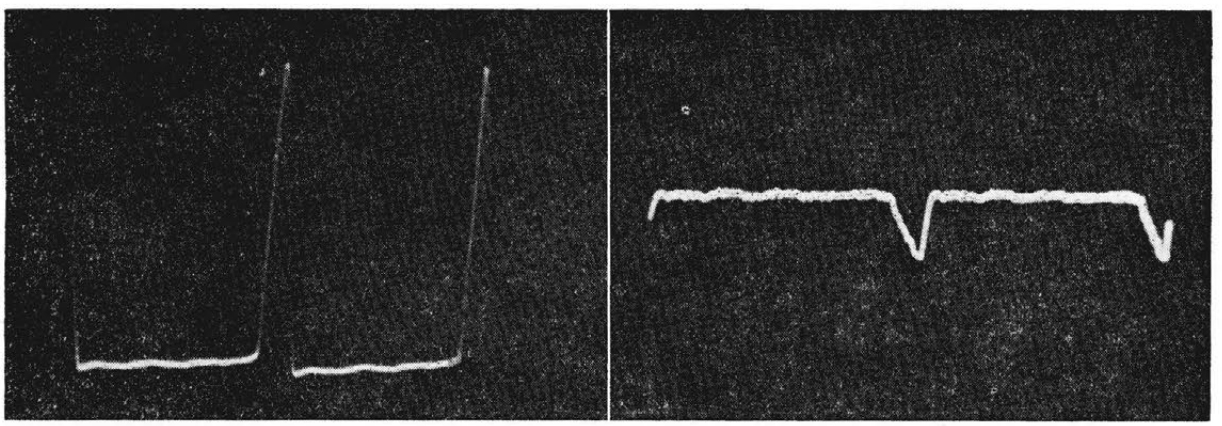

Tangential Strain-Tension Longitudinal Strain-Tension

FIG. 12 OSCILLOGRAPHIC RECORDS OF DYNAMIC STRAINS TO PRODUCE

$$\frac{\sigma_t}{\sigma_z} = \frac{+1.00}{+0.03}$$

(Crosby gage pressure 2550 psi, 880 pulsations per min.)

tangential stresses to longitudinal stresses remained constant with time and were the same for the slightly yielded tubes as for the previously unstressed specimens.

Figs. 11 and 12 show typical oscillographic records of dynamic strains as functions of time for the two heads to produce ratios of tangential to longitudinal stresses of +1.84 to +1.00, and +1.00 to +0.03. It can be seen that the pulsations are sharp triangular-shaped wave forms rather than of the purely sinusoidal type.

MATERIAL AND SPECIMENS

The material investigated is hot-rolled SAE 1020 steel supplied from a 20-ft bar 2 in. diam. The chemical analysis is C-0.20, Mn-0.55, P-0.009, and S-0.027.

Prior to machining, the stock was carefully annealed at 1650 F for 1 hr per in. of thickness and furnace-cooled. Tubular specimens were then machined to the dimensions shown in Fig. 13. The inside-bore surface was micromatic-honed after being reamed. This produced very light spiral scratches, giving no preference to the formation of axial or transverse fatigue cracks. The outside surfaces were polished with No. 000 emery paper. The wall

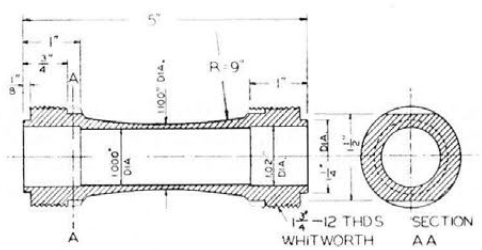

FIG. 13 COMBINED-STRESS TEST SPECIMEN

thickness and outside diameters were measured before and after each test at eight locations by a special ball-point micrometer.

PRELIMINARY UNIAXIAL TESTS

In order to compare the combined-stress results under pure pulsations with the properties of the material under completely reversed stresses, uniaxial rotating bending fatigue tests also were made in both the longitudinal and transverse directions for the annealed bar stock. Similarly, true stress-strain tension tests were made on specimens cut in these same directions.

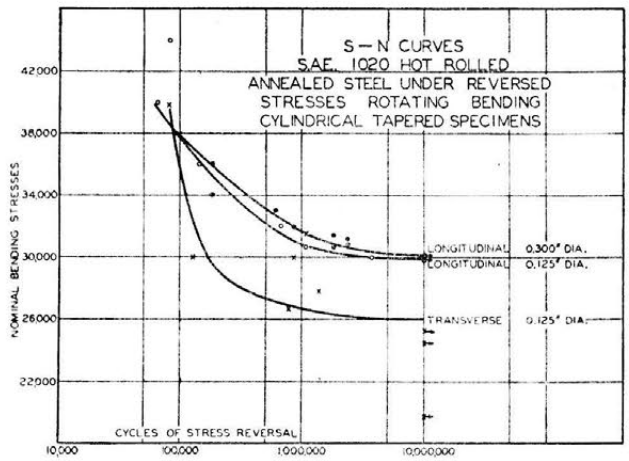

FIG. 14 S-N CURVES FOR SAE-1020 ANNEALED STEEL UNDER COMPLETELY REVERSED ROTATING BENDING ON CYLINDRICAL TAPERED SPECIMENS

Longitudinal R. R. Moore fatigue specimens were machined from the bar stock at the same radial distance from the center as the average tube radius for the combined stress fatigue specimens. This was done to eliminate the effect of variation in properties across the section. The minimum diameter for these test pieces was 0.300 in. after all transverse scratches had been polished out with No. 00 emery paper.

In addition, small 0.120-in-diam tension and Krouse rotating cantilever fatigue specimens were machined from the bar stock in both longitudinal and transverse directions at the same radial distance from the center of the bar as the average tube radius of the combined stress fatigue specimen. Fig. 14 shows the S-N curves for the fatigue tests described.

The preliminary tension and fatigue-test results are summarized in Table 1. The degree of anisotropy present is clearly evident. This is revealed both by the endurance limits in the

TABLE 1 UNIAXIAL REVERSED BENDING FATIGUE AND TENSION-TEST RESULTS

	Longitudinal direction	Transverse direction
Endurance limit, R. R. Moore, psi	30400	...
Endurance limit, cantilever (Krouse), psi	29800	26000
Yield point, psi	36000	31400
Nominal tensile strength, psi	62330	61800
Per cent elongation in 0.50 in.	37.0	31.0
Per cent reduction of area	55.3	51.7
Coefficient of strain-hardening (true stress-strain test), psi	83300	69800
True strain at fracture	0.808	0.724
True stress at fracture, psi	125500	113800

longitudinal and in the transverse directions, and also by the tension-test data. In the latter, while the average nominal tensile strengths for three specimens are nearly the same, the true stress-strain results bring out the degree of anisotropy in a much clearer fashion.

COMBINED-STRESS FATIGUE RESULTS

The S-N curves obtained under combined pulsating stresses for the four stress ratios investigated are shown in Fig. 15 where the dynamic nominal tangential outside fiber stress is plotted as a function of the number of stress pulsations. Tests were carried to 10^7 cycles. For these stress ratios all fatigue fractures occurred parallel to the longitudinal direction, no doubt reflecting the influence of the lower transverse endurance limit. Table 2 gives a summary of the test data, from which it can be seen that the endurance limit in a given direction is not independent of the stresses normal to that direction as has been claimed by other investigators.

TABLE 2 SUMMARY OF COMBINED-STRESS FATIGUE RESULTS; PURE PULSATIONS

Ratio of tangential stress to longitudinal stress	Nominal dynamic tangential stress at outside surface at 10^7 cycles (fatigue limit), psi	Ratio of tangential stress at fatigue limit to tangential stress at fatigue limit for zero longitudinal stress (actually, σ_z = 920 psi)
$\frac{+1.04}{+1.00}$	41850	1.138
$\frac{+1.84}{+1.00}$	38900	1.057
$\frac{+1.00}{+0.025}$	36800	1.000
$\frac{+1.271}{-1.00}$	25300	0.688

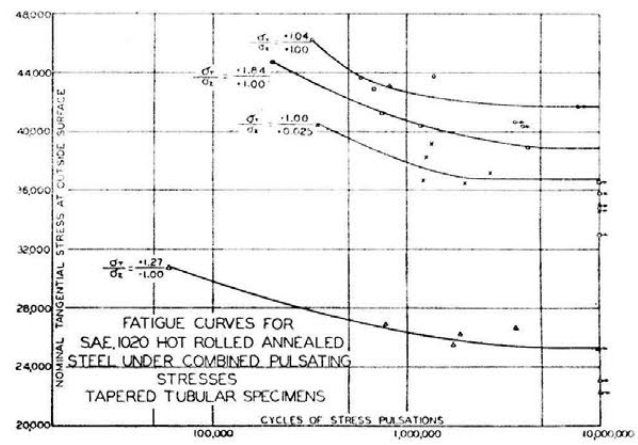

FIG. 15 FATIGUE CURVES FOR SAE-1020 ANNEALED STEEL UNDER COMBINED PULSATING STRESSES FOR TAPERED TUBULAR SPECIMENS

In comparing static combined-stress test results with the various strength theories, it is customary to plot them on a diagram with the ratios σ_1/σ_0 and σ_2/σ_0 as co-ordinates where σ_1 and σ_2 are the principal stresses and σ_0 is the static yield strength. A similar procedure can be followed in the case of combined fluctuating stresses in phase, where σ_1/σ_f and σ_2/σ_f are the co-ordinates. In this case, σ_1 and σ_2 are the maximum principal stresses during a cyclic variation, and σ_f is the maximum uniaxial fatigue strength under the same ratio of mean stress to maximum stress for the cycle. Thus for the two-dimensional problem of combined fatigue stresses, where the maximum principal stresses σ_1 and σ_2 of each cycle are in the same time phase and have the same ratio of mean stress to maximum stress for the cycle, the more common strength theories can be expressed as follows

Maximum-Stress Theory

$$\left.\begin{aligned}\sigma_1 &= \pm\sigma_f \\ \sigma_2 &= \pm\sigma_f\end{aligned}\right\} \quad \ldots\ldots [1]$$

Maximum-Shear Theory

$$\left.\begin{aligned}\sigma_1 &= \pm\sigma_f \\ \sigma_2 &= \pm\sigma_f \\ (\sigma_1 - \sigma_2) &= \pm\sigma_f\end{aligned}\right\} \quad \ldots\ldots [2]$$

Distortion-Energy Theory

$$(\sigma_1^2 - \sigma_1\sigma_2 + \sigma_2^2) = \sigma_f^2 \quad \ldots\ldots [3]$$

Total-Strain-Energy Theory

$$(\sigma_1^2 - 2\mu\sigma_1\sigma_2 + \sigma_2^2) = \sigma_f^2 \quad \ldots\ldots [4]$$

The value of σ_f in Equations [1] to [4], inclusive, can be determined, as in the present tests, by uniaxial fatigue tests under the same ratio of mean stress to maximum stress for the cycle. Thus

σ_f reflects the influence of the uniaxial mean stress for the cycle on the maximum uniaxial cyclic stress for failure. For example, in the case of completely reversed cyclic stresses where the mean stress of the cycle is zero, σ_f becomes merely the endurance limit σ_e.

Various attempts have been made in the past to express empirically σ_f in terms of the mean stress σ_m, the endurance limit σ_e, and the tensile strength σ_u (or the yield strength σ_0). Examples of these are the Modified-Goodman law, the Gerber parabola, the Soderberg linear relation between σ_v/σ_e and σ_m/σ_0, where σ_v is the variable stress, etc. Data of various investigators show that the Soderberg relation is the only conservative one since, although some materials indicate a definite parabolic relation between σ_v/σ_e and σ_m/σ_0, others yield data close to the linear relation. Thus for conservative design, Equations [1] to [4], inclusive, would predict failure when σ_f is obtained from

$$\frac{\sigma_v}{\sigma_e} + \frac{\sigma_m}{\sigma_0} = 1$$

or

$$\sigma_f = \sigma_{max} = \sigma_e + \sigma_m \left(1 - \frac{\sigma_e}{\sigma_0}\right) \quad \ldots\ldots\ldots\ldots [5]$$

It was not the purpose of the present investigation to establish the relation between σ_f, σ_e, σ_m, σ_0, or σ_u for the SAE-1020 steel tested. Sufficient tests were not made to determine this accurately. Since uniaxial reversed bending fatigue tests were made also in the tangential direction as well as uniaxial pulsating tests in this direction, it is possible, however, at least to indicate the probable relationship involved for this material. It was found that either the Modified-Goodman law

$$\frac{\sigma_v}{\sigma_e} + \frac{\sigma_m}{\sigma_u} = 1$$

which for pure pulsation gives

$$\sigma_f = \sigma_{max} = \frac{2\sigma_e\sigma_u}{(\sigma_e + \sigma_u)} \quad \ldots\ldots\ldots\ldots [6]$$

or the Gerber-type parabola

$$\left(\frac{\sigma_v}{\sigma_e}\right)^n + \left(\frac{\sigma_m}{\sigma_0}\right)^n = 1$$

where $n = 3/2$ and which, for pulsation, yields

$$\sigma_f = \sigma_{max} = \frac{2\sigma_e\sigma_0}{[\sigma_0^{3/2} + \sigma_e^{3/2}]^{2/3}} \quad \ldots\ldots\ldots\ldots [7]$$

agrees well with the present tests. From the data of Table 1 for the tangential direction, σ_e = 26,000 psi, σ_0 = 31,400 psi, and σ_u = 61,800 psi. Based upon this, Equations [6] and [7] yield σ_f equal to 36,600 psi, and 35,800 psi, respectively. These agree favorably with σ_f = 36,800 psi found in the uniaxial pulsation tests as listed in Table 2.

Fig. 16 compares the combined-stress fatigue results with the various strength theories listed in Equations [1] to [4], inclusive. As can be seen, data are included in both quadrants. While some scatter is present when viewed from the standpoint of any one theory of strength, in spite of the precautions observed, it is clear that the data check the distortion-energy theory the best.

Dynamic stresses at the mean radius and at the inside radius were also investigated, and when they were plotted as ratios in Fig. 16, identical conclusions were obtained. The test results were recorded in Fig. 16 as outside fiber stresses since measurements were made there.

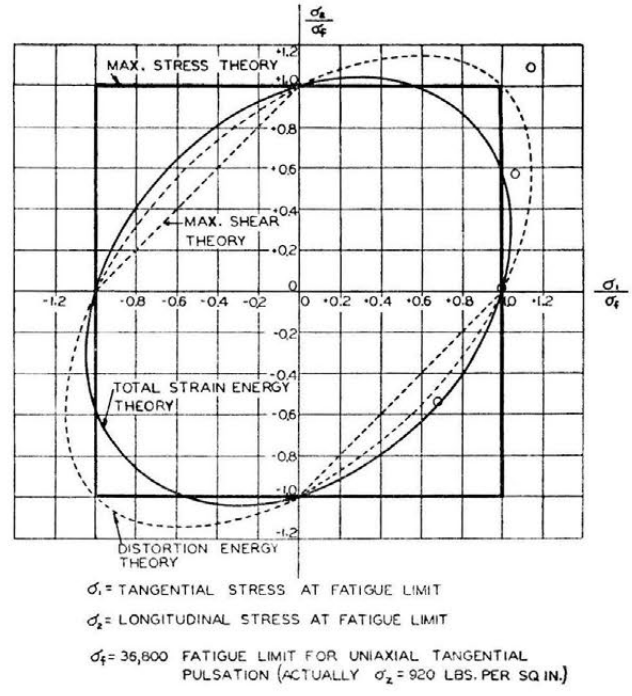

FIG. 16 COMPARISON OF TEST RESULTS UNDER COMBINED PULSATING STRESSES WITH VARIOUS STRENGTH THEORIES

CONCLUSIONS

A special combined-stress pulsator is described which was used to subject thin-walled tubular specimens to various ratios of combined pulsating stresses which were in phase. The material investigated was annealed SAE-1020 steel. Stress ratios in both the (+, +) and the (+, —) quadrants were applied. In addition, tensile tests and completely reversed uniaxial bending fatigue tests were made in both the axial and tangential directions to study the anisotropy of the material. The combined-stress fatigue tests agreed best with the distortion-energy theory.

BIBLIOGRAPHY

1 "Alternating Stress Experiments," by W. Mason, Proceedings of the Institution of Mechanical Engineers, London, England, 1917, pp. 121–158.

2 "The Fatigue of Metals," by H. J. Gough, D. Van Nostrand Company, New York, N. Y., 1926.

"The Fatigue of Metals," by H. F. Moore and J. B. Kommers, McGraw-Hill Book Company, Inc., New York, N. Y., 1927.

3 "Ermüdung," by P. Ludwik, Proceedings of the International Association for Testing Materials, vol. 1, 1931, p. 190.

4 "The Effect of Range of Stress on the Torsional Fatigue Strength of Steel," by J. O. Smith, University of Illinois Engineering Experiment Station, Bulletin Series No. 316, Urbana, Ill., 1939.

5 "Fatigue of Steel Under Combined Bending and Torsion," by A. Ono, Memoirs of the College of Engineering, Kyushu Imperial University, Japan, vol. 2, 1921, pp. 117–142.

6 "Combined Torsional and Repeated Bending Stresses," by F. C. Lea and H. P. Budgen, *Engineering*, vol. 122, 1926, pp. 242–245.

7 See discussion by V. C. Davies of the paper, "Strength of Metals Under Combined Alternating Stresses," by H. J. Gough and H. V. Pollard, Proceedings of the Institution of Mechanical Engineers, London, England, vol. 131, 1935, p. 66.

8 See reference (7), H. J. Gough and H. V. Pollard.

9 "Stress Reversal in Tubes Under Internal Pressure," by A. F. Maier, *Stahl und Eisen*, vol. 54, 1934, pp. 1289–1291.

10 "The Biaxial Fatigue Strength of Low-Carbon Steels," by G. K. Morikawa and LeVan Griffis, *Welding Journal*, vol. 24, Welding Research Supplement, March, 1945, pp. 167s–174s.

11 "Strength of Steel Subjected to Biaxial Fatigue Stresses," by

Joseph Marin, *Welding Journal*, vol. 21, Welding Research Supplement, November, 1942, pp. 554s–559s.

12 "Factors of Safety and Working Stresses," by C. R. Soderberg, Trans. ASME, vol. 52, 1930, p. 13; "Working Stresses," ibid., vol. 55, paper no. APM-55-16, 1933, p. 131; and "Working Stresses," Journal of Applied Mechanics, Trans. ASME, vol. 57, 1935, p. A-106.

13 "Interpretation of Experiments on Fatigue Strength of Metals Subjected to Combined Stresses," by Joseph Marin, *The Welding Journal*, vol. 21, May, 1942, pp. 245s–248s.

The Dynamics of Cavitation Bubbles

By M. S. PLESSET,[1] PASADENA, CALIF.

Three regimes of liquid flow over a body are defined, namely: (*a*) noncavitating flow; (*b*) cavitating flow with a relatively small number of cavitation bubbles in the field of flow; and (*c*) cavitating flow with a single large cavity about the body. The assumption is made that, for the second regime of flow, the pressure coefficient in the flow field is no different from that in the noncavitating flow. On this basis, the equation of motion for the growth and collapse of a cavitation bubble containing vapor is derived and applied to experimental observations on such bubbles. The limitations of this equation of motion are pointed out, and include the effect of the finite rate of evaporation and condensation, and compressibility of vapor and liquid. A brief discussion of the role of "nuclei" in the liquid in the rate of formation of cavitation bubbles is also given.

Introduction

A DISTINCTIVE feature of the hydrodynamics of liquids is the possibility of the coexistence of a vapor or gas phase with the liquid phase. Such two-phase flow is usually called cavitating flow, although it could as well be characterized as liquid flow with boiling. Cavitating flow has great theoretical interest in addition to the hydrodynamics involved because of the relation of this flow condition to the physical-chemical properties of the liquid. The practical significance of cavitation is of course clear. The drag of submerged bodies moving through a liquid rises when cavitation appears; similarly, the efficiency of pumps, turbines, and propellers drops with the development of cavitation; and the damage which may be produced by cavitation in these devices is well known.

The particular flow problem discussed in this paper is the flow of a liquid (water) over a submerged body which will be considered to be at rest. If p_0 denotes the static pressure, and V_0 the uniform flow velocity of the liquid at a great distance from the body, then the general character of the flow in so far as cavitation is concerned is correlated with the cavitation parameter

$$K = \frac{p_0 - p_v}{(\rho V_0^2)/2} \quad \ldots\ldots\ldots\ldots\ldots\ldots [1]$$

where p_v is the vapor pressure of the liquid and ρ its density. Obviously, one cannot expect a single constant to describe so complex a phenomenon as cavitating flow about a submerged body; however, a correlation in a qualitative way may be made with the various types of liquid flow. Three flow regimes for a given suitably shaped body will be indicated here. The first (K sufficiently large) is noncavitating flow. This state of flow consists of a liquid phase only and, with neglect of compressibility effects, follows the same laws as are familiar in air flow. If now K is made smaller, a state of flow is attained in which a relatively small number of bubbles appear near the boundary of the body. This state of flow will be taken as the second regime of flow. If K is further reduced, the number of bubbles increases, until eventually they merge into one large cavity which completely encloses a portion of the body. The state of flow with a single cavity about the body is the third flow regime, and may be called cavity flow. A further reduction of K brings about only an increase in the size of the cavity. These three flow conditions are illustrated in Fig. 1.

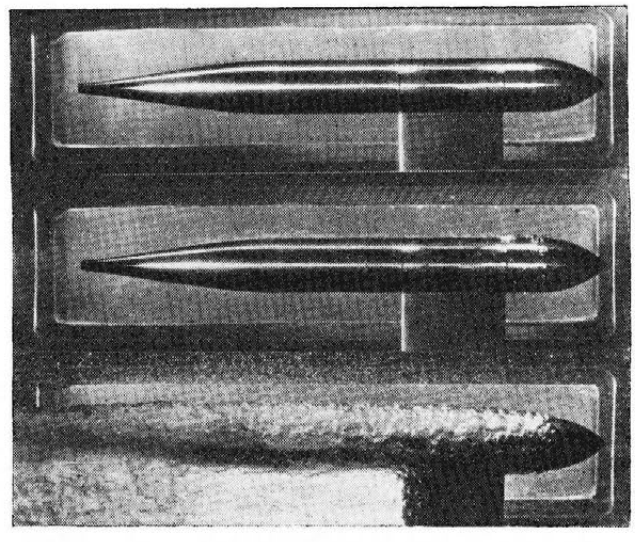

Fig. 1 Views Showing the Three Regimes of Flow
(In the top view, the cavitation parameter K = 0.40; in the center K = 0.28; and in the bottom K = 0.18.)

In the cavity-flow regime, the boundary of the cavity may be taken with reasonably good approximation to be a surface of constant pressure and of constant flow speed. The pressure and velocity in the flow field are fundamentally different from those in noncavitating flow. It may be remarked that, at least for two-dimensional flows, the powerful mathematical methods of the free streamline theory may be applied to the solution of cavity flow problems (1, 2).[2]

The second regime of flow has here been characterized somewhat arbitrarily as the flow condition in which there is only a relatively small number of bubbles in the flow field. This limitation is made in order to get an analytic simplification. If there are only a few small bubbles, the effect of the pressure disturbance of one bubble upon another may be neglected. Further, one may suppose that the pressure field, except at the bubble, is determined in the same way as if there were no bubble cavitation. As is well known for noncavitating flow, if p is the static pressure at any point in the flow field, and if p_0 and V_0 are the static pressure and flow velocity in the uniform flow at a distance from the body, then with neglect of viscous effects, the pressure coefficient

[1] Associate Professor of Applied Mechanics, California Institute of Technology.

Contributed by the Applied Mechanics Division and presented at the Annual Meeting, New York, N. Y., November 28–December 3, 1948, of The American Society of Mechanical Engineers.

Discussion of this paper should be addressed to the Secretary, ASME, 29 West 39th Street, New York, N. Y., and will be accepted until October 10, 1949, for publication at a later date. Discussion received after the closing date will be returned.

Note: Statements and opinions advanced in papers are to be understood as individual expressions of their authors and not those of the Society. Paper No. 48—A-107.

[2] Numbers in parentheses refer to the Bibliography at the end of the paper.

$$C_p = \frac{p - p_0}{(\rho V_0^2)/2} \quad \text{[2]}$$

is independent of p_0 and V_0. The present assumption consists in the calculation of the static pressure p in the second flow regime with the appropriate values of p_0 and V_0 from the pressure coefficient C_p determined for noncavitating flow. This assumption that the pressure coefficient is essentially the same just before the first few cavitation bubbles appear as it is after of course is subject to experimental verification, and the necessary experiments are planned for the high-speed water tunnel in the Hydrodynamics Laboratory of the California Institute of Technology. For the present, this assumption is considered a reasonable one. It may be remarked also that as the number of bubbles increases with decreasing K, the pressure field should go over into that characteristic of the cavity-flow field; but, in the transition, the pressure distribution over the body should show small-scale spatial variations between the limits of the pressure field of noncavitating flow and that of the fully developed cavity flow.

Experimental Observations of Cavitation Bubbles

In the present paper an equation of motion will be developed for a cavitation bubble in a flow regime of the second type. This equation of motion will be applied to an analysis of experimental observations made in the high-speed water tunnel. Since a discussion of these experiments has been given recently by Knapp and Hollander (3), only general features will be mentioned here.

The cavitation experiments were made with a 1.5-caliber ogive for which the noncavitating pressure distribution had been measured, Fig. 2. Runs were made with tunnel velocities V_c

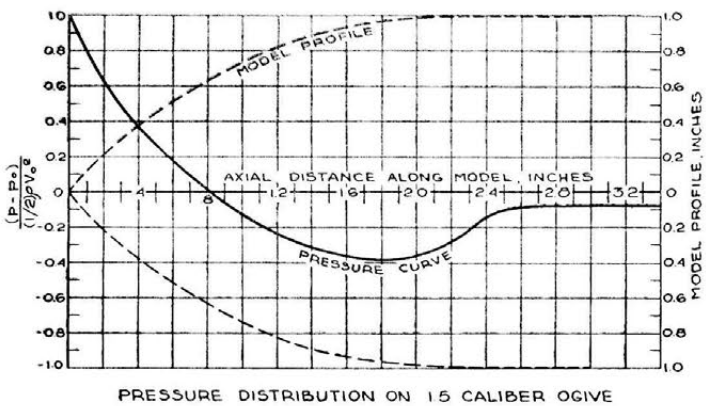

Fig. 2 Experimentally Determined Pressure Coefficient, $C_p = (p - p_0)/2(\rho V_0^2)$, Is Shown as a Function of Axial Distance Along Model

(The model profile is shown in the dotted curves with the associated scale for the profile on the right.)

from 40 fps to 70 fps, and the static pressure p_0, was reduced until a few cavitation bubbles appeared. Photographs of these bubbles were taken on a moving film at a rate of 15,000 per sec to 20,000 per sec; a reproduction of an example of these photographs is shown in Fig. 3.

Equation of Motion for a Cavitation Bubble

Frequent reference has been made in the literature on cavitation to Rayleigh's solution for the problem of the collapse of a spherical cavity in a liquid (4). Rayleigh considered the situation in which the pressure at a distance from the bubble was constant. With this assumption, the variation of the bubble radius with time may be simply and elegantly deduced from the

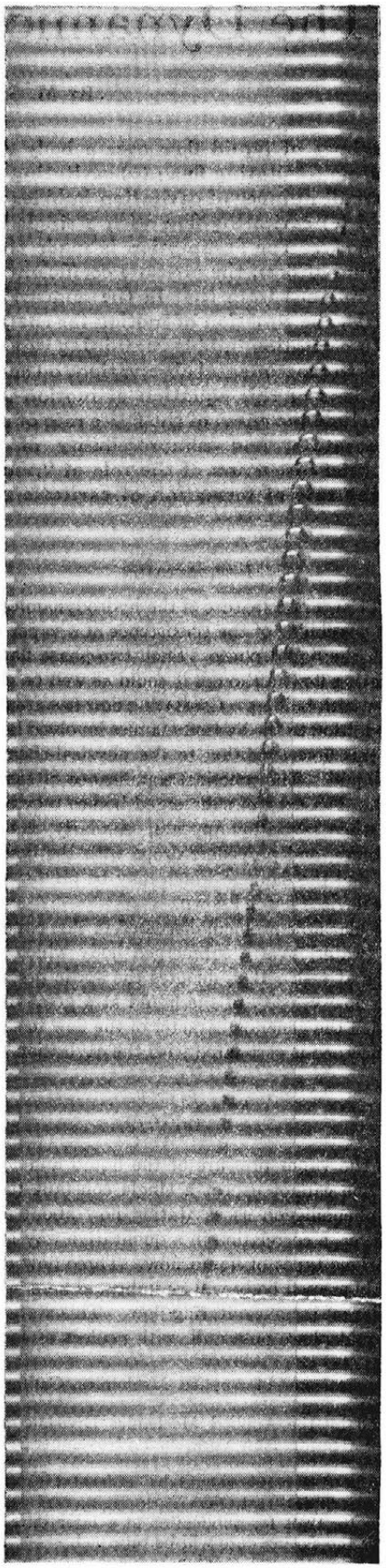

Fig. 3 This Series of Frames Shows the Bubble Denoted as Bubble 1

energy integral of the motion. In the present problem, the bubble moves through a region in which the pressure varies quite rapidly so that an extension of Rayleigh's theory is required. This extension may be readily carried out as follows: Consider a spherical bubble in a perfect, incompressible liquid of infinite extent, and let the origin of co-ordinates be at the bubble center which is at rest. The radius of the bubble at any time t is R, and r is the radius to any point in the liquid. Then, as is well known (5), the velocity potential for motion of the liquid with spherical symmetry is

$$\phi = R^2\dot{R}/r \quad [3]$$

and the Bernoulli integral of the motion is

$$-\frac{\partial\phi}{\partial t} + \frac{1}{2}(\nabla\phi)^2 + \frac{p(r)}{\rho} = \frac{P(t)}{\rho} \quad [4]$$

where $\dot{R} = dR/dt$, $p(r)$ is the static pressure at r, and $P(t)$ is the static pressure at a distance from the bubble. Also, from Equation [3]

$$(\nabla\phi)^2 = R^4\dot{R}^2/r^4 \quad [5]$$

$$\frac{\partial\phi}{\partial t} = \frac{1}{r}(2R\dot{R}^2 + R^2\ddot{R}) \quad [6]$$

Equation [4] will be applied at $r = R$ so that the equation of motion for the bubble radius is determined (5). One notes that

$$(\partial\phi/\partial t)_{r=R} = 2\dot{R}^2 + R\ddot{R}$$

$$(\nabla\phi)^2_{r=R} = \dot{R}^2$$

so that Equation [4] becomes

$$\frac{p(R) - P(t)}{\rho} = \frac{3}{2}\dot{R}^2 + R\ddot{R} \quad [7]$$

Equation [7] is the general equation of motion for a spherical bubble in a liquid with given external pressure $P(t)$, and with the pressure at the bubble boundary $p(R)$. One gets Rayleigh's solution as a special case with

$$P(t) - p(R) = P_0 \text{ (a constant)}$$

and with the aid of the relation

$$\frac{3}{2}\dot{R}^2 + R\ddot{R} = \frac{1}{2\dot{R}R^2}\frac{d}{dt}(R^3\dot{R}^2)$$

Equation [7] is adapted to the present problem with the assumption that

$$p(R) = p_v - 2\sigma/R \quad [8]$$

where p_v is the vapor pressure of the water at the appropriate temperature and σ is the surface-tension constant for water. It is thus supposed that one has to deal with the growth and collapse of a "vapor" bubble. The problem is defined when $P(t)$ is known. It will be assumed, as just discussed, that $P(t)$ is determined from the noncavitating pressure distribution over the body.

The analysis of the experimental data, and the comparison with the theory, are carried out in the following manner: The experimental data given include bubble photographs, Fig. 3, which determine the following:

1 The position of the bubble relative to the body profile as a function of time.

2 The radius R of the bubble as a function of time.

Further, the tunnel temperature (and hence p_v) are given as well as p_0 and V_0; these data are usually combined in the specification of the cavitation parameter K and the tunnel temperature. From this information, and the knowledge of the pressure distribution over the body, Fig. 2, the absolute pressure at the model surface is determined. This absolute pressure as a function of position on the model is now transformed into the function $P(t)$ from the correlation of the bubble position on the model with time. When $P(t)$ has been determined, the integration of the equation of motion (Equations [7] and [8]) may be carried out to get the radius of the bubble R as a function of time. The equation of motion cannot be integrated analytically, and its integration was performed numerically. The solution is determined when two constants are specified, and these were taken to be the observed value of the maximum radius R_m where $\dot{R} = 0$. Thus the theoretical solution has been fitted to the experimental curve only at the peak of the radius-time curve. The theoretical curve was then determined by integrating forward (the collapse portion) and backward (the growth portion) from this one point. A comparison of the calculations with the measured values is shown in Figs. 4, 5, 6, and 7. The agreement is considered satisfactory, particularly since it must be emphasized that precise experimental data are difficult to obtain. The theoretical radius-time curve is quite sensitive to the $P(t)$ function; for the experiments thus far analyzed, it is believed by the experimental workers that the cavitation parameter K has not been determined with quite the necessary accuracy. Further, there are some difficulties in the determination of the bubble outlines with precision. That this is the case is not surprising since one is requiring considerable photographic detail throughout a process which lasts for a time of the order of a millisecond. It must also be pointed out that there are approximations involved in applying the theoretical equation to the experimental situation. These approximations will now be considered.

Theoretical Approximations

The Pressure Field. It has been supposed that the pressure field, $P(t)$, acting on the bubble is determined from the pressure distribution over the model. It is clear that, in the initial stages of cavitation of present interest, the bubbles will form as close to the model surface as possible since the pressures take their lowest values there. However, it also has been assumed that the bubble is acted on by a spherically symmetric field. Since the bubble is of finite extent and since the pressure field has definite pressure gradients both along the model and normal to it, it is clear that a simplification has been introduced. These pressure gradients would be a source of asymmetry in bubble shape, and there is some evidence of this asymmetry. It is believed that the approximation made is not such as to obscure the essential details of the growth and collapse; space gradients in the pressure field are here regarded as a second-order effect.

It also has been assumed that the bubble is in a liquid of infinite extent, and it is evident that the bubble grows and collapses in the neighborhood of the model surface. This asymmetry in the fluid field has an effect which may be pointed out as follows: As compared with the experimental situation, the theory would exaggerate the importance of the liquid inertia (this inertia leads to the term in $\dot{R}^2$ in Equation [7]). Comparison of the theoretical curve with the experimental points would seem to indicate some overestimate of this inertia term where R is small, i.e., near the beginning of the growth and toward the end of the collapse.

The presence of the model surface has an additional effect on the flow field in its neighborhood which arises from the boundary layer. The thickness of this boundary layer may be estimated from the Blasius formula, and for the present flow conditions

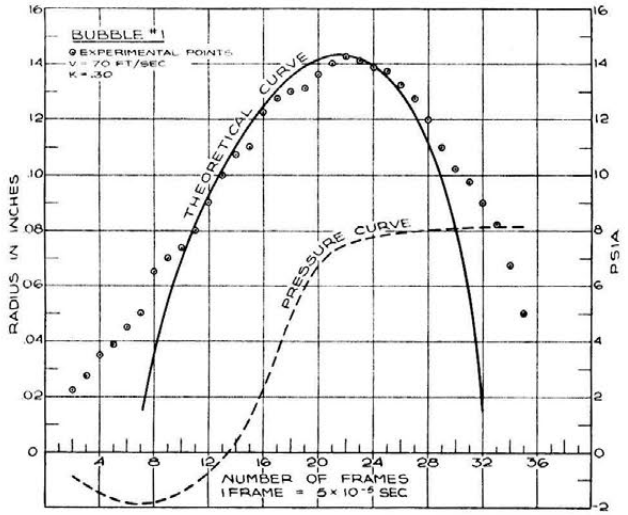

FIG. 4

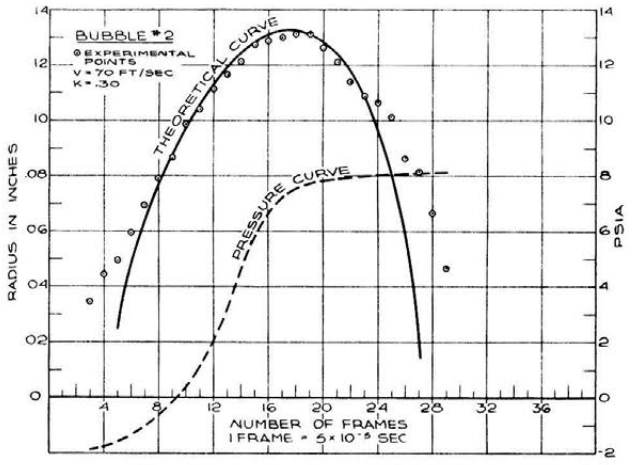

FIG. 5

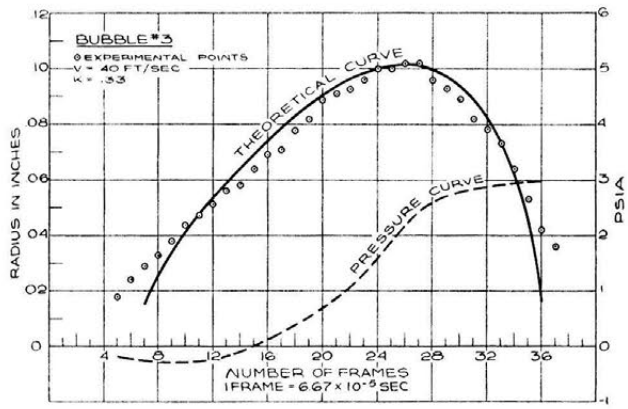

FIG. 6

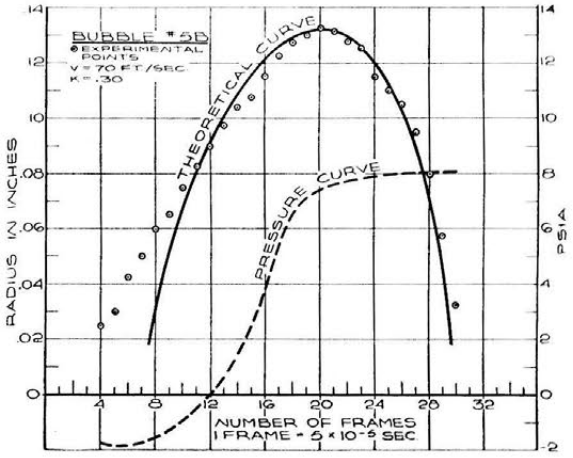

FIG. 7

leads to a thickness of the order of 6×10^{-3} in. On the basis of this estimate, the effect of the boundary layer will be neglected. It should be noted that the present measurements extend to minimum bubble sizes larger than this boundary-layer thickness although some reduction in the effective value of $\dot{R}$ should be expected for very small R.

An experimental source of apparent asymmetry in bubble shape might be supposed to arise from an overestimate of the bubble dimension in the direction of its motion which would be produced by its motion during the time of light exposure (1.5×10^{-6} sec). However, this blurring would give an apparent extension of the image by approximately 10^{-3} in. so that this error is not particularly significant.

Temperature and Pressure Conditions in Bubble. It has been assumed in the theoretical calculations that the vapor pressure, p_v, in the bubble, and hence the bubble temperature, remain constant. Clearly, heat must be applied to the bubble to evaporate water and maintain the vapor pressure during growth, and heat of condensation must be removed during collapse. The temperature changes required may be estimated readily. Consider a bubble with maximum radius R_m which has a growth time τ. The total mass of vapor which is evaporated into the bubble is $(4\pi/3)R_m^3\rho'$, where ρ' is the vapor density. The total heat required is

$$Q = (4\pi/3)R_m^3\rho'L$$

where L is the latent heat of evaporation. Thus for a bubble which grows to a maximum radius $R_m = 0.10$ in. in 20 frames ($\tau = 10^{-3}$ sec), the mass of vapor is 1.17×10^{-6} grams, and $Q = 6.8 \times 10^{-4}$ calories. This heat is taken out of a water layer surrounding the bubble. If the thermal diffusivity of water is D ($D = 1.43 \times 10^{-3}$ sq cm per sec), then the order of magnitude of the thickness d of the water layer from which this heat is conducted is

$$d \approx \sqrt{D\tau}$$

and for $\tau = 10^{-3}$ sec, $d \approx 1.2 \times 10^{-3}$ cm. The volume of the water layer from which this heat comes is of the order of magnitude $4\pi R_m^2 d$, and, in the present example, the corresponding mass of water is 1.0×10^{-3} g. Finally, the temperature drop of this water layer is

$$\Delta T \approx \frac{(4\pi/3)R_m^3\rho'L}{4\pi R_m^2 d\rho c} = \frac{R_m}{3d}\frac{\rho'L}{\rho c}$$

$$\approx \frac{R_m}{3\sqrt{D\tau}}\frac{\rho'L}{\rho c}$$

where c is the specific heat of water. In the present example, ΔT (growth) ≈ 0.7 deg C $= 1.3$ deg F. A typical value of collapse time is $\tau \approx 10$ frames $= 0.5 \times 10^{-3}$ sec, and the corresponding

temperature change, estimated in this same way, is

$$\Delta T \text{ (collapse)} \approx 1 \text{ deg C} = 1.8 \text{ deg F}$$

It is apparent that these temperature changes are insignificant so that one may take the bubble boundary to have a constant temperature, essentially the same as the water temperature, and a constant value of p_v.

This conclusion cannot be accepted unconditionally, however, since evaporation, or condensation, is a process which takes place at a finite rate and, if this rate is not sufficiently high to keep up with the rate of volume change of the bubble, the vapor in the bubble will behave more like a permanent than a condensable gas. This effect definitely limits the range of validity of the particular assumption, p_v = const, toward the end of the collapse phase where the radial velocity $\dot{R}$ increases rapidly. This trend toward rapid increase in the calculated radial velocity is illustrated in Fig. 8. The rate of evaporation,

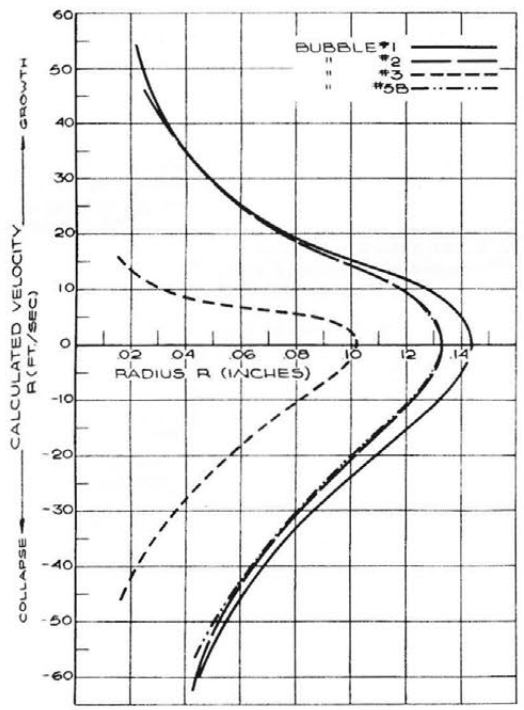

FIG. 8 CALCULATED RADIAL VELOCITIES $\dot{R}$, ARE SHOWN AS A FUNCTION OF BUBBLE RADIUS R

or condensation, can be estimated from elementary kinetic theory which says that the mass of gas evaporated (or condensed) per unit area per unit time at an absolute temperature T is

$$j = p_v \sqrt{\frac{M}{2\pi BT}} \quad \ldots\ldots\ldots\ldots\ldots\ldots [9]$$

where p_v again denotes the vapor pressure for a vapor with molar mass M, and B is the gas constant. If one assumes that the vapor obeys the perfect, gas law

$$p_v = \frac{\rho'}{M} BT$$

which is reasonably accurate in the temperature range of interest (6), Equation [9] may be written

$$j = \rho' \sqrt{\frac{BT}{2\pi M}} = \rho' V \quad \ldots\ldots\ldots\ldots\ldots [10]$$

where $V = \sqrt{BT/2\pi M}$ is the desired velocity to be associated with the rate of the evaporation or condensation process. For the present problem, at 22.2 C = 72 F, V is approximately 150 mps $\approx$ 500 fps. Hence unless $\dot{R}$ is appreciably less than this value, one may not assume the constant value for p_v. During the collapse, when $\dot{R}$ approaches or exceeds this value, the collapse velocity would tend to be decreased because the vapor will begin to show a rising pressure as it behaves like a permanent gas.

A further effect of interest is the shock loss which will appear in the vapor when $\dot{R}$ reaches the gas acoustic velocity. The effects of compressibility both in the vapor and in the liquid will not be considered here, although the problems posed by them are of great interest. A solution of these problems will be decisive for the quantitative determination of the high pressures arising toward the end of the bubble collapse, the regrowth or subsequent oscillations of the bubble, and the sound energy radiated.

Air Content in Bubble and Role of Nuclei in Formation of Bubbles. The assumption has been made that any air contained in the bubble does not affect the dynamics of the bubble growth and collapse over the range of bubble sizes which have been measured and analyzed here. This assumption might be considered questionable since the water-tunnel flow experiments are made with water containing an appreciable concentration of dissolved air. Furthermore in the region of flow in which the bubble behavior is studied, the liquid pressure is considerably below the liquid static pressure p_0 at a distance from the model. Hence one should expect that the water is supersaturated with dissolved air and that diffusion of air into the bubble would take place.

An analytic solution for such a diffusion problem has been carried out by P. S. Epstein and the author, the details of which will be presented elsewhere. For the present discussion it is necessary only to say that the diffusion process is so slow that it does not contribute appreciably to any alteration in the air content of the bubble.

As will be pointed out later, the initial air content of a bubble is very small so that over the range of bubble sizes which are observed and to which the present calculations have been applied, the effect of the air may be neglected. It must be emphasized, however, that the small mass of air in the bubble plays a most important role in the initial stages of bubble growth, and also may enter in the final stages of the bubble collapse. The initial stages of bubble growth in which the air content would be of significance, refer to bubble dimensions which are beyond the present range of experimental observation. Similarly, the final stages of bubble collapse in which the compressibility of air, water vapor, and liquid are of importance, refer to bubble dimensions which lie within the last frame photographed.[3]

A few remarks, nevertheless, may be made concerning the initial formation of the bubble. It is the present view that the formation of a bubble in cavitating flow, or in boiling, begins from a nucleus within the liquid containing air, or vapor, or both. Such gas-phase nuclei are ordinarily submicroscopic in size, and become evident only upon growth of the nuclei through pressure reduction in the liquid (reduction in the function denoted previously by $P[t]$), or through elevation of temperature (increase in the function denoted by $p[R]$). The absence of such nuclei means that the very large forces of surface tension must be overcome to initiate cavitation or boiling. It is well known that degassed pure liquids can withstand very large tensions,

[3] Knapp and Hollander (3) assumed that, over the present range of observation, the bubble contains essentially only water vapor. The present discussion supports this view.

or may be superheated considerably, without the formation of cavities and bubbles.

Recently, Harvey (7) and subsequently Pease and Blinks (8) have shown experimentally that water saturated with air also has high tensile strength, provided it is denucleated. Harvey's method of denucleation of water saturated with air consists in putting the solution under high pressures (of the order of 10,000 psi) for several minutes. The air nuclei are squeezed into solution so that when the solution is brought back to atmospheric pressure it does not cavitate under the tensions which freely produced cavitation before the pressurization. These same pressure-treated air-water solutions also can be superheated by as much as 60 to 80 deg C without boiling.

Presumably in ordinary untreated water the nuclei which contain gas and vapor are stabilized on small solid particles. The presence of a solid, or third phase, is indicated since the surface energy of a bubble bounded by a solid surface and a liquid surface may be very low. Methods whereby the probable rate of formation of nuclei as determined by the surface energy may be calculated have been discussed by Becker and Döring (9) and Kaischew and Stranski (10). The aim of the theory is to calculate the tensile strength of liquids, but it should be applicable also to the statistics of the number of nuclei which should grow to macroscopic bubbles for given conditions of liquid temperature and pressure.

Conclusion

The main purpose of the present discussion, aside from touching upon problems which still await quantitative solution, has been to point out the following: Liquid flow can be divided into the three regimes mentioned; and, since the noncavitating regime and the single-cavity regime may be considered to be on a quantitative basis, the main concern here has been a clarification of the second, or bubble, regime of flow. Also, it has been remarked that an interesting experiment would be the measurement of the pressure distribution over a body in this second regime of flow. It has been shown that the macroscopic behavior of cavitation bubbles may be explained reasonably well by a fairly simple equation.

Finally, it may be pointed out that the macroscopic behavior of the bubbles formed in a boiling liquid may be considered as entirely analogous to the cavitation bubbles more specifically considered here. The growth of bubbles in a liquid has great interest at present in the problem of increasing the heat transfer from a heated solid to a liquid.

Acknowledgments

The study was carried on in the Hydrodynamics Laboratory of the California Institute of Technology. It forms a part of the activities of Contract NOrd-9612 which is jointly supported by the Research and Development Division of the Bureau of Ordnance and the Fluid Mechanics Branch of the Office of Naval Research.

The author wishes also to acknowledge the assistance of Mr. F. H. Brady and Mr. J. M. Green in the numerical computations.

BIBLIOGRAPHY

1 "Hydrodynamics," by H. Lamb, Dover Publications, New York, N. Y., sixth edition, 1945, chapt. 4, pp. 73–78.

2 "Theoretical Hydrodynamics," by L. M. Milne-Thompson, Macmillan & Company, London, England, 1938, chapt. 13.

3 "Laboratory Investigations of the Mechanism of Cavitation," by R. T. Knapp and A. Hollander, Trans. ASME, vol. 70, 1948, p. 419.

4 "Pressure Developed in a Liquid During the Collapse of a Spherical Cavity," by Lord Rayleigh, *Philosophical Magazine*, vol. 34, 1917, pp. 94–98 (Collected Papers, vol. 6, pp. 504–507).

5 "Hydrodynamics," by H. Lamb, Dover Publications, New York, N. Y., sixth edition, 1945, chapt. 5, art. 91a.

6 "Properties of Ordinary Water-Substance," by N. E. Dorsey, Reinhold Publishing Corporation, New York, N. Y., 1940, table 250, pp. 575–576.

7 "On Cavity Formation in Water," by E. Newton Harvey, W. D. McElroy, and A. H. Whiteley, *Journal of Applied Physics*, vol. 18, 1947, p. 162.

8 "Cavitation From Solid Surfaces in the Absence of Gas Nuclei," by D. C. Pease and L. R. Blinks, *Journal of Physical and Colloid Chemistry*, vol. 51, 1947, p. 556.

9 "Kinetische Behandlung der Keimbildung in Übersättigten Dämpfen," by R. Becker and W. Döring, *Annalen der Physik*, vol. 24, series 5, p. 719.

10 "Zur Kinetischen Ableitung der Keimbildungsgeschwindigkeit," by R. Kaischew and I. N. Stranski, *Zeitschrift für Physikalische Chemie*, (B), vol. 26, 1934, p. 317.

Energy Method for Determining Dynamic Characteristics of Mechanisms

By B. E. QUINN,[1] LAFAYETTE, IND.

Two types of problems are dealt with in the paper which are involved in the design of mechanisms required to have specified dynamic characteristics: (1) Determination of applied forces required to produce specified dynamic characteristics. (2) Determination of the dynamic characteristics which will result from the application of known forces. While graphical methods may be used in the solution of type (1) problems involving more or less complex mechanical systems, they do not afford a direct approach to type (2) problems. The energy method which will be outlined can be applied in either case, although this paper will be primarily concerned with the determination of the dynamic characteristics which result when a known force is applied to a given mechanism.

Introduction

WHEN designing circuit breakers and other mechanical devices it is often desirable to determine the time required for these mechanisms to complete a motion cycle. It is also desirable to determine the manner in which the velocity and acceleration of certain moving parts, such as contact tips, will vary during the motion of the mechanism. In designing such devices the desired dynamic characteristics are often the basis upon which the engineer determines the proportions of the various links in the mechanism. Many times these characteristics will determine the forces which will be required to operate the device. Before beginning the design of a new circuit breaker the time required to interrupt the circuit may first be established. In addition, certain velocity characteristics may be desired when the moving contacts are interrupting or closing the circuit. These specified dynamic characteristics may thus be the basis upon which design calculations are made.

If the dimensions of the parts in the mechanism are known, and if the acceleration of one part is given, it is usually possible to determine the corresponding accelerations of all the other moving parts. It is then possible to determine the force which must be applied to the driving member to produce these accelerations.[2] If this analysis is repeated for successive positions of the mechanism, a curve showing the magnitude of the driving force can be determined. A force applied to the mechanism in this manner should then produce the desired dynamic characteristics.

In many cases, however, it may be impractical to supply a driving force to the mechanism which will vary in the desired manner. The engineer is limited to springs, air cylinders, and other devices which have definite force-displacement characteristics. Therefore it may be difficult to modify these devices to obtain a special velocity or acceleration characteristic in the driven mechanism. The problem then arises of determining the velocities and accelerations which will result when an available driving force is used. While other methods[3,4] have been suggested for solving this problem, it is the purpose of this paper to present a simple method which does not require an extensive mathematical background. It may be well to summarize briefly the two types of problems which are involved in the design of mechanisms required to have specified dynamic characteristics:

1 Determination of applied forces required to produce specified dynamic characteristics.

2 Determination of the dynamic characteristics which will result from the application of known forces.

In elementary problems in mechanics there is little difference in the method whereby a solution to either of the foregoing problems can be obtained. In the more complex mechanical systems, however, the graphical method,[2] used for solving type (1) problems, does not afford a direct approach to type (2) problems. The energy method which will be outlined can be applied in either case, although this paper will be primarily concerned with the determination of the dynamic characteristics which result when a known force is applied to a given mechanism.

Fundamental Considerations

It is convenient to consider the mechanical system shown in Fig. 1(*a*). Assume that this mechanism is lying in a horizontal plane, that the links are rigid, and that no friction is present. If a motor is connected to the crankshaft the mechanism can be brought up to a speed such that the crank (2) will rotate with an angular velocity ω_{21}. If the motor is disconnected the mechanism will continue to run. If the piston had maximum velocity at the time of release, it also had the maximum kinetic energy which it would attain during its motion cycle. When it reaches the end of the stroke, however, the velocity will be zero. Where then will be the kinetic energy which was in the piston? Since all members are constrained to move in a horizontal plane there can be no change in the potential energy of the system. If the links are rigid, no strain energy will exist. No external work can be done on the mechanism, since no friction is present. Under these conditions the total kinetic energy which was present at the time of release will remain unchanged. This means that the kinetic energy of the piston must reappear as kinetic energy in other links. This will result in an increase in the velocity of the other members since neither the mass nor the moment of inertia of any member changes. It is thus seen that the velocity of the crank and connecting rod will vary depending upon the amount of kinetic energy which they must possess to keep the total kinetic energy in the mechanism the same at all times. The *distribution*

---

[1] Associate Professor of Machine Design, Purdue University. Mem. ASME.

[2] "Mechanics of Machinery," by C. W. Ham and E. J. Crane, McGraw-Hill Book Company, Inc., New York, N. Y., 1938, pp. 338–342.

Contributed by the Applied Mechanics Division and presented at the Annual Meeting, New York, N. Y., November 28-December 3, 1948, of The American Society of Mechanical Engineers.

Discussion of this paper should be addressed to the Secretary, ASME, 29 West 39th Street, New York, N. Y., and will be accepted until October 10, 1949, for publication at a later date. Discussion received after the closing date will be returned.

Note: Statements and opinions advanced in papers are to be understood as individual expressions of their authors and not those of the Society. Paper No. 48—A-18.

[3] "Mechanics Applied to Vibrations and Balancing," by D. L. Thornton, John Wiley & Sons, Inc., New York, N. Y., 1940, p. 62.

[4] "Dynamical Analysis of Machines," by R. Eksergian, *Journal of The Franklin Institute*, vol. 209, 1930, p. 21.

of the kinetic energy therefore must change for successive positions of the mechanism.

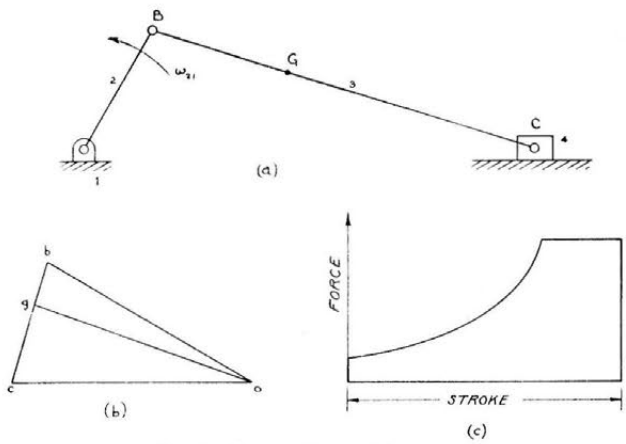

FIG. 1 SLIDER-CRANK MECHANISM

The kinetic energy (KE) of the mechanism in Fig. 1 (*a*) can be computed as follows

$$\text{KE (crank)} = \frac{1}{2} I_c \omega_{21}^2 = \frac{1}{2} I_c \left(\frac{V_b}{OB}\right)^2 \quad \ldots\ldots\ldots [1]$$

$$\text{KE (piston)} = \frac{1}{2} M_p V_c^2 \quad \ldots\ldots\ldots\ldots\ldots\ldots [2]$$

$$\text{KE (con. rod)} = \frac{1}{2} M_r V_g^2 + \frac{1}{2} I_r \omega_{31}^2$$

$$= \frac{1}{2} M_r V_g^2 + \frac{1}{2} I_r \left(\frac{V_{cb}}{CB}\right)^2 \quad \ldots\ldots\ldots [3]$$

It will be noted that these equations are finally expressed in terms of the linear velocities of various points in the mechanism. These velocities can be obtained from the velocity-vector polygon shown in Fig. 1(*b*).

If the velocity of B is doubled for the indicated position of the mechanism, then all other velocities will be doubled. Thus it is seen that a linear relationship exists between the velocities of all the points in the mechanism for a given position. If V_b is doubled, the kinetic energy of the crank will be increased fourfold. A fourfold increase will also result in the kinetic energy of the piston since V_c will be doubled. The connecting rod likewise undergoes a similar increase in kinetic energy. The total amount of kinetic energy in the mechanism will thus be 4 times the original value. It is important to note, however, that the per cent of the total kinetic energy contained by any link will remain the same despite a change in speed. For mechanisms in which there is no change in the mass or moment of inertia of the links with respect to speed, and in which a linear relationship exists between the velocities in a given position, the following theorem is advanced:

"The per cent of the total kinetic energy which the link of a mechanism contains will remain the same in any given position regardless of the speed."

This theorem is the basis of the proposed method for determining the dynamic characteristics of mechanisms.

PROPOSED METHOD

Assume that a force is applied to the head end of the piston shown in Fig. 1 (*a*), which varies along the stroke according to the force-displacement diagram shown in Fig. 1 (*c*). The mechanism could thus represent a single-cylinder steam engine to which the steam is being admitted. It is required to construct the velocity-displacement curve and the displacement-time curve for the piston.

The first step in the energy method is to determine the per cent of the total kinetic energy contained by each link of the mechanism for a series of selected positions. In order to do this, however, the velocities indicated in Equations [1], [2], [3] must be known. According to the theorem, the distribution of the kinetic energy is independent of the speed for a given position. This means that if 20 per cent of the total kinetic energy is in the piston for the position shown in Fig. 1 (*a*), then this value (20 per cent) will be obtained regardless of the speed of the mechanism for which the computation was made. Therefore a convenient value of velocity is assumed for a link of the mechanism, and the kinetic energy of each link is computed for the corresponding velocity. The sum of the kinetic energies of each link gives the total kinetic energy in the mechanism from which the per cent contained by any link can easily be obtained. If this is done for a series of positions the curves shown in Fig. 2 can be drawn.

To conserve space, the numerical computations necessary to construct the curves in Fig. 2 have been omitted. It was necessary to obtain the velocities indicated in Equations [1], [2], [3] for successive positions of the piston. A constant velocity was assumed for point B, and the corresponding velocities were obtained by the use of velocity-vector polygons. The total kinetic energy in the mechanism varied from position to position because of the constant velocity selected for point B. This indicated that the crank would not have constant angular velocity if the total kinetic energy of the mechanism remained unchanged. The following data were used in making these computations:

Weight of connecting rod, lb	3.7
Weight of piston, lb	4.0
Weight of crank, lb	4.0
Moment of inertia of crank, slug-ft^2	0.016
Moment of inertia of connecting rod, slug-ft^2	0.016
Length of crank, in	4
Length of connecting rod, in	16
Distance $\overline{BG}$, in	4

The second step in the procedure consists of drawing the velocity-displacement curve for the piston. An arbitrary displace-

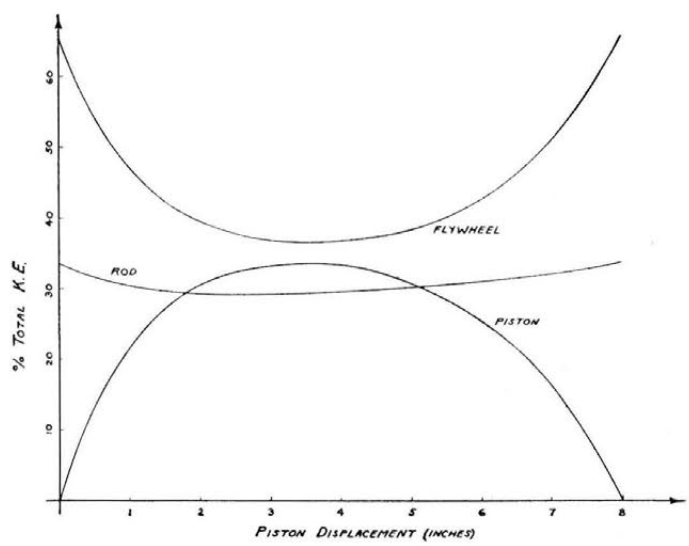

FIG. 2 CURVES SHOWING DISTRIBUTION OF KINETIC ENERGY IN SLIDER-CRANK MECHANISM

ment is selected, and from Fig. 1 (*c*) the work done by the applied force is computed. This of course will be represented by the area under the force-displacement curve for the given displacement. Under the conditions previously outlined, this work must appear as kinetic energy in the mechanism. From Fig. 2 the per cent of the kinetic energy which will appear in each member can be determined; hence the amount of kinetic energy which the piston will contain after the given displacement can be computed. Knowing this value, the velocity of the piston can be obtained by solving Equation [2] for V_c. Thus the velocity-displacement curve can be constructed.

All of the work done by the applied force may not appear as kinetic energy in the mechanism. If the mechanism had been in a vertical plane, then the potential energy of the connecting rod would have changed. Had the mechanism also compressed a spring during the displacement then the amount of work available as kinetic energy would have been still further reduced. In actual mechanisms friction is present, and machine parts may be quite elastic. Therefore care must be taken in determining the amount of work which is available as kinetic energy.

It is possible to determine other dynamic characteristics from the velocity-displacement curve. By using the subnormal construction,[5] the acceleration at any displacement can be obtained. The curve can be integrated to give the time corresponding to a selected displacement, from which the displacement-time curve can be constructed. The other dynamic characteristics can thus be determined from the velocity-displacement curve.

The curves in Fig. 2 could also be used to determine the force which would be required to produce desired dynamic characteristics. Suppose that a velocity-displacement curve was selected for the piston, and that the force-displacement curve was the characteristic to be obtained. The velocity of the piston would then be known in successive positions, and the kinetic energy of the piston could thus be computed. From the curves in Fig. 2 the per cent of the total kinetic energy of the mechanism which is found in the piston for the selected position can be determined. The total kinetic energy in the mechanism can thus be computed. This kinetic energy must be produced by the unknown force applied to the piston acting through the selected displacement. Therefore the average force can be calculated. If small piston displacements are used the force-displacement curve can be constructed.

Example

In Fig. 3 is shown a circular disk cam with a flat-faced follower. A weight is fastened to a string which is wrapped around a drum fastened to the cam. It is required to construct the velocity-time curve for the follower and the weight. The mechanism is shown in the position for which the cam and the follower are considered as having no potential energy. The following data are to be used:

Weight of cam, lb	3.49
Weight of follower, lb	3.49
Weight W, lb	10
Radius of disk cam, in	4
Radius of drum, in	2
Distance B, in	2
Radius of gyration of cam and drum about center of rotation, in	3.46

The first step is to consider the cam to be rotating with a constant angular velocity. The follower will then move with simple harmonic motion, and its displacement and velocity can easily be computed as shown in Table 1. The weight will travel with constant velocity, thus the kinetic energy of the members can be determined easily for successive cam positions. To conserve space the calculations are shown for every 45 deg of an entire revolution of the cam. From the total kinetic energy the per cent contained by each member is calculated and the curves shown in Fig. 4 are plotted. It can be seen from these curves that the calculations need only be made for one half a revolution of the cam, since the values are repeated in the latter portion of cam rotation.

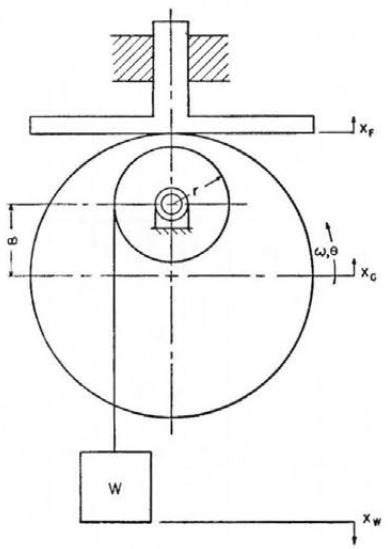

Fig. 3 Cam Mechanism

In accordance with the second step in the solution, the velocity-displacement curves can now be constructed for the follower and the weight. The downward displacement of the weight is computed for a selected angular displacement of the cam, and the work done by the weight in moving this distance is computed. The corresponding increase in potential energy of the cam and follower is calculated, and is subtracted from the work done to obtain the amount of kinetic energy which appears in the system. Of this amount, the per cent which is in the weight, cam, and follower can be obtained from the curves shown in Fig. 4. The velocity of each member can then be computed when the kinetic energy which it possesses is known. The velocity-displacement curves can then be constructed. These computations are shown in Table 2.

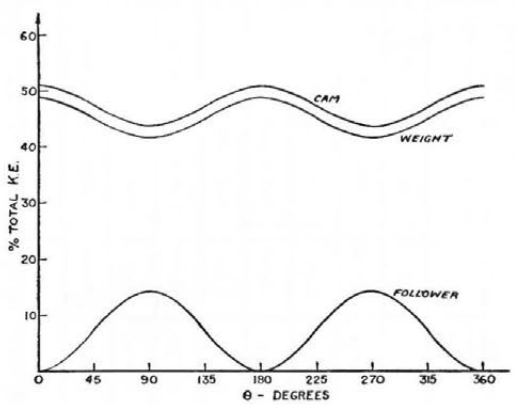

Fig. 4 Curves Showing Distribution of Kinetic Energy in Cam Mechanism

By the well-known method of graphical integration, the desired velocity-time curves can be obtained from the velocity-displace-

[5] "Kinematics of Machinery," by C. D. Albert and F. S. Rogers, John Wiley & Sons, Inc., New York, N. Y., 1938, p. 78.

TABLE 1 TABLE FOR COMPUTING DISTRIBUTION OF KINETIC ENERGY IN CAM MECHANISM
(ω = 30 radians per sec.)

DISPLACEMENTS					KINETIC ENERGY				% KINETIC ENERGY		
ωt (degrees)	$1-\cos \omega t$	$\sin \omega t$	$X_{follower}$ $2(1-\cos \omega t)$	X_{cam} $2(1-\cos \omega t)$	X_{weight} $\frac{-wt\,8\,\pi^2}{360}$	$V_{follower}$ $2\pi \sin \omega t$ 60 $\sin \omega t$	$KE_{follower}$ $\frac{1}{2}\frac{W}{g}V^2$ lb-in	KE_{weight} $\frac{1}{2}\frac{W}{g}V^2$ lb-in	KE_{cam} $\frac{1}{2}I\omega^2$ lb-in	TOTAL KE $KE_f+KE_w+KE_c$ lb-in	$\frac{\%KE_f}{\text{Total KE}}$	$\frac{\%KE_w}{\text{Total KE}}$	$\frac{\%KE_c}{\text{Total KE}}$
0	0	0	0	0	0	0	0	46.56	48.80	95.35	0	48.8	51.2
45	0.293	0.707	0.586	0.586	- 1.5708	42.42	8.12	46.56	48.80	103.48	7.8	45.0	47.2
90	1.0	1.0	2.0	2.0	- 3.1416	60.0	16.24	46.56	48.80	111.60	14.5	41.7	43.8
135	1.707	0.707	3.414	3.414	- 4.7124	42.42	8.12	46.56	48.80	103.48	7.8	45.0	47.2
180	2.0	0	4.0	4.0	- 6.2832	0	0	46.56	48.80	95.36	0	48.8	51.2
225	1.707	-0.707	3.414	3.414	- 7.8540	-42.42	8.12	46.56	48.80	103.48	7.8	45.0	47.2
270	1.0	-1.0	2.0	2.0	- 9.4248	-60.0	16.24	46.56	48.80	111.60	14.5	41.7	43.8
315	0.293	-0.707	0.586	0.586	-10.9956	-42.42	8.12	46.56	48.80	103.48	7.8	45.0	47.2
360	0	0	0	0	-12.5664	0	0	46.56	48.80	95.36	0	48.8	51.2

ment curves. The details of this step are omitted, but the results are given in Fig. 5. Equal intervals of time are shown along the horizontal axis, above which the corresponding intervals of cam rotation are indicated. The slope of the curves thus shown indicates acceleration, and the point where the follower would leave the cam contour could be determined. The dynamic characteristics of the cam mechanism, which will result from the application of the weight, can be obtained.

Although the method is thus illustrated for a very simple mechanism, it can be seen that for analyzing many of the more complex mechanical systems the only additional requirement is sufficient patience.

Conclusions

The proposed method consists of two steps which can be summarized briefly as follows:

1 Determination of the distribution of the kinetic energy in a mechanism.

2 Determination of the velocity of a member by knowing the amount of kinetic energy which it possesses after the applied force has acted through a given distance.

The method has disadvantages which limit the accuracy of the analysis. The effect of friction is cumulative, and the amount of error may increase during the motion cycle. This effect is difficult to determine analytically. If the members are elastic, some of the work done on the mechanism may appear as strain energy rather than kinetic energy. Therefore these factors introduce error in the computations.

There are advantages, however, in this method of analysis. Because accelerations are not required it is not necessary either to construct acceleration polygons or to determine accelerations analytically. Either procedure may be difficult in complex mechanisms. A velocity-vector polygon will supply all the necessary information for any selected position. The required velocities could be determined by instant centers or by any other method familiar to the individual making the analysis. However, the method is versatile since it can be applied to either of the two fundamental problems outlined in the introduction. An extensive mathematical background is not required in order to apply the energy method, although considerable mathematical skill is necessary for using other methods[3,4] of analysis. It is thus

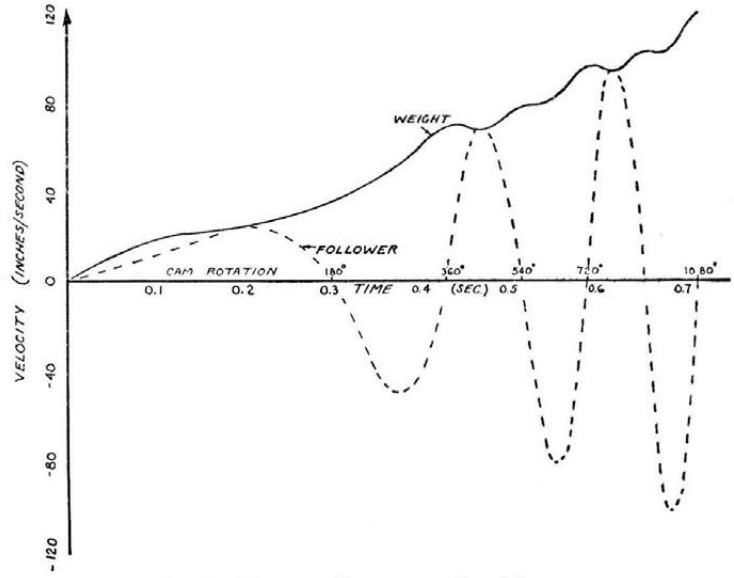

Fig. 5 Velocity Curves for Cam Mechanism

TABLE 2 COMPUTATIONS FOR VELOCITY-DISPLACEMENT CURVES

	θ degrees	X_w in.	PE (available) $=10X_w$ lb-in	X_f in.	PE (cam & follower) $=6.98X_f$ lb-in	KE (available) $=PE(a)-PE(c\&f)$	$KE_f=\%xKE(a)$ %	KE_f (lb-in)	$KE_w=\%xKE(a)$ %	KE_w (lb-in)	$KE_c=\%xKE(a)$ %	KE_c (lb-in)	$V_f=18.1$ KE_f lb-in KE$_f$	V_f (in/sec)	$V_w=8.8$ KE_w KE$_w$	V_w (in/sec)	$w_c=4.3$ KE_c KE$_c$	w_c (rad/sec)
1 REV.	0	0	0	0	0	0	0	0	48.8	0	51.2	0	0	0	0	0	0	0
	45	1.5708	15.71	0.586	4.08	11.63	7.8	0.908	45.0	5.24	47.2	5.49	.95	14.35	2.29	20.15	2.34	10.07
	90	3.1416	31.42	2.0	13.96	17.46	14.5	2.53	41.7	7.28	43.8	7.65	1.59	24.0	2.7	23.8	2.77	11.9
	135	4.7124	47.12	3.414	23.8	23.32	7.8	1.82	45.0	10.5	47.2	11.0	1.35	20.4	3.25	28.6	3.32	14.3
	180	6.2832	62.83	4.0	27.92	34.91	0	0	48.8	17.0	51.2	17.91	0	0	4.13	36.3	4.24	18.25
	225	7.8540	78.54	3.414	23.8	54.74	7.8	4.27	45.0	24.62	47.2	25.8	-2.07	-31.3	4.97	43.7	5.09	21.9
	270	9.4248	94.25	2.0	13.96	80.29	14.5	11.62	41.7	33.4	43.8	35.2	-3.42	-51.6	5.79	51.0	5.93	25.5
	315	10.9956	109.96	0.586	4.08	105.88	7.8	8.25	45.0	47.6	47.2	43.9	-2.88	-43.5	6.9	60.7	7.06	30.4
2 REV.	0	12.5664	125.66	0	0	125.66	0	0	48.8	61.3	51.2	64.3	0	0	7.85	69.0	8.04	34.6
	45	14.1372	141.37	0.596	4.08	137.29	7.8	10.7	45.0	61.8	47.2	64.8	3.27	49.4	7.86	69.0	8.05	34.6
	90	15.7080	157.08	2.0	13.96	143.12	14.5	20.75	41.7	59.6	43.8	62.8	4.55	68.7	7.72	67.9	7.92	34.0
	135	17.2788	172.79	3.414	23.8	148.99	7.8	11.6	45.0	67.0	47.2	70.3	3.4	51.3	8.2	72.2	8.4	36.1
	180	18.8496	188.50	4.0	27.92	160.58	0	0	48.8	78.4	51.2	82.2	0	0	8.85	77.9	9.09	39.1
	225	20.4204	204.20	3.414	23.8	180.40	7.8	14.1	45.0	81.3	47.2	85.1	-3.76	-56.8	9.03	79.5	9.24	39.7
	270	21.9912	219.91	2.0	13.96	205.95	14.5	29.9	41.7	85.8	43.8	90.3	-5.46	-82.5	9.26	81.5	9.51	40.9
	315	23.5620	235.62	0.586	4.08	231.54	7.8	18.08	45.0	104.0	47.2	109.0	-4.25	-64.2	10.3	90.6	10.45	44.9
3 REV.	0	25.1328	251.33	0	0	251.33	0	0	48.8	122.5	51.2	128.8	0	0	11.1	97.5	11.35	48.7
	45	26.7036	267.04	0.586	4.08	262.96	7.8	20.5	45.0	118.5	47.2	124.0	4.53	68.5	10.9	95.9	11.15	47.9
	90	28.2744	282.74	2.0	13.96	268.78	14.5	39.0	41.7	112.0	43.8	118.0	6.25	94.3	10.6	93.2	10.87	46.7
	135	29.8452	298.45	3.414	23.8	274.65	7.8	21.45	45.0	124.0	47.2	130.0	4.64	70.0	11.15	98.2	11.4	49.0
	180	31.4160	314.16	4.0	27.92	286.24	0	0	48.8	140.0	51.2	146.3	0	0	11.85	104.2	12.1	52.0
	225	32.9868	329.87	3.414	23.8	306.07	7.8	23.85	45.0	137.5	47.2	144.5	-4.89	-73.9	11.72	103.0	12.05	51.8
	270	34.5576	345.58	2.0	13.96	331.62	14.5	48.0	41.7	138.0	43.8	145.0	-6.94	-104.8	11.75	103.2	12.07	51.9
	315	36.1284	361.28	0.586	4.08	357.20	7.8	27.8	45.0	160.5	47.2	168.5	-5.28	-79.8	12.69	111.5	13.0	55.9
	0	37.6992	376.99	0	0	376.99	0	0	48.8	184.0	51.2	193.0	0	0	13.56	119.1	13.9	59.8

shown that by considering the kinetic energy in a mechanism the dynamic characteristics can be determined.

ACKNOWLEDGMENT

The author wishes to express appreciation to Mr. Donald Earl Taylor for assistance in preparing this paper.

Appendix

In this paper the theorem has been applied to relatively simple mechanisms. It can be applied, however, to any mechanism which satisfies the previously mentioned conditions. The following proof is thus advanced for a mechanism of p links which have plane motion.

The kinetic energy of link k in a selected position is given by

$$\mathrm{KE}_k = \frac{1}{2}\left[m_k v_k^2 + I_k \left(\frac{V_k}{r_k}\right)^2 \right] \quad [4]$$

in which

m_k = mass of link k
v_k = absolute velocity of mass center
I_k = moment of inertia
V_k = relative velocity of any two points on link k
r_k = distance between these two points

The total kinetic energy of the mechanism is then given by

$$\mathrm{KE}_{\text{total}} = \frac{1}{2}\sum_{k=1}^{k=p}\left[m_k v_k^2 + I_k \left(\frac{V_k}{r_k}\right)^2 \right] \quad [5]$$

The per cent of the total kinetic energy contained in link k is then

$$\text{Per cent total KE} = \frac{100\left[m_k v_k^2 + I_k \left(\frac{V_k}{r_k}\right)^2 \right]}{\sum_{k=1}^{k=p}\left[m_k v_k^2 + I_k \left(\frac{V_k}{r_k}\right)^2 \right]} \quad [6]$$

Substitute v_k' for v_k in which

$$v_k' = Cv_k \quad [7]$$

Since there is a linear relationship between the velocities

$$V_k' = CV_k \quad [8]$$

If there is no change in the mass or moment of inertia with respect to speed (modern machinery does not as yet operate at velocities which justify the use of non-Newtonian mechanics) Equation [6] becomes

$$\text{Per cent total KE} = \frac{100\left[m_k (Cv_k)^2 + I_k \left(\frac{CV_k}{r_k}\right)^2 \right]}{\sum_{k=1}^{k=p}\left[m_k (Cv_k)^2 + I_k \left(\frac{CV_k}{r_k}\right)^2 \right]} \quad [9]$$

Thus it can be seen that C is a factor common to all terms, and Equation [9] reduces to Equation [6].

The per cent of the total kinetic energy contained by link k is therefore independent of the speed.

Press-Forging Thin Sections: Effect of Friction, Area, and Thickness on Pressures Required

By WILLIAM SCHROEDER[1] and D. A. WEBSTER,[2] BURBANK, CALIF.

The application of press forging to parts with thin sections is desirable in many instances. It is generally recognized that in forging such parts, the pressure required may be very high. That this high pressure required is due to friction has been reported;[3] however, very little specific information on the effects of friction, area, and thickness is available. The results of this analysis resemble, in some respects, those presented in an analysis of forces required in rolling by Nadai.[4]

Nomenclature

The following nomenclature is used in the paper:

f = unit friction force
k = constant = 0.577
p = normal pressure at a point
p_a = average pressure
p_c = critical pressure at which the transition from sliding to "sticking" type friction results
r = radius (variable)
R = blank radius
t = blank thickness
$\sigma_r, \sigma_c, \sigma_n$ = principal stresses in radial, circumferential, and normal or axial directions, respectively
$\epsilon_r, \epsilon_c, \epsilon_n$ = principal natural strains in radial, circumferential, and axial directions, respectively
σ_h = hydrostatic component of stress system
σ_0 = flow stress of workpiece
μ = coefficient of friction

Classification of Friction Effects

The basic forging conditions selected for this analysis are illustrated in Fig. 1. It is assumed that the circular blank is reduced in thickness by pressing between two flat-faced dies. For the purpose of this analysis, it may also be assumed that the volume of the part remains constant during deformation; therefore the part grows larger in radius as the thickness is reduced, Fig. 2.

In general, the pressure required for forging depends upon: (*a*) the inherent flow stress of the material; (*b*) the strain pattern as determined by the configuration of the part; and (*c*) the effects of friction.

The flow-stress properties may be represented satisfactorily by a stress-strain diagram. The effect of configuration and friction are interrelated and, generally, must be considered simultaneously. The results of this analysis may be summarized as follows:

Under the conditions assumed the strain is similar to simple

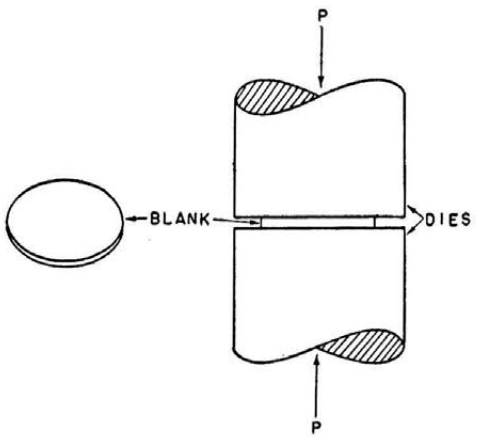

Fig. 1 Die Arrangement for Forging Tests

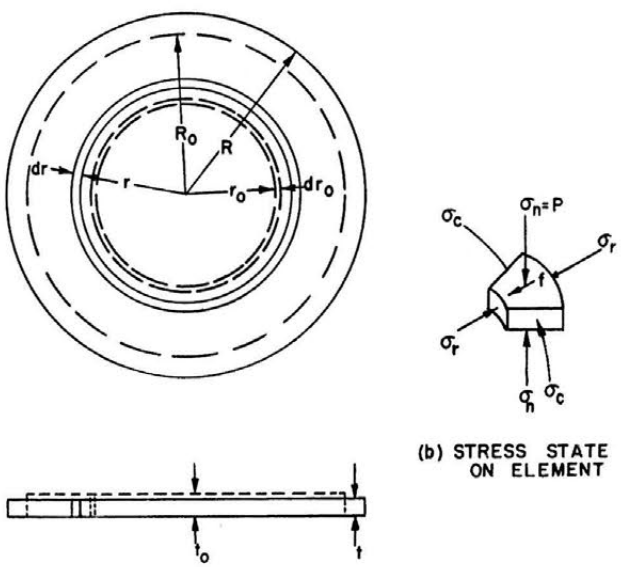

Fig. 2 Nomenclature

[1] Research Engineer, Lockheed Aircraft Corporation. Mem ASME.

[2] Research Engineer, Lockheed Aircraft Corporation.

[3] "Limits of Forging," by George Sachs, *Modern Industrial Press*, March, 1941, pp. 9–10.

[4] "The Forces Required for Rolling Steel Strip in Tension," by A. Nadai, Journal of Applied Mechanics, Trans. ASME, vol. 61, 1936, p. A-54.

Contributed by the Applied Mechanics Division and presented at the Aviation Meeting, Los Angeles, Calif., May 26–29, 1947, of The American Society of Mechanical Engineers.

Discussion of this paper should be addressed to the Secretary, ASME, 29 West 39th Street, New York, N. Y., and will be accepted until October 10, 1949, for publication at a later date. Discussion received after the closing date will be returned.

compression (with some exceptions noted) in that everywhere there is a compression in the one direction and two equal extensions in the two transverse directions. An exception to this strain pattern may result in some cases in the region of the part that is in close proximity to the die surfaces, namely, the surface layers.

In analyzing the effect of friction, three special cases are recognized. For a detailed analysis of these cases, the reader is referred to the Appendix. However, a brief description of the three cases follows:

1 Relative sliding motion occurs between the blank and die surface at all points except the geometric center of the blank.

2 Relative sliding motion between surfaces does not occur, and the spreading action results from shear strain in the blank surface parallel to the die surface.

3 The intermediate condition, where sliding takes place in an annular zone near the edge, and sticking (the term is here used to signify an absence of sliding) results in the central zone.

Case 1 applies when both the coefficient of friction (μ) and ratio of radius to thickness R/t are small.

Case 2 is best understood by considering the law of sliding friction. The unit friction force $f = \mu p$, where p is the unit normal force on the surface. This unit force f superimposes a shear stress of equal value on the existing stress system. For values of f equal to the shear yield stress, large shear deformations will result in the plane of the shear stress. It is demonstrated in the Appendix that for coefficients of friction equal to or larger than some critical value k, the entire spreading action of the parts will proceed by shear deformation within the blank rather than by a relative motion of blank to die surface.

An actual example of this condition of friction is illustrated in Fig. 3. In this figure it may be noted that the original surface of

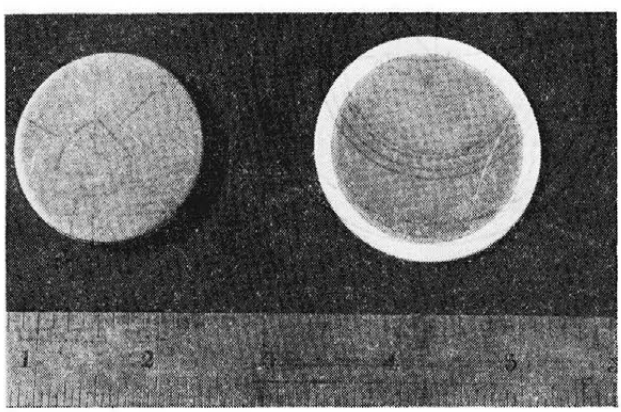

FIG. 3 ILLUSTRATION OF DEFORMATION WHEN FRICTION IS HIGH

the blank, recognizable by the dark circular region, has not increased appreciably in size.

The third condition applies when $\mu < k$ and

$$\frac{R}{t} > \frac{1}{2\mu} \ln \frac{k}{\mu}$$

PRESSURE DISTRIBUTION ON BLANK

The pressure distribution over the blank surface for the foregoing conditions, as derived in the Appendix, are expressed by the following formulas

Case 1: $\dfrac{p}{\sigma_0} < \dfrac{k}{\mu}$

$$\frac{p}{\sigma_0} = e^{2\mu\left(\frac{R}{t} - \frac{r}{t}\right)} \qquad [11]$$

where σ_0 is the flow stress of the material in the blank.

Case 2: $\mu \geq k$

$$\frac{p}{\sigma_0} = 1 + 2k\left(\frac{R}{t} - \frac{r}{t}\right) \qquad [16]$$

Case 3: $\mu < k$ and $\dfrac{p}{\sigma_0} > \dfrac{k}{\mu}$

Within the critical circular zone with radius r_c the pressure may be determined by

$$\frac{p}{\sigma_0} = \frac{k}{\mu} + 2k\left(\frac{r_c}{t} - \frac{r}{t}\right) \qquad [21b]$$

where the value of r_c is expressed by

$$\frac{r_c}{t} = \frac{R}{t} - \frac{1}{2\mu} \ln \frac{k}{\mu}$$

For values of r between r_c and R where sliding of surfaces results

$$\frac{p}{\sigma_0} = e^{2\mu\left(\frac{R}{t} - \frac{r}{t}\right)}$$

AVERAGE PRESSURE REQUIRED

The average pressures p_a, are expressed as follows for the three cases considered

Case 1:

$$\frac{p_a}{\sigma_0} = \frac{2}{C^2}(e^C - C - 1) \qquad [23]$$

where

$$C = \frac{2\mu R}{t}$$

Case 2:

$$\frac{p_a}{\sigma_0} = 1 + \frac{2k}{3}\frac{R}{t} \qquad [24]$$

Case 3:

$$\frac{p_a}{\sigma_0} = \frac{2}{C^2}[(D+1)e^{C-D} - C - 1] + \frac{D^2}{C^2}\left(\frac{k}{\mu} + \frac{2k}{3}\frac{r_c}{t}\right) \qquad [25]$$

where

$$D = \frac{2\mu r_c}{t}$$

GRAPHICAL REPRESENTATION IN TERMS OF NONDIMENSIONAL RATIOS

The equations for pressure as derived are essentially functions of three nondimensional ratios μ, R/t, and p_a/σ_0. Thus the solution for one value of μ and R/t provides a value of p_a/σ_0 for all geometrically similar circular blanks with the same ratio R/t. The ratio p_a/σ_0 is the ratio of average pressure required for the actual press forging to the pressure required under simple compression where friction effects and restraint are negligible.

The pressure equation is represented conveniently by contour plotting of p_a/σ_0 against R/t, for constant values of μ. It is necessary to determine for each value of R/t and μ, which of the

equations are applicable. Computations for several representative values of μ are shown in Fig. 4.

It should be understood that in press-forging the pressure is greatest at the end of the action; hence p_a, σ_0, R, and t refer to the final values. If the forging operation is conducted below the recrystallization temperature, σ_0 must be selected to include an amount of strain-hardening corresponding to that of the forging operation. At elevated temperature where the rate of recrystallization is rapid and the forging operation slow, it may be assumed that σ_0 depends mainly upon the temperature, and to a lesser extent upon the rate of deformation, and strain.

It may be noted that Fig. 4 represents all of the three conditions of friction discussed. The approximate ranges to which each of the cases applies have been indicated.

Experimental Determination of Nondimensional Ratios for Various Conditions of Forging

Test Procedure. An examination of Fig. 4 indicates the extreme importance of maintaining a low coefficient of friction for forging when the R/t ratio is relatively large. For this reason a series of tests were performed to determine the relative effectiveness of a number of lubricants. Suggestions were sought for best lubricant for forging from a study of the technical literature and from individuals in the forging industry. These and some of the authors' selections were tested.

Further tests in which R/t was varied through a wide range were conducted using one of the lubricants which gave best results in the foregoing comparison test.

Tests of forging at elevated temperature without lubricant were conducted because it appeared that this might supply some corroboration for the theoretical deduction that sticking should result over the entire blank surface when the coefficient of friction is large.

The investigation was confined to 61S aluminum alloy, and Dow M and Dow FS magnesium alloys. These were tested both at room and at elevated forging temperature. The elevated temperatures used were 700 F for Dow FS; 750 F for Dow M; and 800 F for 61S-O.

The dies were heated with electric heating coils. Temperatures were measured with an iron-constantan thermocouple mounted in the die near the edge of the blank, using a Leeds and Northrup potentiometer as an indicator. Blanks 1.62 in. diam and with thicknesses of 0.032, 0.064, 0.125, and 0.250 in. were used. The forging pressure was applied with one of two Southwark-Tate-Emery testing machines having capacities of 120,000 and 300,000 lb, respectively. Final thicknesses were measured with a micrometer gage, reading to 0.001 in. Diameters were determined by averaging four measurements made to the nearest 0.01 in. Reductions in thickness, in most cases, were limited to approximately 20 per cent.

Curves of flow stress in terms of strain were determined by compression-testing test cylinders 1 in. high and 1.62 in. diam under conditions of strain rate and temperature similar to the forging tests. The ends of the test cylinders were lubricated with a mixture of silicone grease and flake graphite to reduce friction.

The values of σ_0 used for computational purposes were read from the flow stress-strain curves for values of strain equal to those of the forging tests under consideration, thus incorporating approximately the effect of strain hardening.

The value p_a was obtained by dividing the maximum load applied by the final area. Similarly, R/t was computed on the basis of the final radius and thickness. The results obtained for various lubricants are shown in Figs. 4 and 5.

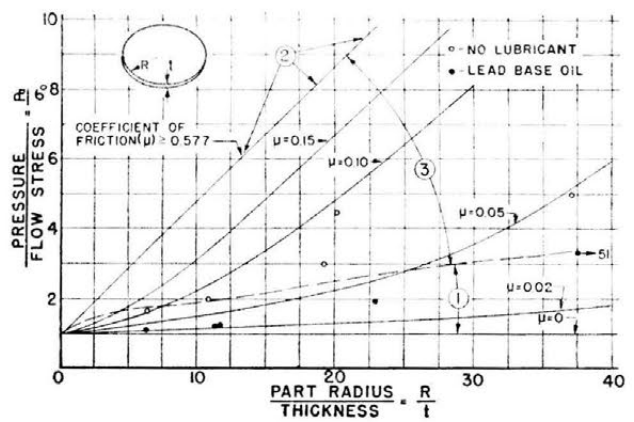

Fig. 4 Nondimensional Representation of Computed and Room-Temperature Forging-Test Results

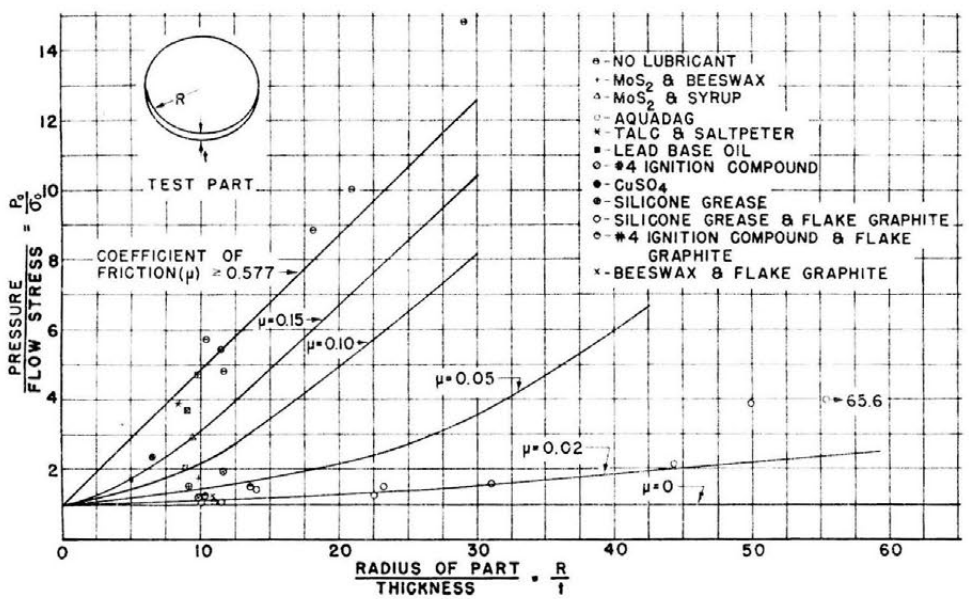

Fig. 5 Nondimensional Representation of Computed and Elevated-Temperature Forging-Test Results

Discussion of Results. The observed effect of friction, area, and thickness on press-forging pressures may be summarized approximately as follows:

1 The results indicate that the p_a/σ_0 value depends upon the R/t and lubricant used, but not upon the alloy tested. This would be expected from the analysis, provided it can be assumed that a particular lubricant gives the same coefficient of friction regardless of the alloy tested and pressure applied. The results indicate that the latter is approximately true for those particular ubricants tested over a range of R/t values.

The curves obtained by plotting p_a/σ_0 against R/t for a specific lubricant follows in general the shape of the curves computed for a constant coefficient of friction.

2 The values, Fig. 5, for the elevated-temperature tests, using no lubricant, agree approximately with the results predicted for Case 2 where sticking of the surface was assumed. Furthermore, as was mentioned before, this sticking of the surfaces was actually observed for these conditions, see Fig. 3.

The experimental results indicate that the curve of p_a/σ_0 versus R/t for "sticking" friction is approximately a straight line; however, the slope of the experimental line appears to be greater than predicted, indicating a value of k possibly larger than the theoretical value of 0.577 assumed for the computations.

3 A marked difference in pressures required was observed for different lubricants when other conditions were similar. This is attributed to the difference in lubricating quality of the lubricant under test conditions.

Although a number of lubricants were tested, no claim can be made that the best lubricants are represented in the list. In view of the extreme importance of lubrication under certain conditions of press forging, it is suggested that a more extensive investigation of lubricants might prove to be valuable.

No absolute check on the validity of the equation for pressure required could be made. Since simplifying assumptions were made for the stress and strain states and the nature of the materials, it may be assumed that the formulas are subject to some approximation. However, the formulas may be expected to be useful for predicting approximately the pressures required for press-forging parts that are relatively similar to those assumed in the analysis. This is particularly true if the coefficient of friction of the lubricant used is evaluated by means of these equations (as in Figs. 4 and 5), for in this case errors will tend to compensate.

In general, the method of approach used in the derivation has been found valuable in analyzing a variety of forging conditions.

Appendix

Referring to Fig. 1, it is assumed that a round blank is being deformed, plastically, between two parallel-faced dies. As the thickness of the blank is reduced, the radius is increased. It is further assumed that the material is incompressible, homogeneous, and isotropic in its properties. For these conditions it follows that the three principal natural strains are related by

$$\epsilon_r + \epsilon_c + \epsilon_n = 0 \qquad [1]$$

where

ϵ_r = radial natural strain
ϵ_c = circumferential natural strain
ϵ_n = normal, thicknesswise, natural strain

The natural strains may be expressed by

$$\left.\begin{aligned} \epsilon_r &= \ln \frac{dr}{dr_0} \\ \epsilon_c &= \ln \frac{r}{r_0} \\ \epsilon_n &= \ln \frac{t}{t_0} \end{aligned}\right\} \qquad [2]$$

where the significance of the symbols is as shown in Fig. 2. (In Fig. 2 the dotted lines indicate the initial while the solid lines indicate the final conditions.)

For the assumed conditions

$$\left.\begin{aligned} \ln \frac{r}{r_0} &= \ln \frac{dr}{dr_0} = -\frac{1}{2} \ln \frac{t}{t_0} \\ \text{or} \\ \epsilon_r &= \epsilon_c = -\frac{1}{2}\epsilon_n \end{aligned}\right\} \qquad [3]$$

These strain conditions are similar to those found in simple compression of a homogeneous isotropic and incompressible material.

Actual conditions will deviate somewhat from these conditions, especially when the unit friction force is large. The effect of a large deviation from these conditions will be considered later.

Differential Equation of Stress Distribution

The differential equation for stress distribution based upon Fig. 2(*b*) is

$$\frac{\partial \sigma_r}{\partial r} + \frac{\sigma_r - \sigma_c}{r} = -\frac{2f}{t} \qquad [4]$$

where f is the unit friction force on each of the two surfaces. Compressive stresses are represented by the positive sign.

Stress State

It is assumed that the shear-strain energy[5] is a criterion for yielding. In terms of Fig. 2 this may be expressed by

$$\sigma_0 = \frac{1}{\sqrt{2}} \sqrt{(\sigma_n - \sigma_r)^2 + (\sigma_r - \sigma_c)^2 + (\sigma_c - \sigma_n)^2} \qquad [5]$$

where σ_0 is the stress to produce yielding under uniaxial loading (simple compression).

It was noted previously that the strain state conforms to that of simple compression. Under these conditions the general stress state is that of uniaxial compression, combined with a hydrostatic pressure in which the n-direction corresponds to the directions of the compression; thus

$$\left.\begin{aligned} \sigma_n &= \sigma_0 + \sigma_h \\ \sigma_r &= \sigma_c = \sigma_h \end{aligned}\right\} \qquad [6]$$

where σ_h is the hydrostatic-pressure component. That these conditions satisfy Equation [5] may be verified readily by substitution.

It may be recognized that by the principle of transmissibility of forces

$$\sigma_n = p \qquad [7]$$

where p is the pressure applied by the die to the element Fig. 2.

[5] "Strength of Metal Under Combined Stresses," by Max Gensamer, American Society for Metals, Cleveland, Ohio 1940, p. 31.

Pressure Distribution

Let

$$f = \mu p \quad [8]$$

By combining Equations [4], [6], [7], and [8]

$$\frac{dp}{p} = -\frac{2\mu}{t}\,dr \quad [9]$$

An expression for pressure may be found by integrating Equation [9] between limits $p = p$ at $r = r$ and $p = \sigma_0$ at $r = R$. Thus

$$\int_p^{\sigma_0} \frac{dp}{p} = -\frac{2\mu}{t}\int_r^R dr \quad [10]$$

Upon rearranging

$$\frac{p}{\sigma_0} = e^{2\mu\left(\frac{R}{t}-\frac{r}{t}\right)} \quad [11]$$

The maximum pressure p_m, results at $r = 0$ and is expressed by

$$\frac{p_m}{\sigma_0} = e^{\frac{2\mu R}{t}} \quad [12]$$

Pressure Distribution Under Conditions of Extreme Friction Force

An examination of Equation [12] indicates that the value of p may become very large, depending upon the value of $\mu R/t$. Since it was assumed that $f = \mu p$, it follows that f will also become large under these conditions. However, from practical considerations it is evident that f represents a shear stress in the surface material and that this value will not increase to a higher value than the value necessary to produce yielding or plastic flow. When these conditions exist the relative sliding between the die and blank surface will be replaced by shear deformation in the surface layers of the blank.

Under these circumstances the stress state is materially different from that previously assumed. For high values of f, the die offers a large restraint to the free spreading of metal near the surface, and produces a condition approximating a hydrostatic pressure equal to p, upon which is superimposed a shear stress f, Fig. 6.

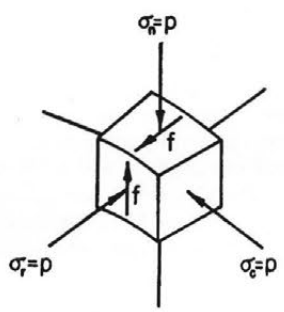

Fig. 6 Stress State in Surface Layer of Blank Under High Coefficient of Friction

For this condition the criterion for yielding may be restated as follows

$$\frac{1}{\sqrt{2}}\sqrt{(2f_0)^2 + f_0^2 + f_0^2} = \sigma_0 \quad [13]$$

or

$$f_0 = 0.577\,\sigma_0 = k\sigma_0 \quad [14]$$

where

$$k = 0.577$$

(It is assumed that the hydrostatic pressure does not affect σ_0.)

The term f_0, Equation [14], represents the maximum value for f. Substituting $f = k\sigma_0$ into Equation [4], the basic differential equation becomes

$$dp = -\frac{2k\sigma_0}{t}\,dr \quad [15]$$

If it is assumed that $\mu \geq k, f = f_0$ everywhere on the blank. The pressure distribution may be found by integrating Equation [15] between the limits $p = \sigma_0$ when $r = R$ and $p = p$ when $r = r$. After integrating and rearranging

$$\frac{p}{\sigma_0} = 1 + 2k\left(\frac{R}{t} - \frac{r}{t}\right) \quad [16]$$

Another condition under which the condition $f = f_0$ exists over a portion of the blank may be found by substituting f_0 from Equation [14] for f, and p_c for p into Equation [8]. Thus

$$k\sigma_0 = \mu p_c \quad [17]$$

and

$$\frac{p_c}{\sigma_0} = \frac{k}{\mu} \quad [18]$$

The equality $f = f_0 = k\sigma_0$ is satisfied at all points where

$$\frac{p}{\sigma_0} \geq \frac{k}{\mu} \quad [19]$$

Therefore sticking will result whenever $p > p_c$ even though $\mu < k$.

The radial range over which Equation [19] is satisfied is found by substituting Equation [18] into Equation [11]. If r_c is the value of r at which $p = p_c$

$$\frac{r_c}{t} = \frac{R}{t} - \frac{1}{2\mu}\ln\frac{k}{\mu} \quad [20]$$

Solving Equation [15] over the range $0 \leq r \leq r_c$

$$\frac{p}{\sigma_0} = \frac{p_c}{\sigma_0} + 2k\left(\frac{r_c}{t} - \frac{r}{t}\right) \quad [21a]$$

or

$$\frac{p}{\sigma_0} = \frac{k}{\mu} + 2k\left(\frac{r_c}{t} - \frac{r}{t}\right) \quad [21b]$$

For the region $r_c \leq r \leq R$ the pressure is expressed by Equation [11].

The foregoing analysis may be summarized briefly as follows:

Condition 1: When

$$\frac{p}{\sigma_0} < \frac{k}{\mu}, \text{ or } \frac{R}{t} < \frac{1}{2\mu}\ln\frac{k}{\mu}$$

everywhere on the blank, sliding between surfaces results.

Condition 2: When $\mu \geq k = 0.577$, the surfaces of the blank will stick to the die surfaces and blank displacement will result in shear deformation within the blank.

Condition 3: When

$$\mu < k \text{ but } \frac{p}{\sigma_0} > \frac{k}{\mu}, \text{ or } \frac{R}{t} > \frac{1}{2\mu}\ln\frac{k}{\mu}$$

sliding between surfaces near the outer edge of the blank and sticking in the central area result.

Average Die Pressures

Average die pressure p_a in the region between $r = a$ and $r = b$ may be obtained for any of the conditions considered by substi-

tuting the appropriate function for p into the following equation and integrating. The basic expression for average pressure is

$$p_a \int_a^b 2\pi\, rdr = \int_a^b 2\pi rp\, dr \quad \ldots\ldots\ldots [22]$$

Condition 1: For the conditions of no sticking, i.e., $R/t < (1/2\mu) \ln (k/\mu)$, the limits of integration are $a = 0$ and $b = R$.

Substituting the value of p from Equation [11] into [22] and integrating between the given limits

$$\frac{p_a}{\sigma_0} = \frac{2}{C^2}(e^C - C - 1) \quad \ldots\ldots\ldots [23]$$

where

$$C = \frac{2\mu R}{t}$$

Condition 2: For the extreme condition where $\mu \geq k$, Equations [16] and [22] may be combined and solved to obtain

$$\frac{p_a}{\sigma_0} = 1 + \frac{2k}{3}\frac{R}{t} \quad \ldots\ldots\ldots [24]$$

for the average pressure ratio for the case of sticking between die and blank.

Condition 3: In the intermediate case where

$$\mu < k \text{ and } \frac{R}{t} > \frac{1}{2\mu} \ln \frac{k}{\mu}$$

Equation [22] may be written

$$p_a \int^R rdr = \sigma_0 \int_{r_c}^R e^{2\mu \frac{2\mu(R-r)}{t}} rdr + \sigma_0 \int_0^{r_c} \left[\frac{k}{\mu} + \frac{2k}{t}(r_c - r)\right] rdr$$

After integrating and simplifying

$$\frac{p_a}{\sigma_0} = \frac{2}{C^2}[(D+1)e^{C-D} - C - 1] + \frac{D^2}{C^2}\left(\frac{k}{\mu} + \frac{2k}{3}\frac{r_c}{t}\right) \quad [25]$$

where

$$D = \frac{2\mu r_c}{t}$$

General Features of Plastic-Elastic Problems as Exemplified by Some Particular Solutions[1]

By RODNEY HILL,[2] SHEFFIELD, ENGLAND

New complete solutions based upon the Reuss equations are obtained for various plastic-elastic problems. These include the expansion of a spherical shell and of a cylindrical hole in an infinite medium. The solutions are used to exemplify certain features common to all plastic-elastic problems, with a view to introducing valid approximations in more complex cases.

Nomenclature

The following nomenclature is used in the paper:

σ_{ij} = stress tensor
σ'_{ij} = deviatoric part of stress tensor
$d\epsilon_{ij}$ = natural strain-increment tensor
$\sigma_x, \sigma_y, \sigma_z$ = Cartesian stress components
$\sigma_r, \sigma_\theta, \sigma_\phi$ = stress components referred to spherical polar co-ordinates
$\sigma_r, \sigma_\theta, \sigma_z$ = stress components referred to cylindrical co-ordinates
p = internal pressure
a, b = internal and external radii of shell or tube
c = radius of plastic-elastic boundary
$\lambda, d\lambda$ = factors of proportionality in the Reuss equations
Y = tensile yield stress
E = Young's modulus
G = modulus of shear
ν = Poisson's ratio
u = radial displacement
v = radial velocity

Introduction

The calculation of stresses and strains in a general problem in plasticity involves following the history of the deformation from the initiation of plastic flow. This implies much more than a determination of the changing shape of plastic surfaces and their influence upon the stress distribution. The basic physical fact of plastic flow is that there is a relation, not between the current stress and the plastic strain, but between the current stress and the increment of plastic strain. The approximate theoretical expression of the experimental determination of this relation is contained in the Lévy-Mises law. Therefore, a process of plastic deformation has to be considered mathematically as a succession of small increments of distortion, even where the over-all strain is so small that the change in external surfaces can be neglected.

The complete solution of a general problem involves the calculation of stresses and strains in both the plastic and elastic regions. In the latter the stress is directly connected with the total strain, and the equations there are fundamentally different from those holding in the plastic region. The solutions in the two regions cannot, moreover, be found separately since both depend on certain conditions of continuity in the stresses and displacements across the plastic-elastic boundary. This boundary is itself one of the unknowns, and is usually of such an awkward shape that even the stress distribution in the elastic region can only be obtained (if at all) by laborious numerical methods.

It is clear that the complete solution of a plastic problem will be practicable in relatively few cases. Complete solutions can only be hoped for where there is some special symmetry or other simplifying property of the problem. Some of these solutions are described in the present paper. From them it is possible to obtain a general insight into the interrelation between the states of stress and strain in the elastic and plastic regions. In particular, an estimate can be made of the influence of the elastic component of strain in the plastic region. Reasonable approximations can then be suggested which allow solutions to be obtained for the more complicated problems of technical importance.

The relations between stress and strain increment for an isotropic element of material, which is being deformed plastically, are taken to be

$$d\epsilon'_{ij} = \frac{d\sigma'_{ij}}{2G} + \sigma'_{ij}\, d\lambda \qquad [1]$$

and

$$d\epsilon_{ii} = \frac{(1-2\nu)}{E}\, d\sigma_{ii} \qquad [2]$$

E, G, ν are the elastic constants, i.e., Young's modulus, modulus of shear, and Poisson's ratio. Tensor $d\epsilon_{ij}$ represents an increment of true or natural strain, measured with respect to the current configuration. Factor $d\lambda$ is a scalar, essentially positive during continued loading, but otherwise unspecified. The first term on the right-hand side of Equation [1] is the deviatoric part of the increment of elastic strain; the second term is the increment of plastic strain. Equation [2] expresses the fact that the elastic compressibility is unchanged by the plastic flow. It is supposed, further, that all the elastic constants remain invariable, provided they are defined in terms of the current configuration. These equations are due to Reuss (1),[3] who based them on the work of Saint Venant, Lévy, von Mises, and Prandtl. When the plastic flow is "free" and takes place under constant stress, the elastic strain increments vanish and the equations are then equivalent to the Lévy-Mises relations

---

[1] The paper is based upon work forming part of the writer's dissertation for a doctorate at Cambridge University, February, 1948.

[2] The British Iron and Steel Research Association, Metal Flow Research Laboratory, Sheffield, England.

Contributed by the Applied Mechanics Division and presented at the Annual Meeting, New York, N. Y., November 28–December 3, 1948, of The American Society of Mechanical Engineers.

Discussion of this paper should be addressed to the Secretary, ASME, 29 West 39th Street, New York, N. Y., and will be accepted until October 10, 1949, for publication at a later date. Discussion received after the closing date will be returned.

Note: Statements and opinions advanced in papers are to be understood as individual expressions of their authors and not those of the Society. Paper No. 48—A-13.

[3] Numbers in parentheses refer to the Bibliography at the end of the paper.

$$d\epsilon_{ij} = \sigma'_{ij} d\lambda \quad [3]$$

The yield criterion will be taken to be either that of von Mises

$$\sigma'_{ij}\sigma'_{ij} = 2Y^2/3 \quad [4]$$

or that of Tresca

$$\text{maximum shear stress} = Y/2 \quad [5]$$

where Y is the yield stress in uniaxial tension or compression. Work hardening will be neglected.

Uniform Extension Under Conditions of Plane Strain

As a first example, consider the uniform deformation of a rectangular tensile specimen in plane strain. This is a simple problem (though its solution has not been given previously), but from it we may draw a general conclusion which applies to all problems of plane strain. Let the z-axis be normal to the planes of flow, and the x-axis be the direction of the applied pull. There is no plastic-elastic boundary to determine since the whole specimen becomes plastic at the same moment. From the Reuss equations

$$\left.\begin{aligned} Ed\epsilon_x &= (2\sigma_x - \sigma_z)d\lambda + d\sigma_x - \nu d\sigma_z \\ 0 &= (2\sigma_z - \sigma_x)d\lambda + d\sigma_z - \nu d\sigma_x \end{aligned}\right\} \quad [6]$$

There is also another equation which determines the transverse strain, if needed. If we adopt Tresca's yield criterion, then $\sigma_x = Y$ throughout the plastic flow. Eliminating $d\lambda$ from Equation [6] and integrating

$$E(\epsilon_x - \epsilon_{x0}) = (1 - 2\nu)(\sigma_z - \nu Y)/2 + \frac{3Y}{4}\log_e\left\{\frac{1 - 2\nu}{1 - \frac{2\sigma_z}{Y}}\right\} \quad [7]$$

where $\epsilon_{x0} = (1 - \nu^2)Y/E$ is the extension at the first yielding (when $\sigma_z = \nu Y$). As the extension increases, the second term becomes relatively unimportant and $\sigma_z \to Y/2$ exponentially. For example, if $\nu = 0.3$, then σ_z is already equal to $0.498\,Y$ after a plastic strain of only 5 times the yield-point strain. Because of this rapid change in σ_z, the elastic strain increment is itself initially comparable with the plastic strain increment for total strains of 3 or 4 times the yield-point strain. The elastic strain increments then rapidly become negligible and σ_z can be taken equal to $Y/2$, i.e. $(\sigma_x + \sigma_y)/2$, to an extremely close approximation.

A similar conclusion follows if the von Mises yield criterion is used. The integration is awkward, but can be simplified by observing that

$$Y^2 = \sigma_x^2 - \sigma_x\sigma_z + \sigma_z^2 = 3\sigma_x^2/4 + (2\sigma_z - \sigma_x)^2/4 \sim 3\sigma_x^2/4$$

to a good enough approximation for the present purpose. Yielding begins when

$$\sigma_x = Y/\sqrt{1 - \nu + \nu^2}; \quad \sigma_z = \nu\sigma_x$$

The tensile stress rapidly increases toward the value $2Y/\sqrt{3}$, an apparent "hardening."

Generalizing, we can expect that in most plane-strain problems it is valid to write

$$\sigma_z = (\sigma_x + \sigma_y)/2 \quad [8]$$

to a very good approximation after a plastic strain of some 5 times the yield-point strain. This relation continues to hold so long as there is no subsequent sharp change in the strain path. A change in the strain path must be regarded as sharp if the change in the stress is of order $E \times$ the strain increment, for then the elastic and plastic strain increments are comparable. The statement also requires an obvious modification if the initial rate of work-hardening is high (of order E). Roughly speaking, the relation, Equation [8], will not then become valid until after a plastic strain corresponding to a greatly reduced hardening rate.

It is perhaps worth while to point out that the foregoing analysis is immediately applicable to the problem of bending a sheet under conditions of plane strain, so long as the curvature is not too large. The longitudinal strain is determined by the usual formula, which may be substituted in Equation [7] to give the longitudinal stress (with obvious modifications on the compression side). The plastic-elastic boundary is found immediately from the known stresses in the elastic region. The transverse strain in the plastic region may be calculated from the third Reuss relation.

Expansion of a Spherical Shell by Internal Pressure

Consider a spherical shell, with current internal radius a and external radius b, which is being expanded by uniformly distributed internal pressure. No restriction is placed on the magnitude of the expansion. The special feature of this problem is that the plastic strain path and the shape of the plastic-elastic boundary are determined by symmetry alone. The reduced stress in the plastic region is a constant uniaxial compression, and so the elastic reduced strain increment is zero in the plastic region.

It is easily shown, in agreement with an intuitive expectation, that plastic flow begins on the inner surface. Let c be the radius of the plastic-elastic boundary at any subsequent stage. The yield criterion is

$$\sigma_\theta - \sigma_r = Y \quad [9]$$

In the elastic regions

$$\left.\begin{aligned} \sigma_r &= \frac{-2Yc^3}{3}\left(\frac{1}{r^3} - \frac{1}{b^3}\right) \\ \sigma_\theta &= \sigma_\phi = \frac{2Yc^3}{3}\left(\frac{1}{2r^3} + \frac{1}{b^3}\right) \end{aligned}\right\} \quad [10]$$

The displacement is

$$u = \frac{2Yc^3}{3E}\left[(1 - 2\nu)\frac{r}{b^3} + \frac{(1 + \nu)}{2r^2}\right]$$

Thus the solution in the elastic region is dependent only on the parameter c. This is a particularly simple form of interrelation between the solutions in the elastic and plastic regions. In the plastic region there are two equations involving only the two unknown stress components, viz., the yield criterion, Equation [9], and the one equilibrium equation which is not identically satisfied. Therefore, the problem is statically determined. Using the condition for continuity of the stresses on $r = c$, and integrating the equilibrium equation, we have immediately

$$\sigma_r = -2Y\log_e\left(\frac{c}{r}\right) - \frac{2Y}{3}\left(1 - \frac{c^3}{b^3}\right); \quad a \leqslant r \leqslant c \quad [11]$$

The internal pressure is

$$p = 2Y\log_e\left(\frac{c}{a}\right) + \frac{2Y}{3}\left(1 - \frac{c^3}{b^3}\right) \quad [12]$$

The whole shell becomes plastic when p has increased to the value $2Y\log_e(b/a)$. Further expansion continues under diminishing pressure and the system would presumably become unstable in practice. To complete the solution we need to relate c to either p or a. It is convenient to regard r and c as independent variables, and to express the compressibility equation in terms of the velocity v defined as

$$v = \frac{\partial u(r, c)}{\partial c}\Big/\left(1 - \frac{\partial u(r, c)}{\partial r}\right) \quad [13]$$

where u is the total displacement, since the first application of pressure. This definition regards the motion of the plastic-elastic boundary as the scale of "time" or progress of the expansion. The compressibility equation is

$$\frac{\partial v}{\partial r} + \frac{2v}{r} = \frac{(1-2\nu)}{E}\left(\frac{\partial}{\partial c} + v\frac{\partial}{\partial r}\right)(\sigma_r + 2\sigma_\theta)$$
$$= \frac{6(1-2\nu)Y}{E}\left[-\frac{1}{c}\left(1-\frac{c^3}{b^3}\right) + \frac{v}{r}\right]$$

by using Equations [9] and [11]. Radius b of course is regarded as a constant while the outer surface is still elastic. Integrating and neglecting Y/E compared with unity

$$v = \frac{3(1-\nu)Yc^2}{Er^2} - \frac{2Y(1-2\nu)r}{Ec}\left(1-\frac{c^3}{b^3}\right) \quad [14]$$

where use has been made of the boundary condition

$$v = \frac{2Y}{E}\left[(1-2\nu)\frac{c^3}{b^3} + \frac{1+\nu}{2}\right] \quad \text{on} \quad r = c$$

Hence the relation between c and the internal radius a is given by

$$\frac{da}{dc} = \frac{3(1-\nu)Yc^2}{Ea^2} - \frac{2Y(1-2\nu)a}{Ec}\left(1-\frac{c^3}{b^3}\right) \quad [15]$$

This holds after the inner surface has become plastic, which happens when

$$\left.\begin{aligned} p_0 &= \frac{2Y}{3}\left(1-\frac{a^3}{b^3}\right) \\ u_0 &= \frac{2Ya}{3E}\left[(1-2\nu)\frac{a^3}{b^3} + \frac{1+\nu}{2}\right] \end{aligned}\right\} \quad [16]$$

For small total strains, a can be treated as constant in the formulas for the stresses. In this case the radius c and the stresses are known in terms of the pressure p without a calculation of the displacements in the plastic region. This is a feature typical of many plastic problems where the strains are small; a limited amount of information can often be obtained without a complete solution. Of course if the internal displacement is regarded as the independent variable, i.e., if it is asked what are the pressure and stress distribution for a certain displacement, a complete solution cannot be avoided. By integration of Equation [15] and use of Equations [16], the total displacement of the internal surface since the first application of pressure is

$$\frac{Ya}{E}\left[\frac{(1-\nu)c^3}{a^3} - \frac{2(1-2\nu)}{3}\left(1-\frac{c^3}{b^3}\right) - 2(1-2\nu)\log_e\left(\frac{c}{a}\right)\right]; \quad c \geq a \quad [17]$$

This can be calculated for any pressure p from Equation [12]. Reuss (1), in 1930, considered this problem (for small strains) and correctly formulated the equation for compressibility in the plastic region in terms of the total displacements. He only gave a partial solution, and did not, for example, explicitly evaluate the displacements in the plastic region.

For strains of any magnitude the displacement u' of the inner surface after the first yielding is obtained from Equation [15] as

$$\left(1+\frac{u'}{a_0}\right)^3 = 1 + \frac{3(1-\nu)Y}{E}\left(\frac{c^3}{a_0^3} - 1\right) - \frac{6Y(1-2\nu)}{E}\left[\log_e\left(\frac{c}{a_0}\right) - \frac{(c^3-a_0^3)}{3b^3}\right] \quad [18]$$

where a_0 is the value of a when pressure is first applied. The total displacement is $u' + u_0$. If a_0 is zero and b is infinite, i.e., the hole is expanded from zero radius in an infinite medium, then the stress and strain configuration is similar at any stage of the expansion. All variables are functions of r/c; c/a is constant and can be found from Equation [15] to be

$$\frac{c}{a} = \left[\frac{E}{3(1-\nu)Y}\right]^{1/3} \quad [19]$$

to the usual approximation. The internal pressure is

$$p = 2Y\left[\log_e\left(\frac{c}{a}\right) + \frac{1}{3}\right] \quad [20]$$

Taking medium-carbon steel as an example with $\nu = 0.287$, $E = 20.9 \times 10^{11}$ dyne/cm^2, $Y = 7.7 \times 10^9$ dyne/cm^2 (50 tn/in.^{2}); $c/a = 5.05$, $p = 3.9\ Y$. For work-hardened copper, $\nu = 0.356$, $E = 12.3 \times 10^{11}$ dyne/cm^2, $Y = 2.8 \times 10^9$ dyne/cm^2, $c/a = 6.1$, $p = 4.3\ Y$. The only previous work on this problem appears to be that of Bishop, Hill, and Mott (2) in 1945. They neglected elastic compressibility in the plastic region. Their value for c/a was $[E/(1+\nu)Y]^{1/3}$, which is equal to Equation [19] only when $\nu = 0.5$. For the steel, their formulas give $c/a = 5.95$, and $p = 4.2\ Y$, an overestimate of 18 per cent in c/a and of 8 per cent in p. A closer approximation actually would be obtained by neglecting volume changes universally. Thus, putting $\nu = 0.5$ in Equation [19], gives $c/a = (2E/3Y)^{1/3}$; for the steel, $c/a = 5.65$ and $p = 4.1\ Y$, an overestimate of 12 per cent in c/a and of 5.5 per cent in p.

Expansion of a Cylindrical Hole by Internal Pressure

We now consider a problem where the shape of the plastic region is determined by symmetry, but where the plastic strain path is not. A long hollow cylinder is expanded by uniformly distributed internal pressure. Longitudinal extension is supposed to be prevented by suitable end forces, so that the problem is one of plane strain. Let a and b be the current internal and external radii, and c the radius of the plastic-elastic boundary. The yield criterion of von Mises can be written in the form

$$\frac{3}{2}(\sigma_\theta - \sigma_r)^2 + 2\left(\sigma_z - \frac{\sigma_r + \sigma_\theta}{2}\right)^2 = 2Y^2 \quad [21]$$

Since σ_z is initially equal to $\nu(\sigma_r + \sigma_\theta)$ and approaches $(\sigma_r + \sigma_\theta)/2$ with increasing plastic strain (as can be verified a posteriori), it is a good approximation to write

$$\sigma_\theta - \sigma_r = 2Y/\sqrt{3} \quad [22]$$

In effect this is Tresca's criterion with a modified yield stress. The approximation effects a considerable analytical simplification, since the problem becomes statically determined with respect to the two stress components in the plane.

In the elastic region

$$\left.\begin{aligned} \sigma_r &= \frac{Yc^2}{\sqrt{3}}\left(\frac{1}{b^2} - \frac{1}{r^2}\right) \\ \sigma_\theta &= \frac{Yc^2}{\sqrt{3}}\left(\frac{1}{b^2} + \frac{1}{r^2}\right) \\ \sigma_z &= \frac{2\nu Yc^2}{\sqrt{3}\,b^2} \end{aligned}\right\} \quad c \leq r \leq b \quad [23]$$

Use has here been made of the yield criterion on $r = c$. The radial displacement in the elastic region is

$$u = \frac{(1+\nu)Yc^2}{\sqrt{3}\,E}\left[\frac{(1-2\nu)r}{b^2} + \frac{1}{r}\right]; \quad c \leq r \leq b \quad [24]$$

In the plastic region, integration of the equilibrium equation with the use of Equation [22] gives

$$\sigma_r = \frac{-2Y}{\sqrt{3}}\left[\log_e\left(\frac{c}{r}\right) + \frac{1}{2}\left(1 - \frac{c^2}{b^2}\right)\right]; \quad a \leqslant r \leqslant c \quad [25]$$

The internal pressure is

$$p = \frac{2Y}{\sqrt{3}}\left[\log_e\left(\frac{c}{a}\right) + \frac{1}{2}\left(1 - \frac{c^2}{b^2}\right)\right] \quad [26]$$

Plastic flow begins at a pressure

$$p_0 = \frac{Y}{\sqrt{3}}\left(1 - \frac{a^2}{b^2}\right) \quad [27]$$

It is again convenient to introduce the velocity v defined in Equation [13]. The compressibility equation is

$$\frac{\partial v}{\partial r} + \frac{v}{r} = \frac{(1-2\nu)}{E}\left(\frac{\partial}{\partial c} + v\frac{\partial}{\partial r}\right)(\sigma_r + \sigma_\theta + \sigma_z) \quad [28]$$

The Reuss equations give also

$$\left.\begin{aligned} 0 &= \lambda(2\sigma_z - \sigma_r - \sigma_\theta) + \left(\frac{\partial}{\partial c} + v\frac{\partial}{\partial r}\right)[\sigma_z - \nu(\sigma_r + \sigma_\theta)] \\ \frac{Ev}{r} &= \lambda(2\sigma_\theta - \sigma_r - \sigma_z) + \left(\frac{\partial}{\partial c} + v\frac{\partial}{\partial r}\right)[\sigma_\theta - \nu(\sigma_r + \sigma_z)] \end{aligned}\right\} \quad [29]$$

On eliminating λ from these equations we have, with Equation [28], two relations to determine v and σ_z as functions of r and c. The relations are hyperbolic, the characteristics in the (r, c) plane being the lines c = const, and the paths of the particles $(dr)/(dc) = v$. When the total strains are small, the characteristics are simply c = const and r = const. Analytic solution appears impossible in general.

In the particular case when the total strain is so small that a can be treated as constant, a method of numerical small-arc integration has been formulated by Hill, Lee, and Tupper (3), 1947, in terms of geometrical quantities in a plane diagram. The case $b = 2a$ was solved completely, and it was found that σ_z approached $(\sigma_\theta + \sigma_r)/2$ soon after the whole cylinder had become plastic. The approach was naturally closer toward the inside of the tube where most plastic flow occurs, but even on the outside surface σ_z was equal to $0.48\,Y$ after a circumferential strain of only $4Y/E$. This illustrates the general conclusion in the second section of the paper.

We see also that the complete stress distribution can be calculated to a good approximation after the tube has become plastic, without needing to know the details of the expansion up to that stage. Components σ_r and σ_θ are known in terms of p at any stage of the expansion from Equations [25] and [26]. This is a further example of the remark made in the third section that limited information can often be obtained without a full solution. Component σ_z, however, cannot be so determined in the early stages when plastic and elastic strains are comparable. Hill, Lee, and Tupper found that the error in σ_z which results from neglecting elastic strains in the plastic region could be as much as 60 per cent.

Many earlier solutions have been proposed for this problem when the strains are small, chiefly because of the connection with the autofrettage of gun barrels. Most are so unsatisfactory as to be not worth mentioning; the following may be cited as stages in the gradual improvement of the theory. Saint Venant (4), in 1872, calculated the stress distribution in a completely plastic tube, and obtained the relation $\sigma_z = (\sigma_r + \sigma_\theta)/2$ from Lévy's equations. Nadai (5), in 1930, established formulas for the stresses and displacements, but neglected elastic strains in the plastic region. This procedure is not only subject to the error already mentioned, but leads to discontinuities in σ_z and the radial strain on the plastic-elastic boundary. The first solution which allowed for elastic compressibility in the plastic region was due to Belayev and Sinitsky (6) in 1938, but the Hencky stress-strain equations were used instead of the Reuss equations. Other end conditions may be considered in this problem, for example, the "free" and "closed" end conditions. The latter has been solved numerically when $b = 2a$ by Hill, Lee, and Tupper (7). The problem is more complicated since the states of stress in the elastic and plastic regions are connected not only by the continuity condition on $r = c$, but also by the end condition in the form of an integral of the axial stress over the whole section.

A complete solution in explicit terms can be found for the case where a cylindrical hole is expanded from zero radius in an infinite medium. All variables are then functions only of the parameter $\theta = r/c$. From Equations [22], [25], and [28]

$$v' + \frac{v}{\theta} = \frac{2(1-2\nu)Y}{\sqrt{3}\,E}\left(\frac{v}{\theta} - 1\right)(\theta\sigma' + 2) \quad [30]$$

where dashes denote differentiation with respect to θ, and σ is written for $\sqrt{3}\,\sigma_z/2Y$. From Equation [29]

$$\frac{2(\sigma - \log_e\theta)}{3/2 + \log_e\theta - \sigma} = \frac{\left(\frac{v}{\theta} - 1\right)(2\nu - \theta\sigma')}{1 - \nu + \nu\sigma'(v - \theta) + \sqrt{3}\,Ev/2Y\theta} \quad [31]$$

In the elastic region σ_z is zero, and therefore equal to $(\sigma_r + \sigma_\theta)/2$, We can expect that σ_z will also be equal to $(\sigma_r + \sigma_\theta)/2$ on $r = a$. where the circumferential strain is infinite. When $\nu = 0.5$, σ_z is universally equal to $(\sigma_r + \sigma_\theta)/2 = (2Y\log_e\theta)/\sqrt{3}$ in the plastic region. It can be verified a posteriori that, when $\nu = 0.3$, the greatest difference of σ from $\log_e\theta$ is about 20 per cent by proportion, and the greatest difference of σ' from $1/\theta$ is about 13 per cent. Hence it is a reasonable approximation to take $\sigma = \log_e\theta$ in Equation [30], in order to find v. Integration of Equation [30] with the boundary condition $\theta = 1$, $v = 2Y(1+\nu)/\sqrt{3}\,E$, then gives

$$v = \frac{-\sqrt{3}(1-2\nu)Y\theta}{E} + \frac{(5-4\nu)Y}{\sqrt{3}\,E\,\theta}; \quad a/c \leqslant \theta \leqslant 1 \quad [32]$$

On the internal surface $v = da/dc$. Since c/a is constant, Equation [32] leads immediately to

$$\frac{c}{a} = \left[\frac{\sqrt{3}\,E}{(5-4\nu)Y}\right]^{1/2} \quad [33]$$

Substituting from Equation [32] into Equation [33] and neglecting Y/E compared with unity

$$q' - \frac{2(5-4\nu)q}{3\theta(\theta^2 - a^2/c^2)} + \frac{(1-2\nu)}{\theta} = 0 \quad [34]$$

where $q = \sigma - \log_e\theta$. A little care is needed in the approximation since c^2/a^2 is of order E/Y. Integration of Equation [34] with the boundary condition $q = 0$, $\theta = 1$, gives

$$q = (1-2\nu)\left(1 - \frac{a^2}{c^2\theta^2}\right)^{E/\sqrt{3}Y}\int_\theta^1 \frac{d\theta}{\theta}\left(1 - \frac{a^2}{c^2\theta^2}\right)^{-E/\sqrt{3}Y} \quad [35]$$

For steel, typical values are $E = 20.9 \times 10^{11}$, $Y = 7.7 \times 10^9$

dyne/cm², $\nu = 0.287$. We find $c/a = 11$, $p = 3.35\ Y$. For hardened copper, $E = 12.3 \times 10^{11}$, $Y = 2.8 \times 10^9$ dyne/cm², $\nu = 0.356$. These give $c/a = 14.6$, $p = 3.75\ Y$.

By numerical integration of Equation [35] it can be shown that q has a maximum value of about 0.077 when $\theta = 0.69$. For smaller values of θ, q tends rapidly to the value zero on $r = a$. This again exemplifies the statement that σ_z approaches closely to the mean of the principal stresses in the plane after a strain of a few times the yield-point strain.

In the present problem, the plastic and elastic strains are still comparable even when $\theta = 0.5$. However, the error in σ_z, which would result from neglecting elastic strains in the plastic region, is here much less than it is for the tube of finite thickness in the initial expansion. We can compare the present solution with that of Bishop, Hill, and Mott (2), in which elastic strains were neglected in the plastic region. They found $c/a = [\sqrt{3}\ E/2(1 + \nu)Y]^{1/2}$. For the steel, this gives $c/a = 13.5$ and $p = 3.65\ Y$. If, in addition, changes of volume are neglected in the elastic region, $c/a = (E/\sqrt{3}Y)^{1/2} = 12.5$, and $p = 3.50\ Y$. These represent fair approximations.

Torsion of a Prismatic Bar

The solution of the torsion of a nonhardening bar of uniform section (the strain being small) is well understood in principle. It is mentioned here very briefly for the sake of completeness and as another example of the interrelation of the elastic and plastic regions.

Primarily the torsion problem is statically determined since there are two equations involving only the two unknown shear-stress components, viz., one equilibrium equation and the yield criterion. The problem is essentially different from those so far considered, in that each plastic element flows under constant stress. The plastic stress distribution is determined only by the shape of the external surface, and this changes by a negligible amount while the over-all strain is still of order Y/E. The determination of the stress in the plastic region is simple; if the normals to the external contour are constructed at all points, then the resultant shearing stress is directed perpendicular to these normals and is of magnitude $Y/\sqrt{3}$. Each shearing-stress trajectory is spaced a constant distance from the external contour; they are in fact the family of evolutes corresponding to the involute of the contour. This can also be thought of in terms of Nadai's membrane-roof analogy; the shape of the roof is fixed in terms of the external contour. In the plastic region the elastic strain increments are therefore zero.

For this reason the Hencky-Nadai and the Prandtl-Reuss equations lead to the same warping function, as observed by Prager (8) in 1934. The plastic-elastic boundary for a given twist is determined by the continuity conditions for the stresses. This is the remaining difficulty of the torsion problem, namely, to find the stress potential ϕ in the elastic region satisfying $\nabla^2\phi = 2G\theta$ (θ = twist per unit length), and such that ϕ and its space derivative are continuous with the known plastic solution across the (unknown) boundary.

Apart from the trivial case of a circular cylinder, there appears to be only one other cross section for which the complete analytical solution is known. This is the oval contour obtained by Sokolowsky (9) in 1942, from an inverse method starting with the assumption of an ellipse for the boundary of the elastic region.

Generally, we see that the distribution of stress in an elastic-plastic torsion specimen is determined (for a given twist) independently of the strains. Of course the relations between the stresses and strains have been used implicitly; for example, in showing that there is a possible solution in which the warping in the plastic region is the same along a line parallel to the axis. The determination of the stresses is independent of the strains in the sense that there finally result self-sufficient differential equations and boundary conditions in the stresses alone. The warping of the specimen in the plastic region has to be calculated afterward, by integrating first through the elastic region and then from the elastic-plastic boundary outward along the common normals to the shearing-stress trajectories. The normals are the characteristics of the linear equation for the warping function.

General Conclusions

Certain broad conclusions can be drawn from a comparative study of the solutions to elastic-plastic problems described in the paper. It is usually essential to allow for the influence of elastic strain increments in the plastic region whenever the plastic material is entirely surrounded by elastic material in which the displacements are small (c.f. the expansion of a spherical shell). If in this case the strains happen to be large throughout a considerable part of the plastic region, then it may be a reasonable over-all approximation to neglect the elastic strain increments throughout the plastic region (c.f. the expansion of a cylindrical or spherical hole from zero radius). This means that the Lévy-Mises relations can be used in place of the Reuss equations, and this is usually a helpful analytical simplification. The procedure may, however, result in discontinuities in some of the stresses across the plastic-elastic boundary. Furthermore, this boundary will probably be determined less accurately than the stresses themselves. In detail the approximation will naturally be less good near the plastic-elastic boundary where plastic and elastic strain-increments are of comparable magnitude.

When the plastic material has freedom to flow in some direction (for example, into the raised coronet round an advancing indenter), then the approximation should be still better. This expectation appears to be well confirmed by experiment. In the extreme case where a body has become entirely plastic, the elastic strain increments can be neglected to a very close approximation indeed after a distortion in which the rate of work hardening has become of order Y. The approximation remains good so long as there is no sharp change in the strain path (c.f. the plane-strain tensile specimen and the cylindrical shell).

A main feature of the previous solutions was that, whereas for a complete determination of all the variables it is necessary to follow the whole history of the deformation, a partial solution for some of the variables can often be obtained without a detailed knowledge of the others. This occurs most commonly when the material does not harden and when the over-all strain is so small that the changes of external surfaces can be neglected in the boundary conditions for the stresses. It may then happen that, with only an implicit use of the stress-strain equations and a general knowledge of the strain path, there can be obtained a self-sufficient set of differential equations and boundary conditions in the stresses alone, or, it may be, in certain stress components only.

Examples of this have been noted in the torsion of a uniform bar and the expansion of spherical and cylindrical shells. The stresses in the plastic and elastic regions can then be calculated in terms of the applied surface forces without considering the strains in detail. Problems of this type are statically determined, but by no means all statically determined problems are of this type. It is not sufficient that there should merely be as many equations in the stresses alone as there are stress components, so that the problem is statically determined in Hencky's sense; there must also be sufficient boundary conditions in the stresses alone.

If, on the other hand, the over-all strain is not small, and the change in external surfaces cannot be neglected and is unknown a priori, then it is clear that the strains must be calculated simulta-

neously with the stresses, at any rate in the plastic region. Certain exceptional cases occur when there is some special symmetry, for example, in the later stages of the expansion of a spherical shell when the strain is so large that elastic compressibility can be ignored.

BIBLIOGRAPHY

1 "Berücksichtigung der elastischen Formänderung in der Plastizitätstheorie," by A. Reuss, *Zeit. für angewandte Mathematik und Mechanik*, vol. 10, 1930, p. 266.

2 "The Theory of Indentation and Hardness Tests," by R. F. Bishop, R. Hill, and N. F. Mott, Proceedings of the Physical Society, vol. 57, 1945, p. 147.

3 "The Theory of Combined Plastic and Elastic Deformation With Particular Reference to a Thick Tube Under Internal Pressure" by R. Hill, E. H. Lee, and S. J. Tupper, Proceedings of the Royal Society of London, England, series A, vol. 191, 1947, p. 278.

4 "Sur l'intensité des forces capables de déformer, avec continuité, des blocs ductiles," by B. de Saint Venant; Comptes Rendus de l'Academie des Sciences, vol. 74, 1872, p. 1009.

5 "On the Mechanics of the Plastic State of Metals," by A. Nadai, Trans. ASME, vol. 52, 1930, p. A-193.

6 "Stress and Strain in Thick Cylinders in the Elastic-Plastic State," by N. M. Belayev and A. K. Sinitsky, Bulletin of the Academy of Sciences of the URSS, vols. 2 and 4, 1938, pp. 3 and 21, respectively.

7 "The Autofrettage of a Closed-Ended Tube," by R. Hill, E. H. Lee, and S. J. Tupper, Armament Research Department, Ministry of Supply, Theoretical Research Report 11/46, 1946.

8 "Mechanik isotroper Körper im plastischen Zustand," by H. Geiringer and W. Prager, *Ergebnisse der exakten Naturwissenschaften*, vol. 13, 1934, p. 310.

9 "A Problem of Elastic-Plastic Torsion," by W. W. Sokolowsky, *Prikladnaia Matematika i Mekhanika*, vol. 6, 1942, p. 241.

Bending of Rectangular Plates Subjected to a Uniformly Distributed Lateral Load and to Tensile or Compressive Forces in the Plane of the Plate

By H. D. CONWAY,[1] ITHACA, N. Y.

This paper presents a method of determining the distribution of deflection and stress in simply supported rectangular plates subjected simultaneously to a uniform lateral load and to uniform tensile or compressive forces in the plane of the plate. The problems are of particular importance in the design of a ship's bottom plating and, for this reason, graphs are given whereby the maximum stress and deflection may easily be calculated. Illustrative examples are included to demonstrate the use of these graphs. An example is also given to illustrate how the method may be extended to include the case of hydrostatic pressure.

Introduction

In considering the design of a ship's hull, the effects of the forces acting in the plane of the plating can be of considerable importance. These forces are caused not only by the bending of the hull as a beam but also by the hydrostatic pressure which will bend the plating and tend to pull it from its attachments. The exact calculation of the forces is difficult but they can be approximated by a method to be indicated later.

The plates covering a hull will be attached to the transverse and longitudinal framing of the ship and, obviously, bending moments will be set up at these attachments. From practical considerations it is probable that the moments are less than those calculated on the assumption that the edges of the plate are completely built-in, since some yielding of the attachment will almost certainly occur under the loading. It will also be observed that although the slopes at the middle of the frames will, from symmetry, be zero, the latter will have finite width and consequently there will still be a slope at what constitutes the edges of the plate. Bearing these points in mind and as a first approximation, the edges of the plates dealt with in this paper are assumed to be simply supported. The clamped-edge case would be very difficult to solve. The particular case of zero force in the plane of the plate and clamped edges has, in fact, only been solved in comparatively recent times (1).[2]

Another important assumption made in the analysis is that the effects of stretching or compressing of the middle plane of the plate due to bending are negligible—the so-called Poisson-Kirchhoff assumption. This assumption is strictly true only when the middle plane is bent into a developable surface, but it will be sufficiently valid if the maximum deflection does not exceed a small fraction of the thickness of the plate. A more exact solution, using von Kármán's (2) equations to take into account this stretching or compressing of the middle plane, would be very difficult to obtain.

The problem has been solved with the limitations mentioned in view. The method of solution is an extension of that used by M. Levy (3) for the particular case in which there is no force in the plane of the plate. Therefore the results obtained may be considered as a more general form of his solution. The maximum deflections and stresses are obtained in the form of rather cumbersome series which are fortunately rapidly convergent. The results, as such, would be of little value to the designer; therefore the series have been summed, and graphs and worked examples are given to facilitate their use in practical problems. B. I. Slepov (4) and F. V. Volkovitch (5) have also investigated the stresses in ship plating by assuming that one pair of opposite edges are rigidly built-in while the other pair are simply supported.

General Solution

The basic equations for the problem are given in books on elasticity, as for example S. Timoshenko's work (1), and it is not necessary to repeat their derivation here. A solution to the problem is also given in this book (6), using the usual Navier method for simply supported rectangular plates. However, this method results in double Fourier series for the deflections and moments which are slowly convergent and not nearly so easy to sum as those given by the Levy solution.

With the usual nomenclature, the differential equation to be solved is

$$\nabla^4\omega = \frac{\partial^4\omega}{\partial x^4} + 2\frac{\partial^4\omega}{\partial x^2\partial y^2} + \frac{\partial^4\omega}{\partial y^4} = \frac{q}{D} \pm \frac{P}{D}\frac{\partial^2\omega}{\partial x^2} \quad \ldots\ldots [1]$$

The positive sign on the right-hand side of the equation denotes that the end load P per unit length of plate is tensile and vice versa.

The bending moments and twisting moments, again per unit length of plate, are given by

$$\left.\begin{aligned} M_x &= -D\left(\frac{\partial^2\omega}{\partial x^2} + \nu\frac{\partial^2\omega}{\partial y^2}\right) \\ M_y &= -D\left(\frac{\partial^2\omega}{\partial y^2} + \nu\frac{\partial^2\omega}{\partial x^2}\right) \\ M_{xy} &= D(1-\nu)\frac{\partial^2\omega}{\partial x\partial y} \end{aligned}\right\} \quad \ldots\ldots\ldots [2]$$

---

[1] Professor, Mechanics of Engineering, Cornell University. Jun. ASME.

[2] Numbers in parentheses refer to Bibliography at end of paper.

Contributed by the Applied Mechanics Division and presented at the Annual Meeting, New York, N. Y., November 28–December 3, 1948, of The American Society of Mechanical Engineers.

Discussion of this paper should be addressed to the Secretary, ASME, 29 West 39th Street, New York, N. Y., and will be accepted until October 10, 1949, for publication at a later date. Discussion received after the closing date will be returned.

Note: Statements and opinions advanced in papers are to be understood as individual expressions of their authors and not those of the Society. Paper No. 48—A-12.

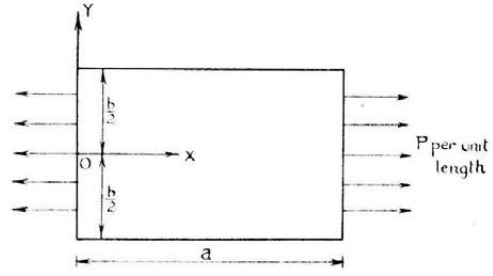

FIG. 1

The unusual nomenclature is again used. Some particular cases are now considered.

Uniform Tensile End Load. Fig. 1 shows a diagram of the plate together with the system of co-ordinate axes adopted. The differential equation to be solved is

$$D\nabla^4\omega = q + P\frac{\partial^2\omega}{\partial x^2} \quad \ldots\ldots [3]$$

Since the edges of the plate are to be assumed simply supported, the deflections at the edges and bending moments acting in planes perpendicular to the edges must vanish. These boundary conditions are expressed mathematically by

$$\left.\begin{aligned} x = 0, a \quad \omega = \frac{\partial^2\omega}{\partial x^2} = 0 \\ y = \pm\frac{b}{2} \quad \omega = \frac{\partial^2\omega}{\partial y^2} = 0 \end{aligned}\right\} \quad \ldots\ldots [4]$$

and the problem is thus completely specified.

Consider the deflected surface of the plate in the form of the series

$$\omega = \sum_{m=1}^{\infty} Y_m \sin\frac{m\pi x}{a} \quad \ldots\ldots [5]$$

where Y_m is a function of y only. This solution, obviously, will satisfy the conditions that ω and $(\partial^2\omega)/(\partial x^2)$ vanish at $x = 0$ and $x = a$, and it remains to choose the function Y_m to satisfy the other conditions. For convenience, the lateral intensity of loading q is represented by a similar series

$$q = \sum_{m=1}^{\infty} q_m \sin\frac{m\pi x}{a} \quad \ldots\ldots [6]$$

Substituting Equations [5] and [6] in Equation [3], the trigonometrical terms vanish to give

$$Y_m^{IV} - 2\alpha_m^2 Y_m'' + \alpha_m^2\left(\alpha_m + \frac{P}{D}\right)Y_m = \frac{q_m}{D} \quad \ldots\ldots [7]$$

where $\alpha_m = m\pi/a$.

The load q is uniformly distributed and, to determine the coefficients q_m

$$\int_0^a q\sin\frac{m\pi x}{a}\,dx = \int_0^a q_m \sin^2\frac{m\pi x}{a}\,dx$$

$$= \frac{1}{2}q_m\int_0^a\left(1 - \cos\frac{2m\pi x}{a}\right)dx$$

$$= \frac{1}{2}q_m a$$

$$\therefore q_m = \frac{2}{a}\int_0^a q\sin\frac{m\pi x}{a}\,dx$$

$$= 0 \text{ for } m \text{ even and } \frac{4q}{m\pi} \text{ for } m \text{ odd.}$$

Therefore the function Y_m can be considered as zero for even values of m and the deflections will be represented by

$$\omega = \sum_{m=1,3,5}^{\infty} Y_m \sin\frac{m\pi x}{a} \quad \ldots\ldots [8]$$

where Y_m is to be found from the solution of the equation

$$Y_m^{IV} - 2\alpha_m^2 Y_m'' + \alpha_m^2\left(\alpha_m^2 + \frac{P}{D}\right)Y_m = \frac{4q}{Dm\pi} \quad \ldots\ldots [9]$$

If this solution is made to satisfy the conditions

$$Y_m = Y_m'' = 0 \text{ for } y = \pm\frac{b}{2} \quad \ldots\ldots [10]$$

the problem is solved.

The general solution of Equation [9] is found to be

$$Y_m = A_m\cosh\gamma_m y\cos\eta_m y + B_m\cosh\gamma_m y\sin\eta_m y + C_m\sinh\gamma_m y\cos\eta_m y + D_m\sinh\gamma_m y\sin\eta_m y + \frac{4q}{Dm\pi}\cdot\frac{1}{\alpha_m^2\left(\alpha_m^2 + \frac{P}{D}\right)} \quad \ldots\ldots [11]$$

where

$$2\gamma_m^2 = \alpha_m^2 + \alpha_m\sqrt{\alpha_m^2 + \frac{P}{D}}$$

$$2\eta_m^2 = -\alpha_m^2 + \alpha_m\sqrt{\alpha_m^2 + \frac{P}{D}}$$

and A_m, B_m, C_m, and D_m are constants of integration. The plate and its loading are, however, symmetrical about the axis of x, and the constants B_m and C_m, therefore must be zero. The remaining constants are found from the foregoing boundary conditions.

These conditions give

$$\left.\begin{aligned} A_m &= -\frac{4q}{Dm\pi}\cdot\frac{1}{\alpha_m^2\left(\alpha_m^2 + \frac{P}{D}\right)}\cdot\frac{\sqrt{\frac{P}{D}}\cosh\frac{\gamma_m b}{2}\cos\frac{\eta_m b}{2} + \alpha_m\sinh\frac{\gamma_m b}{2}\sin\frac{\eta_m b}{2}}{\sqrt{\frac{P}{D}}\left(\cosh^2\frac{\gamma_m b}{2}\cos^2\frac{\eta_m b}{2} + \sinh^2\frac{\gamma_m b}{2}\sin^2\frac{\eta_m b}{2}\right)} \\ D_m &= -\frac{4q}{Dm\pi}\cdot\frac{1}{\alpha_m^2\left(\alpha_m^2 + \frac{P}{D}\right)}\cdot\frac{\sqrt{\frac{P}{D}}\sinh\frac{\gamma_m b}{2}\sin\frac{\eta_m b}{2} - \alpha_m\cosh\frac{\gamma_m b}{2}\cos\frac{\eta_m b}{2}}{\sqrt{\frac{P}{D}}\left(\cosh^2\frac{\gamma_m b}{2}\cos^2\frac{\eta_m b}{2} + \sinh^2\frac{\gamma_m b}{2}\sin^2\frac{\eta_m b}{2}\right)} \end{aligned}\right\} \quad \ldots\ldots [12]$$

The maximum deflection will occur at the center of the plate and from Equation [5] is given by

$$\omega_{max} = \frac{4q}{D\pi} \sum_{m=1,3,5}^{\infty} \frac{1}{m} \frac{1}{\alpha_m^2\left(\alpha_m^2 + \frac{P}{D}\right)} \left\{1 - \frac{\alpha_m \sinh \frac{\gamma_m b}{2} \sin \frac{\eta_m b}{2} + \sqrt{\frac{P}{D}} \cosh \frac{\gamma_m b}{2} \cos \frac{\eta_m b}{2}}{\sqrt{\frac{P}{D}}\left(\cosh^2 \frac{\gamma_m b}{2} \cos^2 \frac{\eta_m b}{2} + \sinh^2 \frac{\gamma_m b}{2} \sin^2 \frac{\eta_m b}{2}\right)}\right\} (-1)^{\frac{m-1}{2}} \quad \ldots\ldots [13]$$

The maximum bending moments $M_{x(max)}$ and $M_{y(max)}$ will also occur at the center and can be found from Equations [2]. They are given by

$$M_{x(max)} = \frac{4q}{\pi} \sum_{m=1,3,5,}^{\infty} \frac{1}{m} \frac{1}{\alpha_m^2\left(\alpha_m^2 + \frac{P}{D}\right)} \left\{\frac{\left[\nu\alpha_m\left(\alpha_m^2 + \frac{P}{D}\right) - \alpha_m^3\right] \sinh \frac{\gamma_m b}{2} \sin \frac{\eta_m b}{2} - \alpha_m^2 \sqrt{\frac{P}{D}} \cosh \frac{\gamma_m b}{2} \cos \frac{\eta_m b}{2}}{\sqrt{\frac{P}{D}}\left(\cosh^2 \frac{\gamma_m b}{2} \cos^2 \frac{\eta_m b}{2} + \sinh^2 \frac{\gamma_m b}{2} \sin^2 \frac{\eta_m b}{2}\right)} + \alpha_m^2\right\} (-1)^{\frac{m-1}{2}}$$

$$M_{y(max)} = \frac{4q}{\pi} \sum_{m=1,3,5,}^{\infty} \frac{1}{m} \frac{1}{\alpha_m^2\left(\alpha_m^2 + \frac{P}{D}\right)} \left\{\frac{\left[\alpha_m\left(\alpha_m^2 + \frac{P}{D}\right) - \nu\alpha_m^3\right] \sinh \frac{\gamma_m b}{2} \sin \frac{\eta_m b}{2} - \nu\alpha_m^2 \sqrt{\frac{P}{D}} \cosh \frac{\gamma_m b}{2} \cos \frac{\eta_m b}{2}}{\sqrt{\frac{P}{D}}\left(\cosh^2 \frac{\gamma_m b}{2} \cos^2 \frac{\eta_m b}{2} + \sinh^2 \frac{\gamma_m b}{2} \sin^2 \frac{\eta_m b}{2}\right)} + \nu\alpha_m^2\right\} (-1)^{\frac{m-1}{2}} \quad \ldots\ldots [14]$$

The results for the particular case of zero end load cannot be obtained from Equations [13] and [14] by merely putting P equal to zero since, if this is done, indeterminate equations of the type 0/0 result. However, a solution is obtained by integrating the differential equation

$$Y_m^{IV} - 2\alpha_m^2 Y_m'' + \alpha_m^4 Y_m = \frac{4q}{Dm\pi} \quad \ldots\ldots [15]$$

The series derived from the solution of this differential equation are given by Timoshenko (1) and will not be considered here.

The problem of the bending of a uniformly loaded rectangular plate subjected to a tensile end load has now been solved. However, the results as they stand are valueless from a practical point of view, and the series for maximum deflection and bending moments have to be summed. Fortunately, the series are all rapidly convergent and it is necessary to consider only the first one or two terms.

The series in Equations [13] and [14] have been summed for various values of P/D and ratio of plate sides a/b. In doing so it is convenient to introduce a nondimensional parameter P/P_E where $P_E = 4\pi^2 D/b^2$. It is then possible to give the maximum values of deflection and bending moments in the forms

$$\omega_{max} = \alpha \cdot \frac{qb^4}{Eh^3}$$

$$M_{x(max)} = \beta \cdot qb^2$$

$$M_{y(max)} = \gamma \cdot qb^2$$

where α, β, and γ are constants dependent upon the ratio a/b and the parameter P/P_E. Values of α, β, and γ are plotted against values of P/P_E for various values of a/b in Figs. 2, 3, and 4, respectively. Poisson's ratio ν is taken as 0.3 for the purpose of these calculations. For convenience in practical examples, α, β, and γ are also plotted against values of a/b for various values of P/P_E in Figs. 5, 6, and 7, respectively.

For small values of a/b, the effect of supporting the short sides of the plate will be negligible and, except at points near the short ends, the deflected surface will be cylindrical. The equations for the maximum deflection and bending moments then become

$$\omega_{max} = \frac{qD}{P^2}\left(\frac{1}{\cosh \frac{a}{2}\sqrt{\frac{P}{D}}} - 1\right) + \frac{qa^2}{8P}$$

$$M_{x(max)} = \frac{qD}{P}\left(\frac{1}{\cosh \frac{a}{2}\sqrt{\frac{P}{D}}} - 1\right)$$

$$M_{y(max)} = 0$$

Uniform Compressive End Load. The differential equation to be solved in this case is

$$D\nabla^4\omega = q - P\frac{\partial^2\omega}{\partial x^2} \quad \ldots\ldots [16]$$

Proceeding in the usual manner, we obtain

$$Y_m^{IV} - 2\alpha_m^2 Y_m'' + \alpha_m^2\left(\alpha_m^2 - \frac{P}{D}\right) Y_m = \frac{4q}{Dm\pi} \quad \ldots [17]$$

The general solution of this equation is

$$Y_m = A_m \cosh \gamma_m y + B_m \sinh \gamma_m y + C_m \cosh \eta_m y + D_m \sinh \eta_m y + \frac{4q}{Dm\pi} \frac{1}{\alpha_m^2\left(\alpha_m^2 - \frac{P}{D}\right)} \quad \ldots [18]$$

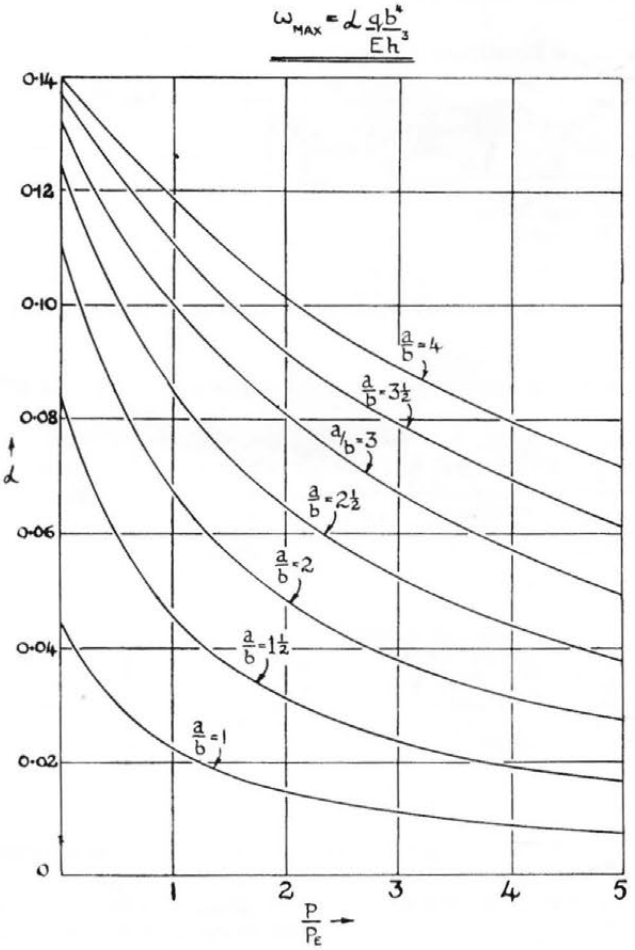

FIG. 2

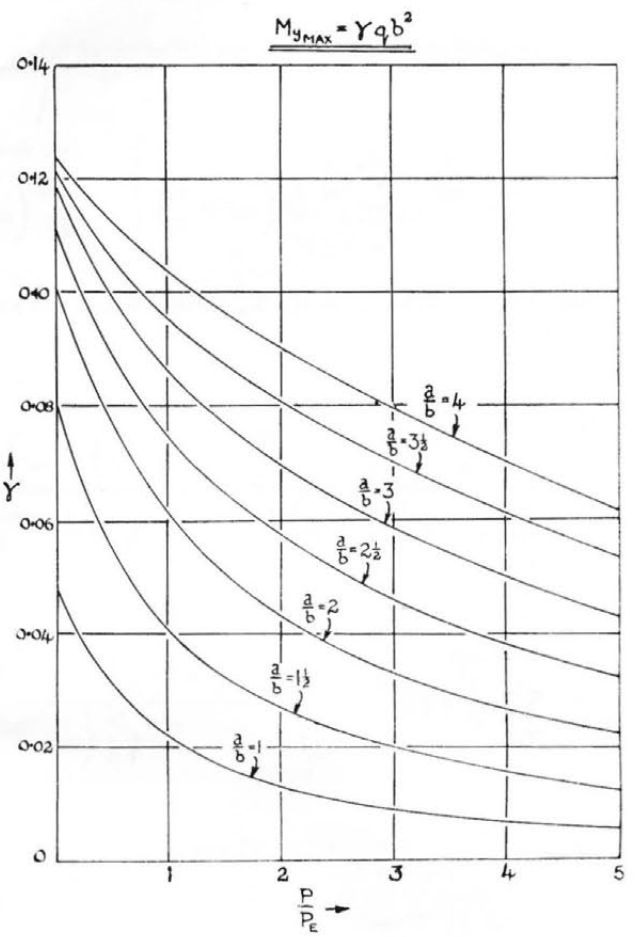

FIG. 4

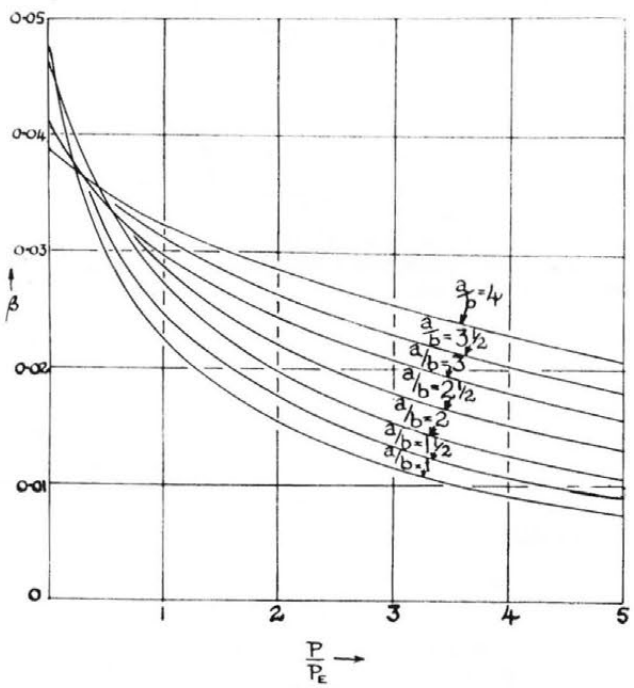

FIG. 3

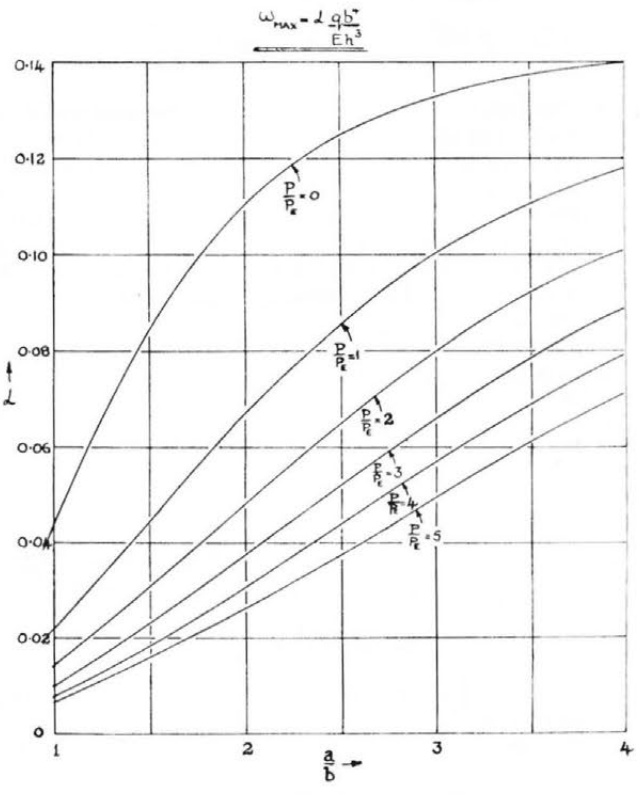

FIG. 5

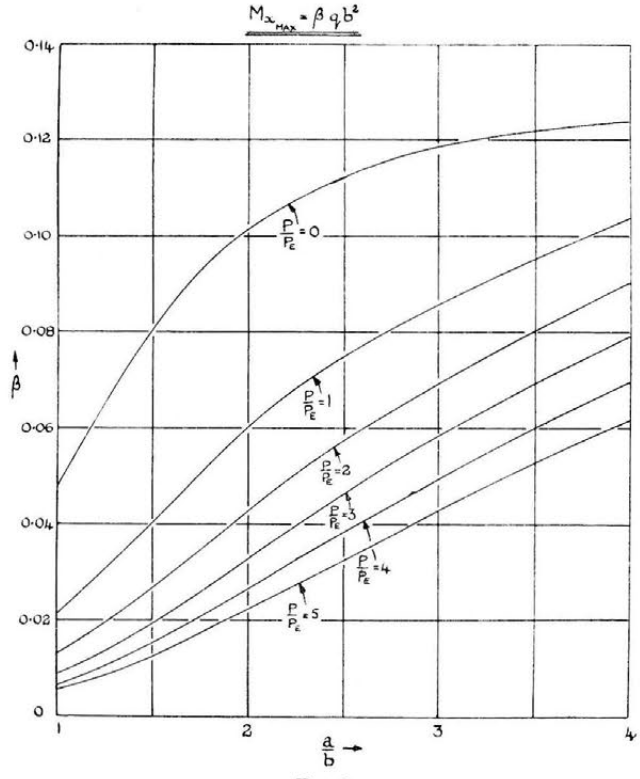
$M_{x_{MAX}} = \beta q b^2$
0·14
0·12
0·10
0·08
β
0·06
0·04
0·02
0
$\frac{P}{P_E}=0$
$\frac{P}{P_E}=1$
$\frac{P}{P_E}=2$
$\frac{P}{P_E}=3$
$\frac{P}{P_E}=4$
$\frac{P}{P_E}=5$
1
2
3
4
$\frac{a}{b}\rightarrow$

FIG. 6

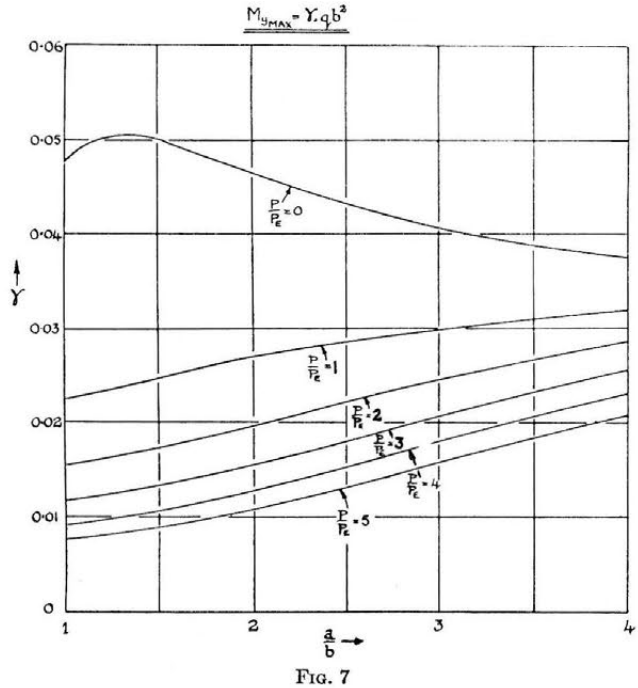
$M_{y_{MAX}} = \gamma q b^2$
0·06
0·05
0·04
γ
0·03
0·02
0·01
0
$\frac{P}{P_E}=0$
$\frac{P}{P_E}=1$
$\frac{P}{P_E}=2$
$\frac{P}{P_E}=3$
$\frac{P}{P_E}=4$
$\frac{P}{P_E}=5$
1
2
3
4
$\frac{a}{b}\rightarrow$

FIG. 7

where

$$\gamma_m^2 = \alpha_m^2 + \alpha_m \sqrt{\frac{P}{D}}$$

$$\eta_m^2 = \alpha_m^2 - \alpha_m \sqrt{\frac{P}{D}}$$

The constants B_m and D_m are again zero, and the remaining constants found from the boundary conditions are

$$\left.\begin{aligned} A_m &= \frac{2q\eta_m^2}{\alpha_m^3 \sqrt{PD}m\pi} \frac{1}{\alpha_m^2 - \frac{P}{D}} \operatorname{sech} \frac{\gamma_m b}{2} \\ C_m &= -\frac{2q\gamma_m^2}{\alpha_m^3 \sqrt{PD}m\pi} \frac{1}{\alpha_m^2 - \frac{P}{D}} \operatorname{sech} \frac{\eta_m b}{2} \end{aligned}\right\} \quad \ldots\ldots [19]$$

Substituting in Equations [18] and [5], the maximum deflection is

$$\omega_{max} = \frac{4q}{D\pi} \sum_{m=1,3,5,}^{\infty} \frac{1}{m} \frac{1}{\alpha_m^2 \left(\alpha_m^2 - \frac{P}{D}\right)} \left[\frac{2\alpha_m \sqrt{\frac{P}{D}} \cosh \frac{\gamma_m b}{2} \cos \frac{\eta_m b}{2} + \eta_m^2 \cosh \frac{\eta_m b}{2} - \gamma_m^2 \cosh \frac{\gamma_m b}{2}}{2\alpha_m \sqrt{\frac{P}{D}} \cosh \frac{\gamma_m b}{2} \cosh \frac{\eta_m b}{2}} \right] (-1)^{\frac{m-1}{2}} \quad \ldots\ldots [20]$$

The maximum bending moments found from Equation [2] are then

$$\left.\begin{aligned} M_{x(max)} &= \frac{4q}{\pi} \sum_{m=1,3,5}^{\infty} \frac{1}{m} \frac{1}{\alpha_m^2 \left(\alpha_m^2 - \frac{P}{D}\right)} \left\{ \frac{\gamma_m^2(\nu\eta_m^2 - \alpha_m^2)}{2\alpha_m \sqrt{\frac{P}{D}} \cosh \frac{\eta_m b}{2}} - \frac{\eta_m^2(\nu\gamma_m^2 - \alpha_m^2)}{2\alpha_m \sqrt{\frac{P}{D}} \cosh \frac{\gamma_m b}{2}} + \alpha_m^2 \right\} (-1)^{\frac{m-1}{2}} \\ M_{y(max)} &= \frac{4q}{\pi} \sum_{m=1,3,5}^{\infty} \frac{1}{m} \frac{1}{\alpha_m^2 \left(\alpha_m^2 - \frac{P}{D}\right)} \left\{ \frac{\gamma_m^2(\eta_m^2 - \nu\alpha_m^2)}{2\alpha_m \sqrt{\frac{P}{D}} \cosh \frac{\eta_m b}{2}} - \frac{\eta_m^2(\gamma_m^2 - \nu\alpha_m^2)}{2\alpha_m \sqrt{\frac{P}{D}} \cosh \frac{\gamma_m b}{2}} + \nu\alpha_m^2 \right\} (-1)^{\frac{m-1}{2}} \end{aligned}\right\} \quad \ldots\ldots [21]$$

As before, the particular case of zero end load cannot be obtained from these equations by merely putting P equal to zero, as indeterminate forms of the type 0/0 result. This case can be solved as previously mentioned.

Another indeterminacy will occur if $\alpha_m^2 = P/D$, i.e., if the term $(Pa^2)/(\pi^2 D)$ happens to be the square of an odd integer. If this is so, the differential equation to be solved simplifies somewhat to

$$Y^{IV}_m - 2\alpha_m^2 Y_m'' = \frac{4q}{Dm\pi} \quad \ldots\ldots [22]$$

the general solution of which is

$$Y_m = A_m + B_m y + C_m \cosh \xi_m y + D_m \sinh \xi_m y - \frac{qa^2y^2}{Dm^3\pi^3} \quad \ldots\ldots [23]$$

where

$$\xi_m^2 = \frac{2m^2\pi^2}{a^2}$$

These equations will of course hold for only one value of m, and for other values the equations previously given will apply.

Proceeding in the usual manner, the following terms in the expressions for ω_{max}, $M_{x(max)}$ and $M_{y(max)}$ are obtained

ω_{max} term =

$$\frac{qa^2}{4\pi^3 Dm^3} \left[b^2 + \frac{8}{\xi_m^2} \left(\operatorname{sech} \frac{\xi_m b}{2} - 1 \right) \right] (-1)^{\frac{m-1}{2}}$$

$M_{x(max)}$ term =

$$\frac{qa^2}{4\pi^3 m^3} \left[b^2\alpha_m^2 - 4(2\nu - 1)\left(\operatorname{sech} \frac{\xi_m b}{2} - 1 \right) \right] (-1)^{\frac{m-1}{2}}$$

$M_{y(max)}$ term =

$$\frac{qa^2}{4\pi^3 m^3} \left[\nu b^2\alpha_m^2 - 4(2 - \nu)\left(\operatorname{sech} \frac{\xi_m b}{2} - 1 \right) \right] (-1)^{\frac{m-1}{2}} \quad \ldots\ldots [24]$$

As in the tensile case, the results are of little value as they stand and the series were summed. Once again, they are found to be rapidly convergent in most cases, and it is necessary to calculate only the first two or three terms. The exception to this is in the cases of large values of a/b where it is sometimes necessary to calculate five or six terms.

For convenience, the nondimensional parameter P/P_E is again introduced where $P_E = 4\pi^2 D/b^2$. It is then possible to write

$$\omega_{max} = \alpha \cdot \frac{qb^4}{Eh^3}$$

$$M_{x(max)} = \beta \cdot qb^2$$

$$M_{y(max)} = \gamma \cdot qb^2$$

where α, β, and γ are constants dependent on a/b and P/P_E. Values of α, β, and γ are plotted against values of a/b for certain values of P/P_E in Figs. 8, 9, and 10, respectively. It was not thought an advantage to plot α, β, and γ against P/P_E for values of a/b.

As would be expected, the curves coincide at a value of a/b somewhat greater than 3, thus signifying that the maximum deflection and bending moments are independent of the end load P. Therefore, at $a/b > 3$, the values can be calculated from

$$\omega_{max} = \frac{5qb^4}{384D} = 0.1422 \frac{qb^4}{Eh^3}$$

$$M_{x(max)} = \nu \frac{qb^2}{8} = 0.0375\, qb^2$$

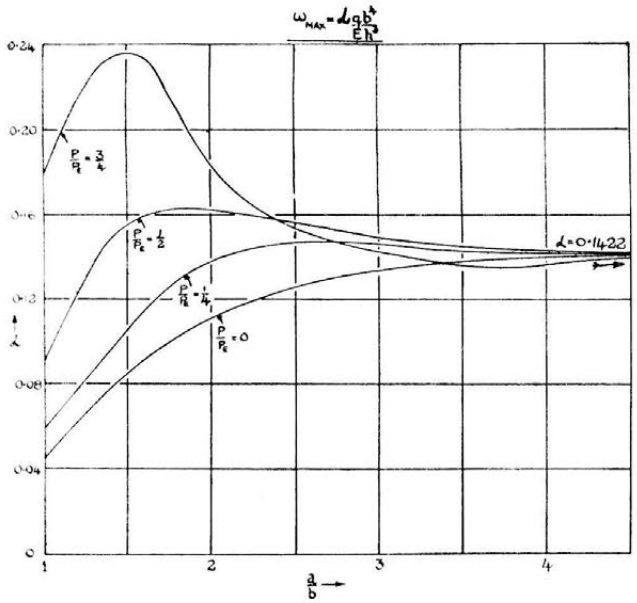

FIG. 8

$$M_{y(\max)} = \frac{qb^2}{8} = 0.1250\ qb^2$$

which refer to a uniformly loaded strip of length b and with zero end load. For small values of a/b, the effect of supporting the short sides of the plate will be negligible. Except at points very near the short ends, the deflected surface will be cylindrical, and the equations for the maximum deflection and bending moments are

$$\omega_{(\max)} = \frac{qD}{P^2}\left(\frac{1}{\cos\frac{a}{2}\sqrt{\frac{P}{D}}} - 1\right) - \frac{qa^2}{8P}$$

$$M_{x(\max)} = \frac{qD}{P}\left(\frac{1}{\cos\frac{a}{2}\sqrt{\frac{P}{D}}} - 1\right)$$

$$M_{y(\max)} = 0$$

A peculiar property of the curves for compressive end loads is observed; viz., that for certain values of a/b the end load may be increased with a decrease in the values of maximum deflection and bending moments. It thus appears that, for certain increases in the compressive force, the central portion of the plate becomes flatter.

NEED FOR FURTHER DATA

Problems of the type dealt with in this paper are of frequent occurrence and few data exist for designers. Information on the following topics would be of considerable value.

1 A treatment of the problems of this paper with graphs for values of a/b from 0–1. Knowledge of the limiting values of a/b for which the formulas for a long plate (cylindrical surface) become invalid.

2 Extension of the problems to include tensile or compressive forces on all four edges.

3 Analysis of the end loads set up by the bending of a plate whose sides are of similar magnitude

BIBLIOGRAPHY

1 "Theory of Plates and Shells," by S. Timoshenko, McGraw-Hill Book Company, Inc., New York, N. Y., 1940, p. 222.

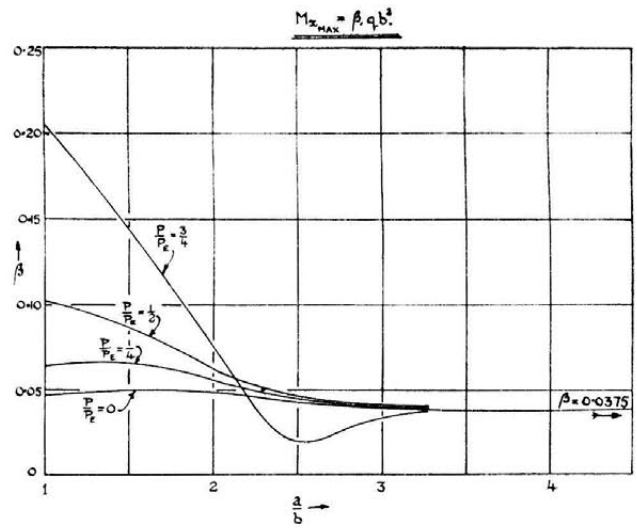

FIG. 9

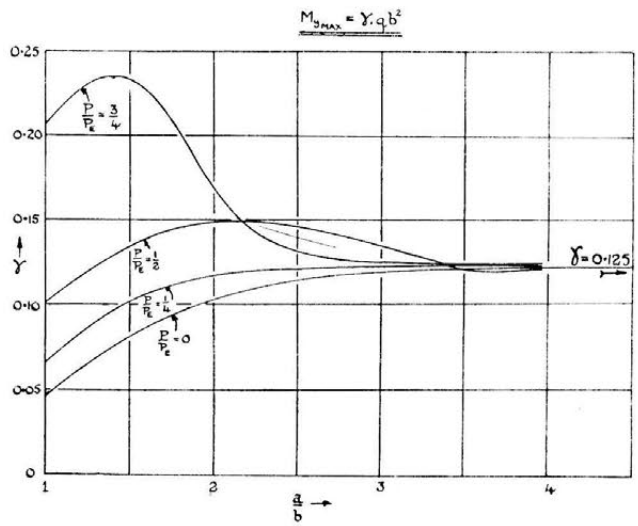

FIG. 10

2 "Festigkeits Probleme in Maschinenbau," by Th. von Kármán, Encyklopädie der Mathematischen Wissenschaften, vol. 4, 1910, p. 349.

3 "Sur l'équilibre élastique d'une plaque rectangulaire," by M. Levy. Comptes Rendus, vol. 129, 1899, pp. 535–539.

4 "The Compound Deflections of a Thin Rectangular Plate Subjected to the Uniformly Distributed Pressure and Compression in the Direction of Fixed Edges," by B. I. Slepov, Transactions of the Scientific Technical Society of Shipbuilding and Marine Engineering, vol. 1, no. 1, 1934, pp. 88–107 (in Russian).

"Compound Bending of a Rectangular Plate Subjected to the Uniformly Distributed Transversal Force and Extended Along the Fixed Edges," by B. I. Slepov, Transactions of the Scientific Technical Society of Shipbuilding and Marine Engineering, vol. 2, no. 1, 1935, pp. 106–128 (in Russian).

5 "Compound Bending of a Thin Plate Fixed at the Long Edges Subjected to the Compression or Tension Along the Short Edges," by F. V. Volkovitch, Transactions of the Scientific Technical Society of Shipbuilding and Marine Engineering, vol. 2, no. 4, 1938, pp. 91–118 (in Russian).

6 "Theory of Plates and Shells," by S. Timoshenko,, McGraw-Hill Book Company, Inc., New York, N. Y., 1940, p. 301.

Appendix 1

CALCULATION OF FORCES IN PLANE OF PLATE

Before calculating the maximum deflection and stress in the

plate, it is necessary to estimate the magnitude of the forces acting in its plane. As has already been indicated, the exact calculation of these forces is difficult but they can be approximated to by a method given by Timoshenko (1).

If, for the purpose of calculating the forces, we may neglect the effects of the longitudinal frames, then we are dealing with long plates carrying forces in the directions of the short sides. The deflected surface of the plates will be cylindrical except near the short sides. If an elementary strip parallel to the short sides is considered, then, on bending, it may be shown that the horizontal distance between the long sides of the strip will decrease by an amount

$$\lambda = \frac{1}{2}\int_0^a \left(\frac{dw}{dx}\right)^2 dx$$

Due to the bending of the hull of the ship as a beam, the ends of the strip are assumed to approach one another by an amount Δ. The amount by which the strip is stretched by the force P per unit length is therefore

$$\frac{Pa}{Eh}(1-\nu^2) = \frac{1}{2}\int_0^a \left(\frac{dw}{dx}\right)^2 dx - \Delta \quad \ldots\ldots [25]$$

If the right-hand side of this expression is negative, the force P will be compressive.

The deflected form of a uniformly loaded and simply supported strip subjected to a tensile end load is easily shown to be

$$\omega = \frac{qa^2x}{8u^2D}(a-x) + \frac{qa^4}{16u^4D}\left[\frac{\cosh u\left(1-\frac{2x}{a}\right)}{\cosh u} - 1\right] \quad [26]$$

where the origin is taken at one end of the strip and $u^2 = Pa^2/(4D)$. Similarly for a compressive end load

$$\omega = -\frac{qa^2x}{8u^2D}(a-x) + \frac{qa^4}{16u^4D}\left[\frac{\cos u\left(1-\frac{2x}{a}\right)}{\cos u} - 1\right] \quad [27]$$

If the end load is tensile, Equation [26] is substituted in Equation [25] to obtain

$$\frac{E^2h^3}{q^2(1-\nu^2)^2a^3}\,\frac{\frac{3a\Delta}{h^2}+u^2}{u^2} = \frac{135}{16}\frac{\tanh u}{u^9} + \frac{27}{16}\frac{\tanh^2 u}{u^8} - \frac{135}{16u^8} + \frac{9}{8u^6} \quad \ldots [28]$$

If the end load is compressive, Equation [27] is substituted in Equation [25] to obtain

$$\frac{E^2h^3}{q^2(1-\nu^2)^2a^3}\,\frac{\frac{3a\Delta}{h^2}-u^2}{u^2} = -\frac{135}{16}\frac{\tan u}{u^9} + \frac{27}{16}\frac{\tan^2 u}{u^8} + \frac{135}{16u^8} + \frac{9}{8u^6} \quad \ldots [29]$$

Fig. 11 shows diagrammatically the longitudinal and transverse cross sections of the ship. Let b be the width of the ship and let

A = total cross-sectional area
I = moment of inertia about neutral axis
c = distance from neutral axis to bottom plates

Denote by A_1, I_1, and c_1 these three quantities when the bottom plates are removed. The relationship between the quantities is then

$$A_1 = A - bh$$

$$c_1 = \frac{Ac}{A_1}$$

$$I_1 = I - bhc^2 - A_1(c_1 - c)^2$$

The total force acting in the plane of the plate is Pb and this produces a displacement Δ_1 where

$$\Delta_1 = \frac{a}{E}\left(\frac{Pb}{A_1} + \frac{Pbc_1^2}{I_1}\right)$$

The displacement Δ_2 due to the bending moment M of the sign shown in Fig. 11 is

$$\Delta_2 = -\frac{Mc_1a}{EI_1}$$

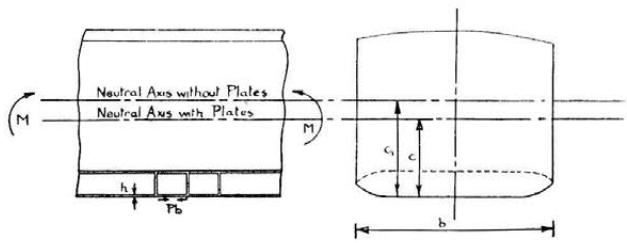

FIG. 11

Hence the resultant displacement is

$$\Delta = \Delta_1 + \Delta_2 = \frac{a}{E}\left[\frac{Pb}{A_1} + \frac{(Pbc_1 - M)c_1}{I_1}\right] = \frac{u^2h^3}{3a(1-\nu^2)}\left(\frac{b}{A_1} + \frac{bc_1^2}{I_1}\right) - \frac{Mac_1}{EI_1} \quad \ldots\ldots [30]$$

Having due regard to sign and substituting Equation [30] in Equation [28] or [29], depending upon whether the end load is tensile or compressive, an expression for u and hence P may be obtained. This may be solved by trial and error.

Appendix 2

Examples in Use of Graphs

To clarify the use of the graphs, two practical examples have been worked out; one of a plate having a tensile end load, and the other of a plate having a compressive end load.

Tensile End Load:

Length of plate = a = 80 in.
Breadth of plate = b = 40 in.
Thickness of plate = h = 0.5 in.
Uniform hydrostatic pressure = q = 9 psi
Tensile end load = P = 10,000 lb per in.

$$\text{Flexural rigidity} = D = \frac{Eh^3}{12(1-\nu^2)} = \frac{30\times10^6\times(0.5)^3}{12(1-[0.3]^2)} = 344{,}000 \text{ lb-in.}$$

$$P_E = \frac{4\pi^2D}{b^2} = \frac{4\pi^2\times344{,}000}{40\times40} = 8500 \text{ lb per in.}$$

$$\therefore \frac{P}{P_E} = 1.18$$

From Figs. 2, 3, and 4, it is found, for this particular value of P/P_E and $a/b = 2$, that

$$\alpha = 0.063,\ \beta = 0.0255,\ \gamma = 0.057$$

Hence

$$\text{Maximum deflection } \omega_{max} = \frac{\alpha q b^4}{Eh^3} = \frac{0.063 \times 9 \times 40^4}{30 \times 10^6 \times (0.5)^3} = 0.387 \text{ in.}$$

$$\text{Maximum bending moment } M_{x(max)} = \beta \cdot qb^2 = 0.0255 \times 9 \times 40^2 = 368 \text{ lb-in. per in.}$$

$$\text{Maximum bending moment } M_{y(max)} = \gamma \cdot qb^2 = 0.057 \times 9 \times 40^2 = 820 \text{ lb-in. per in.}$$

$$\text{Longitudinal bending stress} = \frac{6M_{x(max)}}{h^2} = \frac{6 \times 368}{(0.5)^2} = 8830 \text{ psi}$$

Direct stress = 20,000 psi

$\therefore$ Resultant stresses = $20{,}000 \pm 8830$
= 28,830 and 11,170 psi (both tensile)

$$\text{Transverse bending stress} = \frac{6M_{y(max)}}{h^2} = \frac{6 \times 820}{(0.5)^2} = 19{,}700 \text{ psi}$$

Direct stress is zero.
Resultant stresses = 19,700 psi (tensile and compressive)

Compressive End Load. Data as in tensile case but with a longitudinal compressive load of 2000 lb per in.

$$\frac{P}{P_E} = \frac{2000}{8500} = 0.236$$

From Figs. 8, 9, and 10, it is found that

$$\alpha = 0.136,\ \beta = 0.055,\ \gamma = 0.155$$

As before

$$\omega_{max} = \alpha \cdot \frac{qb^4}{Eh^3} = \frac{0.136 \times 9 \times 40^4}{30 \times 10^6 \times (0.5)^3} = 0.835 \text{ in.}$$

$$M_{x(max)} = \beta \cdot qb^2 = 0.055 \times 9 \times 40^2 = 792 \text{ lb-in. per in.}$$

$$M_{y(max)} = \gamma \cdot qb^2 = 0.115 \times 9 \times 40^2 = 1655 \text{ lb-in. per in.}$$

$$\text{Longitudinal bending stress} = \frac{6M_{x(max)}}{h^2} = \frac{6 \times 792}{(0.5)^2} = 19{,}000 \text{ psi}$$

Direct stress = 4000 psi

$\therefore$ Resultant stresses = $4000 \pm 19{,}000$
= 23,000 (compressive), 15,000 (tensile), psi

$$\text{Transverse bending stress} = \frac{6M_{y(max)}}{h^2} = \frac{6 \times 1655}{(0.5)^2} = 39{,}700 \text{ psi}$$

Direct stress is zero
$\therefore$ Resultant stresses = 39,700 psi (tensile or compressive)

In many practical problems the lateral loading is not uniformly distributed because the top edges of the plate are nearer the water surface. Therefore it is necessary to be able to analyze the problem in which the intensity of loading varies uniformly from zero along the top edge to a maximum q along the bottom edge.

It will be obvious that if the end loads are unaltered, the values of the deflections and stresses at the center of the plate will be one half of those obtained for the case of q uniformly distributed. These deflections and stresses will vary but little from the maximum values.

A further example will serve to illustrate how the solution to such a problem may be obtained.

Tensile End Load. Data as in previous tensile case but with a hydrostatic pressure varying from 9 psi along one edge to 11 psi along the opposite edge.

From Figs. 2, 3, and 4, it is found, as before, that

$$\alpha = 0.063,\ \beta = 0.0255,\ \gamma = 0.057$$

Therefore, for a uniformly distributed loading of $\frac{1}{2}(11-9) = 1$ psi

$$\text{Maximum deflection } \omega_{max} = \alpha \cdot \frac{qb^4}{Eh^3} = \frac{0.063 \times 1 \times 40^4}{30 \times 10^6 \times (0.5)^3} = 0.043 \text{ in.}$$

$$\text{Maximum bending moment } M_{x(max)} = \beta \cdot qb^2 = 0.0255 \times 1 \times 40^2 = 40.8 \text{ lb-in. per in.}$$

$$\text{Maximum bending moment } M_{y(max)} = \gamma \cdot qb^2 = 0.057 \times 1 \times 40^2 = 91.2 \text{ lb-in. per in.}$$

Hence the total values of the deflection and bending moments are

$$\omega_{max} = 0.043 + 0.387 = 0.430 \text{ in.}$$
$$M_{x(max)} = 40.8 + 368 = 408.8 \text{ lb-in. per in.}$$
$$M_{y(max)} = 91.2 + 820 = 911.2 \text{ lb-in. per in.}$$

and the stresses follow as before

The Dynamic Response of a Simple Elastic System to Antisymmetric Forcing Functions Characteristic of Airplanes in Unsymmetric Landing Impact

By JOSEPH B. WOODSON,[1] WASHINGTON, D. C.

This paper presents an analysis of the dynamic response of an undamped mechanical system with one degree of freedom subjected to disturbances which are described by antisymmetric forcing functions. The analysis was undertaken to throw light on the effect on the vibration of the wings caused by unsymmetric landing impact of an airplane. Two types of disturbances are considered; a full-sine-wave pulse, and a pulse which is the difference between two overlapping half sine waves. The results are presented in the form of dynamic-response curves and dynamic-response-factor curves. The numerically greatest dynamic-response factors, approximately 3.24 and —3.26, resulted for a full-sine-wave pulse disturbance with a ratio of duration of impact to natural period, $T_i/T \cong 1.11$. When T_i/T is in the neighborhood of 1, the first positive peak of dynamic response is numerically less than the negative and positive peaks which follow it. For much of the range, the positive and negative dynamic-response factors are numerically approximately equal. The analysis was confined to values of T_i/T between 0.33 and 12. As T_i/T increases without limit, the positive and negative dynamic-response factors tend to 1 and —1, respectively.

Introduction

CONSIDERATION of the velocity of descent of large airplanes, the possible angle of roll just prior to landing impact, and the measured duration of impact for large airplanes indicated that for planes using tricycle landing gears the time difference between contact of the two main wheels might be comparable to the duration of impact at each wheel. Recent tests by Westfall,[2] of a large bomber-type airplane confirm this speculation. Such landings may develop as much dynamic response in the antisymmetric modes of the airplane as in the symmetric modes. It was considered desirable therefore to develop dynamic-response curves for typical antisymmetric forcing functions, and to show how they might be used to determine the dynamic behavior due to landing impact of an airplane with two main landing wheels.

The analysis in this report is based on the general mathematical theory of transients in an undamped elastic structure given by Biot and Bisplinghoff.[3] The results of the investigation are expected to be of use in analyzing experimental data obtained in unsymmetric-model drop tests performed as part of a project on landing impact of structural models. This project was initiated by the Bureau of Aeronautics, Department of the Navy, to provide an experimental check on analytical methods for determining the transient oscillations in the structure of an airplane during landing impact.

Equations for Transient Wing-Tip Displacement in Any Mode; Forcing Functions

In this paper we consider an airplane making initial contact with the ground in two-point landing. We denote the landing impact force-time relation for the first alighting gear by $P_1(t)$ and for the second alighting gear by $P_2(t)$. For both $P_1(t)$ and $P_2(t)$, the origin of time is taken as the instant when the first alighting gear touches the ground. Any one of four following landing conditions is possible:

(1) The landing impact forces, $P_1(t)$ and $P_2(t)$, begin simultaneously and have identical time histories, so that $P_1(t) = P_2(t)$.

(2) The landing impact forces, $P_1(t)$ and $P_2(t)$, begin simultaneously but have different time histories.

(3) There is a time delay T_d between the beginning of $P_1(t)$ and the beginning of $P_2(t)$, but except for this time delay their time histories are identical, so that $P_1(t) = P_2(t - T_d)$.

(4) There is a time delay T_d between the beginning of $P_1(t)$ and the beginning of $P_2(t)$, and their time histories are essentially different, so that $P_1(t) \neq P_2(t - T_d)$.

We shall show that for a symmetrically constructed airplane each symmetric mode of vibration is excited by a quantity proportional to $P_1(t) + P_2(t)$, while each antisymmetric mode is excited by a quantity proportional to $P_1(t) - P_2(t)$. For such an airplane, therefore, when landing condition (1) occurs, the symmetric modes only are excited; while, for conditions (2), (3), and (4), we have unsymmetric impact and both symmetric and antisymmetric modes are excited. Most actual airplane landings probably satisfy condition (4) (the most general condition), but can be approximated by condition (3). In the present report the impact problem is simplified by neglecting damping and aerodynamic forces.

It can be shown that the deformation of an airplane due to landing impact may be represented by the superposition of an infinite number of modes, as long as the airplane acts as a linear elastic structure. If damping is neglected, the modes are un-

[1] Mechanical Engineer, Engineering Mechanics Section, National Bureau of Standards.

[2] "Measurements of Landing-Gear Forces and Horizontal-Tail Loads in Landing Tests of a Large Bomber-Type Airplane," by J. R. Westfall, NACA Technical Note No. 1140, September, 1946.

Contributed by the Applied Mechanics Division and presented at the Annual Meeting, New York, N. Y., November 28–December 3, 1948, of The American Society of Mechanical Engineers.

Discussion of this paper should be addressed to the Secretary, ASME, 29 West 39th Street, New York, N. Y., and will be accepted until October 10, 1949, for publication at a later date. Discussion received after the closing date will be returned.

Note: Statements and opinions advanced in papers are to be understood as individual expressions of their authors and not those of the Society. Paper No. 48—A-16.

[3] "Dynamic Loads on Airplane Structures During Landing," by M. A. Biot and R. L. Bisplinghoff, NACA ARR 4I10, October, 1944.

coupled, and the response in each mode under the landing impact force will be independent of every other mode.

We now fix our attention upon a particular mode which we call (j), and employ the following notation:

$q_{(j)}(t)$ is the transient wing-tip displacement in the mode, positive upward for the wing tip on the side of the plane which first contacts the ground

$\phi^{(j)}$ is the normalized deflection function describing the wing mode shape

$\omega_{(j)}$ is the circular natural frequency in the mode

$T_{(j)}$ is the natural period in the mode and equals $2\pi/\omega_{(j)}$

$Q_{(j)}(t)$ is the "generalized force" in the mode, defined by

$$Q_{(j)}(t) = \phi^{(j)}{}_{P1}\, P_1(t) + \phi^{(j)}{}_{P2}\, P_2(t)$$

where $\phi^{(j)}{}_{P1}$ is the normalized deflection in the mode at the station where $P_1(t)$ is applied, etc.

M_j is the "generalized mass" in the mode, defined by

$$M_{(j)} = \int [\phi^{(j)}]^2\, dm$$

where dm is an element of mass

As shown by Biot and Bisplinghoff[4] $q_{(j)}(t)$ satisfies the equation

$$M_{(j)}\ddot{q}_{(j)}(t) + M_{(j)}\omega^2{}_{(j)}q_{(j)}(t) = Q_{(j)}(t)$$

and $q_{(j)}(t)$ may be found provided $Q_{(j)}(t)$ and the constants of the equation are known. If we keep in mind that this equation applies to any mode (j), we may drop the (j)'s and write

$$M\ddot{q}(t) + M\omega^2 q(t) = Q(t) \quad \ldots\ldots [1]$$

If the mass distribution of the airplane is the same on either side of the center of gravity, and if the alighting gears are symmetrically located with respect to the center of gravity (conditions which are closely realized, usually), then it is true that in each symmetric mode, $\phi_{P1} = \phi_{P2}$ and

$$Q(t) = \phi_{P1}[P_1(t) + P_2(t)] \quad \ldots\ldots [2]$$

while in each antisymmetric mode, $\phi_{P1} = -\phi_{P2}$ and

$$Q(t) = \phi_{P1}\,[P_1(t) - P_2(t)] \quad \ldots\ldots [3]$$

In symmetric modes the quantity $P_1(t) + P_2(t)$ is designated $P(t)$ and called the symmetric forcing function

$$P(t) = P_1(t) + P_2(t) \quad \ldots\ldots [4]$$

Similarly, in antisymmetric modes the quantity $P_1(t) - P_2(t)$ is designated $P(t)$ and called the antisymmetric forcing function

$$P(t) = P_1(t) - P_2(t) \quad \ldots\ldots [5]$$

Either Equation [4] or Equation [5] may be written in the form $P(t) = P_{\max}p(t)$, where $p(t)$ is the dimensionless forcing function or "disturbance" (for symmetric or antisymmetric modes as the case may be) and has maximum value 1. Either Equation [2] or Equation [3] may be written in the form

$$Q(t) = [\phi_{P1}]P_{\max}\,p(t), \quad \text{or} \quad Q(t)/Q_{\max} = p(t)$$

where

$$Q_{\max} = [\phi_{P1}]P_{\max}$$

We now define $q_s = Q_{\max}/M\omega^2$. The ratio $q(t)/q_s$ is called "dynamic response," or more briefly "response," and is denoted by $u(t)$. Equation [1] may be written

$$\omega^{-2}\ddot{u}(t) + u(t) = p(t) \quad \ldots\ldots [6]$$

As an aid to visualization, we note that Equation [1] is the equation of motion for an undamped mechanical system of one degree of freedom, consisting of a linear spring of stiffness K and a mass M acted upon by a force $Q(t)$, Fig. 1. In this system, $K = M\omega^2$; thus we see that q_s is the static displacement which would result from the application of a static force equal to $Q_{\max}$.

Nature of Forcing Functions in Unsymmetric Impact

We define t_i as the duration of time for which $P_1(t)$ is different from zero, and T_d as the time delay separating the beginning of $P_1(t)$ and the beginning of $P_2(t)$. The total duration of impact T_i, is given by the equation

$$T_i = T_d + t_i \quad \ldots\ldots [7]$$

The ratio, total duration of impact to natural period, is given by

$$\frac{T_i}{T} = \frac{T_d + t_i}{T} = \left(\frac{1}{2} + \frac{T_d}{2t_i}\right)\frac{2t_i}{T} \quad \ldots\ldots [8]$$

Consideration will now be given to forcing functions produced by landings in which $P_1(t)$ and $P_2(t)$ are identical, except, in gen-

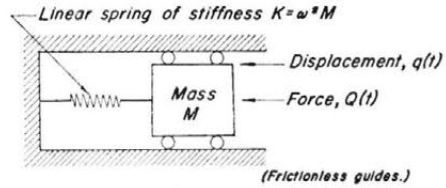

Fig. 1 Equivalent Mechanical System for Any Mode of Vibration of an Aircraft Structure

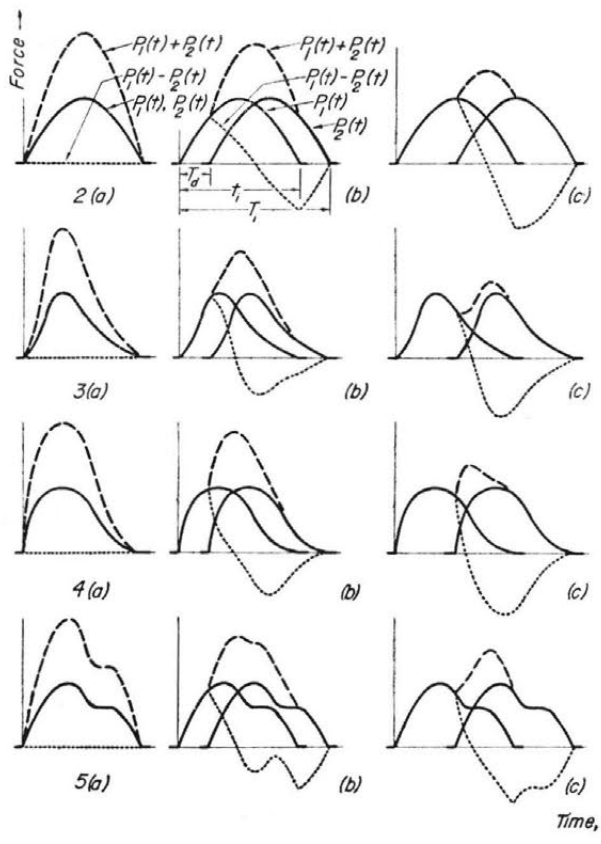

Figs. 2, 3, 4, 5 Symmetric and Antisymmetric Forcing Functions for Various Landing Impact Forces
(In each figure for [a], $T_d = 0$; for [b], $T_d \cong [1/4]t_i$; for [c], $T_d \cong [1/2]t_i$.)

[4] Appendix 1, reference 3.

eral, for a time delay between them (compare conditions [1] and [3] of the preceding section). It is assumed that the airplane is nearly symmetrically constructed, so that we may obtain the forcing functions from Equations [4] and [5].

Figs. 2, 3, 4, and 5 illustrate four assumed shapes of the landing impact force, similar to shapes recorded in model drop tests. In each figure, the symmetric and antisymmetric forcing functions which result for three different values of T_d, ranging from zero to about $t_i/2$ are illustrated. As T_d increases from zero to $t_i/2$, the figures show that (1) the total duration of impact is increased; (2) the peak value of the symmetric forcing function $P_1(t) + P_2(t)$ decreases; (3) the peak value of the antisymmetric forcing function $P_1(t) - P_2(t)$ increases. Thus the relative importance of the antisymmetric forcing function increases as T_d increases relative to t_i. For any particular value of T_d, the duration of the antisymmetric forcing function is the same as the duration of the symmetric forcing function; each has the duration T_i. For $T_d = 0$, $P_1(t) - P_2(t) = 0$, and therefore the antisymmetric modes are not excited.

Dynamic Response to Simple Antisymmetric Forcing Functions

Case I: Dynamic Response to Full Sine-Wave Pulse. We may approximate antisymmetric forcing functions like those of Figs. 2(*b*, *c*), 3(*c*), and 4(*c*) by a full sine wave having the same duration T_i and the same maximum positive value P_{max}. The disturbance (Fig. 6) is

$$\left.\begin{aligned} p(t) &= \sin(2\pi t/T_i) \text{ for } 0 \le t \le T_i \\ p(t) &= 0 \text{ for } t > T_i \end{aligned}\right\} \quad \ldots\ldots\ldots [9]$$

As shown in the Appendix, the resulting dynamic response is

$$\left.\begin{aligned} u(t) &= q(t)/q_s \\ &= \frac{1}{(T/T_i) - (T_i/T)} [\sin \omega t - (T_i/T) \sin(2\pi t/T_i)] \\ &\qquad \text{for } 0 \le t \le T_i \end{aligned}\right\} \quad \ldots [10]$$

$$u(t) = q(t)/q_s = \frac{2 \sin(\omega T_i/2)}{(T/T_i) - (T_i/T)} \cos \omega(t - T_i/2) \text{ for } t > T_i \quad \ldots\ldots [11]$$

Since $\omega t = (T_i/T) \times (t/T_i)2\pi$, it is seen that $u(t)$ is a function of the dimensionless time t/T_i and of the ratio of total duration of impact to natural period T_i/T.

In Fig. 7 dynamic-response curves resulting for various values of T_i/T are plotted. The dynamic-response curve for $T_i/T = 1$, for which Equations [10] and [11] are indeterminate, was computed from Equation [14] in the Appendix. It is seen from Fig. 7 that the response $u(t)$ follows the forcing function $p(t)$ closely for $T_i = 12T$, the longest duration of impact considered. For

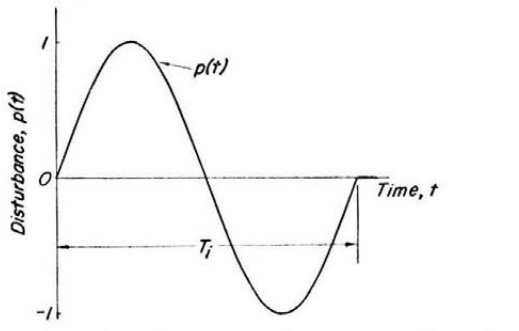

Fig. 6 Full-Sine-Wave Pulse Disturbance, Case I

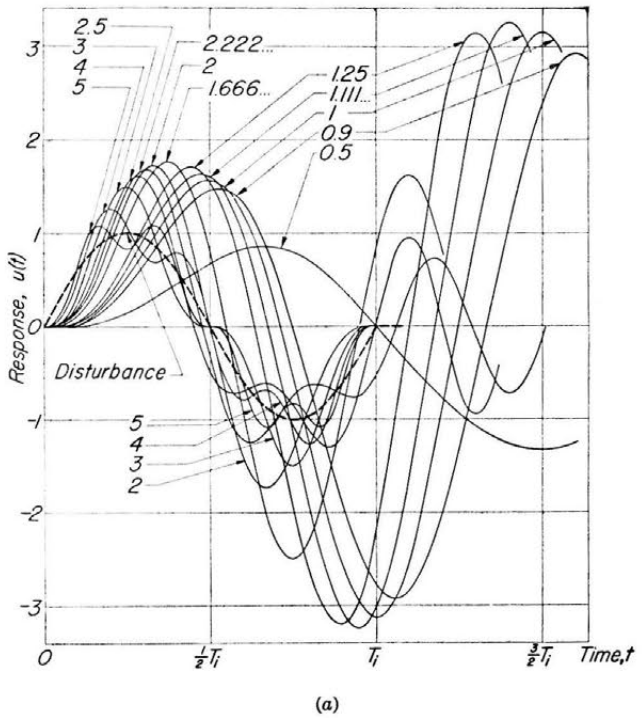

(*a*)

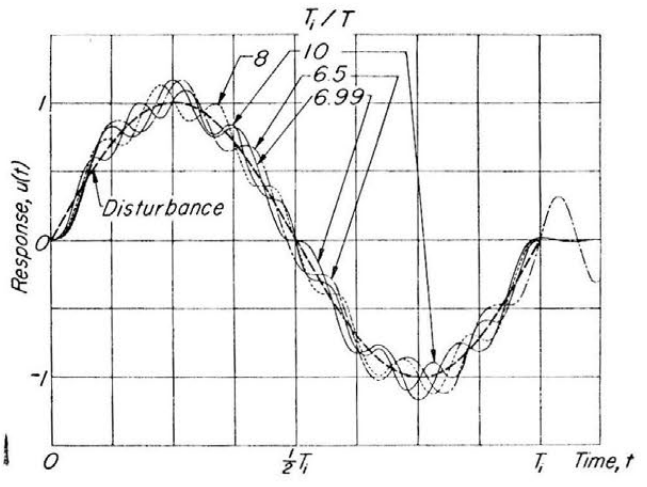

(*b*)

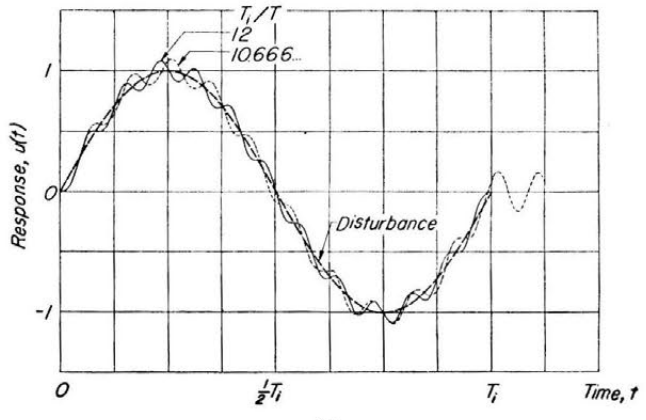

(*c*)

Fig. 7 Dynamic Response to a Full Sine-Wave Pulse, Case I for Various Values of T_i/T

smaller values of T_i the amplitude of oscillation of $u(t)$ around $p(t)$ increases until for $T_i = 1.11T$, Fig. 7, $u(t)$ has maximum positive and negative peak values more than 3 times as large as the maximum value of $p(t)$. For $T_i < 1.11\ T$ the peak value of $u(t)$ decreases, until for $T_i = 0.5T$, the shortest duration of impact considered, the peak values of $u(t)$ and $p(t)$ are nearly equal. For still smaller values of T_i, Equations [10] and [11] show that $u(t)$ becomes progressively smaller compared with $p(t)$, and becomes zero for $T_i = 0$.

To obtain the dynamic-response factors, the peak positive and peak negative values (γ_p and γ_n, respectively) of $u(t)$ occurring during the impact (i.e., for $0 \leq t \leq T_i$) were determined from the curves in Fig. 7. Similarly, the peak positive and peak negative values (γ_p' and γ_n', respectively) of $u(t)$ occurring after the impact (i.e., for $t > T_i$) were determined from these curves. Values γ_p, γ_n, γ_p', and γ_n' are plotted as functions of the corresponding values of T_i/T in Fig. 8. The discontinuities in the slopes of γ_p and γ_n result from the fact that for some values of T_i/T the first peak in $u(t)$ is most serious, while for other values of T_i/T the second or subsequent peaks may be more serious.

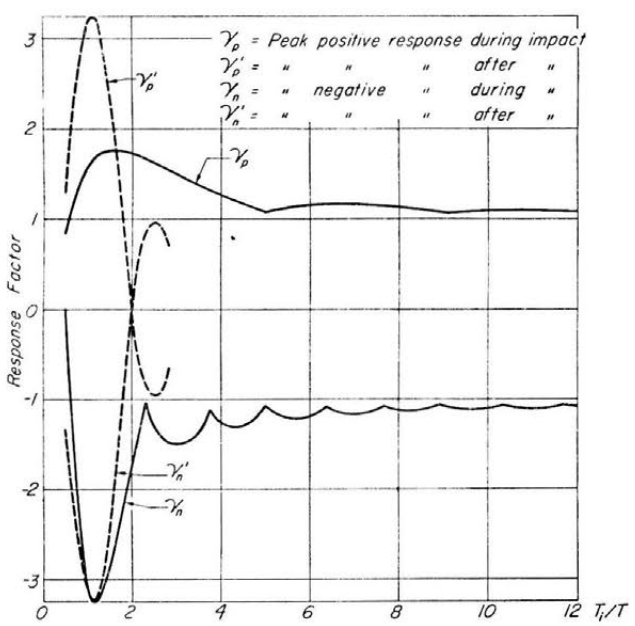

FIG. 8 DYNAMIC-RESPONSE FACTOR FOR A FULL SINE-WAVE PULSE, CASE I

When T_i/T is an integer greater than 1, $\gamma_p = \gamma_n$ because $u(t)$ has symmetry about the point $(T_i/2, 0)$; and $\gamma_p' = \gamma_n' = 0$ because of the absence of free response after $t = T_i$.

For the range of duration of impact $1 < T_i/T < 2$, γ_n is numerically greater than either γ_p or γ_p'. Furthermore, it can be noted from Fig. 8 that for $0.5 \leq T_i/T \leq 1.6$ (approximately), $\gamma_p' > \gamma_p$; that is to say, for values of T_i/T near 1, the most serious peak of positive response occurs after the impact is over. For $T_i/T < 1$, the most serious peak of negative response likewise occurs after the impact is over; whereas for $T_i/T > 1$, the most serious peak of negative response is reached at a time somewhat less than T_i.

For values of T_i/T in excess of about 1.6, the most serious peaks of positive and negative response always occur during the impact and are approximately in phase with the maximum positive and negative values of the driving force $p(t)$. For values of t in excess of T_i, the idealized system discussed here shows an oscillatory response which continues indefinitely (except when T_i/T has integral values greater than 1). Most actual airplane structures, however, would have enough damping to reduce this response to a negligible amount after a few cycles.

Biot and Bisplinghoff[5] give a dynamic-response-factor curve which is an envelope for the dynamic-response factors due to various forcing functions in symmetric impact. It is probable that this curve will also serve as an envelope for the dynamic-response factors due to many symmetric forcing functions which arise in unsymmetric impact. In view of the fact that the numerically greatest values of dynamic-response factor given by that curve are only 1.91 and —1.85, respectively, it appears that, for sufficiently short impacts, the gravest antisymmetric mode may show more dynamic response than any symmetric mode. In actual landings so abrupt that the duration of impact is nearly equal to the natural period of the gravest antisymmetric mode, we may expect dynamic response as great as 3 in that mode only.

Case II: Dynamic Response to Pulse Which Is Difference Between Two Overlapping Half Sine Waves. We shall consider here antisymmetric forcing functions having a shape shown by the solid curve in Fig. 9. Such an antisymmetric forcing function would occur if the force on each main landing wheel of the airplane were a half sine-wave pulse of duration t_i, (dotted curves a and b in Fig. 9), and if the time delay between contact of the two main wheels were T_d. We shall limit ourselves to values of $T_d \leq t_i/2$. The antisymmetric forcing function is obtained as the difference between curves a and b.

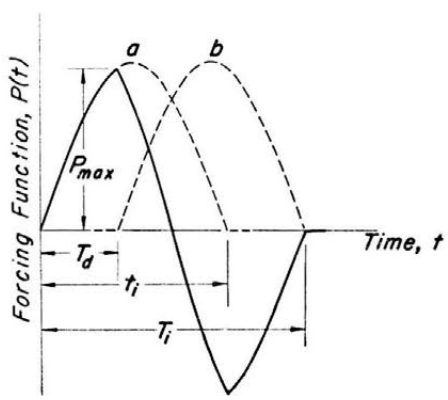

FIG. 9 ANTISYMMETRIC FORCING FUNCTION RESULTING FROM OVERLAPPING HALF SINE-WAVE LANDING IMPACT FORCES

The dynamic-response equations which result are given in the Appendix, Equations [15], [16], [17], and [18]. Dynamic-response curves were calculated for two different values of T_d as follows:

Case II(a): $T_d = t_i/2$. By using Equation [7] or Equation [8], this relation may be expressed

$$T_d = T_i/3 \quad \text{or} \quad T_i/T = (3/4) \times (2t_i/T)$$

Case II(b): $T_d = t_i/3$, that is

$$T_d = T_i/4$$

or

$$T_i/T = (2/3) \times (2t_i/T)$$

The dynamic-response curves for Cases II(a) and (b) are shown in Figs. 10 and 11, respectively. Dynamic-response-factor points are shown plotted in Fig. 12. The response-factor curves for Case

[5] Fig. 13, reference 3.

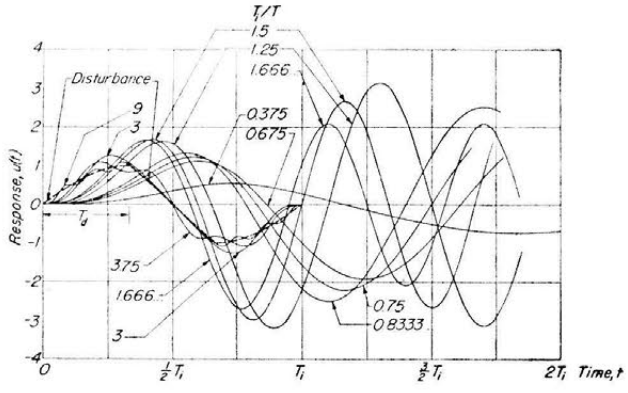

FIG. 10 DYNAMIC RESPONSE TO A PULSE WHICH IS DIFFERENCE BETWEEN TWO OVERLAPPING HALF SINE WAVES WITH $T_d = (1/3)\ T_i$; CASE II(a)

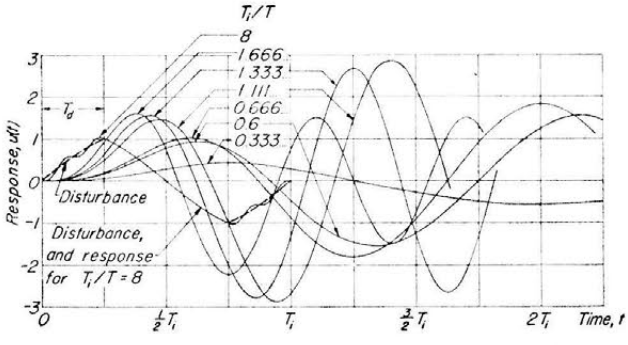

FIG. 11 DYNAMIC RESPONSE TO A PULSE WHICH IS DIFFERENCE BETWEEN TWO OVERLAPPING HALF SINE WAVES WITH $T_d = (1/4)\ T_i$; CASE II(b)

I, Fig. 8, are also shown in part in Fig. 12, to show the effect of shape of the forcing function on dynamic-response factor. The good agreement (generally within about 20 per cent) shows that the shape of the forcing function, over the range considered, has only a minor effect on the dynamic response.

COMPARISON BETWEEN CASES I, II(a), AND II(b)

Figs. 13, 14, 15, and 16 correspond to four different ratios of T_i/T and show superimposed plots of dynamic response for Case I and Case II(a) and/or Case II(b). In each figure, T_i is the same for each case, as is the maximum value of $p(t)$. For a given ratio of T_i/T, it is seen that the dynamic responses are similar, but not identical, because of the effect of the different disturbance profiles.

The response for Case I is initially greater than the response for either Case II(a) or Case II(b). This is probably due to the higher rate of application of the disturbance for Case I during $0 \leq t \leq T_i/4$.

DISCUSSION

It has been pointed out that due to time delay between contact of the two main landing wheels of an airplane, during landing impact, antisymmetric forcing functions arise which may cause the response of the airplane in antisymmetric modes to be as serious as the response in symmetric modes.

The method of computing the antisymmetric forcing functions from the force-time history at the two main wheels has been presented. Dynamic-response curves have been obtained for three simple antisymmetric forcing functions which approximate the functions which might be expected in landing impact of airplanes. A range of values of duration of impact to natural

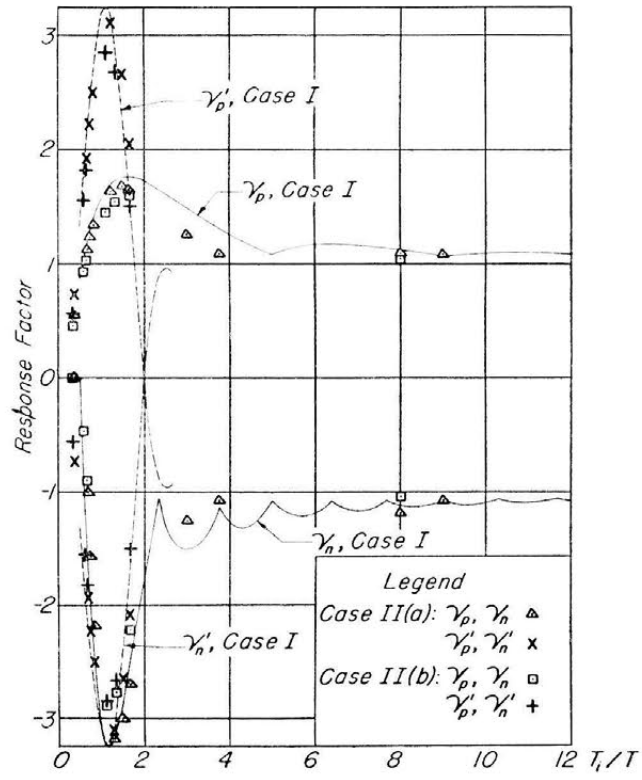

FIG. 12 DYNAMIC-RESPONSE FACTOR FOR A PULSE WHICH IS DIFFERENCE BETWEEN TWO OVERLAPPING HALF-SINE WAVES; CASES II(a) AND II(b)
(The Case I response factor is shown for comparison.)

period of mode is considered. It is shown that for the functions considered, the peak response is insensitive to the shape of the forcing function.

ACKNOWLEDGMENT

Acknowledgment is gratefully made to the Bureau of Aeronautics, Department of the Navy, for its active co-operation and financial support of the investigation. The author wishes to express appreciation to Mr. Samuel Levy of the National Bureau of Standards for his guidance in the preparation of this paper.

Appendix

DERIVATION OF DYNAMIC-RESPONSE EQUATIONS

General. Frankland[6] gives the results of integration of Equation [6] when $p(t)$ is a half-sine-wave pulse of duration t_i; the disturbance is

$$\left.\begin{aligned} p_1(t) &= 0 && \text{for } t < 0 \\ p_1(t) &= \sin\ (\pi t/t_i) && \text{for } 0 \leq t \leq t_i \\ p_1(t) &= 0 && \text{for } t > t_i \end{aligned}\right\} \quad \ldots\ldots\ldots [12]$$

and the resulting dynamic response is

$$\left.\begin{aligned} u_1(t) &= \frac{1}{(T/2t_i) - (2t_i/T)} \times \\ &\qquad [\sin \omega t - (2t_i/T) \sin\ (\pi t/t_i)] \text{ for } 0 \leq t \leq t_i \\ u_1(t) &= \frac{1}{(T/2t_i) - (2t_i/T)} \times \\ &\qquad [(1 + \cos \omega t_i) \sin \omega t - \sin \omega t_i \cos \omega t] \quad \text{for } t > t_i \end{aligned}\right\} \quad \ldots [13]$$

[6] "Effects of Impact on Simple Elastic Structures," by J. M. Frankland, David W. Taylor Model Basin, Report 481, April, 1942.

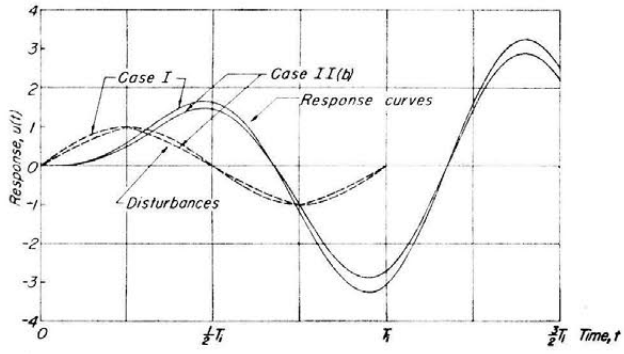

FIG. 13 DYNAMIC RESPONSE FOR CASES I AND II(b) WITH $T_i/T = 1.111\ldots$

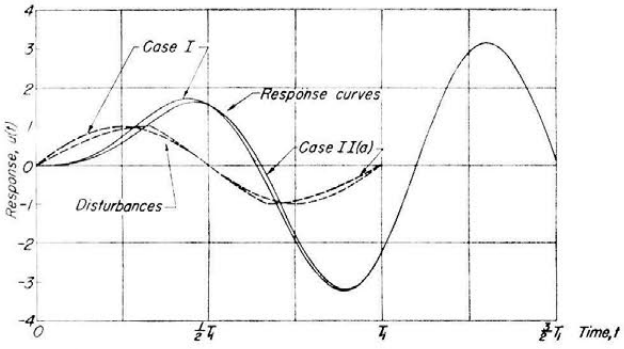

FIG. 14 DYNAMIC RESPONSE FOR CASES I AND II(a) WITH $T_i/T = 1.25$

Case I. We make use of these results as follows: Consider the system in Fig. 1 to be acted upon by a disturbance $p_1(t)$ followed by a disturbance $p_2(t)$ defined by

$$p_2(t) = -p_1(t - t_i)$$

It follows that $u_2(t) = -u_1(t - t_i)$. Also $p_1(t) + p_2(t) = p(t)$, where $p(t)$ is the full sine-wave pulse of duration $2t_i = T_i$, defined by Equations [9]; thus $u(t)$, the response to $p(t)$, is given by $u(t) = u_1(t) + u_2(t)$.

For $0 \leq t \leq T_i$ we may use Equations [13] merely by substituting T_i for $2t_i$

$$u(t) = \frac{1}{(T/T_i) - (T_i/T)} \times [\sin \omega t - (T_i/T) \sin (2\pi t/T_i)] \text{ for } 0 \leq t \leq T_i$$

For $t > T_i$ we write

$$u(t) = u_1(t) + u_2(t) = \frac{1}{(T/T_i) - (T_i/T)} \{[1 + \cos(\omega T_i/2)] \times \sin \omega t - \sin(\omega T_i/2) \cos \omega t - [1 + \cos(\omega T_i/2)] \sin \omega(t - T_i/2) + \sin(\omega T_i/2) \cos \omega(t - T_i/2)\} \text{ for } t > T_i$$

which reduces to

$$u(t) = \frac{1}{(T/T_i) - (T_i/T)} [\sin \omega t - \sin \omega(t - T_i)]$$

or

$$u(t) = \frac{2 \sin(\omega T_i/2)}{(T/T_i) - (T_i/T)} \cos \omega(t - T_i/2) \text{ for } t > T_i$$

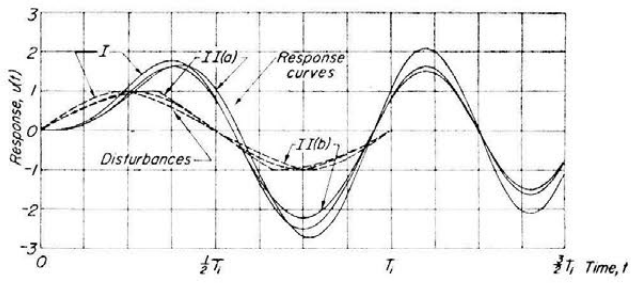

FIG. 15 DYNAMIC RESPONSE FOR CASES I, II(a) AND II(b) WITH $T_i/T = 1.666\ldots$

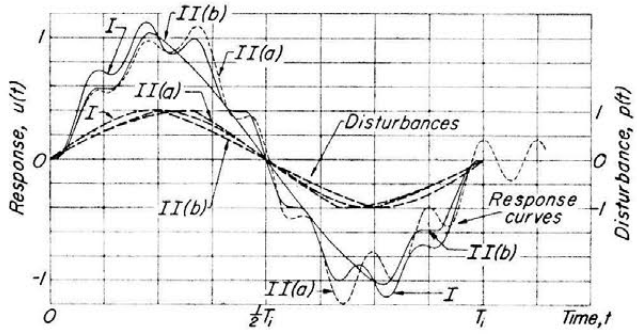

FIG. 16 DYNAMIC RESPONSE FOR CASES I, II(a), AND II(b) WITH $T_i/T = 8$

In case $T_i/T = 1$, Equations [13] are indeterminate. The proper equations are[6]

$$u_1(t) = (1/2)(\sin \omega t - \omega t \cos \omega t) \text{ for } 0 \leq t \leq t_i$$
$$u_1(t) = -(\pi/2) \cos \omega t \quad \text{for } t > t_i$$

From these equations we obtain

$$\left.\begin{aligned} u(t) &= (1/2) \times (\sin \omega t - \omega t \cos \omega t) \text{ for } 0 \leq t \leq T_i \\ u(t) &= -(\pi/2) \cos \omega t + (\pi/2) \cos \omega(t - T_i/2) \\ &= -\pi \cos \omega t \quad \text{for } t > T_i \end{aligned}\right\} \ldots [14]$$

Case II. Consider the system in Fig. 1 acted upon by a disturbance $p_3(t)$ defined by

$$p_3(t) = \frac{1}{\sin(\pi T_d/t_i)} p_1(t) \qquad [T_d \leq t_i/2]$$

followed by a disturbance

$$p_4(t) = -p_3(t - T_d)$$

Since the Case II disturbance, $p(t)$, is given by $p(t) = p_3(t) + p_4(t)$, the response is given by $u(t) = u_3(t) + u_4(t)$ or

$$p(t) = \frac{1}{\sin(\pi T_d/t_i)} [p_1(t) - p_1(t - T_d)]$$

$$u(t) = \frac{1}{\sin(\pi T_d/t_i)} [u_1(t) - u_1(t - T_d)]$$

We therefore obtain

$$u(t) = \frac{1}{[\sin(\pi T_d/t_i)] \times [(T/2t_i) - (2t_i/T)]} \times [\sin \omega t - (2t_i/T) \sin(\pi t/t_i)] \text{ for } 0 \leq t \leq T_d \ldots\ldots [15]$$

$$u(t) = \frac{1}{[\sin(\pi T_d/t_i)] \times [(T/2t_i) - (2t_i/T)]} \times \{\sin \omega t - (2t_i/T) \sin(\pi t/t_i) - \sin \omega(t - T_d) + (2t_i/T) \sin[\pi(t - T_d)/t_i]\} \text{ for } T_d < t \leq t_i \quad [16]$$

$$u(t) = \frac{1}{[\sin(\pi T_d/t_i)] \times [(T/2t_i) - (2t_i/T)]} \{(1 + \cos \omega t_i) \sin \omega t - \sin \omega t_i \cos \omega t - \sin \omega(t - T_d) + (2t_i/T) \sin[\pi(t - T_d)/t_i]\} \text{ for } t_i < t \leq T_d + t_i = T_i \quad [17]$$

$$u(t) = \frac{1}{[\sin(\pi T_d/t_i)] \times [(T/2t_i) - (2t_i/T)]} [(1 + \cos \omega t_i) \sin \omega t - \sin \omega t_i \cos \omega t - (1 + \cos \omega t_i) \sin \omega(t - T_d) + \sin \omega t_i \cos \omega (t - T_d)] \text{ for } t > T_i \quad [18]$$

Since $T_i/T = (1/2 + T_d/2t_i)(2t_i/T)$, we see that for any particular ratio of T_d/t_i, $u(t)$ is a function of dimensionless time t/t_i and of T_i/T.

Discussion

Flow Through a Pipe With a Porous Wall[1]

H. Poritsky.[2] The author mentions the difficulty of solving the highly nonlinear equations which represent the flow in a pipe with n openings. It is worth pointing out that a convenient method of treating these is afforded by the direct-current board. This is merely a collection of resistances with a telephone switchboard which allows them to be connected in any manner so as to correspond to any network. By connecting them as a filter so that the series resistances correspond to the fluid-flow resistances in the pipe, while the parallel resistances correspond to the duct-flow resistances, one obtains an electrical analogy to the fluid-flow problem. The nonlinear features are obtained by adjusting the resistances as proper functions of the currents, by trial and error, that is, an assumed set of resistances is first used to represent an initial (best) guess; readings of voltages and currents are then taken, and the relation between the currents and the resistances checked against the fluid-flow pressure drop; the resistances are then readjusted to correspond to the currents, and the process is repeated until no further adjustment is needed.

In addition to ventilating-sterilizing applications of the author's theory, it is of interest to point out a further, physiological, application of it, namely, to the flow of blood in a blood vessel. Blood vessels are permeable to flow of plasma, resulting in a continuous seepage through the vessels. In shock, as is well known, the permeance of the blood vessels becomes large and the seepage increases to a degree disastrous to the individual.

E. A. Richardson.[3] Unfortunately, the author is interested in a specific and not a general case. He deals with one condition which is not typical of the normal porous tube. In the case of the tube under discussion, the author assumes that the fluid passes through orifices with practically no friction. As a result, the jet issues with the velocity head which exists along the length.

In the normal porous tube there is a relatively high pressure drop with only a small, perhaps even negligible, portion of the pressure drop as velocity head of outflow.

The writer of this discussion has taken as an example a high-resistance porous wall with negligible velocity head on outflow for detailed consideration. Obviously, this marks the other extreme. Obviously, also, most of the practical cases will lie somewhere between these limits.

It is felt that this subject is of sufficient importance to warrant an extended discussion. Porous tubes, as a whole, will become increasingly important in various ways. One of the important fields of application is high-temperature protection in aviation. This happens to be only one of many possibilities.

In order to make this discussion an extension of the paper and tie in with it, the equation numbers used by him are retained and a continuation of these numbers used in presenting the new work.

It is assumed that $dW/dx = -KDP^{1/2}$. This is equivalent to assuming that each hole in the pipe wall is substantially frictionless so that the full potential head appears as velocity of outflow.

Now, in the case of a considerable proportion of true porous tubes the very high resistance to permeation may result in a velocity of outflow which corresponds to a kinetic energy very small compared with the potential energy inside of the tube. In such a case the equation corresponding to Equation [1] of the paper will be

$$dW/dx = -KDP \quad [20]$$

It seems well to investigate the solution in this special case and it is recommended to the author that in the closure he expand his paper to cover the intermediate cases, if that should seem practicable and desirable to him. In what follows, the assumption of laminar flow in the tube will be retained.

Equations [2], [3], and [4] of the paper remain unchanged

$$d^2P/dx^2 = k_0k_1P \quad [21]$$

The auxiliary equation is

$$a^2 = k_0k_1 \quad [22]$$

so that

$$a = \pm\sqrt{k_0k_1} = \pm\sqrt{(128\,\mu K)/(g\pi\rho D^3)} \quad [23]$$

and

$$P = A\sinh ax + B\cosh ax \quad [24]$$

From Equation [1] of the paper

$$W = -(A/a)k_1\cosh ax - (Bk_1/a)\sinh ax + C \quad [25]$$

Substituting in Equation [2] of the paper, it is seen that $C = 0$

When

$$x = 0,\ W = W_0;\ \text{when } x = L,\ W = 0$$

$$W_0 = -(Ak_1/a)$$

Hence

$$A = -aW_0/k_1 = -\sqrt{k_0/k_1}\,W_0 \quad [26]$$

$$0 = W_0\cosh aL - (Bk_1/a)\sinh aL \quad [27]$$

Hence

$$B = (aW_0/k_1)\coth aL = \sqrt{k_0/k_1}\,W_0\coth aL \quad [28]$$

and

$$P = -\sqrt{k_0/k_1}\,W_0\sinh ax + \sqrt{k_0/k_1}\,W_0\coth aL\cosh ax \quad [29]$$

The flow

$$W = W_0(\cosh ax - \coth aL\sinh ax) \quad [30]$$

The rate of outflow per foot of length is easily found as

$$dW/dx = aW_0(\sinh ax - \coth aL\cosh ax) \quad [31]$$

where the minus sign indicates outflow.

It is always important to make sure that flow does occur through the wall throughout the length of the pipe, for with certain coefficients in these equations, it will be found that practically the whole discharge occurs in the first portion of the pipe and little or none from the rest. Term a is really the reciprocal of a characteristic length L_a, so that if $L/L_a = aL$ is small, outflow will occur throughout the pipe length; but if large, most of the flow will be found in the first portion of the pipe.

[1] By F. C. W. Olson, published in the March, 1949, issue of the Journal of Applied Mechanics, Trans. ASME, vol. 71, pp. 53–54.

[2] Consulting Engineer, General Electric Company, Schenectady, N. Y. Mem. ASME.

[3] Special Engineer, Publication and Consultation, Bethlehem Steel Company; Partner, Edward (Nellie), and George Richardson, Bethlehem, Pa. Mem. ASME.

It is interesting to note that these equations are closely related mathematically to the temperatures in a shaft which is heated locally over a short length, with the rest of the shaft free to give up heat by convection and radiation to the surrounding air. In such cases it is surprising how rapidly the temperature falls so that within a very few diameters the temperature is close to that of the air.

A. H. Shapiro.[4] The type of problem which the author has formulated may in time prove to have many more practical applications than seem apparent now, and therefore the writer feels that this type of analysis is of considerable utility.

The type of solution obtained by the author not only represents a limiting case, but is in fact the limiting case of a limiting case. Within the assumptions of the paper, it is applicable only when the amount of flow through the wall per unit length of wall is vanishingly small. For the more general case, Equation [2] of the paper must be modified to take into account momentum effects.

Following the author's convention that dW represents the "increase" in mass flow through the duct in the length dx, and assuming that the leakage flow as it enters the porous wall has no forward component of velocity (this must be so if the hole is small compared to the pipe diameter), the incoming momentum flux to the length dx is

$$\frac{\pi}{4} D^2 G(G/\rho g)$$

while the outgoing momentum flux is

$$\frac{\pi}{4} D^2 (G + dG)\left(\frac{G + dG}{\rho g}\right)$$

Hence the momentum equation is

$$-\frac{\pi}{4} D^2\, dP - \tau_w \pi D dx = \frac{\pi D^2}{4\rho g}\left[(G + dG)^2 - G^2\right] = \frac{\pi}{4} D^2 \left(2G\frac{dG}{\rho g}\right)$$

where τ_w is the shearing stress at the wall. Noting that

$$f = \frac{\tau_w}{G^2/2\rho g}$$

and that

$$G = W\Big/\frac{\pi}{4} D^2;\quad dG = dW\Big/\frac{\pi}{4} D^2$$

and using

$$f = \frac{16}{DG/\mu}$$

there is finally obtained

$$\frac{dP}{dx} = -\frac{128\mu}{\pi g \rho D^4} W - \frac{32}{\pi^2 g \rho} W \frac{dW}{dx}$$

in place of the author's Equations [3] and [4].

In many practical problems, the second term on the right-hand side of this equation, representing inertia effects, cannot be ignored compared to the first term on the right-hand side, representing frictional effects.

It may also be worth noting that if dW/dx is not negligible, the laminar-flow formula, $f = 16/\mathrm{R}$, will not be applicable because the flow pattern, especially near the wall where frictional effects are most important, will not correspond to Hagen-Poisseuille flow.

[4] Associate Professor of Mechanical Engineering, Massachusetts Institute of Technology, Cambridge, Mass. Mem. ASME.

Author's Closure

The interest shown in the author's paper is appreciated and, to a certain degree, unexpected, particularly since it was the author's intention merely to present an instance where the use of Weierstrass functions leads to a simple solution of ready applicability. Perhaps for this reason, sufficient attention was not paid to the choice of title, which, as the last two discussers show, implies more than is given in the paper.

It seems that a mathematical treatment of the intermediate cases mentioned by Mr. Richardson hardly would be advisable. This would involve raising P in Equation [20] of the paper to some power between $1/2$ and unity. Only for a few particular cases could one hope to obtain closed analytical solutions and these no doubt would be of such complexity as to render them of little value. An electrical analyzer of the type described by Dr. Poritsky would be of definite value in this case.

Finally, the author would like to call attention to an excellent paper by J. D. Keller.[5] In it, the momentum effects discussed by Professor Shapiro are taken into consideration.

On the Impact Behavior of a Material With a Yield Point[1]

E. H. Lee.[2] There is one difficulty in the theory used by the author, which, in principle, is clarified by some work now being carried out at Brown University. It is assumed in the paper that it is necessary to reach the upper yield stress before plastic flow occurs, but that instantaneously the elastic stress falls to the lower dynamic yield stress. It would seem that, since elastic loading is possible up to the upper yield stress, the initial elastic stress would produce an elastic wave starting with the same magnitude. In order to consider this change from upper to lower yield stress, it is necessary to use a stress-strain relationship involving overstress, and such a relationship of the simplest type is

$$E_0 \frac{d\epsilon}{dt} = \frac{d\sigma}{dt} + k[\sigma - \sigma_0(\epsilon)]$$

where E_0 is Young's modulus, k a viscosity constant, and $\sigma_0(\epsilon)$ the static stress-strain relationship for plastic flow. This relationship considers the rate of strain to be a combination of elastic and viscoplastic components. Using such a relationship, the plastic wave equations become more complicated but soluble by the method of characteristics. The upper yield-point stress, to which a section of the rod is subjected prior to plastic flow, initiates an elastic wave, the magnitude of which decreases toward the lower yield stress as the wave propagates. The rate of decrease depends upon k, and for a certain range of k the stress decreases to the lower yield stress very rapidly to give agreement with the analysis in the paper.

It would seem that this agreement would be closer for long specimens than for short, since the longer times involved would permit the excess stress to dissipate itself. Solutions using a simpler form of this type of law have been considered by Sokolovski.[3]

[5] "The Manifold Problem," by J. D. Keller, Journal of Applied Mechanics, March, 1949, Trans. ASME, vol. 71, pp. 77–85.

[1] By M. P. White, published in the March, 1949, issue of the Journal of Applied Mechanics, Trans. ASME, vol. 71, pp. 39–52.

[2] Graduate Division of Applied Mathematics, Brown University, Providence, R. I. Mem. ASME.

[3] "The Propagation of Elastic-Viscous-Plastic Waves in Bars," Akad. Nauk SSSR, *Prikladnaia Matematika i Mekhanika*, vol. 12, 1948, pp. 261–280. (See *Mathematical Reviews*, March, 1949, p. 219.)

A. NADAI.[4] The author of this paper refers to a number of important experimental facts which may deserve further careful considerations when the mechanism under which a localized deformation propagates along a tension bar is described. It is highly to be commended that the author calls attention to the dependence of the upper yield stress in mild steel on the rate of strain. Without entering into further details, it may prove useful to extend the way in which a localized deformation propagates along a tension bar by including also in the analysis a plausible assumption as to the nature of the speed dependence. It seems that most recent tests have indicated that the upper yield point increases with the elastic strain rate preceding yielding, according to a logarithmic function.

There is another point which might be mentioned. It has been brought out by P. P. Bijlaard that in compact specimens subjected to tension the first plastic layer (Lüders' flow layer) usually forms under an angle of 45 deg with respect to the axis of the bar, while the inclination of flow layers in flat specimens in materials having a sharp yield point is by no means 45 deg, and may vary. It is also interesting to note that the state of stress and strain within the first flow layer in the case of a compact specimen is a state of simple shear. According to the theory of the octahedral shearing stress, yielding under simple shear requires a yield stress 15 per cent higher when expressed in terms of shearing stress than the uniform yielding of the entire cross section in a round bar under simple tension. Furthermore, after the first formation of a thin layer, in which a state of simple shear prevails, a "working zone" forms with which the plastic zone advances along a specimen under static conditions of testing. In this working zone the strains change from the front in which they are of the order of 0.001 to the higher values of 2–3 per cent strain as observed after the yield-point elongation is completed in static testing. This may have the consequence that within the working zone again a complex state of stress and strain must exist through which all material elements must gradually pass when the plastic zone advances along the tensile specimen. The hope may be expressed that some of these most interesting mechanical conditions might be further investigated in the future analysis of the way bars yield of material having a sharp yield point both under static as well as under dynamic conditions.

AUTHOR'S CLOSURE

The author is grateful to Drs. Lee and Nadai for their valuable and interesting contributions. He agrees with Dr. Lee that the actual process of yielding is probably less simple than that assumed in the original paper. The data that were analyzed there showed enough scatter to make any attempt at refinement, such as that mentioned by Dr. Lee, entirely useless. However, as better data are obtained this and similar refinements in theory will be useful. The author does not feel that the assumption of discontinuous behavior in a material is necessarily a difficulty. Certainly, discontinuities are useful concepts in shock-wave theory, and they appear to be useful in the theory of propagation of plasticity as well. The author believes that in metals with well-defined yield points, a steady-state plastic wave form is possible. This wave is a shock wave, or wave of very nearly zero length, the length being determined by the dependence of stress on strain rate, as in a shock wave in a gas. In this case the magnitude of the stress in the wave, and the residual strain produced by it are constant along the specimen to the point where interference with another wave occurs.

As Dr. Nadai points out, the region of yielding in a specimen with a definite yield point is certainly behaving in a very complicated way. It seems likely that this behavior is basically the same under static and under dynamic conditions in spite of the great difference in speeds of propagation. It appears only that in dynamic yielding the amount of yielding is not constant but increases with the intensity of the propagating stress wave. It seems likely that careful investigation of what happens dynamically may help cast light on what happens statically, and vice versa. Certainly, both investigations might be pursued simultaneously with profit.

[4] Consulting Mechanical Engineer, Westinghouse Electric Corporation, Research Laboratories, East Pittsburgh, Pa. Mem. ASME.

Investigation of the Variation of Point Unit Heat-Transfer Coefficients for Laminar Flow Over an Inclined Flat Plate[1]

E. B. PENROD.[2] This paper makes an important contribution to the technical literature by presenting information on heat transmission from a nonisothermal inclined flat plate in laminar flow. It was stated that the temperature at the center of the ribbon was kept only a few degrees above the free air temperature in all runs. Nevertheless, it would be of interest to know (*a*) what the temperature gradient was in the direction of the length of the ribbon, and (*b*) the magnitude of the temperature deviation for a similar isothermal flat plate in laminar flow.

In making a study of heat transfer from a cylindrical surface to air in parallel flow, Jakob and Dow[3] took into consideration the effect of the hydrodynamic starting length of the specimen (the ratio of the surface area of the starting piece to the perimeter of the heating cylinder). Was the apparatus used here, designed so that the effect of the hydrodynamic starting length was negligibly small?

The coefficients of heat transfer from a solid surface to a gas according to Jakob and Dow are about 31 per cent smaller than that reported by Slegel and Hawkins.[4] The former investigators used a cylindrical surface, while the latter a flat plate. It would be of considerable interest if the author would calculate the value of the coefficient of heat transfer from his data for a flat plate and convert it by the use of the curvature factor to the equivalent value for a cylindrical surface 1.3 in. OD. If this could be done, the author's results could be compared with those of Jakob and Dow, and also those of Slegel and Hawkins.

AUTHOR'S CLOSURE

The temperature at the center of the nichrome ribbon was, at the downstream end of the plate for any run, not more than 15 F above free stream air temperature, nor less than 10 F above free stream air temperature. The leading edge of the plate was at essentially the free stream air temperature. The comparable isothermal surface plate then would be at a 10 F to 15 F temperature difference with the free stream air temperature, over the whole plate surface.

As is stated in the paper, the ratio of the unheated starting length to the total length is 0.0313 and thus is negligibly small.

[1] By R. M. Drake, Jr., published in the March, 1949, issue of the JOURNAL OF APPLIED MECHANICS, Trans. ASME, vol. 71, pp. 1–8.

[2] Head, Department of Mechanical Engineering, University of Kentucky, Lexington, Ky. Mem. ASME.

[3] "Heat Transfer From a Cylindrical Surface to Air in Parallel Flow With and Without Unheated Starting Sections," by Max Jakob and W. M. Dow, Trans. ASME., vol. 68, 1946, pp. 123–134.

[4] "Heat Transfer From a Vertical Plate to an Air Stream," by L. Slegel and G. A. Hawkins, Research Series no. 97, Engineering Experiment Station, vol. 30, May, 1946.

The experimental data of Jakob and Dow have been to some extent substantiated by Slack[5] in experiments on a 1.90-in-OD probe having a hemispherical nose. In this experiment, the nose was to some extent heated and no starting length correction was applied. It is thus concluded that the average heat-transfer coefficient from such a probe may be specified by the equation

$$\frac{hx}{k} = 0.028 \left(\frac{Ux}{\nu}\right)^{0.80} \quad \ldots\ldots\ldots\ldots\ldots\ldots [1]$$

for air in axial flow, under conditions in which the preponderant amount of heat transfer occurs from the cylindrical surface of the probe. The dimension x in the given correlation is the ratio of the surface area to the perimeter of the cylinder, which in the case of a hemispherical nose as was used by Slack, results in a length measured along the axis of symmetry of the probe. Such a measurement can be valid only when the length of the cylinder is large compared with its diameter.

Considering the state of knowledge concerning the boundary-layer flow on a body of the type considered, the comparison to flat plate conditions is to some extent unwarranted. The correction for boundary-layer curvature as calculated by Jakob and Dow, should indeed apply if the boundary layer would begin with zero thickness at some point along the cylindrical surface, when x could be considered zero. Unfortunately, the development of the boundary layer on the spherical nose section is of such character as to make fallacious the comparison with flat-plate conditions as implied in the characteristic length as quoted in the given equations.

To make a comparison with the flat plate, some boundary-layer dimension should be chosen as significant, and it is expected that in a relation of the type

$$\frac{h\delta}{k} = C \left(\frac{U_\infty \delta}{\nu}\right)^{0.8} \quad \ldots\ldots\ldots\ldots\ldots\ldots [2]$$

the constant C would be related for probe and plate only by the curvature relation previously cited. On the basis of this reasoning, it appears that the boundary-layer thickness implicitly assumed in Equation [1] is too small.

On the Design of Large Elevator Platforms[1]

L. R. Rissler.[2] The usefulness of the principle of superposition for the solution of statically indeterminant structures is quite evident in this paper. It has been the writer's experience that, in general, the simpler approach to the solution of a statically indeterminant structure is by the use of the theorem of Castigliano. The author's straightforward solution of this problem is obvious.

The distribution of load in a mat has rather a wide application, especially in the building industry. The author's paper points the way for a rational method of approach in the selection of floor members for many types of structures. It is particularly useful for elevator-platform design, because it is necessary for them to be as light in weight as possible. It would seem that an expanded application of the author's paper must take into account the two assumptions upon which it has its foundation. There are cases, which the writer can visualize, where the assumptions will not hold. One case would be where the stringer stiffness is large compared to the beam stiffness. Under this condition, an appreciable part of the load would be carried by more than three beams.

Author's Closure

I wish to thank Mr. Rissler for his discussion of my paper. The problem dealt with in it is of course one with far too many redundant elements for the application of Castigliano's theorem. With reference to the last three paragraphs of the discussion, I wish to refer Mr. Rissler to the explanation offered early in the paper in justification of Assumption I. Later in the paper, in connection with the numerical examples, he will find a discussion of its validity. Obviously, this or any other assumption is permissible as long as it leads to results that are on the safe side.

The Manifold Problem[1]

R. W. Powell.[2] The effort to collect and codify the scattered material on the flow in manifolds is very commendable. However, the author has overlooked some of the publications of civil engineers on the subject. It is desired especially to call attention to an article on the manifold for navigation locks,[3] and discussions of it by John S. McNown and the writer. These discussions were prepared independently, and are efforts to explain and evaluate the discrepancies between the author's Equation [8] and the actual situation. At each lateral-discharge opening there is an increase in pressure due to the deceleration, but it is not as much as Equation [8] would indicate, that is, there is an energy loss at each opening besides the ordinary friction loss in the pipe between openings.

The original treatment by Enger and Levy of a continuous side slot assumed that the liquid leaving through the slot keeps all of its forward velocity. On this basis the momentum treatment checks the energy treatment (Bernoulli's theorem) without loss. But with lateral pipes at right angles to the main pipe, if it is assumed that the liquid flows into the lateral perpendicularly to the direction of flow in the main pipe, the momentum treatment shows that the recovery of head is twice that given by Bernoulli's equation without loss. The actual fact is that the liquid as it leaves through the port has not been turned through the whole 90 deg.

Soucek and Zelnick called the flow in the main pipe upstream from the port Q_1, and downstream Q_2. The flow out through the port Q_3, was taken as $P_d Q_1$. Then $Q_2 = (1 - P_d)Q_1$. Thinking of Q_1 as $Q_2 + Q_3$, they assumed that the momentum of only $Q_2 + k_d Q_3$ would need be considered in the equation, as a forward momentum corresponding to $(1 - k_d)Q_3$ would be carried out into the port. This gives an equation

$$A(p_2 - p_1) = \frac{(Q_2 + k_d Q_3)V_1}{gv} - \frac{Q_2 V_2}{gv}$$

which reduces to

$$gv(p_2 - p_1) = 2(P_d + k_d P_d - P_d^2)V_1^2$$

This agrees with Equation [8] if $k_d = P_d/2$, which is the same as taking McNown's c as 0.5, that is, the author's treatment considers the energy loss in the port as zero. But the experiments recorded in the reference cited[3] show that, with the possible

---

[5] "Turbulent Heat Transfer With High Surface Temperature; Experimental Investigation With a Cylindrical Probe in an Axial Air Flow," unpublished Master of Science Thesis, 1948, by E. G. Slack, University of California, Berkeley, Calif.

[1] By F. Hymans, published in the March, 1949, issue of the Journal of Applied Mechanics, Trans. ASME, vol. 71, pp. 9–18.

[2] Section Engineer, Apparatus Development, Westinghouse Electric Corporation, Jersey City, N. J.

[1] By J. D. Keller, published in the March, 1949, issue of the Journal of Applied Mechanics, Trans. ASME, vol. 71, pp. 77–85.

[2] Professor of Mechanics, Ohio State University.

[3] "Lock Manifold Experiments," by Edward Soucek and E. W. Zelnick, Trans. ASCE, vol. 110, 1945, pp. 1357–1400.

exception of the case of the continuous slot, this energy loss is far from negligible. The writer's discussion also points out the effect of the nonuniform distribution of velocity in both the downstream main pipe and the lateral. These statements will not be repeated here, nor the important remarks made by McNown in the latter part of his discussion, and the reply of Soucek and Zelnick thereto.

R. H. Solem.[4] The scope of the paper is of course the proper proportioning of flow through a series of ports in a manifold. The author has given an excellent analysis of a common problem in practical everyday gas and heating applications which it seems has had very little attention in the past.

The author has assumed a discharge coefficient of 0.62 for K in Equation [1]. It would be well for the author to discuss further the effects of wide variations in this K-factor as experienced in practice. In the writer's experience, it generally has been found that it is good practice to use ports drilled from a No. 28-MTD (or $^1/_8$ in.) down to a No. 60-MTD. However, these practical limits vary widely in the field, depending upon whether raised ports are used or simple drilled ports. Mr. Bartholomae of Pittsburgh recommended use of rather large ports ranging from No. E-MTD (or $^1/_4$ in.) down to $^1/_8$ in. Such a range of port sizes might change this K-factor from a high of 80 per cent to as low as 40 per cent in the case of very small ports occasionally used.

Another item discussed by the author is the area ratio. It has been the writer's experience that a safe rule is to use a factor of 1.0 to 1.2; if this is exceeded, rather uneven and often unstable flames result. This is also borne out by the author's calculations. In an article by B. E. Bartholomae,[5] the author recommends that a total port area of a drilled-pipe burner may be from 1.75 to 2 times the cross-sectional area of the pipe. With fairly large ports and reasonably long burner pipes with L/D = 60 to 80, no doubt reasonably good results were obtained.

The author of the present paper recommends that, to compensate for variations in flow through ports at various locations, the ports must be placed on closer or greater centers depending upon the portion of the burner requiring more or less flow. In a burner there is of course the important factor of flame travel, and, if these centers were to spread and the ports were small, flame travel would become quite a problem. In a short burner, where the ratio of L/D = 10, the pipe would be so short generally that it hardly would be practical to vary the spacing over the burner length.

To some extent in practice, the amount of preheating of the gas-air mixture in the pipe burner will reduce the specific gravity of the gas and, at the same time, expand it so the effective port area is reduced at the end of the run. This to some extent occasionally tends in a practical manner to offset the importance of the L/D factor.

The design of the "simple" drilled pipe burner so commonly employed deserves some real comprehensive research. The paper concerns itself primarily with proper distribution of flow to all ports. The writer would like to propose an additional step, namely, to lay out tables on various popular pipe sizes from $^3/_8$ to 4 in. for various lengths. Such a study would involve the factors in the present paper, that is, the ratios of L/D, the ratio of areas of ports to cross-sectional area; a determination of ideal port sizes for universal gas use involving: (*a*) elimination of backfiring or flashback; (*b*) noise; (*c*) clogging; (*d*) flame travel; and port centers, as discussed in this paper, for proper flow distribution and proper maintenance of flame travel. Such tables could be calculated and would, it is believed, then standardize all commercial gas-drilled pipe burners, or the homemade burner, when drilled in the average shop. This would then "refine" an item which is now so commonplace that it has been neglected.

[4] Solem Machine Company, Rockford, Ill.

[5] Equitable Gas Company, article by B. E. Bartholomae, Pittsburgh, December, 1943, reprinted *Industrial Gas*.

Author's Closure

The discussions by Professor Powell and by Mr. Solem are appreciated.

The reference by Professor Powell to the Soucek-Zelnick work is a valuable one, but two limitations should be pointed out. First, Soucek and Zelnick did not make tests on a *number* of ports along a conduit; they had six ports, but only one at a time was discharging. This does not correspond to a manifold, where the flow conditions at any outlet are certainly influenced by the flow distortions which have occurred at the other outlets further upstream. Second, Soucek and Zelnick based their discharge coefficients on an "effective head" obtained by extrapolating the upstream gradient to the center line of the port, that is, they took no account of the rise of pressure in the manifold at or beyond the port caused by the longitudinal deceleration.

Nevertheless, in view of Professor Powell's discussion, it appears, in reference to the present paper, that a sharper distinction must be made between (1) a continuous slot in the side of a manifold, and (2) a series of separate holes, especially when the holes are comparatively few in number and far apart relative to the diameter of the manifold. For many small holes close together, it is believed that the derivation for the continuous slot is practically correct. As ΔQ changes to dQ, the momentum-theory results coincide with the energy-theory results, as shown in the discussion of Vazsonyi's theory in the Appendix.

A point not sufficiently emphasized in the paper is the erratic character of the flow from the manifold openings when the area ratio is considerably greater than unity, and the author is glad to note that Mr. Solem has pointed this out. To cite a specific case, in the manifold shown in Fig. 3, the greatest care was required in its construction, to obtain even the moderately uniform variation of jet heights indicated by the photographs. Without the outlet tubes (that is, with plain drilled holes) it was impossible to obtain any uniformity. Even with the tubes, with water, Fig. 3(*b*), occasional slight variations of unknown origin would cause some one of the jets near the inlet end to spurt much higher than its neighbors; this variation would persist for a time, then disappear, and later occur at some other outlet. The flames in Fig. 3(*a*) were photographed when burning a mixture of gas and air, but with raw natural gas, by impressing ever so slight a variation of pressure at the inlet, the flames could be made to dance along the manifold length, alternately high at the inlet end and low at the dead end, and vice versa. As a flow-distributing device, a manifold of large area-ratio is therefore extremely unreliable.

Mr. Solem raises the question of the effect of variation of the discharge coefficient. In the paper it was explained how this can be taken care of in a simple manner, provided the coefficient is the same for all ports; but if it varies from one port to another (with the pressure or head, for example) the correction is more difficult.

The effect of the transfer of heat to the combustible mixture in pipe burners, as pointed out by Mr. Solem, is to produce an acceleration which tends to counteract the effect of the deceleration and hence to equalize the discharge; but in most cases, with pipe burners in the open, the magnitude of this effect is believed to be negligible in practice. With pipe burners in ovens, it may in some cases be of importance.

In the present paper it was desired to cover many other mani-

fold problems besides those of pipe burners, but a more intensive study of this particular device, as suggested by Mr. Solem, would certainly be desirable. Perhaps he will carry this out in the comprehensive manner he has outlined.

References which should be added to those given in the paper, aside from those cited by Professor Powell and Mr. Solem, are as follows:

"Jets From Manifold Tubes," by Jacob Kunz, Trans. ASME, vol. 53, 1931, Paper No. APM-53-14, p. 181.

"Hydraulic Losses in Short Tubes Determined by Experiments," by J. R. Oakey, *Engineering News-Record*, vol. 110, June 1, 1933, pp. 717–718.

"Hydraulics of Sprinkling Systems for Irrigation," by J. E. Christiansen, Trans. ASCE, vol. 107, 1942, pp. 220–239 and discussion.

"Flow Through a Pipe With a Porous Wall," by F. C. W. Olsen. JOURNAL OF APPLIED MECHANICS, Trans. ASME, vol. 71, 1949, pp. 53–54.

Book Reviews

Fluid Mechanics

FÜHRER DURCH DIE STRÖMUNGSLEHRE (Abriss der Strömungslehre.) By L. Prandtl. F. Vieweg and Son, Brunswick, Germany, fifth edition, 1949. Bound in cardboard, 6¼ × 9¼ in., 247 figs., 407 pp., no price listed.

REVIEWED BY J. P. DEN HARTOG[1]

THIS book is a substantially enlarged new edition of a volume which first appeared in 1931 under the title "Abriss der Strömungslehre." An English translation was published in 1936, entitled "The Physics of Solids and Fluids," Blackie & Sons, Glasgow, Scotland.

The next edition, much larger than the first one, appeared in the middle of the war in Germany and was renamed "Führer" instead of "Abriss." A few copies of that edition were picked up in Germany in 1945 and found their way to allied countries, but its existence remained virtually unknown outside of Germany. Now, during the postwar years, the great master of fluid mechanics has not only revised the text, incorporating in it all the new material discovered by the Germans during the war, but has increased its size from 300 to 400 pages. The new material deals principally with applications to meteorology and to heat transfer.

Readers of the earlier edition will remember it as a beautiful book, simple and lucid, with many striking explanations of physical experiments as well as mathematical developments, giving much understanding for comparatively little difficulty. In its present new edition the book covers the entire field of fluid mechanics in its broadest sense, describing and explaining the fundamental laws as well as all important technical applications.

Many of the topics in the book originated or were materially advanced by either Professor Prandtl himself or by his advice to the great number of students and assistants who did their work in his laboratory. This book is a fitting monument to the father of modern fluid mechanics. An English translation will be published early in 1950 by Blackie & Sons, Glasgow, Scotland.

Reissner Anniversary Volume

REISSNER ANNIVERSARY VOLUME—Contribution to Applied Mechanics. Edited by The Staff of the Department of Aeronautical Engineering and Applied Mechanics of the Polytechnic Institute of Brooklyn. J. W. Edwards, Ann Arbor, Mich., 1949. Cloth, 9¼ × 6¼ in., viii and 493 pp., figs., illus. $6.50.

REVIEWED BY W. R. SEARS[2]

THESE papers on applied mechanics were contributed in honor of Prof. Hans J. Reissner on the occasion of his seventy-fifth birthday. The volume begins with a biographical sketch prepared by three of his colleagues at the Polytechnic Institute of Brooklyn, and a list of his more than ninety published works. There follow thirty-two papers in the fields of aerodynamics, elasticity and structures, electricity, mathematical methods, plasticity, and propulsion, contributed by investigators on both sides of the Atlantic.

It is impossible for the reviewer to report on each of the papers presented, but perhaps it is permissible for him to mention a few that seemed particularly interesting to him, in order to give some idea of the character of the volume. If so, he would mention L. H. Donnell's extension of the concept of critical axial loads in bars to include both compression and tension, by virtue of generality of end conditions; Theodore von Kármán's note on thrust augmentation, which shows that surprising results may appear if nonuniform entrance conditions are permitted; and J. J. Stoker's idea of prestressing a circular plate to stiffen it against normal buckling. An important section of the book is devoted to a series of five papers on concentrated load effects in reinforced monocoque structures, submitted by personnel of the Airplane Structures Research Staff at the P.I.B.

The range of subject matter covered in the volume is broader than might be suggested by these samples. It includes, for example, Reinhold Rüdenberg's paper on the electron gun, Rufus Oldenburger's discussion of a new type of constant-speed drive, and Alexander Weinstein on separation theorems for eigenvalues. The list of contributors is impressive, including, as it does, D. P. Riabouchinsky writing on the open-channel analogy to compressible flow, Walter Tollmien on a hodograph method, K. O. Friedrichs, Eric Reissner, R. Grammel, R. von Mises, and others of comparable scientific stature.

In style and appearance, as well as in content, the Reissner volume is a complete success, and its editors are to be complimented. It stands as an appropriate tribute to one of the Grand Old Men of applied mechanics.

Elements of Mechanical Vibration

ELEMENTS OF MECHANICAL VIBRATION. By C. R. Freberg and Emory N. Kemler. John Wiley & Sons, Inc., New York, N. Y., Second edition, 1949. Cloth, 6 × 9 in., figs., illus., bibliography, xiii and 227 pp., $3.75.

REVIEWED BY DANA YOUNG[3]

AN understanding of vibration phenomena has become a necessity in many engineering applications, and courses dealing with vibrations have been introduced into many engineering colleges. As a result a need has arisen for elementary texts on vibrations for those who do not have sufficient theoretical background or the time to study the subject very deeply. This book, which is now in its second edition, has been planned to fit this type of demand.

As stated in the preface, it is the purpose of this book to discuss the more elementary phases of vibrations and reduce them to a form in which they can be applied to practical problems. In order to achieve these aims it has been necessary to sacrifice mathematical rigor and, to a certain extent, some of the more fundamental principles of vibrating systems. A theoretically inclined reader will find much to criticize.

The first part of the book follows along conventional lines. Vibrations of a one-degree-of-freedom system are discussed in reasonable detail. This is followed by a brief treatment of systems with several degrees of freedom including the application of Holzer's method. A chapter is devoted to vibration isolation and absorbers, and another chapter discusses methods of reducing various mechanical systems to equivalent disk and shaft systems.

[1] Professor of Mechanical Engineering, Massachusetts Institute of Technology, Cambridge, Mass. Mem. ASME.

[2] Director, Graduate School of Aeronautical Engineering, Cornell University, Ithaca, N. Y.

[3] Professor of Applied Mechanics, University of Texas, Austin, Texas. Mem. ASME.

The vibration of beams is treated with principal emphasis upon Rayleigh's energy method.

The latter part of the book includes three subjects of a more specialized nature, namely, noise and its reduction, the mobility method, and electrical-analog systems.

Theory of Propellers

THEORY OF PROPELLERS. By Theodore Theodorsen. McGraw-Hill Publications in Aeronautical Science. McGraw-Hill Book Company, Inc., New York, N. Y.,1948. Cloth, 6 × 9 in., illus., viii and 164 pp., $3.50.

REVIEWED BY HUGH L. DRYDEN[4]

IN THIS monograph of 164 pages, Theodorsen paints in broad terms the theory of propellers in a nonviscous incompressible fluid with very brief discussions of approximate allowances for the effects of the profile drag of the blades and of the general nature of compressibility effects. The main content is the potential theory of the flow about propellers with finite number of blades and with the optimum lift distribution along the blades to give minimum losses. It is thus comparable to the theory of airfoil systems of minimum induced drag in the potential flow of a nonviscous fluid.

Theodorsen has made many original contributions to this subject, starting from Goldstein's solution for a lightly loaded single-rotation propeller of small advance ratio. Theodorsen showed that the Goldstein functions are applicable to heavily loaded propellers provided that parameters of the helix surface far behind the propeller are used rather than the parameters of the surface at the propeller itself. He also developed an electrical-analog method of determining the potential function for optimum load distribution on single and dual rotation propellers, which is rather inadequately described in chapter 5 of the book.

The practical designer will find the presentation difficult to understand and will consider the restriction of applicability of the theory to design operating conditions and low tip speeds where the flow approximates potential flow as a severe limitation. Nevertheless, if he does master the fundamental concepts, he will have a powerful aid in assessing the general effects of changes in the design variables and of body interference.

Chapter 1 is an exceedingly brief introduction which outlines the general content of the book. Chapter 2 presents various general theorems with regard to optimum loading. Chapter 3 sketches the solution of the optimum-distribution problem, giving tabular results for two-blade and four-blade single-rotation propellers as computed by various authors. Chapter 4 introduces the propeller mass coefficient as a parameter for heavily loaded propellers, and gives formulas for thrust, torque, energy loss in wake, and ideal propeller efficiency, as well as the distribution of energy losses in the wake between the axial, tangential, and radial motions. Chapter 5, as already mentioned, describes an electrical analog for determining the loading function and the mass coefficient.

Chapter 6 presents design relations and procedures for single and dual propellers. The design proceeds from assumptions as to the power, density, velocity, rotation speed, diameter, and number of blades. The power coefficient is computed, thence the corresponding ratio of helix displacement velocity at infinity to forward speed. From tables, the mass coefficient, advance ratio of the helix, and load distribution are obtained. Choosing a selected ideal lift coefficient, the chords at various radii are computed. The loss from profile drag is then computed and used to correct the estimated efficiency and useful power.

Chapter 7 discusses the slip-stream contraction; Chapter 8 describes propeller-selection problems, and Chapter 9 sketches the treatment of body-interference problems.

The reviewer considers the compact presentation as an excellent commentary on propeller theory by a leading expert in the field.

[4] Director of Aeronautical Research, National Advisory Committee for Aeronautics, Washington, D. C. Mem. ASME.

Theory of Oscillations

THEORY OF OSCILLATIONS by A. A. Andronow and C. E. Chaikin. English language edition by S. Lefschetz. Princeton University Press, Princeton, N. J., 1949. Cloth, 5¾ × 9 in., 313 figs., ix and 358 pp, price $6.

REVIEWED BY J. P. DEN HARTOG[5]

ONCE upon a time, in 1877, Lord Rayleigh published a book entitled "Theory of Sound," which was the first textbook on vibration. The subject has grown greatly since that day and many other books have followed it. These newer books usually contain discussions of many modern applications, but all of those are explained on the basis of Rayleigh's original theories, so that it can be stated without much exaggeration that no book on vibration has appeared since 1877 which differs essentially from the great classic.

Now, however, we have before us a publication in an entirely different class, written by two Russian scientists, originally published in Moscow in 1937, and recently made available in an English edition. (March, 1949.) The work of Rayleigh and of most of his successors deals with the vibrations of *linear* systems only. Scattered papers have appeared on *nonlinear* vibrations, most of which go back to an epoch-making one by Van der Pol on "Relaxation Oscillations," in 1926. Other papers in this field are on the general mathematical theory, primarily by the great French mathematician Poincaré, but these are so difficult as not to be understandable to most engineers, even to those specialized in vibration, such as the reviewer.

The present book by Andronow and Chaikin is written by engineers for engineers. It treats the general theory of nonlinear systems, but in each chapter a number of rather familiar physical cases are discussed in detail first, before the generalizations are drawn. Thus each step of abstract theory is made much more easily understandable by reference to the behavior of a familiar example. These examples include the squeaking door, the pendulum with a rotating axle in its pivot with friction, vibrating systems with dry friction or square velocity damping, vacuum-tube oscillators, cathode-ray sweep circuits, and many others. Most of the examples deal with mechanical or electrical systems, but they extend beyond that: the case is discussed of the two kinds of fish in the ocean, one of which feeds on plants and the other of which feeds on the first kind of fish. Thus the second kind cannot exist without the first; the population of either kind goes up and down with time in regular cycles.

The mathematical methods by which all of these rather complicated phenomena are discussed are surprisingly simple: the principal feature is that for each case a diagram is made where displacement is plotted against velocity. This has been done in the past (among others inevitably by Rayleigh in 1877 for linear systems, and later by Van der Pol), but the innovation is that a systematic study of these displacement-velocity diagrams reveals the most significant properties of the behavior of all nonlinear systems.

It is clear that we have before us an important publication. The English edition is not just a translation; it has been "edited" by Professor Lefschetz of Princeton University, who explains in

[5] Professor of Mechanical Engineering, Massachusetts Institute of Technology, Cambridge, Mass. Mem. ASME.

the preface that he has shortened the book considerably by retaining all the physical examples and by omitting many existence and convergence proofs. This undoubtedly has made the book very much easier and more profitable to engineers. Many readers will be grateful to Professor Lefschetz for the service he has thus rendered the profession.

It is unfortunate indeed that the authors, Andronow and Chaikin, are now spiritually separated from us by a set of circumstances which are even more complicated and certainly more serious than nonlinear vibrations. The reviewer ends by expressing his regret that such is the case and by stating his conviction that if these authors could appear before us at one of our Society's meetings they would be given a warm welcome and receive well-deserved applause for a beautiful job well done.

Distribution of Deformation

DISTRIBUTION OF DEFORMATION (a New Method of Structural Analysis). By C. V. Klouček. Translated from the Czech and German editions by A. H. Waddell-Zalud and F. H. Zalud. Published by C. V. Klouček, Prague, Czechoslovakia, 1949. Paper, 9½ × 6½ in., 215 figs., 510 pp. (This first English edition has been printed only in 350 copies for the information of foreign specialists.)

REVIEWED BY JACK R. BENJAMIN[6]

THE method of rigid frame analysis developed in this book is based on a consideration of the deformation of the frame when the joints rotate. The term "distribution of deformation" refers to the distribution of angular joint rotation throughout the frame when one joint is rotated. This is not a method of successive approximation, but an algebraic method wherein the structural action is evaluated before loads are applied. Application of loads then results in direct computation of joint rotations which, when combined with the action of the loads, yields the span-end moments. The solution of simultaneous equations is not required and accuracy is limited only by the normal structural assumptions. The fundamental equations are simple and easily applied with results comparable in speed with those of moment distribution.

Almost the exact same method has been presented in the United States by Evans, "Rigid Frames"; in Sweden by Efsen, "Method of Primary Moments." By an extension the results of Lin, "A Direct Method of Moment Distribution" are obtained. These and other comparable methods are derived on a different basis, but the end results and equations are fundamentally the same.

The extension of the method to include chord rotations is standard until the problem of multistoried frames is attacked. Solution of sidesway in multistoried frames is handled by the use of a substitute cantilever beam with knots of stiffness at each floor level. The substitute cantilever is then used to calculate story deflections from which moments are obtained. The substitute cantilever works well for simple structures, but with more difficult problems the method increases greatly in complexity. Extension of the cantilever beam with knots to a horizontal beam with knots affords a new solution to the Vierendeel truss.

The theoretical development is logical and thorough and the investigation of accuracy of the method and simplifications is complete. The operation of the method is illustrated by many examples.

This book once again points out that purely algebraic methods can compete with the methods of successive approximation. The method used by any designer then is a matter of personal preference and experience.

[6] Assistant Professor of Civil Engineering, Stanford University, Stanford University, Calif.

International Association for Bridge and Structural Engineering

INTERNATIONAL ASSOCIATION FOR BRIDGE AND STRUCTURAL ENGINEERING. Third Congress, Liége, Belgium, Sept. 13–18, 1948, preliminary publication. Edited by F. Stuessi and P. Lardy. Eidgenössische Technische Hochschule, Zurich, Switzerland; École Polytechnique Fédérale, Zurich; Swiss Federal Institute of Technology, Zurich, 1948. Cloth, 7 × 9¾ in., illus., diagrams, charts, tables, 697 pp., 400 Belgian fr; 300 Belgian fr to members of IABSE.

REVIEWED BY N. J. HOFF[7]

THIS carefully printed and illustrated volume contains advance copies of papers prepared for presentation at the Third Congress of the International Association for Bridge and Structural Engineering which was held in Liége, Belgium, in September, 1948. The association was organized in 1929 and has its offices at the Federal Polytechnic Institute of Zurich, Switzerland. It is of some interest to compare the publication of this first congress after World War II with those of the two earlier ones.

The first congress of the association was held in Paris in 1932. It was attended mostly by Central European engineers who had started the organization. The papers were submitted to the congress in French, German, or English and were printed in the 683-page Preliminary Publication in the original language—predominantly German—and in French translation. Only two contributions were accepted from England and one from the United States. Summaries of all papers were published in the three working languages of the congress. The preliminary publication of the second congress, held in Berlin in 1936, has all the earmarks of the lavishness of a dictatorship which wants to impress other countries with its appreciation of engineering science. A separate volume was published in each of the official languages—French, English, and German—containing the original or a complete translation of every paper accepted by the general secretaries and technical advisers. The English edition contained 1583 pages. In spite of the large number of papers there were only three English and five French authors with a sprinkling of Scandinavians and men from the Low Countries. All the other contributions were of Central European origin.

Judging from the present volume, the geographic center of the activities of the association shifted to the West and North after World War II. Contributions from the various countries are distributed as follows: France 18, England 9, Sweden 8, Belgium 7, Holland 4, Switzerland 3, U. S. A. 3, Czechoslovakia 2, Poland 2, Denmark 1, and Spain 1. Papers were accepted in one of the three official languages and printed as received. It appears, however, that many of the European, particularly Scandinavian, authors prefer English to the other two languages. The volume contains altogether 32 papers in French, 21 in English, and 5 in German. Again, all summaries appear in each of the three languages.

The papers are arranged in five groups. Those in the first deal with connections and design details of steel structures. Their importance follows from the observation that failures of bridges are almost always caused by incorrect detail design rather than errors in the general layout and analysis. One of the details that has caused much trouble in recent years is the welded joint—one has to think only of the Liberty ships. Four papers deal with problems of welding. It is observed that triaxial states of stress prevailing because of the residual stresses lead to brittle failure. The "weldability" of a steel depends just as much upon design details as upon the composition of the material. Other problems of

[7] Professor of Aeronautical Engineering, Polytechnic Institute of Brooklyn, Brooklyn, N. Y. Mem. ASME.

interest are the optimum arrangement of stiffeners to retard the buckling of the web of a beam subjected to bending, the calculation of the buckling stress of plates beyond the elastic limit, and the behavior of thin sheet elements of built-up girders after buckling.

The second part, comprising more than one third of the book, deals with concrete, reinforced concrete, and prestressed concrete structures. The trend toward rational, instead of empirical methods is noticeable in this part as well as in the preceding one. The first eight papers contain analytical and experimental studies of the optimum grain sizes and the composition of concrete; of the properties of vibrated concrete; resistance of concrete to frost; crack formation in reinforced concrete; the supersonic method of testing concrete structural elements; the determination of the bending moment that causes failure in a rectangular reinforced-concrete beam; and the effect of transverse grate-type reinforcements upon the strength of rectangular concrete columns.

The remaining thirteen papers of the second part describe reinforced-concrete structures, mostly bridges, erected since 1936 in Belgium, Holland, Spain, France, Czechoslovakia, England, and Sweden. Reasons are given for the choice of the particular type of construction; dimensions, loads, bending moments, and stresses are quoted; photographs show the completed structures, sketches explain design features, and methods of erection are discussed. It is worth noting that some of the reinforced-concrete bridges described replace earlier suspension bridges. Of particular interest are descriptions of a number of structures utilizing prestressed concrete. Prestressing eliminates cracks in the concrete to such an extent that pipe lines can be constructed which remain watertight when subjected to internal pressure.

Part 3 is entitled "Developments in Long-Span Steel Bridges." It deals mostly with suspension bridges which have become the preferred choice for very long spans. Because of the intrinsic complexity of the theory of the suspension bridge, research men in this field have to make use of advanced mathematical methods. The "elastic" theory has long been superseded by the "deflection" theory, but even the accuracy of the accepted version of the latter is put to the test in the first three articles of this section. It is found by means of worked out numerical examples that the maximum moments in the stiffening girder may be in error up to 7 per cent if the horizontal displacements of the cable are disregarded (Melan's equation), and up to about 4 per cent if the effect of the hanger deflections is neglected. Results of preliminary wind-tunnel tests are given on the influence of design details of stiffening truss, deck construction, handrailing, etc. upon the aerodynamic instability of suspension bridges. Plans for the construction of a special wind-tunnel accommodating bridge models up to a length of 50 feet are disclosed.

Reinforced-concrete slabs and thin-walled shells are the subject matter of Part 4. In the analytical treatment of these problems difficulties arise, as a rule, from satisfying the boundary conditions. At the same time the complexity of an exact mathematical treatment is often not warranted because of the uncertainties involved in the evaluation of the actual boundary conditions. Three papers in this group treat of the rigorous, approximate, and experimental determination of the strength and stability of continuous slabs. Two more describe actually completed structures.

The fifth and last part of the volume deals with questions of safety and dynamic loads. Six papers discuss the general concept of safety and point out the need for a statistical approach to the problem. It is shown that results of strength tests do not follow the probability curve of Gauss. One article emphasizes the importance of inelastic deformations in the load-carrying capacity of structures. Advances made in the understanding of dynamic effects are described in five papers. Of particular interest are two articles on the vibration of beams under the influence of moving loads.

In conclusion, it may be stated that the average level of the papers is high and it is regrettable that so little interest was shown on this side of the Atlantic in the work of the Congress. The only three American contributors are O. H. Amman, "General Report on Developments in Long-Span Steel Bridges"; G. Winter, "Performance of Thin Steel Compression Flanges"; and A. M. Freudenthal, "Inelastic Behavior and Safety of Structures." A greater participation by American civil engineers in the deliberations of the next congress should benefit the art and contribute to a better understanding between at least one group of people in Europe and the United States.

The Aeronautical Quarterly

THE AERONAUTICAL QUARTERLY. Vol. 1, Part I, May 1949. Published by the Royal Aeronautical Society, London, England. Stiff paper, $6^3/_4 \times 9^3/_4$ in., 10s.

REVIEWED BY ALEXANDER KLEMIN[8]

EVERY branch of applied science proceeds steadily from the simple to the complex. Before World War I several men could justifiably say that they had read all the technical aeronautical literature of the day. Today that would be an impossible task. When in every scientifically minded country there issues a flood of research reports and technical studies in aviation, the problem for the serious worker is to select what should be read and what should be retained or at least indexed, and what to discard as of ephemeral interest. The new *Aeronautical Quarterly* should help the situation. The first number is impeccably edited, the mathematics are well set out, the editorial board has selected its seven papers or articles wisely.

The first paper is on "Control Reversal Effects on Swept-Back Wings" by Haydn Templeton, which is one of the most difficult and most modern problems in airplane design. The author in his summary says "With the descriptive treatment adopted, the analysis is of necessity broad and general but is designed to appeal to those not too familiar with the subject." It is this sentence which shows why the *Quarterly* will be valuable. Authors and editorial board apparently understand that it is impossible for any technician to understand the specialized mathematics of every field without proper background.

G. N. Ward in "Calculation of Downwash Behind a Supersonic Wing" makes use of the thought that once the linearized lift-problem for a supersonic wing has been solved, the complete flow round the wing and the downwash behind the wing may be found. His treatment is difficult and ultramathematical.

It is a nuisance when studying airplane dynamic stability and changing a parameter to have to solve all the equations. K. Mitchell in "Estimation of the Effect of a Parameter Change on the Roots of Stability Equations" shows how the effects of such changes on the roots may be determined fairly quickly.

W. J. Duncan is an international authority on flutter. In "Flutter of Systems With Many Freedoms" he discusses the choice of a minimum set of freedom and how to conduct flutter calculations *so as to minimize labor*, an objective that will appeal to many readers.

E. C. Pike's "Note on Propeller-Turbine Reduction Methods" deals with an interesting topic. Methods of presentation and reduction in this field have not yet become standardized.

That the *Quarterly* will be catholic in its viewpoint is proved by G. W. Trevelyan and D. R. Blundell's "Determination of Drag of Jet-Propelled Aircraft in Flight" because this is a practical topic discussed by practicing engineers. F. Ursell's "Notes on

[8] Greenwich, Conn. Mem. ASME.

the Linear Theory of Incompressible Flow Round Symmetrical Swept-Back Wings at Zero Lift" is a fine linearized treatment of a difficult problem.

The foreword says in part "It is the primary object of the editorial board of *The Aeronautical Quarterly* to encourage workers to submit papers describing new and original work, or papers reviewing the progress in some specialized field of activity and .... to make the results of these researches available to all workers or design groups concerned with aviation." If the *Quarterly* continues as it has begun, it should achieve the object thus defined.

Advances in Applied Mechanics

ADVANCES IN APPLIED MECHANICS. Edited by Richard von Mises and Theodore von Kármán. Vol. 1. Academic Press Inc., New York, N. Y., 1948. Cloth, 6 × 9 in., 293 pp., illustrated. $6.80.

REVIEWED BY ERIC REISSNER[9]

THE present book is the first of a series intended for graduate students, scientists, and engineers who are familiar with the contents of textbooks and handbooks in the field of applied mechanics, but who feel in need of integrated surveys of the results and methods contained in the recent periodical literature. This need becomes more and more pressing with the increased volume of research which is carried on in fluid and gas dynamics, in elasticity and plasticity, and related subjects. Both experimental and mathematical techniques are becoming more refined and more and more we are witnessing extreme specialization among research workers. While twenty or so years ago many a man could claim familiarity with the state of knowledge in applied mechanics in general, today we find many who are having difficulties in keeping up with progress outside their own specialty. In view of this trend it is extremely commendable that the two world-renowned editors have undertaken the task of assembling surveys of various fields which will facilitate, for those who feel that this is worth while, the task of becoming acquainted with recent progress in many of the subdivisions of applied mechanics. It is valuable advice which the editors give by saying "the more research in mechanics expands, the more interconnections of seemingly far distant fields become apparent." One needs to think only how mathematical methods from supersonic aerodynamics are now being utilized in the theory of plasticity and how early methods in plasticity have been rediscovered by gas dynamicists.

Coming to the contents of volume 1, we find first a summary of advances since 1938 concerning boundary-layer flow, written by H. L. Dryden. Among these advances is the experimental verification of mathematical-stability theory by means of low-turbulence wind-tunnel tests and the phenomenon of stabilization of the boundary layer by means of suction through slots or porous walls.

N. Minorsky gives an informative account of qualitative and quantitative procedures for the solution of second-order nonlinear ordinary differential equations. In particular we find discussion of periodic solutions and analysis of nonlinear resonance.

C. B. Biezeno surveys contributions to elasticity published during the period 1940 to 1946 in Holland. Quite a large number of papers on plane stress, beams, plates, and shells are abstracted in this article.

J. M. Burgers is concerned with the statistical theory of turbulence. This is an enlightening discussion of a mathematical model, that is, of a system of equations simpler than the Navier-Stokes equations but incorporating essential features of these equations. Although progress is evident, much work appears still to be required before one can speak of a rational solution of even the simplest problems of the statistical theory of turbulence.

Hilda Geiringer presents two finite difference methods for the analysis of problems of one-dimensional wave propagation in compressible fluids. One of these methods is by the author, the other one by J. von Neumann. Both have not been generally available heretofore.

R. von Mises and M. Schiffer offer a lucid introduction to the method of Stefan Bergman for integration of the linear partial differential equation which governs the problem of two-dimensional steady compressible flow when velocity components instead of space co-ordinates are introduced as independent variables. The discussion is carried out for an isentropic gas and for a hypothetical gas more nearly isentropic than the one with linear pressure-volume relation. One may hope that a future article will bring a discussion of associating the solutions which are obtained with the physical flow problems which are here of interest.

The appearance of this volume 1 of "Advances in Applied Mechanics" is a noteworthy event. One looks forward to additional volumes of this series, assembled and written in the spirit of the present first volume.

Memoires et Travaux

MEMOIRES ET TRAVAUX DE LA SOCIÉTÉ HYDROTECHNIQUE DE FRANCE. Vol. 1, 1948. Published by Société Hydrotechnique de France, 199 Rue de Grenelle, Paris 7, France. Paper, 8 1/2 × 11 1/2 in.

REVIEWED BY ARTHUR T. IPPEN[10]

INTEREST in hydrodynamics and especially applied hydraulics has expanded to a very remarkable degree in France since the war's end as evidenced by the opening and remarkable growth of several excellent laboratories and by the already well-known periodical *La Houille Blanche*. The Société Hydrotechnique de France has now ventured to publish by agreement with *La Houille Blanche* two editions yearly of its own "Memoires et Travaux." These will appear as special numbers of *La Houille Blanche* dedicated exclusively to the committee work and field of interest of the Société Hydrotechnique. The first number in this series contains the minutes of two meetings of the technical committee of the society held on November 19, 1946, and April 29, 1947, with extensive discussions of a number of papers published in *La Houille Blanche* or other scientific journals by the members. This number thus is to bring up to date the records of the society since the break in publication in 1945. Summaries of later meetings are to appear in the following issue. A series of papers are also contained therein, the titles of which may be given here to elucidate the scope of the scientific field covered.

Mr. R. Legendre introduces corrective terms into the Kármán logarithmic equation for velocity distribution in pipes to extend the validity to the zone near the pipe axis, in his paper on "The distribution of mean velocities for turbulent flow in cylindrical pipes." Mr. L. Escande extends the water-hammer theory to the case of "The maximum pressure surge obtained in the governing of hydroelectric units equipped with relief valves." Mr. G. Labaye has summarized and evaluated critically the results on the "transport of sediments by streams" obtained in the past by investigators of all countries.

Mr. A. Nizery compares the problem of "Constant-depth waves in the neighborhood of a jetty" to the optical problem of diffraction of light at the edge of a large screen. Mr. G. Remenieras investigates the "possibility of direct conversion of the energy of a fluid stream into electric power" by passing the stream

[9] Professor of Mathematics, Massachusetts Institute of Technology, Cambridge, Mass. Jun. ASME.

[10] Professor of Hydraulics, Massachusetts Institute of Technology, Cambridge 39, Mass. Mem. ASME.

through a magnetic field. The conclusion is that this would be practical only for the hypothetical case that the energy of the primary fluid could be efficiently transmitted to an intermediate fluid of high electric conductivity. The direct application of the method for velocity measurements by A. Kolin is well known and will probably remain its primary function. Nevertheless, it is often instructive to speculate. Mr. M. Pardé comprehensively and appreciatively surveys the American attacks on the problem of floods in "American studies of floods" with conclusions applied to his own country.

Judging from the variety of problems dealt with in this first issue of "Memoires et Travaux" in such a useful and excellent manner, it can be well recommended to all hydraulic engineers in the U. S. as representative of the best efforts of their European colleagues.

Computation Curves for Compressible Fluid Problems

COMPUTATION CURVES FOR COMPRESSIBLE FLUID PROBLEMS. By C. L. Dailey and F. C. Wood. John Wiley & Sons, Inc., New York, N. Y., and Chapman and Hall, Ltd., London, England. 1949. Paper, 8½ × 11 in., graphs, figs., x and 33 pp., $2.

REVIEWED BY ASCHER H. SHAPIRO[11]

TO THE growing number of useful aids in working out design problems in the high-speed flow of gases may be added this compilation of charts covering many of the compressible-flow functions most commonly employed.

The scope of the work may best be indicated by outlining the various groups of curves:

Isentropic Flow. Curves of temperature ratio, pressure ratio, density ratio, and area ratio, all versus Mach number (from 0 to 4), and for specific-heat ratios from 1.25 to 1.40.

One-Dimensional Heat Addition Without Friction in a Constant-Area Channel. Curves for finding final Mach number, pressure ratio, and stagnation pressure ratio as functions of initial Mach number (from 0 to 4) and of stagnation temperature ratio, for specific-heat ratios from 1.25 to 1.40.

Oblique Shocks. With initial Mach number (from 0 to 4) and turning angle (from 0 to 38 deg) as independent parameters, curves of shock angle, stagnation pressure ratio, pressure ratio, density ratio, temperature ratio, final Mach number, and entropy change. The normal shock is shown as a limiting case. All curves are for a specific-heat ratio of 1.4.

Prandtl-Meyer Flow. For a specific-heat ratio of 1.4, stream turning angle versus Mach number (from 0 to 4.0).

Conical Shocks. With initial Mach number (from 0 to 4.0) and cone angle (from 0 to 52 deg) as independent parameters, curves for finding shock angle, stagnation pressure, Mach number, velocity, pressure, and stream direction at the surface of the cone and in the region between the shock and the cone.

The curve sheets are preceded by a short text giving the underlying assumptions and derivations of the formulas on which the curves are based.

Although curves can hardly be expected to yield the precision of tables, the scales of the curves are sufficiently large for the accuracy required of most engineering computations. Great care has obviously been given to the organization, drawing, and binding of the charts. This, together with the importance of the subject matter, makes the collection of graphs a valuable tool as a supplement to some of the extensive numerical tabulations which are already available.

[11] Associate Professor of Mechanical Engineering, Massachusetts Institute of Technology, Cambridge, Mass. Mem. ASME.

Practical Solution of Torsional Vibration Problems

PRACTICAL SOLUTION OF TORSIONAL VIBRATION PROBLEMS. By W. Ker Wilson. John Wiley & Sons, Inc., New York, N. Y., 1948. Cloth 5⅝ × 8⅝ in. Vol. I, xx and 731 pp., illus.; Vol. II, xxi and 694 pp., illus. Each volume $10, U. S. A.

REVIEWED BY G. S. CHERNIAK[12]

AFTER being out of print for several years, the second edition of this book has been reprinted and is again available. The purpose of this review is primarily to announce the reissue of this valuable publication to many who, like the reviewer, have been fruitlessly attempting to locate a copy for the past several years. It also might not be remiss to examine briefly the content or the benefit of those who have not had occasion nor the opportunity to use this reference.

Dr. Wilson's books represent one of the most complete but by no means all-inclusive sources of data on techniques for the analysis of torsional systems and the measurement of such vibrations. Volume I comprises chapters on the following: Torsional Vibration, Natural Frequency Calculations, Equivalent Oscillating Systems, Flexible Couplings, Geared Systems, Determination of Stresses Due to Torsional Vibration at Nonresonant Speeds, Effective Inertia Method of Torsional-Vibration Analysis, Aero-Engine Air-Screw Systems. Volume II deals with the following: Determination of Stresses Due to Torsional Vibration at Resonant Speeds, Measurement of Torsional Vibration Amplitudes and Stresses, Analysis of Torsiograph Records, Torsional Vibration Damping Devices, Rotating Pendulum Vibration Absorbers, Dynamic Characteristics of Electrical Generating Sets.

The presentation of this material is lucid and amply illustrated by numerous examples. An excellent bibliography is included, as well as a selected list of patents relating to vibration study. Naturally, the current printing does not contain any references to recent publications such as the SAE compilations on "Evaluation of Effects of Torsional Vibration" and "Co-Operative Testing of Torsiographs and Calibrations." It is also regrettable that the very recently published methods of extending the Holzer method to forced damped vibrations (J. P. Den Hartog and J. P. Li, Trans. ASME 1946; and T. W. Spaetgens' ASME paper 49—APM-12) could not of course be included.

[12] Chief Engineer, Lessells and Associates, Inc., Boston, Mass. Jun. ASME.

AN ASME PAPER

Its Preparation, Submission and Publication, and Presentation

To a large degree the papers prepared and presented under the ASME sponsorship are evidence by which its professional standing and leadership are judged. It follows, therefore, that to qualify for ASME sponsorship, a paper must not only present suitable subject matter, but it must be well written and conform to recognized standards of good English and literary style.

The pamphlet on "AN ASME PAPER" is designed to aid authors in meeting these requirements and to acquaint them with rules of the Society relating to the preparation and submission of manuscripts and accompanying illustrations. It also includes suggestions for the presentation of papers before Society meetings.

CONTENTS

Price 35¢, No discount allowed. ***A remittance must accompany all orders for $2.00 or less. U. S. Postage Stamps are acceptable.***

THE AMERICAN SOCIETY OF MECHANICAL ENGINEERS

29 West 39th Street, New York 18, N. Y.